

X-RAY OBSERVATIONS OF DWARF NOVAE

Thesis by

France Anne-Dominic de Córdoba

In Partial Fulfillment of the Requirements
for the Degree of
Doctor of Philosophy

California Institute of Technology
Pasadena, California

1979

(Submitted 1979 May 3)

DEDICATED TO

my parents

Joan McGuinness Córdova and Frederick Ben Córdova, Jr.

and my brothers and sisters

Thomas Martin

Declan Francis

Kathleen Thérèse

Zoe Teresa

Vincent Paul

Frederick Benedict III

Lu Marie de Montfort

Leslie Joan Paul

Mary Elizabeth

William Vincent

Jeanne Robert

PREFACE

The idea of making a survey for X-ray emission from cataclysmic variable stars with the HEAO-1 instruments came several months before the satellite was launched. In the winter of 1977 there was an epidemic of AM Her fever. The "accidental" discoveries of soft X-ray emission from AM Her and SS Cyg were the X-ray astronomer's first introduction to some very old and lively stars, possible relatives of the hard X-ray emitting neutron stars in close binary systems. Bill Priedhorsky, *Voytek* Krzeminski and I eagerly pointed the telescopes of Mt. Wilson and Palomar Mtn. that winter, using Kukarkin's catalogue of some 27000 variable stars like a telephone directory. We were gearing up for simultaneous optical/HEAO-1 observations of all the CVs the X-ray eye would detect.

Preparations also included sending HEAO-1 ephemerides of 130 CVs to the American Association of Variable Star Observers and the Royal Astronomical Society of New Zealand Variable Star Section. From the time the satellite was launched in August of 1977 until it ran out of gas in January of 1979, the amateur astronomers of these organizations faithfully and carefully monitored these stars for us. Without their observations, the survey described herein would not have had as much meaning. I especially thank the directors of the AAVSO and VSS, Janet Mattei and Frank Bateson, for organizing

the optical observations and sending us beautiful light curves of outbursting dwarf novae. It was AAVSO member Jim Morgan who alerted us to the outbursts of U Gem and SS Cyg, in time to point the X-ray detectors of HEAO-1 while the stars were still in outburst. It was during those pointings that X-ray oscillations were first detected.

There were a number of other astronomers who contributed whenever possible to the simultaneous monitoring of CVs; Rob Robinson and Joe Patterson at the University of Texas were especially helpful. And I would like to thank the staffs of Mt. Wilson, Palomar Mt. and the Cerro Tololo Inter-American Observatory for allowing me to use their facilities for this project, and Steve Kent and Chip Williams for their assistance at the telescope.

In spite of the preparations and all the simultaneous observations, the first nine months of HEAO-1 produced few positive detections of CVs. But then, in 1978 June, things started to happen -- a combination of luck, timing, and perhaps the novena my mother was making, and with a lot of persistence (and faith!) on the part of my advisor Gordon Garmire who gently, but deliberately, prodded NASA/TRW into making the crucial pointings of SS Cyg and U Gem.

Much preparation goes into arranging a satellite pointing observation; the nominal requirement is one month's advance notice for a pointing. Yet these observations had to be accomplished

immediately; an object transits in the HEAO-1 detectors only every six months, and the coincidence of an optical outburst during this time is a rare and important "target of opportunity." Other people who contributed much towards getting these pointings accomplished were Jean Swank of GSFC and John Aiello of NASA/TRW.

Many people assisted in various aspects of the data analysis: John Nugent with the superposition code, Ian Tuohy with the spectral analysis, and Spencer Klein with much of the handling of the magnetic tapes. I thank them for their unqualified help, and for their friendship as well.

The person I would most like to single out with respect to this project of understanding the X-ray behavior of CVs, and to thank for a beautiful collaboration, and for his cheer and grace, is Tom Chester who did much of the timing analysis described here. It was Tom who first saw in the pattern of the superposed pulses of U Gem a powerful way of quantifying a phenomenon that we had been told was "impossible" to analyze.

For reading and commenting on our preliminary manuscripts and/or offering their ideas about models of the pulsation, we thank Drs. Roger Blandford, Steve Weber, Peter Goldreich, Richard Wade, Joe Patterson, Keith Mason, Paula Szkody, and Jim Pringle.

Janine Boyer and Sharon Hage typed the papers that went into this dissertation; I thank them for their enthusiasm and warmth as well as their skill.

Lastly, I would like to mention some people who go by the name of "Rothschild et al." in all HEAO-A2 publications. These are the people who conceived, tested and calibrated the A2 experiment which accomplished much more than just its "mission objectives." The et al. are: E. Boldt, S. Holt, P. Serlemitsos, G. Garmire, P. Agrawal, G. Riegler, S. Bowyer, and M. Lampton.

ACKNOWLEDGEMENTS

It seems somewhat artificial to distinguish among those who gave me advice in my research, those who helped me in the laboratory or at the telescope, those who gave me inspiration, and those who made me laugh. So I lump here, in random order, colleagues, friends, heroes, mentors, dancing and climbing partners, and a few who were all of these -- with much thanks for the adventure and the belay:

Gerry Neugebauer, Tom Chester, Prune, Boz, Sally and Bill Hurt, Gordon Garmire, Zoe and Lu, Page Lee Hufty, Kay and Alan Hanson, Mr. and Mrs. Big Honey Priedhorsky and Anna Beth, Richard Wade, John Nugent, Walter Lewin, Keith Matthews, Jerry Nelson, Rick Ridgeway, Voytek, the Jesters (Marty, Moose, George, Kris, Tyrone, Margly and Stroke) and the Cowboys (Waylon and Willie, D. Rutherford Hayes and D. Bobo Laney), Eric Persson, Jerry Kristian, Lee and Sonny Tatum, Bev Johnson and Mike Hoover, Ian Tuohy, Bill and Joan Moore, Larry Petro, Barbara Zimmerman, Vic, Bogdan Paczynski, Joe Patterson, Rick Brenner, T.S. Eliot, Chuck Wilts and Jim Campbell, Paula Szkody, BDO, Janet Mattei, Normroff, V. Nabokov, Jay Frogel, Steve van Bogart Beckwith, John Aiello, Sandor and R.B.Miel, the Herb, Sharon Hage and Janine Boyer, Vagn and Mel, Farrout, Tom Tombrello, Jim Morgan, John Nousek, Spencer Klein, Jon Mathews, Jean Swank, Keith Mason, Bob Leighton, El Touton, Kris Sellgren, Ian Gatley, Rob Robinson, Andy Hunter, Mary at Mt. Wilson, Saint Catherine of Siena, my Zapotec Indian comadres and copadres of Villa Diaz Ordaz, Grandma, Mom and Dad, and Ollie Bear.

ACKNOWLEDGEMENTS

(continued)

And I thank the Deity or Singularity who through grace or a toss of the dice has allowed that I should be healthy and happy.

ABSTRACT

The details of a survey of the X-ray properties of ~ 65 dwarf novae are presented: four objects are discussed in detail and the null results for the remaining stars are summarized.

Pulsed soft X-rays (0.1 - 0.5 keV) with a period of 9s and a pulsed fraction that varies between 0 and 100% were detected from the dwarf nova SS Cygni at the peak of an optical outburst. This detection confirms for the first time the supposed high-energy origin of the optical pulsations seen from dwarf novae. The pulse shape is remarkably sinusoidal for such a large amplitude oscillation. The pulsation is not coherent, in contrast to previous claims for the related optical oscillations. Instead, the phase of the pulsation apparently executes a random walk with a Q of ~ 25 , whereas the period is quite stable: $\dot{P} \sim -1 \times 10^{-5} \text{ s s}^{-1}$. There is no evidence for any other periodic behavior on timescales between 160 ms and 3 h. A blackbody fit to the observed spectrum yields $T \sim 3.5 \times 10^5 \text{ K}$ and a flux at the Earth of $\sim 4.5 \times 10^{-11} \text{ erg cm}^{-2} \text{ s}^{-1}$ in the 1/4 keV band. This in turn implies a total luminosity (integrated over all frequencies) at the source of $\sim 1.8 \times 10^{33} \times (d/200 \text{ pc})^2 \text{ erg s}^{-1}$.

continued

A soft X-ray pulsation has also been detected from the dwarf nova U Geminorum on the declining portion of an optical outburst. The pulsation is quasi-periodic with periods ranging from 20 to 30s and present throughout all binary phases, including eclipse, with an average amplitude of $\sim 15\%$. Although superficially the quasi-coherent pulsation from U Gem seems qualitatively different from the more coherent soft X-ray pulsation of SS Cygni, we find that a change in only the strength of the random walk in phase can account for the difference between the two stars. We have developed a simple, powerful technique for analyzing the unstable pulsations; our analysis shows that the phase noise in U Gem is from 10 to 30 times greater than in SS Cyg. A blackbody spectral fit to the U Gem data gives the best-fit parameters $kT \sim 25$ eV and $N_H \leq 5 \times 10^{18} \text{ cm}^{-2}$, which imply a flux at the Earth of $3 \times 10^{-10} \text{ erg cm}^{-2} \text{ s}^{-1}$ in the energy interval 0.13 - 0.5 keV.

Previous models for the optical oscillations fail to account for the properties of the X-ray pulsations. It is possible that an as yet unspecified instability in the boundary layer between the white dwarf and the accretion disk is the origin of the pulsation.

A low-intensity soft X-ray source has been discovered in a region of the sky containing the dwarf nova AY Lyrae. The upper limit to the temperature of the source is $T \leq 5 \times 10^6$ K. X-ray emission below 2 keV has also been detected for the first time

from a source whose X-ray variability and position favor identification with EX Hydrae. The soft X-ray intensity was observed to vary by a factor of three in less than one hour. A temperature in excess of 1×10^7 K was measured for the dwarf nova, which was in an optically quiescent state during the X-ray observation. A thermal bremsstrahlung spectrum with $kT = 4.5$ keV and a column density of $1.7 \begin{smallmatrix} +1.4 \\ -1.0 \end{smallmatrix} \times 10^{21} \text{ cm}^{-2}$ gives the best fit to the data, and implies a total X-ray luminosity (between 0.15 and 10 keV) of $\sim 2.4 \times 10^{32} \times (d/100 \text{ pc})^2 \text{ erg s}^{-1}$. Models for the production of X-rays by accretion onto a white dwarf are discussed in light of this new evidence.

The HEAO-1 X-ray satellite was used to make these observations. HEAO-1 fortuitously scanned ~ 20 dwarf novae while they were undergoing optical outbursts, yet soft X-ray emission was detected only from SS Cyg and U Gem. The 3σ limits to the flux from the non-detected objects, several of which were observed by the spacecraft during more than one outburst, range from 1 to 10% of U Gem's mean flux. We present these limits and discuss various hypotheses for the failure to detect soft X-rays from the majority of erupting dwarf novae.

A preliminary survey of the soft X-ray emission from ~ 65 dwarf novae during quiescence has also been made. Thus far, soft X-rays have been detected only at positions coincident with those

continued

of AY Lyr and EX Hya. We report the average 3σ upper limits to the flux from the nondetected dwarf novae. These limits are $\sim 7 \times 10^{-12}$ erg cm⁻² s⁻¹ in the energy interval 0.18 - 0.43 keV, and $\sim 3 \times 10^{-11}$ erg cm⁻² s⁻¹ in the interval 0.74 - 2 keV. We compare the quiescent state spectra of dwarf novae with their outburst spectra and deduce that variations in the mass accretion rate can account for the variety of X-ray behavior we observe.

TABLE OF CONTENTS

	page
PREFACE	iii
ACKNOWLEDGEMENTS	vii
ABSTRACT	ix
TABLE OF CONTENTS	xiii
INTRODUCTION	xvi
PART I: DWARF NOVAE IN OUTBURST	1
<u>A Review of Previous Observations</u>	2
Figure	4
PAPER 1: <u>Soft X-ray Pulsations from SS Cygni</u>	5
I. Introduction	6
II. The Observations	8
III. Detailed Analysis of the Pulsation	16
IV. Discussion	23
V. Implications for Future Observations	33
Table	35
References	36
Figures	39
PAPER 2: <u>The Quasi-Periodic Soft X-ray Oscillation in U Geminorum</u>	52
I. Introduction	53
II. The Observations	54
III. A New Technique for Analyzing Unstable Pulsations	62
IV. Discussion	67
V. Implications	69
References	71
Figures	72

PAPER 3:	<u>A Soft X-ray Survey of Dwarf Novae in Outburst</u>	86
I.	Introduction	87
II.	The Experiment and the Survey	88
III.	Results	89
IV.	Discussion	91
V.	Conclusion	99
	Table	101
	References	102
	Figures	104
PART II: DWARF NOVAE IN QUIESCENCE		109
	<u>A Review of Previous Observations</u>	110
PAPER 4:	<u>The Detection of Soft X-rays from EX Hydrae</u>	112
I.	Introduction	113
II.	The Observations	114
III.	Discussion	118
	Table	124
	References	125
	Figures	127
PAPER 5:	<u>Soft X-ray Emission from the Vicinity of AY Lyrae</u>	131
	The Observations	132
	References	137
	Figures	138

PAPER 6:	<u>A Soft X-ray Survey of Dwarf Novae in Quiescence</u>	142
	I. Introduction	143
	II. The Experiment and the Survey	144
	III. Results	146
	IV. Discussion	146
	V. Conclusions	151
	Table 1	153
	Table 2	154
	References	155
SUMMARY		157
	Table	158
	References	165
APPENDIX A:	<u>Experiment Description</u>	168
	1. Introduction	168
	2. LED1 Characteristics	169
	3. How an (X-ray) Event Gets Processed and Telemetered	191
	4. Data Reduction	196
	References	241
APPENDIX B:	<u>Pulse Timing</u>	242
	1. The Computer Program	243
	2. The Arrival Times for SS Cygni 's Pulses	247

INTRODUCTION

HEAO-1 was the first of three satellites (designated High Energy Astronomical Observatories) designed to make a comprehensive study of the high-energy universe. The specific mission of HEAO-1 was to conduct an all-sky survey of radiation ranging from the softest X-rays of 0.1 keV to higher energy gamma rays of 10 MeV.

Scientists at Caltech collaborated on one of several HEAO-1 experiments, the Cosmic X-ray Experiment, whose purpose was to map the entire diffuse X-ray sky and to study the temporal and spectral characteristics of discrete X-ray sources. The Caltech investigators shared the low-energy portion of the experiment (0.1 - 3 keV) with scientists at the Jet Propulsion Laboratory and the University of California at Berkeley, while Goddard Space Flight Center investigators had responsibility for analysis of the medium and hard X-ray data. A description of the low-energy detector which was used to collect the data forming the subject material of this thesis is given in Appendix A.

This dissertation is a study of the soft X-ray emission from dwarf novae, a subset of cataclysmic variable stars, using HEAO-1 data. The results of an extensive search for soft X-ray emission from about sixty of the most prominent members of this class are reported, and the fast temporal behavior of two prototype dwarf novae, SS Cygni and U Geminorum, is investigated.

In the standard picture of a dwarf nova, mass is transferred from a late-type star via Roche-lobe overflow onto an accretion disk surrounding a white dwarf. Approximately every few weeks the systems have "dwarf" outbursts (relative to the **large** outbursts of the classical novae), during which they visually brighten by ten to one-hundred times. The rise from quiescent to peak light occurs in less than a day; thereafter the systems slowly fade to their pre-outburst level over the course of several days.

The origin of the eruptions is not well understood. It is commonly believed that an instability in the cool component or in the disk itself causes additional material to be transferred to the compact star, resulting in the conversion of gravitational potential energy into radiation throughout the disk and at the white dwarf surface. An alternative model is the nuclear burning of material accumulated on the degenerate star's surface. Excellent reviews of cataclysmic variables in general may be found in Robinson (1976) and Warner (1976); the theoretical aspects are treated in more detail in Bath (1976; 1978).

The first detections of soft X-ray/EUV emission from the dwarf nova SS Cygni during outbursts (Rappaport et al. 1974, Hearn, Richardson and Li 1976; Margon et al. 1978) raised speculations that the high-energy emission came either from a "bright spot" where the high-velocity ejecta from the late-type donor impacts the disk (Warner 1974) or from a region of retarded velocity ("boundary layer") between the inner disk and the white dwarf surface (Bath

et al. 1974; Pringle 1977). Alternatively, the discovery of hard X-rays (1-7 keV) and possibly very weak soft X-rays (0.16-0.28 keV) from SS Cyg during quiescence (Heise et al. 1978), could be interpreted as evidence for a weak white dwarf magnetic field ($B \leq 10^6$ gauss) which disrupts the disk at a few white dwarf radii or less, and channels the gas spherically onto the degenerate star (Fabian, Pringle and Rees 1976). The resulting spectrum would have both a hard X-ray component due to bremsstrahlung in a standoff shock above the white dwarf, and a soft X-ray component due to thermalization and reradiation of the hard X-ray emission absorbed by the white dwarf (Kylafis et al. 1978).

One of the most distinctive properties observed in dwarf novae is the appearance of low-amplitude visual pulsations during outburst (see the previously mentioned reviews). The pulsation is usually categorized as either "coherent" or "quasi-coherent." The former have periods between about 10 and 30s, while the latter have periods between about 30 and 150s. The coherent oscillation is observed to drift in frequency over the course of the outburst with a Q of $\sim 10^5$; the quasi-coherent oscillation is damped after only a few cycles.

Various models have been proposed to account for the pulsation: for the coherent oscillation Bath (1973) has suggested rotating temperature fluctuations in the inner accretion disk; Warner and Robinson (1972) have proposed non-radial g-mode pulsations of the white dwarf; and Papaloizou and Pringle (1978) have evoked non-radial

modes of a rotating white dwarf surface layer (these modes are similar to the Rossby waves in the Earth's atmosphere and oceans). All models predicted that the origin of the visual pulsation was in a high-energy component; the visual pulsation was due either to reprocessing (Paczynski 1978; Warner and Brickhill 1978) or was part of the direct spectrum of an EUV/soft X-ray component (Bath 1973). For the quasi-periodic oscillation, on the other hand, Robinson and Nather (1979) have proposed an origin in hot spots in the accretion disk a few white dwarf radii from the compact star. These oscillations are presumably triggered by an increased mass flux through the disk.

In the last year and a half, several X-ray observations have been made using the HEAO-1 and Ariel V satellites which make it possible to evaluate the applicability of these models for the dwarf novae X-ray emission, and for the origin and nature of the visual oscillations. Specifically, a relatively hard spectrum has now been measured for at least three dwarf novae during both quiescent and outburst phases. In addition, highly modulated soft X-ray pulsations of both "coherent" and "quasi-coherent" character have been discovered from two dwarf novae during outbursts.

Several of these observations are reported here for the first time; others, in particular many of the hard X-ray observations, have been reported elsewhere but are summarized here for completeness.

This dissertation is organized into two Parts: Part I is an analysis of the observations of dwarf novae during outburst and Part II is an analysis of the observations of these objects during

quiescence. Each Part contains three papers which have either been accepted for publication in various scientific journals, have been submitted for publication, or are still in preparation for eventual submission. The specific journals involved are designated on the title pages for each paper. Collaboration is also acknowledged on the title pages.

In the preface to Part I the first detections of soft X-rays (reported previously) from SS Cyg and U Gem are summarized. In the first two papers the discoveries of soft X-ray pulsations from these objects are presented and a detailed analysis of the pulsation is made. A new technique for analyzing unstable pulsations is described and applied to the pulsations from SS Cyg and U Gem. In Paper 3 the results of a survey for soft X-ray emission from about 20 erupting dwarf novae are reported and possible hypotheses for the failure to detect X-rays from most of these systems are examined.

In the beginning of Part II the previous reports of X-ray emission from SS Cyg and EX Hya during quiescence are reviewed. Papers 4-6 present the results of a search for X-ray emission from about 65 dwarf novae in their quiescent states: the positive detection for the first time of X-rays below 2 keV from EX Hya, the detection of very soft X-rays from a source in the vicinity of AY Lyrae, and the upper limits to soft X-ray emission from the remainder of the stars in the survey.

The dissertation concludes with a summary of all the X-ray observations of dwarf novae and a discussion of how these observations have enhanced our understanding of the dynamics of these

close binary systems.

Since the format of the work is a collection of scientific papers, many of the details of the experiment and the data reduction techniques could not be included. Therefore, these are described in full in Appendix A, which is at the end of the dissertation. In Appendix B the computer program used to generate the arrival times for the pulses of both SS Cyg and U Gem is listed, together with a brief description of the program and an example of its output.

REFERENCES

- Bath, G.T. 1973, Nature Phys. Sci., 246, 84.
- _____ 1976, IAU Symposium No.73, Structure and Evolution of Close Binary Systems, ed. P. Eggleton et al. (Dordrecht: Reidel), p. 173.
- Bath, G.T., Evans, W.D., Papaloizou, J. and Pringle, J.E. 1974, M.N.R.A.S., 169, 447.
- Fabian, A.C., Pringle, J.E. and Rees, M.J. 1976, M.N.R.A.S., 175, 43.
- Hearn, D.R., Richardson, J.A., and Li, F.K. 1976, Bull. A.A.S., 8, 447.
- Heise, J., Mewe, R., Brinkman, A.C., Gronenschild, E.H.B.M., den Boggende, A.J.F., Schrijver, J., Parsignault, D.R. and Grindlay, J.E. 1978, Astr. and Ap., 63, L1.
- Kylafis, N.D., Lamb, D.Q., Masters, A.R., and Weast, G.J., Proc. of the IAU/COSPAR Symposium on X-ray Astronomy, Innsbruck, Austria, June 1978.
- Margon, B., Szkody, P., Bowyer, S., Lampton, M. and Paresce, F. 1978, Ap.J., 224, 167.
- Paczyński, B. 1978 in Nonstationary Evolution of Close Binaries, ed. A. Zytkow (Warsaw: Polish Scientific Publishers).
- Papaloizou, J. and Pringle, J.E. 1978, M.N.R.A.S., 182, 423.
- Pringle, J.E. 1977, M.N.R.A.S., 178, 195.
- Rappaport, S., Cash, W., Doxsey, R., McClintock, J. and Moore, G. 1974, Ap.J. (Letters), 187, L5.
- Robinson, E.L. 1976, Ann. Rev. Astr. Ap., 14, 119.
- Robinson, E.L. and Nather, R.E. 1979, preprint
- Warner, B. 1974, M.N.R.A.S., 167, 47p.

Warner, B., 1976, in IAU Symposium No. 73, Structure and Evolution of Close Binary Systems, ed. P. Eggleton et al. (Dordrecht: Reidel), p.85.

Warner, B. and Brickhill, A.J. 1978, M.N.R.A.S., 182, 777.

Warner, B. and Robinson, E.L. 1972, Nature Phys. Sci., 239, 2.

PART I:
DWARF NOVAE IN OUTBURST

PREVIOUS X-RAY OBSERVATIONS OF DWARF NOVAE
IN OUTBURST

The first detection of a stellar X-ray source in the 1/4 keV band happened to be that of SS Cygni during a 1973 MIT rocket flight. The source was discovered by Rappaport et al. (1974) in a scan over Cygnus X-2. The identification with the dwarf nova was proposed on the basis of positional coincidence and because SS Cyg was undergoing an optical outburst ($m_V = 8.5$) at the time. The intensity measured for the source was 5×10^{-10} erg cm⁻² s⁻¹; to date this is the highest reported intensity for SS Cyg.

Subsequently, the SAS-3 group at MIT reported a detection of SS Cyg, again in the 1/4 keV band and again during an optical outburst (Hearn, Richardson and Li 1976). The observed flux for that observation was $(3-5) \times 10^{-11}$ erg cm⁻² s⁻¹.

Observations of SS Cyg were made on three consecutive days during an outburst, using the extreme ultraviolet telescope on the Apollo Soyuz Test Project. The first observation was made three days after the rise to optical maximum. For this observation (the star was at $m_V = 8.9$), the EUV (0.08 - 0.25 keV) flux was 9×10^{-11} erg cm⁻² s⁻¹. On the following day it was measured at the same EUV flux, but on the third day of observing it was not detected above the background, even though the optical brightness had increased slightly ($m_V = 8.6$). The upper limit to the flux on this day was 1.5×10^{-11} erg cm⁻² s⁻¹. These EUV observations are detailed by Margon et al. (1978).

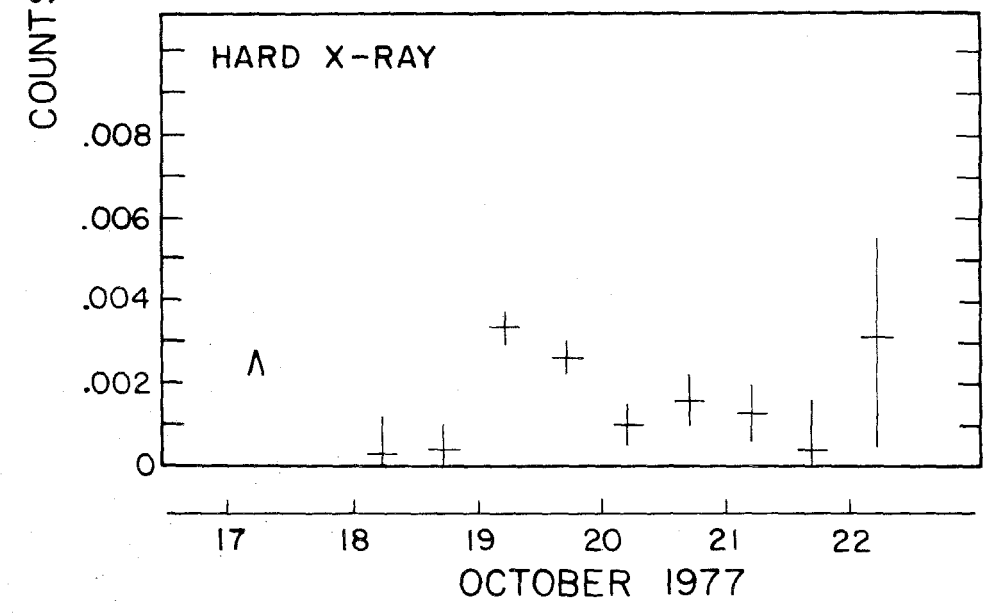
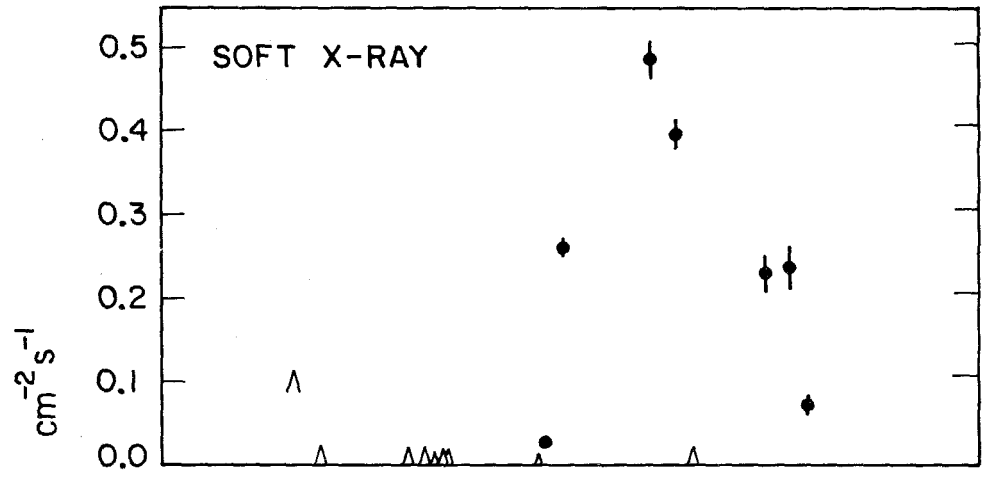
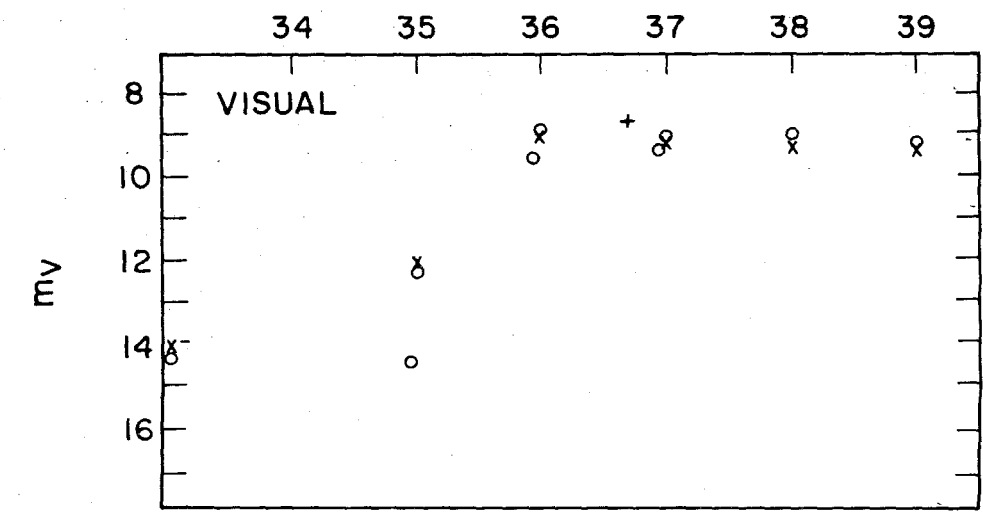
U Geminorum was first detected in scanning observations using the HEAO-1 satellite. During an optical eruption of the source in 1977 October, both soft and hard X-rays were detected (Mason et al. 1978; Swank et al. 1978). Figure 1 shows the outburst light curves for the visual (a), the soft X-ray (b), and the hard X-ray (c) observations. The peak soft X-ray flux was $3.2 \times 10^{-10} \text{ erg cm}^{-2} \text{ s}^{-1}$ (for $kT = 30 \text{ eV}$), while the peak hard X-ray flux was $2.4 \times 10^{-11} \text{ erg cm}^{-2} \text{ s}^{-1}$ (for $kT = 5+3 \text{ keV}$).

As Figure 1 shows, both X-ray components showed an increase over their quiescent (unobservable) levels. In soft X-rays, the quiescent phase flux was at least 100 times less than the peak outburst flux. An OSO-8 satellite upper limit to U Gem's hard X-ray flux during quiescence is three times less than the outburst flux (Swank et al. 1978).

During the outburst the soft X-ray flux from U Gem was highly variable on a timescale of a few hours (or less). This variability is consistent with an orbital dependence for the limited data sample available (Mason et al. 1978). It must be stressed that this apparent dependence may be fortuitous. The hard X-ray light curve showed no orbital dependence (Swank et al. 1978).

These observations are listed, together with the observations of dwarf novae during quiescence, in the Table accompanying the Summary of this dissertation; the references mentioned here may be found with that Table.

J.D. 2443400.0+



OCTOBER 1977

U GEMINORUM

PAPER 1:

SOFT X-RAY PULSATIONS FROM SS CYGNI

submitted for publication to the

Astrophysical Journal

in collaboration with

T.J.Chester, I.R.Tuohy and G.P.Garmire

April 1979

I. INTRODUCTION

Although our understanding of dwarf novae has progressed rapidly in the last 20 years, some of the most fundamental facts remain unexplained. (For general reviews of cataclysmic variables see Warner 1976; Bath 1976; Robinson 1976; and Bath 1978.) This situation can be largely traced to our ignorance regarding the basic process that fuels the observed luminosity in these close binary systems; that is, we do not know the precise manner in which mass is transferred from the red star via the accretion disk to the surface of the white dwarf.

Like many other dwarf novae, SS Cygni shows low amplitude, short period optical pulsations during outbursts. For SS Cyg, periods ranging from 8.5 to 10.6 s have been measured (Patterson, Robinson, and Kiplinger 1978; Horne and Gomer 1979; Patterson 1979). The optical pulsations are thought to be reprocessed pulsed X-ray or EUV emission produced in the vicinity of the compact star (Warner and Brickhill 1978), although the origin of the pulsation itself remains unclear. It was hoped that high energy observations could test this hypothesis.

Hard X-rays (2-25 keV) have been detected from SS Cyg during optical quiescence by HEAO-1 with a flux of 1.6×10^{-10} erg cm⁻² s⁻¹ (Mason, Córdova, and Swank 1978). It is unlikely, though, that hard X-rays are the source of the optical pulsation. Fabbiano et al. (1978) report a 3σ upper limit to the pulsed fraction of SS Cyg during quiescence of $\sim 13\%$ for periods consistent with those of the optical

pulsations. In addition, the hard X-ray flux decreases during eruption (Ricketts et al. 1979). Swank (1979) reports that during the outburst described herein there was a residual hard X-ray flux of $\sim 4 \times 10^{-11}$ erg $\text{cm}^{-2} \text{s}^{-1}$, and that the preliminary upper limit to a hard X-ray pulsation during this outburst is $\sim 10\%$.

In soft X-rays (0.1-0.5 keV), on the other hand, there is an increase in intensity during outbursts by about an order of magnitude. Our own HEAO-1 pointing observation of SS Cyg on 1977 December 12 during quiescence gives an upper limit of 5×10^{-12} erg $\text{cm}^{-2} \text{s}^{-1}$. This is consistent with the marginal detection of 1/4 keV X-rays from SS Cyg during quiescence by Heise et al. (1978). During outbursts, however, soft X-rays and EUV from SS Cyg have been detected with an average flux of 5×10^{-11} erg $\text{cm}^{-2} \text{s}^{-1}$ by several experimenters (Rappaport et al. 1974; Hearn et al. 1976; and Margon et al. 1978). The observed correlation between soft X-ray and optical brightenings made it important to search for soft X-ray pulsations during eruptions.

In 1978 June we were fortunately able to point HEAO-1 at SS Cyg during an outburst. This was the first X-ray pointing at an erupting dwarf nova, and hence the first experiment capable of looking for rapid X-ray variability during a maximum. The soft X-rays from SS Cyg were indeed highly modulated at a period close to observed optical periods in the object, confirming the soft X-rays as the ultimate source of the optical pulsations. The large amplitude allowed us to study the properties of the pulsation in detail.

This paper is organized as follows: §II presents the soft X-ray observations from this pointing; §III is devoted to a detailed analysis of the pulsation; §IV includes a discussion of possible models for the origin and nature of the pulsation; and §V is a summary of the implications of this analysis for future investigations.

II. THE OBSERVATIONS

On 1978 June 13 HEAO-1 investigators were alerted by the American Association of Variable Star Observers that SS Cyg was undergoing an optical outburst. A HEAO-1 pointing at SS Cyg commenced June 14.8 U.T. and lasted ~ 6 h. The inset in Figure 1 displays the visual light curve and shows that the satellite observation took place near the peak of the outburst. We reproduce in Figure 1 a representative portion of the X-ray data, showing the large amplitude pulsations with a period of ~ 9 s.

a) The Instrumentation

The low energy detector LED1 of the A2 experiment^{*} on HEAO-1 was

* The A2 experiment of HEAO-1 is a collaborative effort led by E. Boldt of Goddard Space Flight Center (GSFC) and G. Garmire of the California Institute of Technology (CIT) with collaborators at CIT, Jet Propulsion Laboratory, University of California at Berkeley, and GSFC.

used for this observation. A complete description of the experiment is given in Rothschild et al. (1979). Briefly, LED1 is a gas

proportional counter with sensitivity in the range 0.1-3 keV. The collimator in front of the detector has a 3° FWHM field of view along the satellite meridian, and coaligned fields of view of 1.5° and 3° FWHM along the satellite azimuth. The data from both fields of view, representing a combined geometrical area of 380 cm^2 , were used for this analysis. All of the data were taken with a time resolution of at least 1.28 s; portions of the observation had 80 ms resolution.

b) The X-ray Light Curve

We used the ratio of the fields of view to subtract the contribution from the X-ray sky background and found that SS Cyg was detectable only below 0.5 keV. This ratio technique confirmed that the substantial flux in the energy band 0.5-2 keV was due to a background feature, probably associated with the large Cyg X-6 background enhancement (Davidsen et al. 1977). SS Cyg is completely resolved spectrally from this feature, which is cut off below 0.5 keV. Thus the data used for the analysis described here are taken only from the interval 0.1-0.5 keV, except as noted. Summing the count rates from both fields of view, the X-ray sky background contributed $\sim 45\%$ to the total count rate.

Figure 2 shows the background-subtracted, aspect-corrected soft X-ray light curve for the entire observation. Each point represents an average over ~ 41 s of data. The X-ray signal is interrupted by Earth occultations of the source which last for $\sim 1/2$ of each 90 min satellite orbit. For convenience in referring later in the text to the

disjoint sections of data, the sections are labeled OB1, 2, etc. The few low data points occur at times when the aspect corrections are large. Spacecraft aspect wandering results in larger uncertainties for the count rates during the first halves of OB1, 2, 3 and 4, and the last half of OB5 (see error bars in Figure 2). Within the large uncertainties for the individual data points, the amplitude is consistent with being constant during each OB.

Since the data in the first 4 OBs were taken with the same detector gain, the average count rates from these sections may be compared. The average intensities during OB1, 2 and 3 were 0.045 ± 0.002 , 0.045 ± 0.002 , and 0.047 ± 0.002 ct cm⁻² s⁻¹, respectively, while that of OB4 was 0.038 ± 0.001 ct cm⁻² s⁻¹. Hence the signal from SS Cyg was lower (4σ) during OB4 by 16%. OB5 was taken with a different detector gain and cannot be compared with the other OBs unless some assumption about the spectrum is made. Assuming the best-fit spectral parameters (see §IIc), the average intensity of OB5 is $\sim 0.033 \pm 0.002$ ct cm⁻² s⁻¹. (Any choice of spectral parameters within the 90% confidence limits given in §IIc will give a value for the intensity of OB5 which is at least as low as the value for OB4.) This apparent monotonic decrease may represent a cooling of the source. Alternatively, the decrease of OB4 and 5 may be correlated with the 6.6 h binary period of SS Cyg. A longer observation is required to differentiate between these two possibilities. There is no evidence of any periodic modulation of the X-ray intensity on timescales from a few minutes to ~ 3 h.

c) The Spectrum

We analyzed the SS Cyg pulse-height data taken when the LED1 high voltage was increased above its nominal value. The higher voltage extended the detector bandpass by reducing the lower threshold from 0.18 keV to 0.13 keV, as determined from an on-board X-ray calibration which immediately followed the SS Cyg observation. Background data for the pointing were derived from data taken while LED1 was scanning a region of sky close to SS Cyg.

The spectral data below 0.5 keV were parameterized in turn with a blackbody spectrum and a thermal bremsstrahlung spectrum which we approximated with an exponential plus an energy dependent Gaunt factor (Kellogg, Baldwin, and Koch 1975), allowing for absorption in the interstellar medium (Brown and Gould 1970). The measured flux and the best-fit spectral parameters are given in Table 1. Figure 3 shows the observed count rate spectrum and the best-fit blackbody model, together with the 90% confidence chi-squared contours (Lampton, Margon and Bowyer 1976) for both types of spectra. From the chi-squared contours, we can set the following limits on the source temperature:

$$5.04 < \text{Log } T < 5.82 \text{ (Blackbody)}$$

$$5.21 < \text{Log } T < 6.34 \text{ (Thermal Brem.)}$$

For both models, the upper limit to the column density is $6.3 \times 10^{20} \text{ cm}^{-2}$. The bremsstrahlung model sets a lower limit of $1 \times 10^{19} \text{ cm}^{-2}$ on the column density, but in contrast, the blackbody model is consistent with zero column at the 90% confidence level.

The best-fit blackbody spectrum of 30 eV yields a total luminosity at the source (integrated over all frequencies) of $\sim 1.8 \times 10^{33} \times (d/200 \text{ pc})^2 \text{ erg s}^{-1}$, with about 30% of this luminosity in the energy range accessible to our detector. (The distance of 200 pc is selected as a compromise between various distance estimates; see Warner 1976.) The spectral resolution of the LED1 proportional counter for energies less than 0.5 keV is $> 80\%$, resulting in large uncertainties in the estimation of the temperature (see inset to Figure 3). Therefore, the best-fit temperature and luminosity derived here should only be used as a guide. In addition, a line emission model may be more appropriate for temperatures \sim a few $\times 10^5$ K and would systematically increase the temperatures quoted above.

The above spectral data were acquired in a special telemetry mode with a temporal resolution of 20 ms per event. In order to search for possible variability of the source spectrum during the 9 s pulse, the data were folded at the appropriate period into 10 phase bins. A spectral hardness ratio for each bin was computed from the ratio of the (0.23-0.41) to (0.13-0.23) keV count rates. No correlation of the hardness ratio with the sinusoidal pulse light curve was evident, as confirmed by a fit of the data to a constant hardness ratio ($\chi^2_{\nu} = 1.3$ for 9 degrees of freedom).

d) The Pulsations

The power spectra from discrete Fourier transforms using 1.28 s binning are shown for two of the OBs in Figure 4. There is an overall period drift evident in the Fourier transforms of $\dot{P} \sim -1 \times 10^{-5} \text{ s s}^{-1}$ that will be discussed in §III. There are no detectable harmonics or subharmonics of the 9 s period, with a 90% confidence upper limit of 2% of the average X-ray flux. This is only a "formal" upper limit since the inherent phase jitter (discussed below) of the 9 s pulsation will selectively wash out higher harmonics.

We have analyzed the 80 ms data available for OB4 and OB5 in order to search for pulse structure that might have been smeared out in the Fourier transform by the period variability. We determined the time of maximum for each pulse (discussed in detail in §III), and superposed each pulse so that the maxima coincided. The resulting composite profile is shown in the inset of Figure 4b. The figure represents a superposition of 427 pulses. The source signal in this data is only 30% of the total intensity. The large background contribution results from the lack of spectral resolution in the 80 ms data; hence the 80 ms data include the entire broadband energy range of 0.1-3 keV.

The best-fit sinusoid yields $\chi^2 = 108$ with 106 degrees of freedom, and is shown as a solid line through the pulse profile. Care must be used in deriving upper limits on harmonic amplitudes because, as we now show, spurious harmonics are introduced by the superposition. Noise power always increases the fitted pulsed amplitude (because amplitudes

are always nonnegative) and shifts the observed time of maximum of each pulse. When the pulses are aligned at their peaks, the peak amplitude is thus increased by noise. The amplitudes of other portions of the pulse, however, are progressively reduced by smearing caused by the shifts in the observed time of maximum away from the true peak of each pulse. A complete explanation of this effect is given in Córdova et al. (1979).

After allowance for the effects of noise, the 90% confidence upper limit to the amplitudes of harmonics, relative to the fundamental amplitude, is 12% for the first harmonic, and $\sim 7\%$ for the other harmonics. However, the accuracy in the determined time of maximum for each pulse reduces our sensitivity to the harmonics with periods less than ~ 2.4 s. This remarkably sinusoidal pulse profile is perhaps the simplest pulse profile yet observed in X-ray astronomy.

A Fourier transform of the 80 ms data for OB4 and 5 revealed no excess power at periods between 160 ms and 9 s. We have also searched for power near 0.031 Hz because of the reported quasi-periodic oscillation in visual light at ~ 32 s (Robinson and Nather 1979). Adding the power between 29 and 35 s gives a 90% confidence upper limit to the equivalent pulsed fraction of 2%. Thus we conclude that there is no apparent periodic behavior in SS Cyg, other than the 9 s pulsation, on timescales from 160 ms to 3 h.

We have employed several techniques in order to examine the short term behavior of the pulsation. In one type of analysis, short

segments of continuous data were folded over many periods in the neighborhood of the 9 s pulsation period, and the amplitudes were plotted as a function of period. The resulting "periodograms" (illustrated in Córdova 1979) show a pulsation behavior strikingly similar to the optical pulsations observed from other dwarf novae: large amplitude variability, a long term period drift, period excursions on short timescales, and the occasional presence of multiple periods. A problem with this type of analysis is that amplitude and/or phase changes can produce sidelobes of the pulsation, creating a false impression of multiple periodic structure. Furthermore, if the pulsation has an overall drift, the segmenting of the data and subsequent folding can create the appearance of discrete periods with a frequency separation correlated with the length of the segments. (See Warner and Brickhill 1978 for an explanation of the periodogram technique and applications to visual pulsations from several dwarf novae.)

A more successful approach is illustrated in Figure 5, which is a three-dimensional "phase diagram" of a small portion of the data from the beginning of the observation. Each of the curves in the figure represents 128 s of data folded into 10 phase bins using an 8.76 s pulsation period, which was the best-fit period for the latter part of the observation. The curves are sequential with a 50% overlap. Three cycles of the fold are repeated in each curve to show more clearly the phase excursions about the mean period drift. Note also the apparent amplitude changes.

We have used essentially the above method to derive the amplitude and phase of the pulsation as a function of time. A quantitative analysis of these parameters is presented in the next section. That this refinement over techniques used in analyzing the optical pulsations was possible is due to the large amplitude of the soft X-ray pulsations ($\sim 30\%$ as compared to $\sim 0.1\%$ in the visual).

III. DETAILED ANALYSIS OF THE PULSATION

We determine pulse arrival times by cross-correlating individual pulses or groups of pulses with a master pulse profile. For SS Cyg, the master pulse is a simple sinusoid, and hence the procedure reduces to fitting short segments of the data with a sinusoid, obtaining the amplitude and phase of the pulsation. These quantities are shown in Figure 6 from a fit to every independent set of four consecutive pulses (28 bins of 1.28 s each) in each orbit. We have similarly fit sets of individual pulses and, separately, sets of up to ten consecutive pulses, obtaining nearly identical results.

An important point must be appreciated with regard to the phase of the pulsations. Whenever the amplitude of the pulsation becomes small enough to be comparable to the uncertainty in the determination of the amplitude, the phase of the pulsation becomes undefined. We wish to obtain a set of arrival times that are well enough defined so that a statistical analysis will give reliable results. Thus we must consider only those points for which the amplitude is nonzero at

a high enough confidence level to be sure that fewer than one arrival time in our set is expected to be spurious. We have used a cutoff at the 99.0% confidence level to ensure that this will be true in the set of 209 arrival times shown in Figure 6b, which represents 72% of the data.

What stands out above all in Figure 6 is the apparently independent variability in both the amplitude and phase of the oscillation. The amplitude can change by a factor of ~ 6 within ~ 15 pulses with no effect on the pulse phase (see the middle of the third orbit). The pulse phase not only wanders around slowly, but it also jumps rapidly at times. Near the end of OB1 the phase jumps by $134^\circ \pm 26^\circ$ (1σ) from one group of 4 cycles to the next group with no effect on the amplitude. Also, in the middle of OB2, there is a phase jump of $234^\circ \pm 24^\circ$ from one set of 4 cycles to another set separated by three sets not shown in the figure. The phases of those sets were $24^\circ \pm 24^\circ$, $101^\circ \pm 32^\circ$, and $197^\circ \pm 24^\circ$, which implies a phase change of $173^\circ \pm 34^\circ$ within ~ 10 pulse cycles. (The amplitudes of those sets were nonzero by more than 1σ . Thus fewer than one phase is expected to be spurious in this set of three phases.) Note that the rapid rise in amplitude occurs after this phase shift. Examination of individual pulses does not yield any further information on the jumps except for their probable sign, because of the larger uncertainties in the individual pulse quantities.

The mean pulsed fraction of the source is $\sim 30\%$. (The mean determined from Figure 6a includes noise from counting statistics, which increases that mean to 0.34.) Amplitude variability is definitely

present; for each orbit, the reduced χ^2 about a constant value is ~ 4 . Thus the intrinsic variability in the pulsed fraction is roughly twice the observational error.

We display the pulse-to-pulse variation of the amplitude in the form of the two histograms shown in Figure 7. Two different definitions of pulsed fraction are used, each of which gives different information. Consider a pulse $A + B \cos(\omega t)$. In Figure 7a, as in Figure 6a, the pulsed fraction for each pulse is defined as $B/\langle A \rangle$, where $\langle A \rangle$ is the mean intensity for the entire OB containing that pulse. Thus this figure reflects the pulsed amplitude distribution of all pulses since the mean intensity acts only as an overall normalizing factor. In Figure 7b, the pulsed fraction is defined as B/A . Hence this figure reflects the pulsed fraction distribution. (Recall that the pulsed fraction so defined ranges between 0 and 200%; a pulse $1 + \cos(\omega t)$ has a pulsed fraction of 100%, whereas a δ function, which equals $1 + 2 \cos(\omega t) + \dots$, has a pulsed fraction of 200%.) For example, if $B \propto A$, with A variable, Figure 7a would give the distribution of A , whereas all the pulses in Figure 7b would fall in the same pulsed fraction bin, B/A . The similarity of the two distributions testifies to the constancy of the mean intensity from SS Cyg and the true variability of the pulsed fraction, which ranges from ~ 0 to $\sim 100\%$. (Examination of the individual pulses with pulsed fractions over 100% shows that they are all consistent with a pulsed fraction of 100% within measurement errors.) Note that the mean of both histograms is now 44% due to the increased noise amplitude ($\sim 28\%$ for a fit to individual pulses).

The magnitude of the phase variability prevents connecting the phase of the pulsation between OBs. Hence the binary orbital time delay with an expected amplitude of ~ 1.5 s (Walker and Chincarini 1968) cannot be seen. However, there is no ambiguity in pulse numbering within each orbit except for the two large phase jumps noted above.

This variability also appears in the distribution of χ^2 values obtained in fitting a constant plus sinusoid to every group of n pulses. Although the observed χ^2 distribution closely resembles the expected χ^2 distribution for $n = 1$ or 2 , it deviates noticeably from the expected χ^2 distribution as n increases.

If we attempt to fit short stretches of the arrival time with a constant period, we obtain a poor fit in general. That is, an intrinsic uncertainty in the arrival times must be (quadratically) added to the measured uncertainties in order to obtain a fit with a reduced χ^2 of unity. Following this procedure, we show in Figure 8a how the period varies with time on short timescales. We have chosen time intervals in such a way as to show the full range of variability of the period. In Figure 8b, the period and its uncertainty as derived from each orbit of data are given by the solid error bars. The period shows an irregular general decrease, to be discussed further below.

The noise properties of the phase of the oscillation can be investigated by examining how the variance of the phase about a constant

period depends on time. We do this in the following way. Consider all sets of arrival times spanning n pulse periods. We determine the best-fit period and the intrinsic uncertainty for each set as detailed above. From all these sets, we obtain a mean intrinsic uncertainty σ_{int} and its standard deviation, taking into account the degree of dependence of the overlapping sets. Figure 8 shows how σ_{int}^2 depends on n . In interpreting Figure 8, be aware that each point is partially dependent on its neighbors.

The variance increases approximately linearly with time, which is consistent with a random walk in phase caused by white noise in the period of the oscillation. Although meaningful statistical estimates of σ_{int} cannot be made for time intervals longer than those shown in Figure 9, point estimates are available from the entire length of each satellite orbit. From OB1 and 5 ($n \sim 100$), σ_{int} equals 36° and 54° , and from OB2, 3, and 4 ($n \sim 300$), σ_{int} equals 69° , 78° , 37° . These estimates are consistent with the extrapolation of Figure 9. It is important to note that all these estimates of σ_{int} are lower bounds to the true variance in the data because the period that was fit to each stretch absorbed a large portion of the variance.

To determine the strength of the random walk, we construct artificial data and analyze the data in the same fashion as above. Let $\{T_N\}$ be a set of arrival times generated by $T_N = T_{N-1} + P$, where $P = P_0 + P_1x$, P_0 and P_1 are fixed numbers, and x is a normally distributed random variable with a mean of zero and unit standard deviation. An "observational uncertainty" was assigned

to these times by utilizing the actual measurement errors of the real data.

For $P_0 = 8.77$ s, we find that $P_1 = 0.44 \pm 0.06$ s (subjective 1 σ error) produces a curve consistent with Figure 9. For illustration, we show in Figure 10 the first set of artificial data given by the random number generator on our computer. Note how similar the "structure" of Figure 10 is to Figure 6b, and how the period seems to assume several discrete values, with sudden transitions between periods, not to mention a few phase jumps here and there. Our prescription also produces occasional sections of data with smaller variances which resemble OB4.

There have been several reports in the literature of multiple periods or erratic period shifts in the optical oscillations from dwarf novae (Robinson 1973; Warner and Brickhill 1978). The evidence in Figure 10 suggests that both these effects may be due to a random walk noise process.

Although we know that phase steps must occur at least as often as once per cycle, we do not know the true frequency of the steps. Thus, instead of specific values of P_0 and P_1 , our simulation gives us the strength of the random walk, which is defined as a rate of phase steps times the mean square phase step:

$$S = R \langle (\Delta\phi)^2 \rangle = \frac{1}{P_0} \left(\frac{2\pi P_1}{P_0} \right)^2 = 0.011 \pm 0.003 \text{ s}^{-1}. \quad (1)$$

This strength is just the slope of the phase variance versus time relation that would be found if the generating period P_0 were known.

In a random walk of this strength, the phase of the oscillation changes by 90° on the average every 25 ± 7 pulses!

As noted before, however, the full variability implied by this strength of random walk is not seen directly in the data because the "true" period of the oscillation is unknown. Typically, solving for the period reduces the variance by a factor of ~ 12 here, which makes the pulsation seem more coherent. Our artificial data allow us to estimate the period variation caused by the random walk. For time intervals similar to OB1 and 5, the period uncertainty is ~ 0.05 s; for OB2, 3 and 4 it is ~ 0.03 s. These period uncertainties are ~ 10 times larger than the formally derived uncertainties in the periods for each orbit, and are shown as the dotted error bars in Figure 8b.

We can now understand the erratic period shifts shown in Figure 8 as due to the random walk. Furthermore, any possible long term period change can now be meaningfully determined. Using the period uncertainties given by the random walk and the best-fit periods for each OB, we find the following: 1) a fit to a constant period gives $P = 8.811$ s and $\chi^2 = 13.2$ with 4 degrees of freedom, with a probability of 0.01 that this is a good fit; 2) a fit to P and \dot{P} yields $P = (8.906 \pm 0.031)$ s - $(8.9 \pm 2.6) \times 10^{-6} t$ (single parameter 1σ errors), where t is measured from the beginning of OB1 and $\chi^2 = 1.2$ with 3 degrees of freedom. An F test confirms that \dot{P} is significant at the 99.0% confidence level. The result of the latter fit is shown in Figure 8b as a solid line; 3) a fit to a constant period $P = 8.88$ s for OB1-2 and a different constant period $P = 8.76$ s for OB3-5 yields $\chi^2 = 1.3$ with 3 degrees of freedom; thus this interpretation cannot be ruled out.

If a random walk in period were also present, the phase variance found using the true period would equal $St + S't^3$. A firm upper limit to S' can be obtained by requiring that the contribution of the term in S' be less than the contribution of the term in S to the last point in Figure 9. This gives $S' < 10^{-8} \text{ s}^{-3}$. (If $S' = 10^{-8} \text{ s}^{-3}$, σ_{int} would be $\sim 300^\circ$ for time intervals of 300 periods; this is much greater than our point estimates from OB2, 3, and 4.)

IV. DISCUSSION

a) General

The discovery of a 9 s pulsation in the soft X-rays from SS Cygni confirms the general expectation that high energy pulsations are the ultimate source of the optical pulsations observed during outbursts of dwarf novae (Bath 1973; Warner and Brickhill 1978; Paczyński 1978). It is interesting that the origin of the pulsation is in soft X-rays, rather than hard X-rays. (In fact, hard X-rays were observed simultaneously during this pointing but no short period was detected at the 10% level; Swank 1979.) Although the X-ray pulsed fraction was expected to be larger than the optical pulsed fraction, the large pulsation amplitude actually observed is perhaps surprising. The direct implication is that the pulsation cannot be merely a small perturbation of the X-ray source; it is instead an intrinsic part of the X-ray production mechanism.

The large pulsation amplitude also makes the near absence of harmonics in the pulse profile all the more surprising. Although the

sinusoidal nature of the optical pulsations from dwarf novae had been emphasized before, Papaloizou and Pringle (1978) have pointed out that optical harmonics would be suppressed by the strong optical flickering and perhaps by smoothing if the optical light is reflected off the disk. Neither of these mechanisms affects the X-ray pulse profile. Thus this almost featureless pulse profile may constrain models for the pulsation.

Because of the high energies required to produce soft X-rays and the shortness of the pulsation period, it is probable that these X-ray observations probe the region near the compact star's surface. We can calculate a characteristic area of X-ray emission from the observed flux if we assume that the source emits a blackbody spectrum:

$$A = \frac{L}{\sigma T^4} \approx 2 \times 10^{15} \left(\frac{d}{200 \text{ pc}} \right)^2 \left(\frac{30 \text{ eV}}{kT} \right)^4 \text{ cm}^2. \quad (2)$$

The radiating area is much smaller than the area of a white dwarf surface ($\sim 3 \times 10^{18} \text{ cm}^2$).

We can model the source area in two ways. If the X-rays come from a hot spot in the disk with $A = 2\pi R^2$, similar to the model proposed by Bath (1973),

$$R \approx 2 \times 10^7 \left(\frac{d}{200 \text{ pc}} \right) \left(\frac{30 \text{ eV}}{kT} \right)^2 \text{ cm}. \quad (3)$$

We can then set an upper limit on the temperature of the remaining part of the ring of the disk containing the spot by demanding that this ring contribute less X-ray luminosity ($E > 0.15 \text{ keV}$) than the spot. This

implies $T < 1/2 T_{\text{spot}}$, assuming thermal emission. Thus, in this model, the spot has a temperature enhancement by at least a factor of two.

Alternatively, a radiating ring close to the degenerate star of area $2 \times 2\pi R_{\text{WD}} \Delta R$ must have

$$\Delta R \approx 3 \times 10^5 \left(\frac{d}{200 \text{ pc}} \right)^2 \left(\frac{30 \text{ eV}}{kT} \right)^4 \left(\frac{5 \times 10^8 \text{ cm}}{R_{\text{WD}}} \right) \text{ cm}. \quad (4)$$

This is about the thickness calculated for an optically thick boundary layer where the accreting disk material settles on the white dwarf surface (Pringle 1977).

We summarize below the characteristics of the X-ray pulsation:

- (1) The pulsation is strong only during optical outbursts.
- (2) The period is 9 s, and $\dot{P} \sim -1 \times 10^{-5} \text{ s s}^{-1}$.
- (3) The phase apparently random walks, with $Q \sim 25$.
- (4) The pulse profile is closely sinusoidal and of large amplitude (mean amplitude $\sim 30\%$, but individual pulsed fractions vary from 0 to 100%).
- (5) The pulsation comes from a region of typical size 1-100 km with a temperature of $\sim 30 \text{ eV}$ and a total luminosity of $\sim 10^{33} \text{ erg s}^{-1}$.

Optical pulsations sharing some of the above properties (1, 2, and 4) but with a much smaller amplitude have been observed in about twenty CV systems (Patterson, Robinson, and Nather 1977; Warner and Brickhill 1978, and references in both). In fact, optical oscillations have been detected in SS Cyg itself during two different outbursts (neither of which correspond to the outburst reported here). Patterson, Robinson,

and Kiplinger (1979) recently reported a period of 9.76 s for SS Cyg. The pulsation amplitude was 0.02% when the system was at $V = 8^m.5$. For a different SS Cyg outburst, Horne and Gomer (1979) measured a pulsation period of 8.5 s and an amplitude $\sim 0.05\%$ for the system at $8^m.2$. Several days later, when the visual brightness had decreased to $9^m.6$, Patterson (1979) measured a pulsation period of 10.6 s and an amplitude of $\sim 0.1\%$. Upper limits (90% confidence) to the optical pulsation amplitude during the 1978 June outburst reported here are 0.05% for June 12.4 U.T. (Stiening and Hildebrand 1978), and 0.1% for June 14.3 U.T. from our own observations.

Our estimates of the X-ray flux and pulsed fraction yield an upper limit to the optical pulsation amplitude that could be due to reprocessed X-ray pulsation. The soft X-ray flux listed in Table 1 is the flux at the Earth in the energy band 0.13-0.48 keV; when corrected for absorption and extrapolated over all frequencies, the total flux is $\sim 4.5 \times 10^{-10} \text{ erg cm}^{-2} \text{ s}^{-1}$, of which $\sim 30\%$ is pulsed. The ratio, then, of the flux in the high-energy pulsed component to the observed optical flux in the band 3400-6000 Å is $\sim 1\text{-}2\%$. This is a comfortable order of magnitude greater than the maximum reported optical pulsation amplitude.

The direct contribution of the pulsed 30 eV blackbody spectrum to visible light is $\sim 3 \times 10^{-13} \text{ erg cm}^{-2} \text{ s}^{-1}$ (3400-6000 Å). We estimate from the optical observations quoted above that the maximum energy in the visual pulsation is $\sim 1\text{-}2 \times 10^{-12} \text{ erg cm}^{-2} \text{ s}^{-1}$. Thus we cannot yet definitely rule out the possibility that the X-ray and optical pulsation merely come from different portions of the same $\sim 30 \text{ eV}$ spectrum. A

clear test of this would be either multicolor optical pulsation observations throughout the outburst and/or simultaneous X-ray/optical pulsation observations.

A possible correlation between the pulsation period and optical luminosity has emerged from the optical observations of a few dwarf novae in outbursts: near the beginning of the outburst the optical pulsation period decreases until it reaches a minimum at, or just after, the peak visual brightness (e.g., Patterson, Robinson, and Nather 1977). Then the period may increase throughout the decline to visual minimum. The X-ray period of SS Cyg is observed to decrease at peak visual light, yet the X-ray intensity may also be steadily decreasing. More observations are required to investigate any period/X-ray brightness correlation.

The most striking characteristic of the X-ray pulsations is their simultaneous phase incoherence and period stability. Superimposed on the long term period drift is a random walk in phase. That is, the pulsation does not remember where its phase should be on any timescale, yet it knows very well what its period should be. This property and the fact that 9 s is approximately the Keplerian period of matter orbiting near the surface of a $1 M_{\odot}$ white dwarf give strong evidence that the X-ray pulsation period is connected to that Keplerian period. The phase incoherence may then be connected to the growth and decay times of disturbances in the orbiting matter.

Before considering possible models for the pulsation, we note that Robinson and Nather (1979) have proposed that there are two distinct types of pulsation seen in cataclysmic variables: "coherent"

oscillations claimed to have phase coherence but otherwise having the properties discussed above, and "quasi-periodic" oscillations with phase incoherence, longer periods, a broad range of simultaneously excited periods, and no evidence of long term period stability. Obviously, the observed phase incoherence of the X-rays from SS Cyg, which otherwise fall into the "coherent" pulsation class, force a reanalysis of the basis of the classification. (Note how Figure 8 of Patterson, Robinson, and Nather 1977, which shows how the variance of the quasi-periodic oscillation in the dwarf nova RU Peg grows in time, resembles our Figure 9.) While two classes of pulsation may still exist, our analysis points to the need for quantitative observational estimates of the degree of coherence of all the observed periodicities in cataclysmic variables.

b) Previous Models for the Pulsations

The instability of the X-ray pulsations excludes a magnetic rotator model. A critique of the hypothesis of nonradial g-modes in a slowly rotating star as the origin of the optical pulsations is given in Papaloizou and Pringle (1978, hereafter PAP); the arguments against the g-mode theory can be applied to the X-ray pulsations as well.

PAP have investigated the modes of a rotating pulsing star and find that either toroidal "r" modes concentrated in the white dwarf surface layer, or g-modes modified to originate in a rotating surface layer, may produce the observed optical pulsations. The periods of these modes are of order $1/m$ times the rotation period of the outer

layers of the white dwarf (m is the azimuthal wave number). For this theory to be able to produce the large amplitude X-ray pulsations, m must be small.

There are several difficulties with the model of PAP. For the predicted periods to fit the observations, the rotation rate of the surface layers of nearly all white dwarfs must be about the same, i.e., roughly twice the pulsed period (or ~ 20 -60 s). There is no direct observational evidence to support this hypothesis (or, of course, to reject it). On the other hand, since the pulsation periods are approximately the same as the Keplerian periods in the inner accretion disk (Bath 1973), we believe that this timescale, and not the rotation period of the white dwarf, provides the "clock" for the pulsation.

It is also hard to believe that pulsation from the outer layers of the white dwarf could have the necessary instability in phase that is required. In addition, the model of PAP deals specifically with the surface layer of the white dwarf. In a continuously accreting system most of the energy is liberated in the outer portion of the boundary layer; this interface between the white dwarf and the disc is likely to have highly variable properties.

c) The Nature and Origin of the X-ray Oscillations

For the dwarf novae, it is apparent that many features of the pulsations, such as their transience and their systematic changes in period, are related to the phase of the outburst. It may be that the change in the mass accretion rate is critical in the evolution of the pulsations.

We identify the boundary layer, the region of retarded velocity between the rapidly rotating inner accretion disk and the more slowly rotating white dwarf surface, as the source of the pulsation. Most of the accretion energy will be dissipated where the velocity gradient is largest, i.e., in the outer portion of the boundary layer. The temperature of the X-ray source measured for SS Cyg (3×10^5 K) is approximately that predicted for a heated, optically thick boundary layer (Pringle 1977). The pulsation mechanism in the boundary layer must depend on the stability and properties of the mass flow. The mechanism must produce almost sinusoidal pulsations whose amplitude and phase can suffer sudden, and apparently random, changes.

In the theory of boundary layers of the type usually considered in fluid mechanics, there exist instabilities which have the above properties (e.g., see the reviews by Morkovin 1958 and Roshko 1976). The theory is complicated, owing to the nonlinear processes it attempts to describe, and only very simple laboratory experiments have been attempted to demonstrate the existence of these instabilities (Schlichting 1968; Greenspan 1968). The instabilities can manifest themselves as sinusoidal oscillations whose coherence is a function of the shear flow parameters. Although the boundary layers considered in these references are quite different from the one we consider, we merely wish to point out that such instabilities are not unprecedented.

There are many ways in which the boundary layer could give rise to pulsed X-rays, which can be broadly classified into nonradial and radial instabilities. Consider first the nonradial instabilities.

One type of instability which has been discussed in relation to cataclysmic variables is the Kelvin-Helmholtz instability. PAP point out that the interaction at the boundary layer may allow a nonlinear cycle of a quasi-coherent nature. Alternatively, weak, oblique shocks in the boundary layer may produce the X-rays (Pringle and Savonije 1978). The shocks probably have lifetimes of only a few pulses or less, and hence can easily give phase incoherence. Finally, the presence of the boundary layer gives rise to a region where the angular velocity of material rotating in the disk/boundary layer reaches a maximum. It is possible that an unstable density wave trapped in this region produces the X-ray pulsation. The dispersive properties of this wave may then account for the phase instability. These waves might even be the agent allowing matter to accrete onto the white dwarf.

Radial pulsation models in the disk are also viable because the radial pulsation periods are close to the Keplerian periods at the outer edge of the boundary layer (Novikov and Thorne 1973). A variation in the boundary layer thickness, in either the radial or the axial direction or both, would necessarily affect the X-ray production. If, for example either the stellar rotation axis or a stellar magnetic field axis were not aligned with the orbital angular momentum vector, a periodic radial push would be applied to the rotating matter. Alternatively, the boundary layer may itself be unstable to radial perturbations.

The development of these and other models will require much further theoretical work which we will not pursue here. However, we emphasize that if the pulsations are tied to the Keplerian period of matter rotating near the white dwarf surface, as we propose, the pulsation period alone measures M_{WD}/R_{WD}^3 , independent of the usual geometric unknowns (such as the inclination of the binary system). Thus a theory which can compute how the observed pulsation period depends on the white dwarf mass is of fundamental importance. Such a theory will be necessary to derive actual estimates of the white dwarf mass because of the range of periods present in the boundary layer. As an illustration, if the observed X-ray pulsation period gives an upper limit to the Keplerian period at the white dwarf surface, we find a mass for SS Cyg in excess of $0.9 M_{\odot}$, using white dwarf models given in Schwarzschild (1958). This speculative lower limit is consistent with previous mass estimates quoted in Robinson (1976).

In conclusion, none of the existing models for the optical pulsations correctly explains the X-ray oscillation behavior. We believe that the pulsations arise from an as yet unspecified instability in the boundary layer. The fact that this instability only occurs for dwarf novae in outburst, yet is observed to occur sporadically in other subclasses of cataclysmics that are in nonflaring states, indicates that a critical flow must be reached before these instabilities may occur. If this is true, we expect that the coherence, amplitude, and pulse shape of the oscillations should also depend on the accretion flow parameters.

In support of this hypothesis, we also offer as evidence the detection of large-amplitude X-ray pulsations of a quasi-periodic nature in U Geminorum on the decline from maximum ($P \sim 20\text{--}30$ s; Córdova et al. 1979). Preliminary analysis suggests that the main difference between U Gem and SS Cyg is that the random walk is stronger in U Gem or, equivalently, a broader range of periods is simultaneously excited.

V. IMPLICATIONS FOR FUTURE OBSERVATIONS

It has proven difficult to develop theories of dwarf novae because of the many unknowns of the mass accretion process. Hence observations must play a fundamental role in guiding theory. Our results point to the need for the following observations of dwarf novae:

- (1) The soft X-ray light curve must be sampled over the entire outburst, especially near the beginning.
- (2) Other systems must be observed in X-rays to investigate the effects of the orbital inclination, M_{WD} , and accretion rate.
- (3) More sensitive detectors must be employed to better define how sinusoidal the pulses are, and to test if the X-ray spectrum changes during the pulse.
- (4) The coherence properties of all the observed pulsations (optical as well as X-ray) must be quantitatively investigated.
- (5) Optical observations must investigate the wavelength dependence of the pulsation amplitude in order to test whether the optical

pulsation is the tail of the X-ray pulsation spectrum or whether it is reprocessed X-ray radiation. Simultaneous X-ray/optical observations could not only decide this question, but may also constrain disk parameters if the optical pulsation is due to reprocessed X-ray radiation (Chester 1979).

Hopefully, the new insights gained from the X-ray observations will stimulate the development of theories that can fruitfully interact with observations. While it would be satisfying just to understand how the X-ray pulsation is produced, successful theories may allow the fundamental parameters of these interesting systems to be better defined.

TABLE 1

SS CYGNI BEST-FIT SPECTRAL PARAMETERS

Model	Energy (keV)	Flux (erg cm ⁻² s ⁻¹)	T (10 ⁵ K)	N _H (10 ²⁰ cm ⁻²)	χ^2_{ν} (23 d.o.f.)
Blackbody	0.13-0.48	$\sim 4.5 \times 10^{-11}$	3.5	1.0	1.4
Thermal Brem.	0.13-0.48	$\sim 4.5 \times 10^{-11}$	4.7	1.4	1.4

REFERENCES

- Bath, G. T. 1973, Nature Phys. Sci., 246, 84.
- Bath, G. T. 1976, in P. Eggleton et al., IAU Symposium No. 73, Structure and Evolution of Close Binary Systems (Dordrecht: Reidel), p. 173.
- Bath, G. T. 1978, Q.J.R.A.S., 19, 442.
- Brown, R. L., and Gould, R. J. 1970, Phys. Rev. D., 1, 2252.
- Chester, T. J. 1979, Ap. J., 230, in press (May 15, 1979).
- Córdova, F. A. 1979, Ph.D. thesis (Caltech).
- Córdova, F. A., et al. 1979, in preparation.
- Davidson, A. F., Henry, R. C., Snyder, W. A., Friedman, H., Fritz, G., Naranan, S., Schulman, S., and Yentis, D. 1977, Ap. J., 215, 541.
- Fabbiano, G., Gursky, H., Schwartz, D. A., Schwarz, J., Bradt, H. V., and Doxsey, R. E. 1978, Nature, 275, 721.
- Greenspan, H. P. 1968, The Theory of Rotating Fluids, (London, New York: Cambridge University Press).
- Hearn, D. R., Richardson, J. A., and Li, F. K. 1976, Bull. A.A.S., 8, 447.
- Heise, J., Mewe, R., Brinkman, A. C., Gronenschild, E. H. B. M., den Boggende, A. J. F., Schrijver, J., Parsignault, D. R., and Grindlay, J. E. 1978, Astr. and Ap., 63, L1.
- Horne, K., and Gomer, R. 1979, private communication.
- Kellogg, E., Baldwin, J. R., and Koch, D. 1975, Ap. J., 199, 299.

- Lampton, M., Margon, B., and Bowyer, S. 1976, Ap. J., 208, 177.
- Margon, B., Szkody, P., Bowyer, S., Lampton, M., and Paresce, F.
1978, Ap. J., 224, 167.
- Mason, K. O., Córdova, F. A., and Swank, J. H. 1978, Proc. of the
COSPAR Symposium, Innsbruck, Austria, June 1978.
- Morkovin, M. V. 1958, ASME, 80, 1121.
- Novikov, I., and Thorne, K. S. 1973, in Black Holes, Les Houches, ed.
C. De Witt and B. S. de Witt (New York: Gordon and Breach), p. 344.
- Paczyński, B. 1978, in Nonstationary Evolution of Close Binaries, ed.
A. Zytkow (Warsaw: Polish Scientific Publishers).
- Papaloizou, J., and Pringle, J. E. 1978, M.N.R.A.S., 182, 423.
- Patterson, J. 1979, private communication.
- Patterson, J., Robinson, E. L., and Kiplinger, A. L. 1978, Ap. J.
(Letters), 226, L137.
- Patterson, J., Robinson, E. L., and Nather, R. E. 1977, Ap. J., 214,
144.
- Pringle, J. E. 1977, M.N.R.A.S., 178, 195.
- Pringle, J. E., and Savonije, G. J. 1978, preprint.
- Rappaport, S., Cash, W., Doxsey, R., McClintock, J., and Moore, G.
1974, Ap. J. (Letters), 187, L5.
- Ricketts, M. J., King, A. R., and Raine, D. J. 1979, M.N.R.A.S., 186,
233.
- Robinson, E. L. 1973, Ap. J., 183, 193.
_____. 1976, Ann. Rev. Astr. Ap., 14, 119.
- Robinson, E. L., and Nather, R. E. 1979, Ap. J. Suppl., 39, no. 4.
- Roskho, A. 1976, AIAA J., 14, 1349.

- Rothschild, R., Boldt, E., Holt, S., Serlemitsos, P., Garmire, G.,
Agrawal, P., Riegler, G., Bowyer, S., and Lampton, M. 1979,
Space Sci. Inst., in press.
- Schlichting, H. 1968, Boundary Layer Theory, (New York: McGraw-
Hill).
- Schwarzschild, M. 1958, Structure and Evolution of the Stars (New
York: Dover).
- Stiening, R. F., and Hildebrand, R. 1978, private communication.
- Swank, J. H. 1979, private communication.
- Walker, M. F., and Chincarini, G. 1968, Ap. J., 154, 157.
- Warner, B. 1976, in P. Eggleton et al., IAU Symposium No. 73,
Structure and Evolution of Close Binary Systems (Dordrecht:
Reidel), p. 85.
- Warner, B., and Brickhill, A. J. 1978, M.N.R.A.S., 182, 777.

FIGURE CAPTIONS

Figure 1. A portion of the X-ray data with 1.28 s binning, showing the 9 s pulsations. The dotted line marks the background level. The inset shows the AAVSO visual light curve of SS Cygni for the 1978 June outburst.

Figure 2. The aspect-corrected soft X-ray light curve for the entire SS Cygni pointing. Each point is a ~ 40 s average corrected for background by subtracting the different detector fields of view. Dropouts are due to earth occultation. The satellite orbits are designated OB1, 2, etc. for future reference. Satellite drift motion results in larger uncertainties for the intensities during the first values of OB1, 2, 3, and 4 and the last half of OB5; this is illustrated in the figure by the unequal error bars below OB2.

Figure 3. The SS Cygni observed spectrum (crosses) and the best-fit blackbody model (solid line), which represents a kT of 30 eV and an N_H of $1 \times 10^{20} \text{ cm}^{-2}$. The inset shows the 90% confidence χ^2 contours for both a blackbody and a thermal bremsstrahlung fit.

Figure 4. Power spectra for OB2 and OB4. The inset in (b) shows the superposition of pulses from OB4 and OB5, with all pulses aligned at their peak. The solid line through the pulse profile is the best-fit sinusoid.

Figure 5. A phase diagram for a portion of the X-ray data illustrating the phase wanderings and large apparent changes in the pulsation

amplitude. Each trace is a fold of 128 s of data at a period of 8.76 s. There is a 50% overlap between traces.

Figure 6. a) The pulsed amplitude for every set of 4 consecutive pulse periods, in units of the average count rate from SS Cygni for each orbit, plotted versus a reference time near the beginning of each spacecraft orbit. Counting statistics introduces a noise amplitude of ~ 0.14 . b) The time delay (or phase) of each arrival time relative to a constant period plotted versus time in the same way as in (a). Only points that are significant at the 99% level are shown. The periods used were 8.893, 8.876, 8.785, 8.757, and 8.745 s respectively. Positive residuals imply tardy pulses.

Figure 7. The amplitude distribution for each pulse. Note the x-axis scale change at a pulsed fraction of 100%. a) The pulsed fraction is here defined as the ratio of the pulsed amplitude for each pulse to the mean intensity for the entire OB containing that pulse. All 1166 pulses are displayed. b) The pulsed fraction is here defined as the ratio of the pulsed amplitude for each pulse to the mean intensity determined during each pulse. The 4% of all pulses with mean intensities less than \sim half the mean intensity for each OB are excluded because of the large uncertainty in their pulsed fraction.

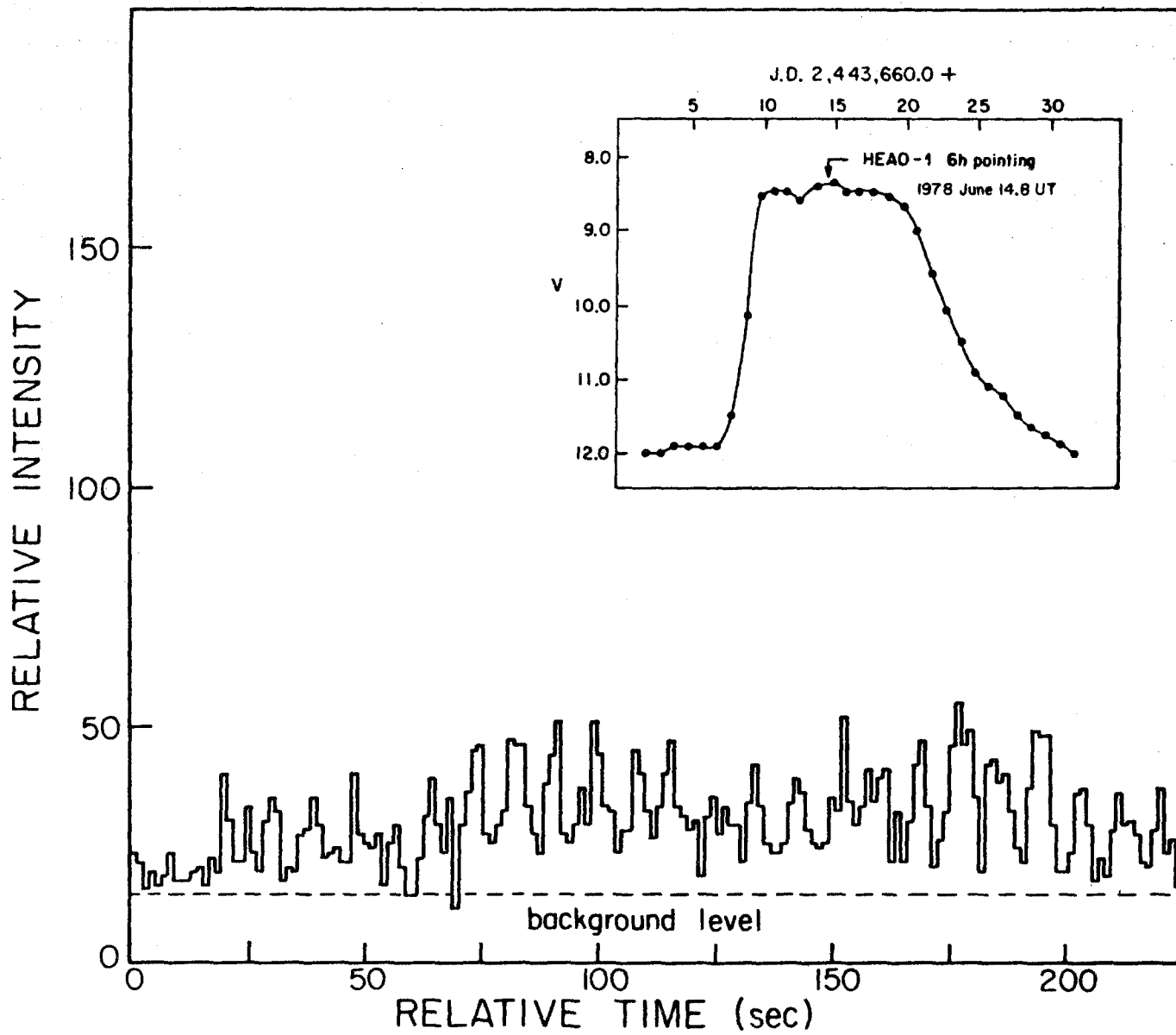
Figure 8. a) The period of the oscillation plotted as a function of time as determined from short sections of the data. b) The period for each orbit plotted as a function of time. The solid error

bars give the formal errors, and the dotted error bars give errors derived from artificial data assuming a random walk.

Figure 9. The mean intrinsic variance derived from all sets of arrival times spanning n periods plotted versus n .

Figure 10. The time delay relative to a constant period of every fourth artificial pulse arrival time plotted versus time for $P_0 = 8.77$ s and $P_1 = 0.44$ s (see text). Uncertainties were taken from Figure 6b. The periods found were 8.82, 8.71, 8.76, 8.78, and 8.79 s respectively.

Figure 1



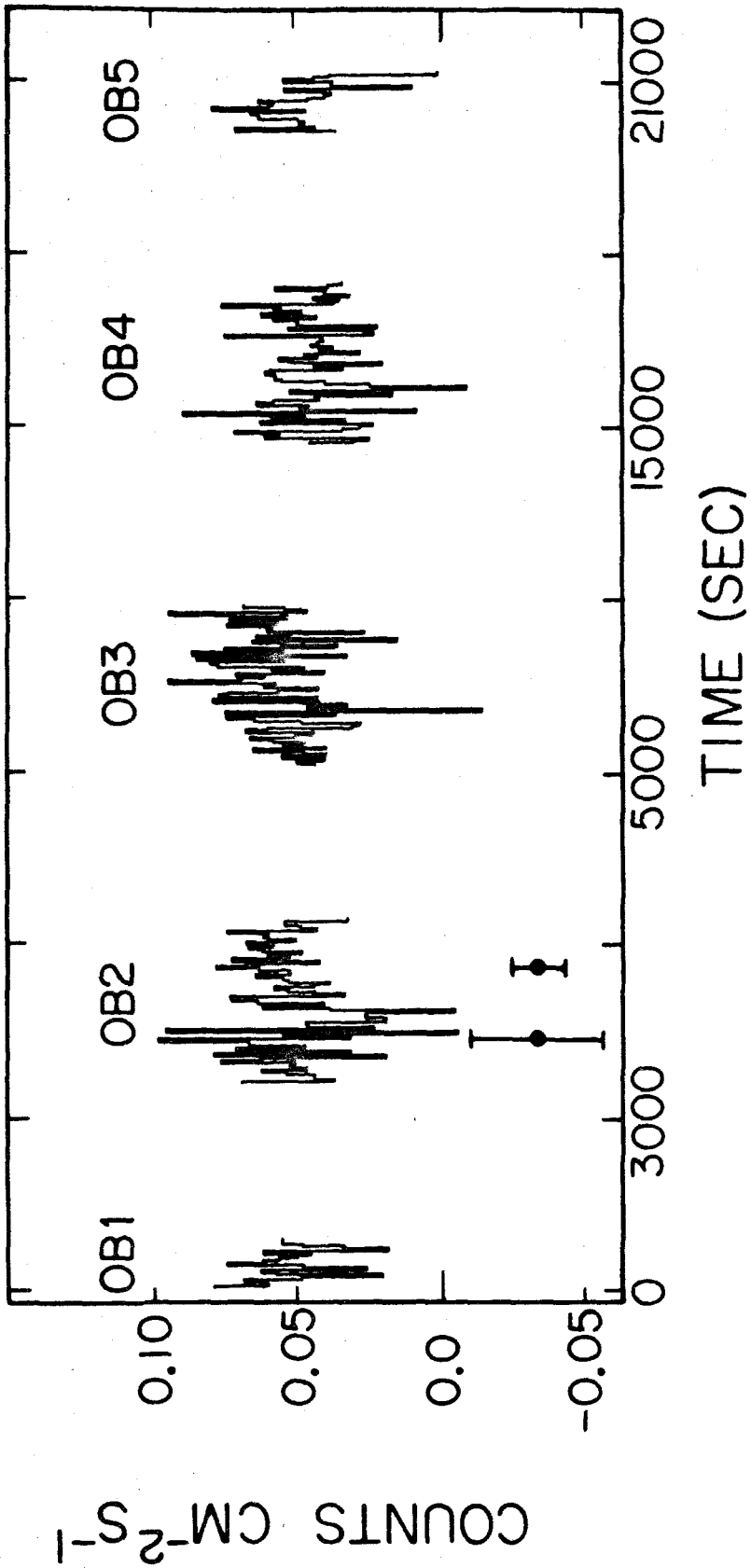


Figure 2

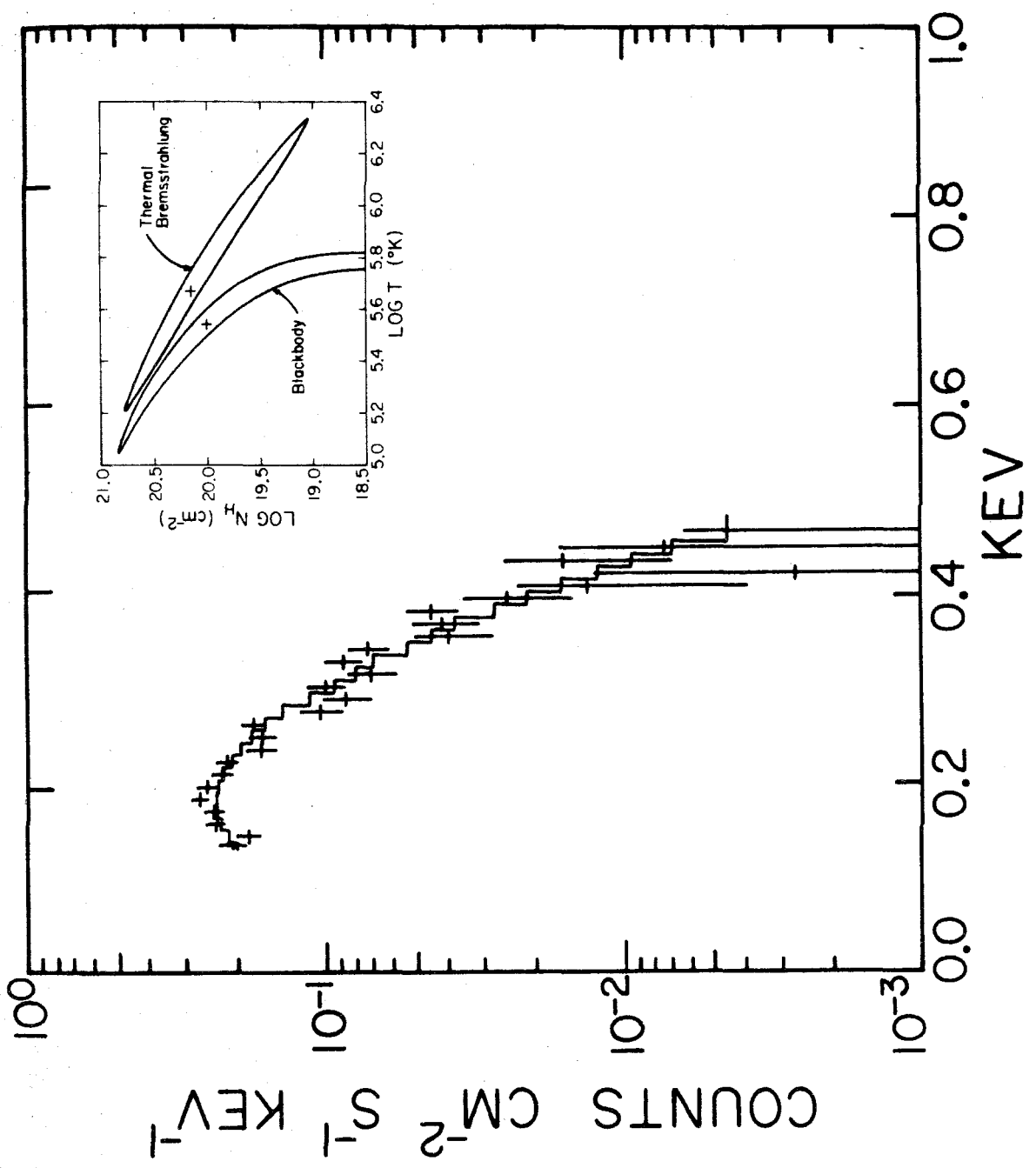


Figure 3

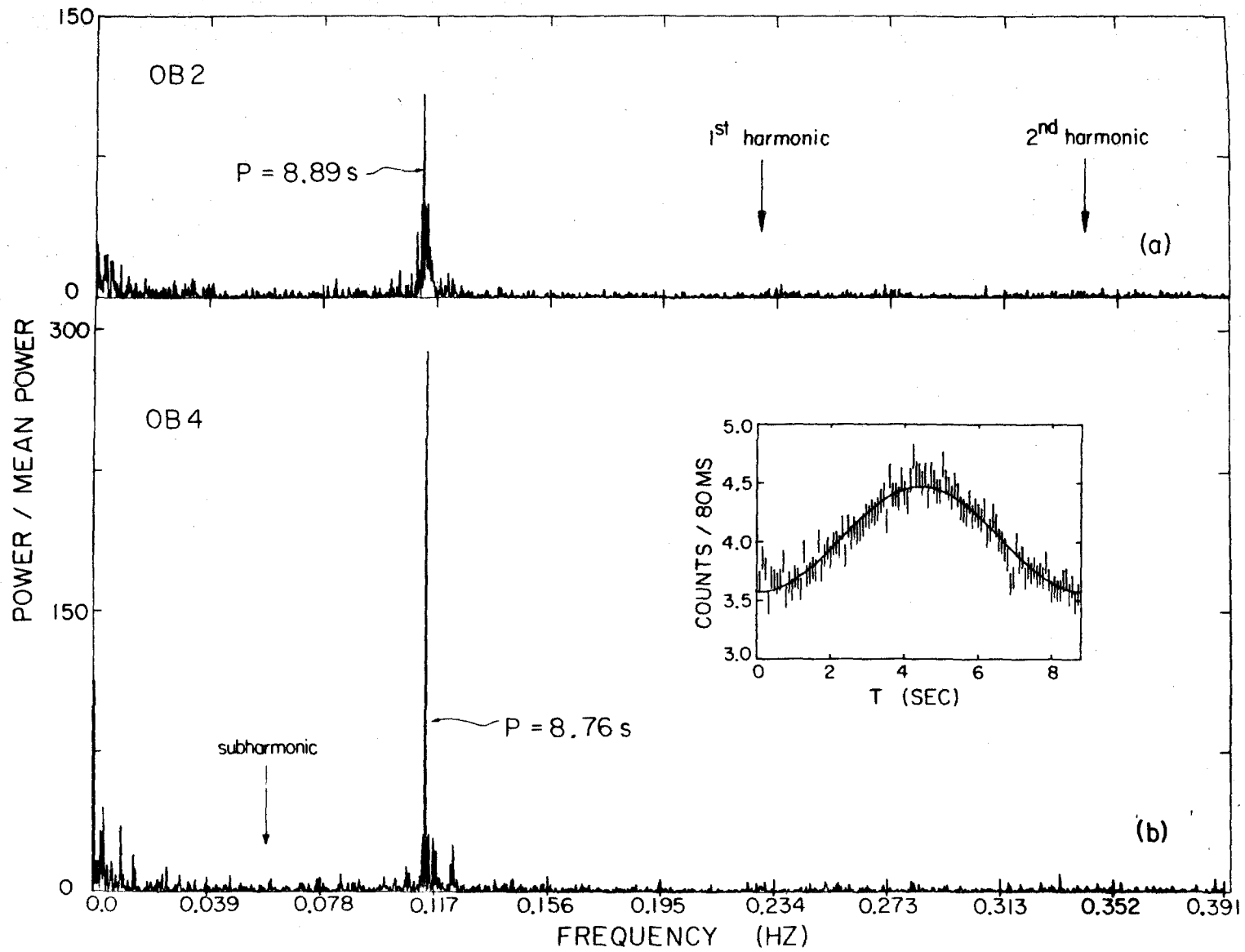


Figure 4

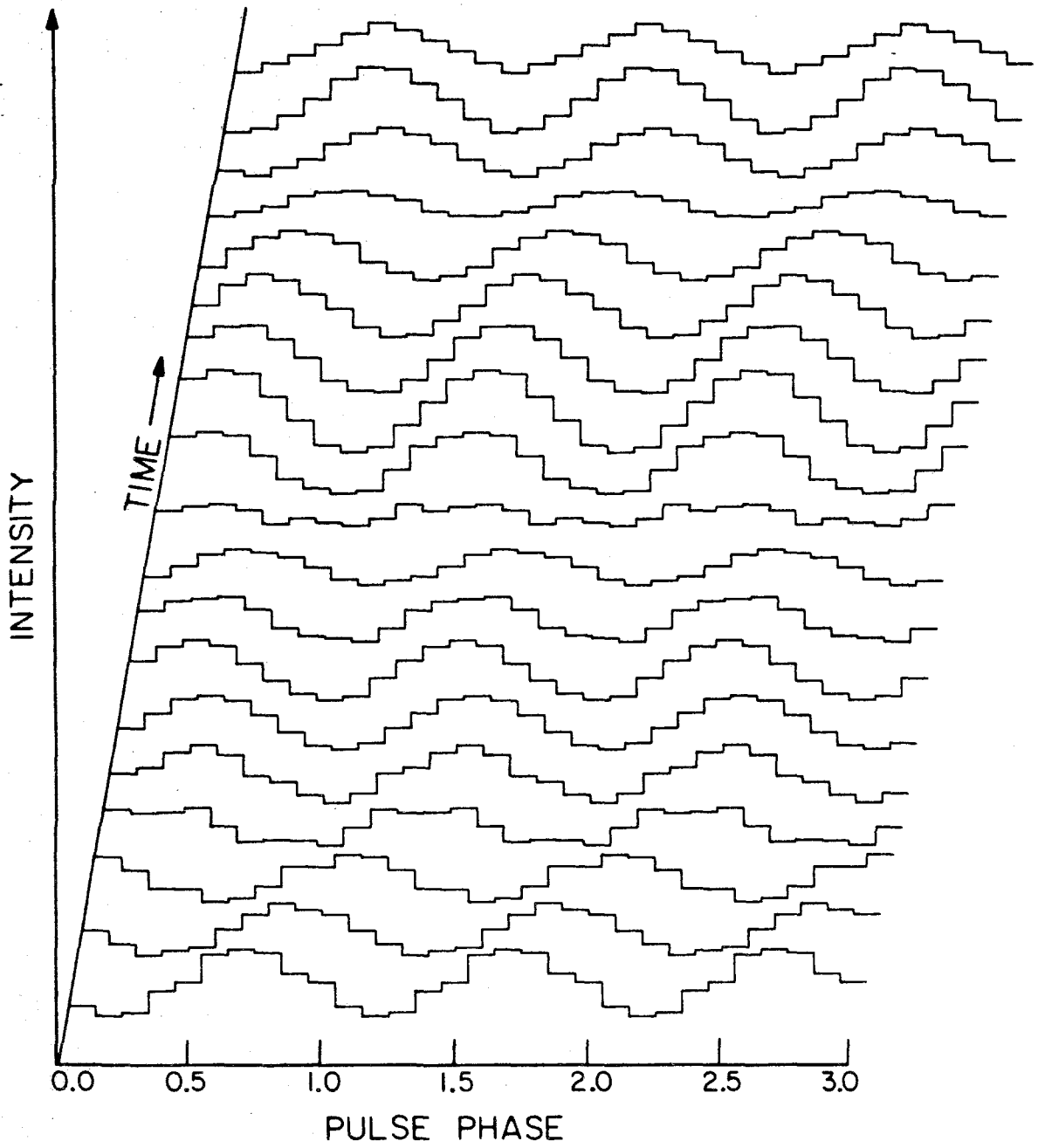


Figure 5

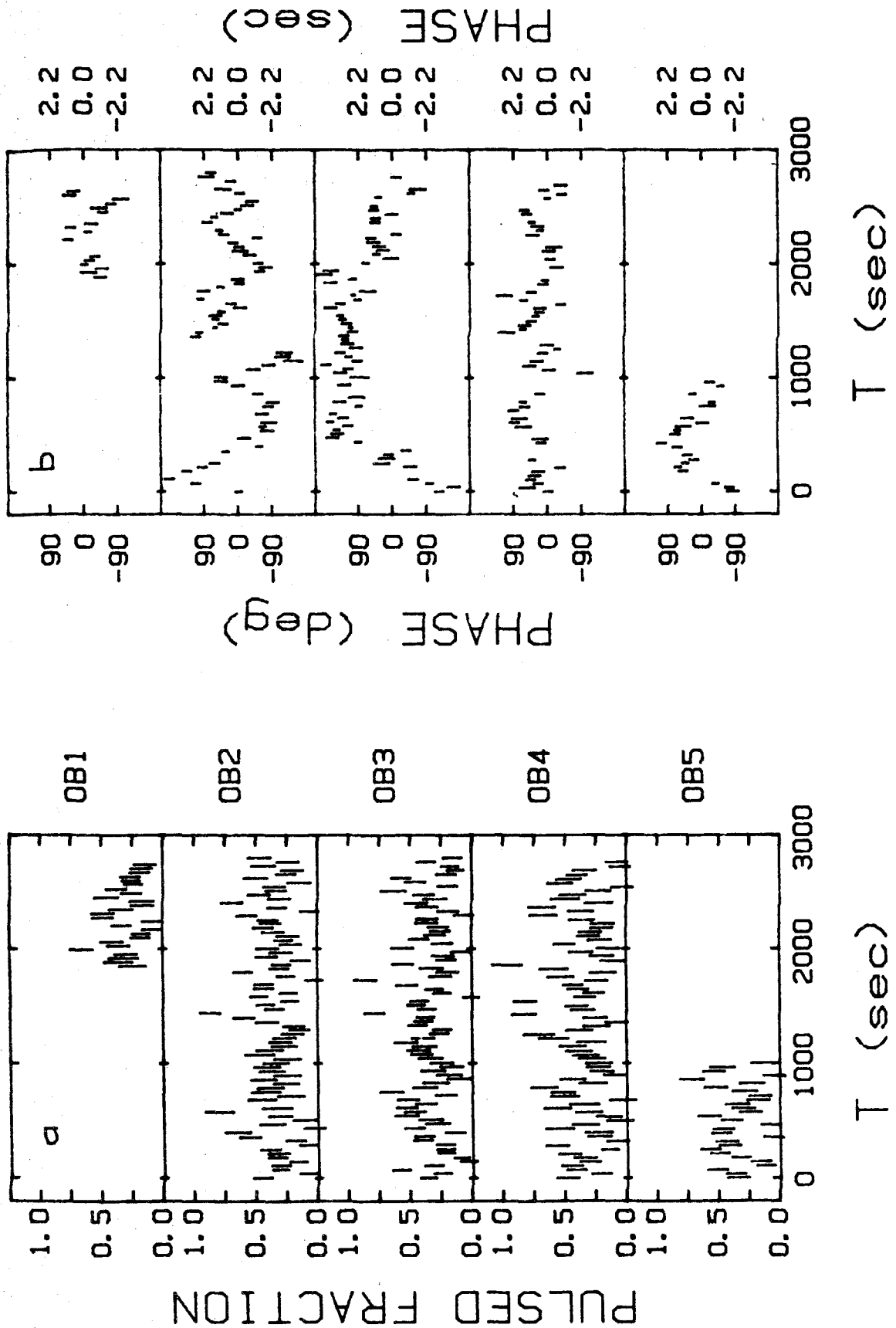


Figure 6

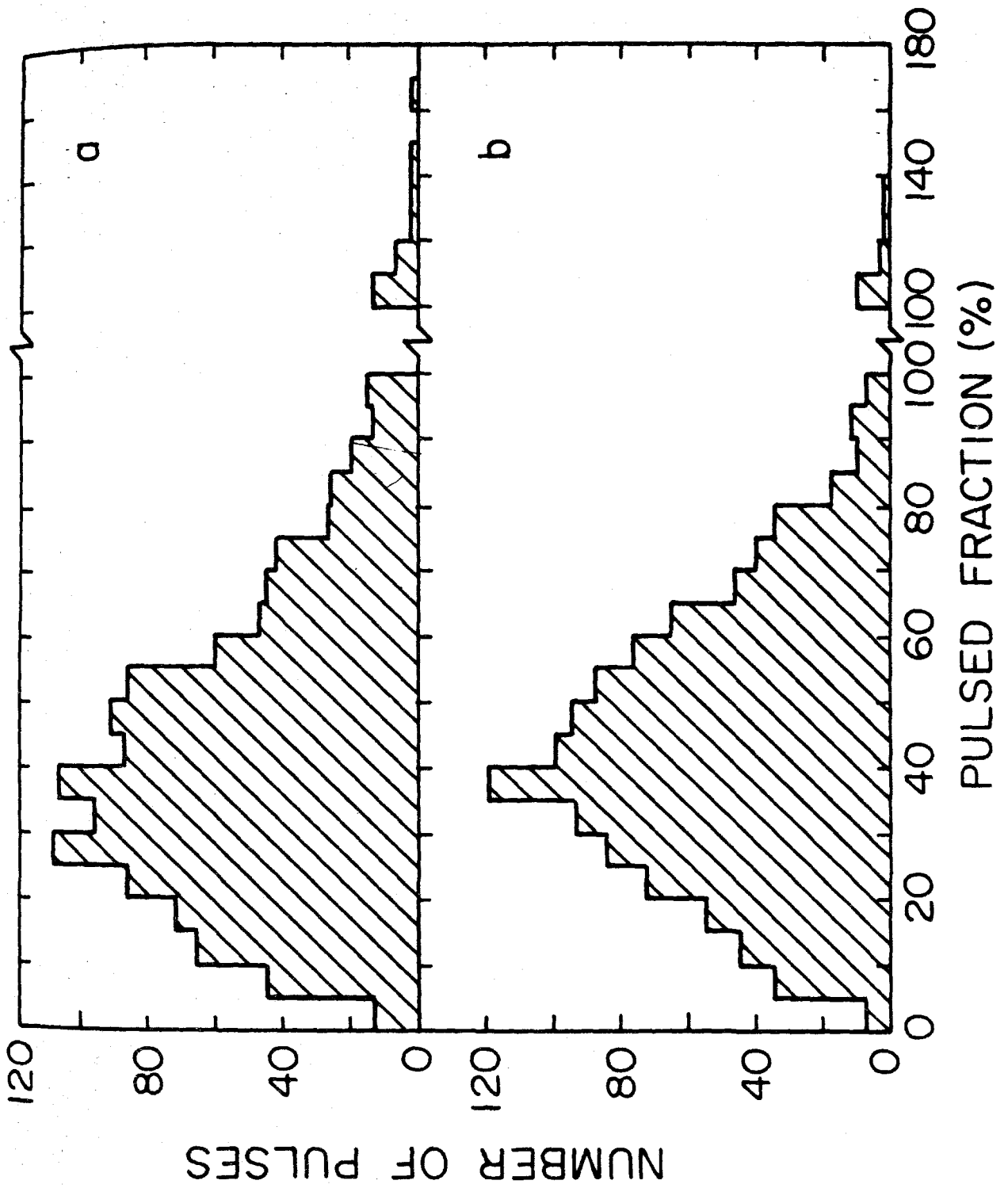


Figure 7

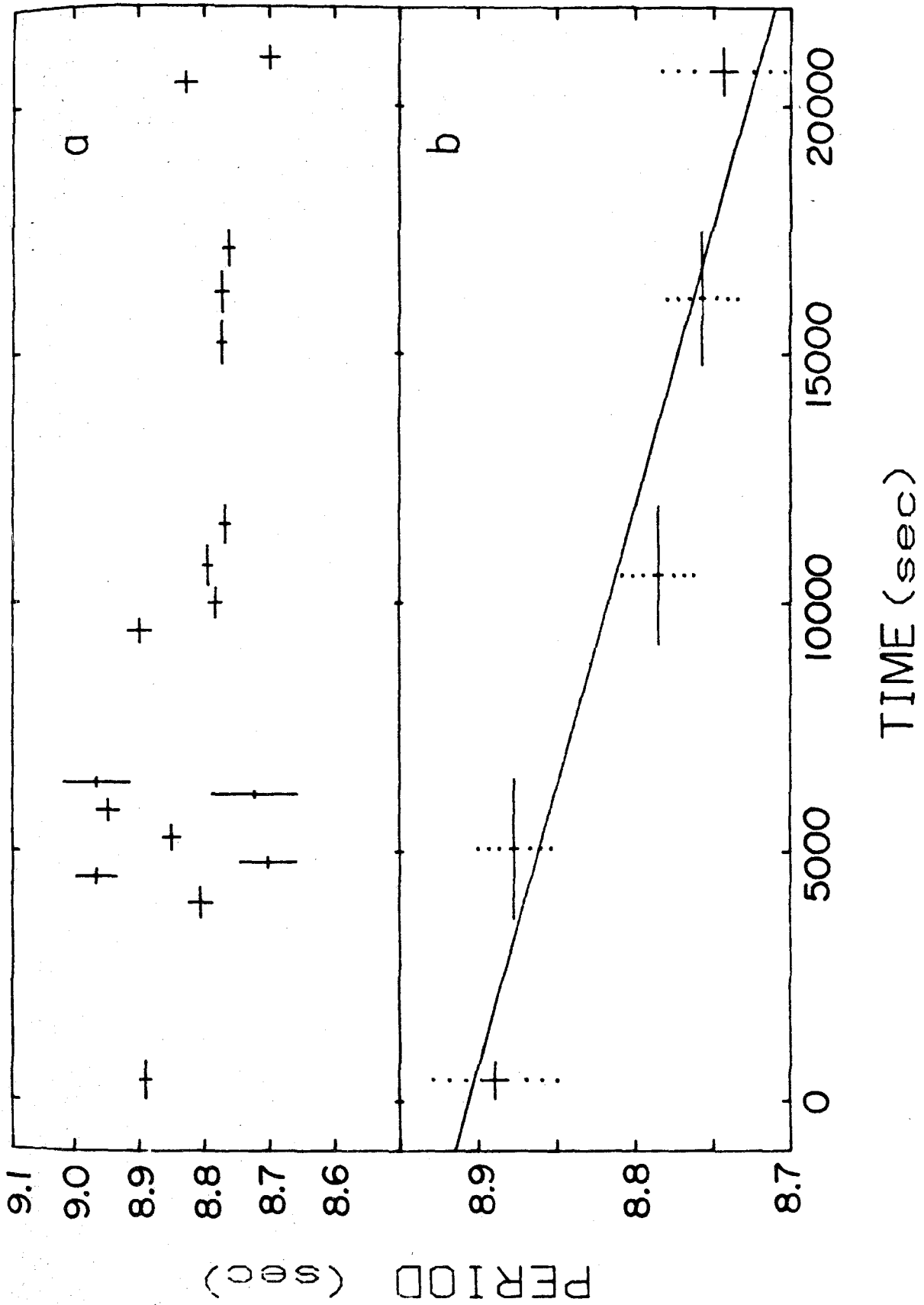


Figure 8

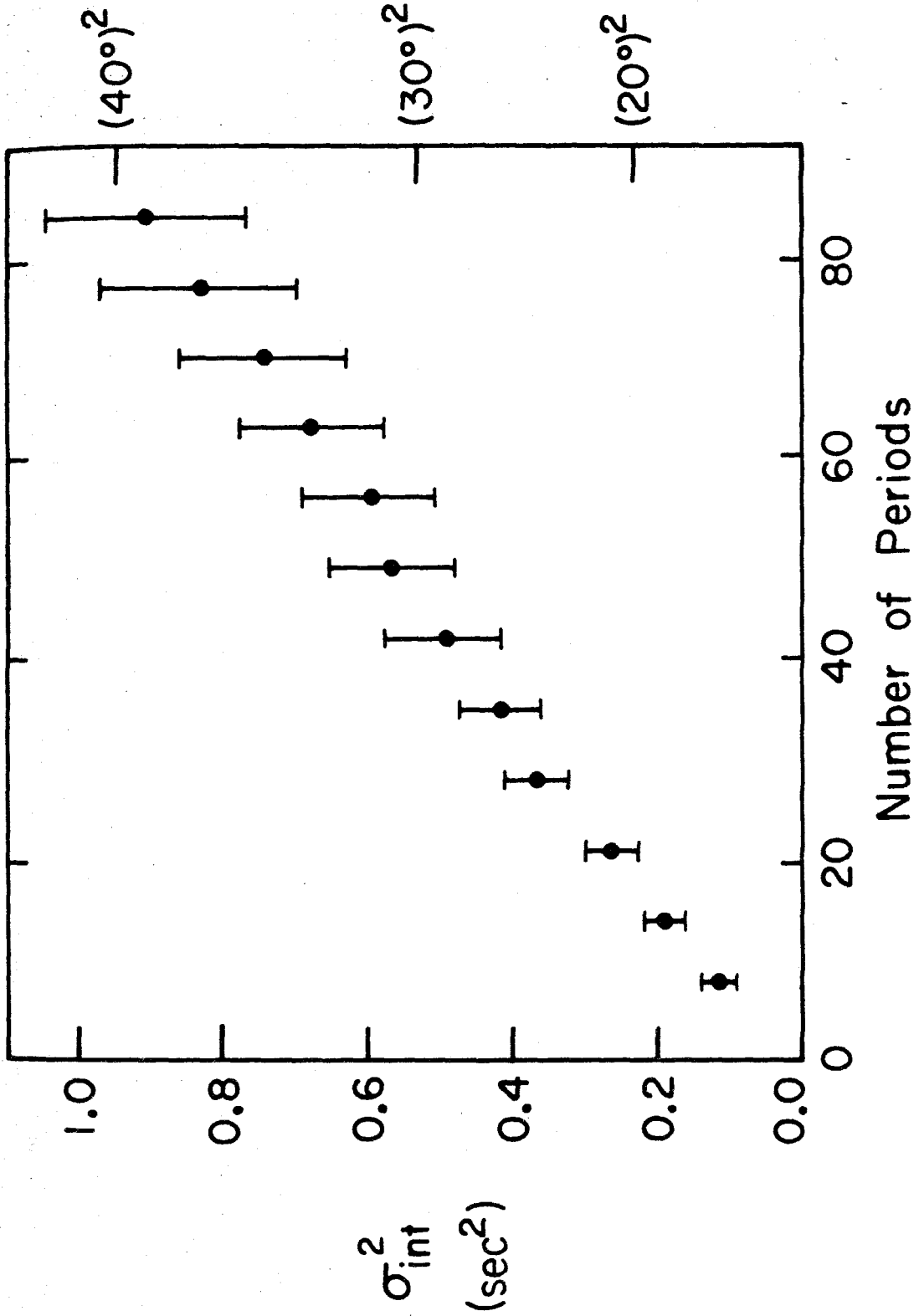


Figure 9

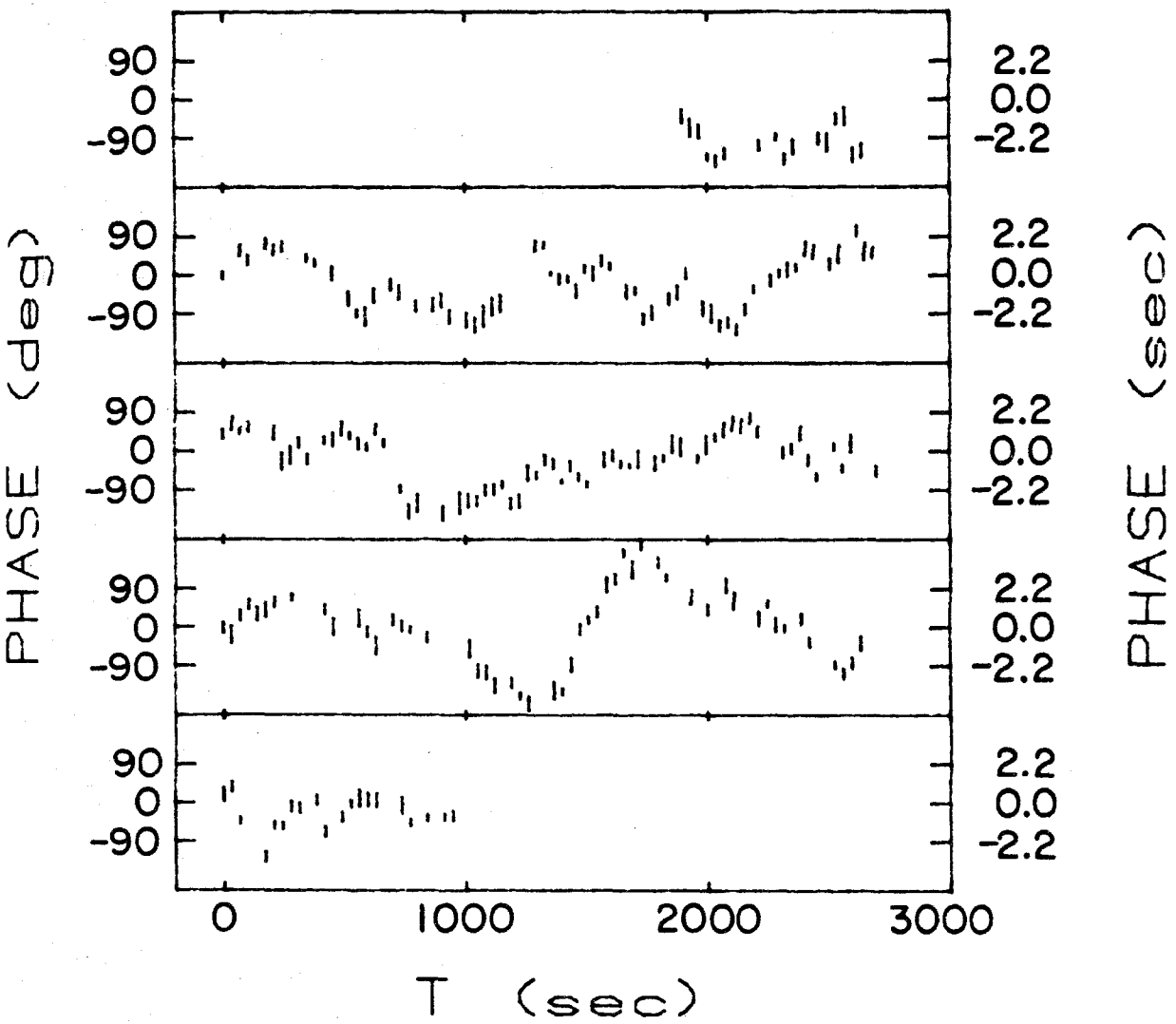


Figure 10

PAPER 2:

THE QUASI-PERIODIC SOFT X-RAY OSCILLATION IN U GEMINORUM

in preparation with

T.J.Chester and G.P.Garmire

I. INTRODUCTION

U Geminorum is the prototype for a class of close binary systems which undergo frequent, relatively low-amplitude visual eruptions. These objects are designated "dwarf" novae to distinguish them from the historical and recurrent novae that have rare and much more luminous outbursts (see the reviews by Robinson 1976 and Warner 1976). Every ~ 100 days U Gem brightens by 4-6 magnitudes from an apparent magnitude $V \sim 14.3^m$. The rise to peak brightness occurs in less than a day; the star thereafter slowly declines to its preoutburst level over several days.

During such an outburst in 1977 October both soft and hard X-ray components in U Gem were first detected with the HEAO-1 satellite (Mason et al. 1978; Swank et al. 1978). The observations were made while the satellite was in a scanning mode, thus precluding a search for fast time variability. During a subsequent outburst one year later, HEAO-1 was pointed continuously at U Gem for 10 h. A large-amplitude quasi-periodic oscillation was detected with a period centering on 25 s.

This is the second dwarf nova found to be a soft X-ray pulsator during outburst. The detection of a 9 s pulsation from SS Cygni confirmed that the origin of the low-amplitude visual pulsations seen in numerous dwarf novae during outburst is a soft X-ray/EUV source (Córdova et al. 1979; hereafter, Paper I). Although a search has been made for visual pulsations from U Gem, none has yet been detected (Patterson 1979).

In §II of this paper we give the details of the HEAO-1 pointing at U Gem; we present the soft X-ray light curve, the energy spectrum, and the characteristics of the pulsation. In §III we describe a new method for analyzing a pulsation whose phase random walks, and we apply this technique to the X-ray pulsation in U Gem and SS Cyg. In §IV we show from artificially generated data that the pulsation behavior in both SS Cyg and U Gem can be duplicated by varying only the strength of the random walk. Our simulation reproduces many other properties associated with the optical pulsations in dwarf novae such as the absence of harmonics and the simultaneous presence of multiple periodicities. Finally, in §V we discuss the implications of our analysis.

II. THE OBSERVATIONS

HEAO-1 was pointed at U Gem for 10 h commencing at 09:30 UT on 1978 October 16, about two days after the peak of an optical outburst. A short, representative portion of the soft X-ray light curve is displayed in Figure 1; the X-rays are highly modulated with a period of about 25 s. The inset to the figure is the AAVSO visual light curve for the eruption.

a) The Instrumentation

The data described here were taken with the low-energy detector LED1 of the HEAO-A2 experiment which is described in detail by Rothschild et al. (1979). LED1 is a collimated gas proportional

counter with sensitivity between 0.1 and 3 keV. A special collimator design, whereby sources were viewed with two coaligned fields of view having different solid angles, made it possible to subtract the X-ray sky background; the fields of view were $1.5 \times 3^\circ$ and $3^\circ \times 3^\circ$.

Aspect information acquired from an on-board star camera was used to correct the source intensity for spacecraft pointing wandering. We use the nominal value of 380 cm^2 for the LED1 effective geometrical area.

b) The Soft X-ray Light Curve

The background-subtracted, aspect-corrected soft X-ray light curve covering the entire U Gem pointing is illustrated in Figure 2. A differencing technique making use of the unequal fields of view reveals that the source is present only at energies less than 0.5 keV. The 10 h observation contained 7 satellite orbits of ~ 90 min each. The dropouts in the data are due to Earth occultations of the source. In the figure the satellite orbits are designated OB1, 2, etc. for later reference. The data comprising Figure 2 were output from scalers which count the X-ray events occurring in consecutive 1.28 s intervals. Each data point in the figure is an average over 32 such intervals.

With the nominal detector high-voltage setting, discriminators at the input of the scalers used for this analysis accept only events within the energy interval 0.18-0.43 keV. Increasing the high-voltage by a fixed amount changes this bandpass to 0.13-0.28 keV, thus extending the detector sensitivity to lower energies. Figure 2 shows the data for both the nominal voltage setting (a) and the higher voltage setting (b). The count rate is much higher in the 0.13-0.28 keV band, suggesting that the source spectrum is relatively unabsorbed (see §IIc).

Two striking features are apparent in the X-ray light curve. 1) There is no obvious correlation of the X-ray intensity with binary phase. The observation spanned 2.5 binary orbits, including the eclipse. 2) There is a slow decline in intensity in the 0.18-0.43 keV band from OB1 through OB5, yet there is an increase in intensity in the 0.11-0.28 keV band from OB5 through OB7.

The variations in the light curve may be interpreted as due to (a) a decrease in the area of the emitting region over the first half of the observation (OB1-5), followed by an increase in the area for the remainder of the observation, or (b) a cooling of the source for the first half of the observation, with a subsequent heating after OB5, or (c) a combination of a monotonic change in the source area coupled with a monotonic change in the source temperature.

In addition to the scaler data, we also have pulse-height data with finer energy resolution. Using these data we will be able to compute a hardness ratio for the entire observation and thus, hopefully,

understand how the source is behaving over the whole observation; this analysis is in progress.

The first two interpretations that we gave for the shape of the light curve required a reversal in the source behavior during, or following, OB5. It will be shown in §III that the pulsation period also apparently changes near the time of OB5. Unfortunately, with the limited data available, it is not possible to determine whether the change in period is correlated with the hypothesized reversal, or is merely a coincidence.

c) The Spectrum

For the pulse-height analysis we used data taken with the higher voltage setting to increase our sensitivity to a possible low-energy spectral turnover. In Figure 3 we show the observed countrate spectrum and the best-fit blackbody model, which had a temperature $kT = 25$ eV and a column density $N_H \leq 5 \times 10^{18} \text{ cm}^{-2}$. In the inset to Figure 3 we display the 90% confidence χ^2 contours for fits to both a blackbody spectrum and a thermal bremsstrahlung spectrum (i.e., exponential plus Gaunt factor), assuming Brown and Gould (1970) cross-sections for interstellar absorption. The limits on the source temperature are:

$$5.04 < \text{Log } T < 5.47 \text{ (Blackbody)}$$

$$5.15 < \text{Log } T < 5.78 \text{ (Thermal Brem.)}$$

The detector is insensitive to a decrease in N_H below $\sim 5 \times 10^{18} \text{ cm}^{-2}$; thus both models are consistent with zero hydrogen column. The 90% confidence upper limit to N_H for both models is $2.5 \times 10^{20} \text{ cm}^{-2}$.

The flux at the Earth in the energy interval 0.13-0.48 keV is $3.4 \times 10^{-10} \text{ erg cm}^{-2} \text{ s}^{-1}$, assuming the best-fit spectral parameters from either model. Using the best-fit blackbody parameters, we calculate a luminosity at the source, integrated over all frequencies, of $1.9 \times 10^{33} \times (d/100 \text{ pc})^2 \text{ erg s}^{-1}$. The value of 100 pc was chosen because it is consistent both with the low N_{H} value from the X-ray observation, and with the distance of $76 \left(\pm \begin{smallmatrix} 36 \\ 24 \end{smallmatrix} \right) \text{ pc}$ calculated by Wade (1979), using optical spectrophotometry. For comparison, the luminosity derived in Paper I for SS Cyg using the above procedure was $\sim 1.8 \times 10^{33} \times (d/200 \text{ pc})^2 \text{ erg s}^{-1}$. The best-fit (blackbody) parameters for SS Cyg were $kT = 30 \text{ eV}$ and $N_{\text{H}} = 1 \times 10^{20} \text{ cm}^{-2}$.

For the spectral fitting we used only data from OB7. The other OBs were taken in an unusual telemetry format which had 20 ms direct pulse-height readouts; the analysis of these data is in progress. Therefore, at this time we cannot remark on whether the spectrum depends on the phase of the pulsation.

d) The Pulsations

A power spectrum from a discrete Fourier transform using 1.28 s binning is shown for OB5 in Figure 4a. This power spectrum is typical of the other sections as well. Note the chaotic distribution of power over many periods centered roughly near 25 s. The Fourier transforms of shorter sections of data often show sharp spikes at periods that differ for each section. Clearly, tremendous period variability is present.

Power spectra summed over OB1-5 and over OB6-7, displayed in Figure 4b and 4c, respectively, show more clearly the distribution of power. Note that the power in OB1-5 is centered on 25 s whereas the power in OB6-7 is centered on 29 s. It is difficult to set an upper limit to harmonics of the signal using the power spectra. The method described in §III is a more sensitive way of deriving such limits.

Due to the large range of periods present, any attempt to fit more than a few pulse cycles with a sinusoid must fail. However, individual pulses can be fit fairly well by a constant plus a sinusoid of period 25 s. The distribution of χ^2 values obtained from such a fit resembles a χ^2 distribution with 21 degrees of freedom instead of a χ^2 distribution with the actual 17 degrees of freedom in the fit. That is, a constant plus a sinusoid accounts for most, but not all, of the variance in the data. This result remains true even if the period of each pulse is allowed to be different.

This slight increase in the χ^2 distribution is precisely that found for SS Cyg when a constant plus a sinusoid is fit to more than a few consecutive pulses. For SS Cyg, with its weaker phase noise, an acceptable χ^2 distribution is obtained by fitting sets of one or two pulses. For U Gem, an acceptable χ^2 distribution can be obtained only by fitting a fraction of a pulse at a time. In other words, the phase noise is so strong in U Gem that it significantly affects individual pulses.

Nevertheless, since a sinusoidal fit to individual pulses accounts for most of the variance in the data, the amplitude and arrival time of each pulse are meaningful quantities, and are shown in Figure 5.

We have plotted only those phases significant at the 99.0% level to eliminate spurious phases from our set. The periods used to plot the phases are the best-fit periods for each OB found in §III (see Fig. 7b).

Note how similar both the amplitudes and phases are to the same quantities shown for SS Cyg in Paper I. The major differences are 1) the pulsed fraction for U Gem ranges between 0 and $\sim 40\%$ with a mean of 15%, whereas the pulsed fraction for SS Cyg ranges between 0 and $\sim 100\%$ with a mean of 30%; and 2) the phase variability is much greater for U Gem. There is about the same pulse to pulse variability in U Gem as there is between groups of ~ 20 pulses in SS Cyg.

With such strong phase variability, it is hopeless to try to phase the pulsation over an entire OB. For example, a plot of χ^2 versus period from such an attempt shows only erratic variation over the entire period range from ~ 15 s to ~ 35 s. However, on shorter time intervals of ~ 300 s, χ^2 shows a nice quadratic minimum at a period which is different for each such section of data. Thus we can test the time dependence of the variance of the phase for U Gem in the same manner as we tested for SS Cyg in Paper I, provided that we restrict the analysis to intervals no longer than ~ 300 s.

The result of this calculation is that the intrinsic variance of the phase of U Gem grows linearly with time just as it did for SS Cyg. The observed slope is $\sim (22^\circ)^2/\text{cycle}$ for U Gem versus $\sim (4.5^\circ)^2/\text{cycle}$ for SS Cyg. Thus the only apparent difference between the seemingly "chaotic" pulsation of U Gem and the much more "regular" pulsation of SS Cyg is the strength of the random walk in phase! This is an

important point, because superficially the X-ray pulsations from the two stars seem fundamentally different. We will come back to this point in §IV.

Finally, we have constructed artificial data sets as in Paper I in order to estimate the intrinsic slope of the variance increase versus time that would be found if the true period of the pulsation were known. Let successive arrival times be generated by $P_0 + P_1 x$, where x is a gaussian random variable of zero mean and unit standard deviation. For $P_0 = 25$ s, $P_1 = 5 \pm 1$ s reproduces the observed variance slope. Thus the intrinsic slope for U Gem is $\sim (70^\circ)^2/\text{cycle}$ versus $\sim (20^\circ)^2/\text{cycle}$ for SS Cyg.

We have not presented the above analysis in detail because it is identical to the procedure given in Paper I and because we have discovered a more powerful technique for analyzing the properties of the pulsation. We present this method in §III.

III. A NEW TECHNIQUE TO ANALYZE UNSTABLE PULSATIONS

Our previous methods allowed us to deduce that the phase of the X-ray pulsations from U Gem and SS Cyg seems to undergo a random walk. In order to deduce the intrinsic strength of the random walk, however, we had to first tediously analyze all possible continuous sets of arrival times to derive the observed variance increase with time, and then generate artificial data sets and analyze the artificial data sets in the same fashion. With this method, only the average strength of the random walk over the whole observation could be reliably deduced

because the method required a fairly large set of arrival times to give accurate results. Also, when the strength is large, it becomes impossible to derive the intrinsic variance of the data because it becomes impossible to phase the pulsation on other than short timescales.

We have discovered a much simpler, more powerful technique that lacks the above drawbacks. A pulse train with a phase that random walks can be represented by

$$f(t) = A \cos(\omega t + \phi_t), \quad (1)$$

where ϕ_t is the sum of normally distributed phase steps. We do not need to specify how often phase steps occur; we only require the well-known properties of a random walk variable that $\langle \phi_t \rangle = 0$ and $\langle \phi_t^2 \rangle \propto |t|$. If N such pulse trains are superposed such that their peaks at $t = 0$ coincide and the result is divided by N , the expectation of the resulting function is

$$F(t) = \langle A \cos(\omega t + \phi_t) \rangle, \quad (2)$$

where the average is over the random variable ϕ_t . A simple calculation gives

$$F(t) = A e^{-S|t|/2} \cos \omega t, \quad (3)$$

where $\langle \phi_t^2 \rangle$ has been replaced by $S|t|$, where S is defined as the strength of the random walk. Note that S is the intrinsic strength, not the observed strength found after fitting a period to the arrival times, and that ω is the intrinsic frequency of the pulsation. Also, all of the data can be included to a fit to $F(t)$, instead of just the arrival times

used in our previous method. The use of all of the data (instead of only the arrival times) allows better resolution in finding S.

We form $F(t)$ in the following way. We first derive t_i , the time of maximum for each pulse, as before. Then an estimate of $F(t)$ is formed by

$$F(t) = \frac{1}{N} \sum_{i=1}^N f(t - t_i), \quad (4)$$

where f is an observed continuous data train (for example, one of the OB sections) and N is now the number of pulses in the data train. Thus for every pulse in a given pulse train, the entire pulse train is superposed on itself, with every pulse acting once in turn as the center of the superposition. Since the superposition results from data which is binned, finite pulse trains can easily be taken into account by a normalization using the number of data points in each bin.

$F(t)$ is somewhat similar to an autocorrelation function (ACF), although there are the following important differences:

1. Unlike an ACF, there is almost no amplitude information in $F(t)$ other than the mean pulsation amplitude because every pulse in $f(t)$ appears in every pulse of $F(t)$. Thus $F(t)$ is virtually unaffected by any change in the amplitude of the pulsation (other than a secular change), or by any correlation between amplitudes. (A finite pulse train allows a small residual amplitude dependence due to end effects, which is negligible for large N .)

2. $F(t)$ is linear in $f(t)$ whereas an ACF is quadratic in $f(t)$. Thus $F(t)$ is much more sensitive to any harmonics present in $f(t)$. For example, if

$$f(t) = A \cos \omega(t + \phi_t) + A_2 \cos\{2\omega(t + \phi_t) + \psi\} \quad (5)$$

then

$$F(t) = A e^{-S|t|/2} \cos \omega t + A_2 e^{-2S|t|} \cos(2\omega t + \psi). \quad (6)$$

This was the method used in Paper I to derive the upper limits to harmonics of SS Cyg's pulsation; a similar analysis for U Gem is in progress.

3. $F(t)$ preserves the phase of harmonics whereas an ACF is an even function of t and hence discards phase information.

4. An ACF is contaminated by a white noise spike near $t = 0$ and by low frequency noise. While $F(t)$ is almost unaffected by these noise processes, white noise decreases the amplitude of the damped sinusoid because it shifts the observed arrival time t_i away from the true arrival time by some random amount σ_n . Thus $F(t)$ becomes

$$F(t) = A \langle \cos \omega \sigma_n \rangle e^{-S|t|/2} \cos \omega t. \quad (7)$$

Thus the measured amplitude includes an average attenuation due to errors in the pulse arrival times. Finally, the pulse centered on $t = 0$ has an increased amplitude because noise power always increases the amplitude of the pulse (since amplitudes are nonnegative). These

noise effects are important only when the noise pulsation amplitude (due to white noise) is comparable to the true pulsation amplitude.

We have applied this method to both SS Cyg and U Gem, and display fits to representative data sections in Figure 6. For SS Cyg, the fit to $F(t)$ is acceptable when the middle pulse is excluded from the fit, even though no account was taken of either the error in the data points due to systematic errors in the aspect determination or any error due to the finite number of pulses in the superposition. For U Gem, the middle pulse is included in the fit even though this systematically affects the derived amplitude and random walk strength by a small amount. This was done because the noise pulsation amplitude is smaller in comparison to the true pulsation amplitude for U Gem, and because the strong random walk of U Gem overpowers the noise pulsation amplitude even within the middle pulse. Also, because fewer pulses have been superposed for U Gem, the incomplete statistical averaging also increases the χ^2 of the fit. Figure 6 emphasizes that only the strength of the random walk is different between SS Cyg and U Gem.

We have fit all our data in a similar manner, and display the results in Figures 7a (for SS Cyg) and 7b (for U Gem). Together with the random walk strength (S) are also shown the average intensities in $\text{ct cm}^{-2} \text{ s}^{-1}$ (I), pulsed fractions (A), and periods (P) for each OB. The last three quantities were derived using the $F(t)$ method. For U Gem, the 1σ errors for each parameter have been obtained by searching the χ^2 surface for the number obtained by adding the value of the reduced χ^2 (~ 1.6 instead of 1.0) to the minimum χ^2 .

SS Cyg serves as a check on our procedures because we had previously determined in different ways most of the parameters shown in Figure 7 for SS Cyg. It is reassuring that the average random walk strength found for SS Cyg using the pulse train superposition method ($F(t)$) agrees with the strength deduced using our earlier method. The amplitudes and periods are also consistent with our previous determinations. Note that this period agreement implies that the periods found through $F(t)$ are not identical to the intrinsic periods of the oscillation when only a finite number of pulses are superposed because the statistical nature of the phase noise ensures variability in finite samples.

It is interesting to speculate on the existence of any trends in the derived quantities although our observations, which sample less than 10% of the total optical outburst, are not long enough to securely define any long term trends. With this in mind, the clearest trends apparent in Figure 7 are 1) the decline of the X-ray intensity for both stars; 2) the probable decrease of period for SS Cyg (P significant at the 99% confidence level: see Paper I); 3) the possible decline of the pulsed fraction in U Gem; 4) the possible increase of period for U Gem (which depends on the reality of change in only 2 points); and 5) the possible quadratic change for S for U Gem (again dependent on only a few points). Furthermore, for SS Cyg there may be a long term decrease in S and a trend of the pulsed fraction, but we have too few data points to tell.

Without any theory to place these results in perspective, one can only speculate on their significance. Observationally, however, it will be important to verify the existence of any such correlations in more extensive data sets.

IV. DISCUSSION

In Paper I we examined previous hypotheses for the origin of the optical pulsations observed in dwarf novae and found that these models could not account for the X-ray pulsation behavior in SS Cyg. The observation of U Gem discussed here strengthens the view we expressed in Paper I that the pulsation is due to a density wake or shocks in the turbulent shear flow near the white dwarf surface. The observed phase noise and amplitude strength and variability should provide important clues to the mechanism producing the pulsation.

To demonstrate in a simple way the characteristics of a pulsed signal subject to phase noise, we have generated artificial data sets showing what happens to a pulsation when the strength of the random walk is increased. Figure 8 shows three power spectra generated by

$$f(t) = 100 + 20 \cos(\omega t + \phi_t) + 20 \cos(2\omega(t + \phi_t)), \quad (8)$$

where ϕ_t is a step function which changes its value every cycle:

$$\phi_t = \phi_{t-P_0} + \frac{2\pi P_1}{P_0} x. \quad (9)$$

P_0 is the basic pulsation period, chosen to be 25s, P_1 is the standard deviation of P_0 , and x is a gaussian random variable of zero mean and unit standard deviation.

We have chosen values for P_1 equal to 1.5, 3, and 5 in Figure 8a, b, and c, respectively. Our artificial data set consisted of 256 pulses. The figure illustrates several important points:

1. A variation in the strength of the random walk can change the "coherent" pulsation of SS Cyg to the "incoherent" pulsation of U Gem. Figure 8a shows a strong pulsation at 25 s with a appearance similar to that for SS Cyg (Paper I). Figure 8c, on the other hand, shows only an enhancement in the power spectrum at periods clustering around 25 s, a profile similar to that for U Gem.
2. Harmonics will be even more strongly affected by phase noise than the fundamental is affected. In (c) the harmonic that showed up strongly in (a) has completely disappeared even though it has an amplitude equal to that of the fundamental! This could explain the absence of harmonics in the observed dwarf novae pulsations.
3. The phase noise produces random period shifts. In (a), where the phase noise was weak, the peak is 0.1 s away from the true pulse period. In (b) it is shifted by 0.2 s.
4. The random walk can produce multiple pseudo-periodicities (see the two spikes in Figure 8c).

Thus the behavior of the so-called "coherent" visual oscillations (Patterson, Robinson, and Nather 1977; Patterson, Robinson, and Kiplinger 1978) can be explained by intrinsic phase instability; these

pulsations resemble the X-ray pulsations in SS Cyg. The "quasi-coherent" visual oscillations observed for several dwarf novae on the decline from maximum brightness (Robinson and Nather 1977) have a behavior similar to the X-ray pulsation in U Gem. Figure 8 shows that the difference between the "coherent" and "quasi-coherent" pulsations may be only in the strength of the random walk in phase. It is possible that all of the optical and X-ray oscillations are produced by the same mechanism.

V. IMPLICATIONS

The observation that most of the soft X-rays in SS Cyg and U Gem are pulsed suggests that the production of soft X-rays is intimately tied to the pulsation mechanism. The actual detectability of the pulsation will be affected by obscuring material near the source, so that a failure to detect pulsation does not necessarily imply absence of pulsation. An X-ray scanning observation of U Gem during an outburst previous to the one reported here revealed a possible delay of one-half to one day in the turn-on of the soft X-rays (Mason et al. 1978). This delay, if real, might be due to either a belated involvement of the white dwarf in the outburst (e.g., after a critical mass accretion flow has been reached), or a transient obscuration of the pulsation emission region.

It is possible that for the X-ray/EUV pulsation the degree of phase noise is related to the amount of interaction between the white dwarf and the accretion disc. A more turbulent boundary layer implies a thicker boundary layer. If most of the X-rays are produced at the

outer edge of the boundary layer where the velocity gradient is the largest, we might expect to find a correlation between the phase noise and the pulsation period. X-ray and visual observations of the dwarf novae pulsations should be made throughout the entire outburst to look for a relationship between these parameters. A particularly interesting question which could be resolved through such observations is whether the strength of the random walk in phase is intrinsic to the individual dwarf nova or depends on the outburst phase. If the latter is true, the random walk strength may describe how much of the boundary layer is active in producing X-rays; this, in turn, would constrain models for the pulsation.

REFERENCES

- Brown, R. L., and Gould, R. J. 1970, Phys. Rev. D., 1, 2252.
- Córdova, F. A., Chester, T. J., Tuohy, I. R., and Garmire, G. P.
1979, submitted to Ap. J.
- Mason, K. O., Lampton, M., Charles, P., and Bowyer, S. 1978, Ap. J.
(Letters), 226, L129.
- Patterson, J. 1979, private communication.
- Patterson, J., Robinson, E. L., Kiplinger, A. L. 1978, Ap. J. (Letters),
226, L137.
- Patterson, J., Robinson, E. L., Nather, R. E. 1977, Ap. J., 214, 144.
- Robinson, E. L. 1976, Ann. Rev. Astr. Ap., 14, 119.
- Robinson, E. L., and Nather, R. E. 1979, Ap. J. Suppl., 39, No. 4.
- Rothschild, R., Boldt, E., Holt, S., Serlemitsos, P., Garmire, G.,
Agrawal, P., Riegler, G., Bowyer, S., and Lampton, M. 1979,
Space Sci. Instr., in press.
- Swank, J. H., Boldt, E. A., Holt, S. S., Rothschild, R., and Serlemitsos,
P. J. Ap. J. (Letters), 226, L133.
- Wade, R. A. 1979, A. J., in press.

FIGURE CAPTIONS

Figure 1. A portion of the soft X-ray light curve of U Gem showing the quasi-periodicity centered at ~ 25 s. The inset is the AAVSO visual light curve for the 1978 October outburst.

Figure 2. The X-ray light curve covering the entire HEAO-1 10 h pointing at U Gem. The data have been corrected for aspect and the X-ray sky background has been subtracted. Each data point is an average over 41 s. The dropouts are due to Earth occultations. Each satellite orbit (~ 90 min. duration) is labeled OB1, 2, etc. The high voltage on the detector anode was switched back and forth during the observation between two settings, resulting in different bandpasses for the low-energy scaler. The data in the figure have been separated according to this bandpass.

Figure 3. The observed energy spectrum for U Gem (crosses) and the best-fit blackbody spectrum (solid line), which has a $kT \approx 25$ eV and $N_H \lesssim 5 \times 10^{18} \text{ cm}^{-2}$. The inset shows the 90% confidence χ^2 contours for both blackbody and a thermal bremsstrahlung model fits.

Figure 4. Power spectra for U Gem resulting from discrete Fourier transforms of (a) a single satellite orbit (OB5), (b) OB1-5, and (c) OB6-7. For (b) and (c) the power spectra for the individual OBs were added together.

Figure 5. The amplitude (a) and arrival time (b) of individual U Gem pulses plotted versus a time referenced to the beginning of the observation. Only points that are significant at the 99% level

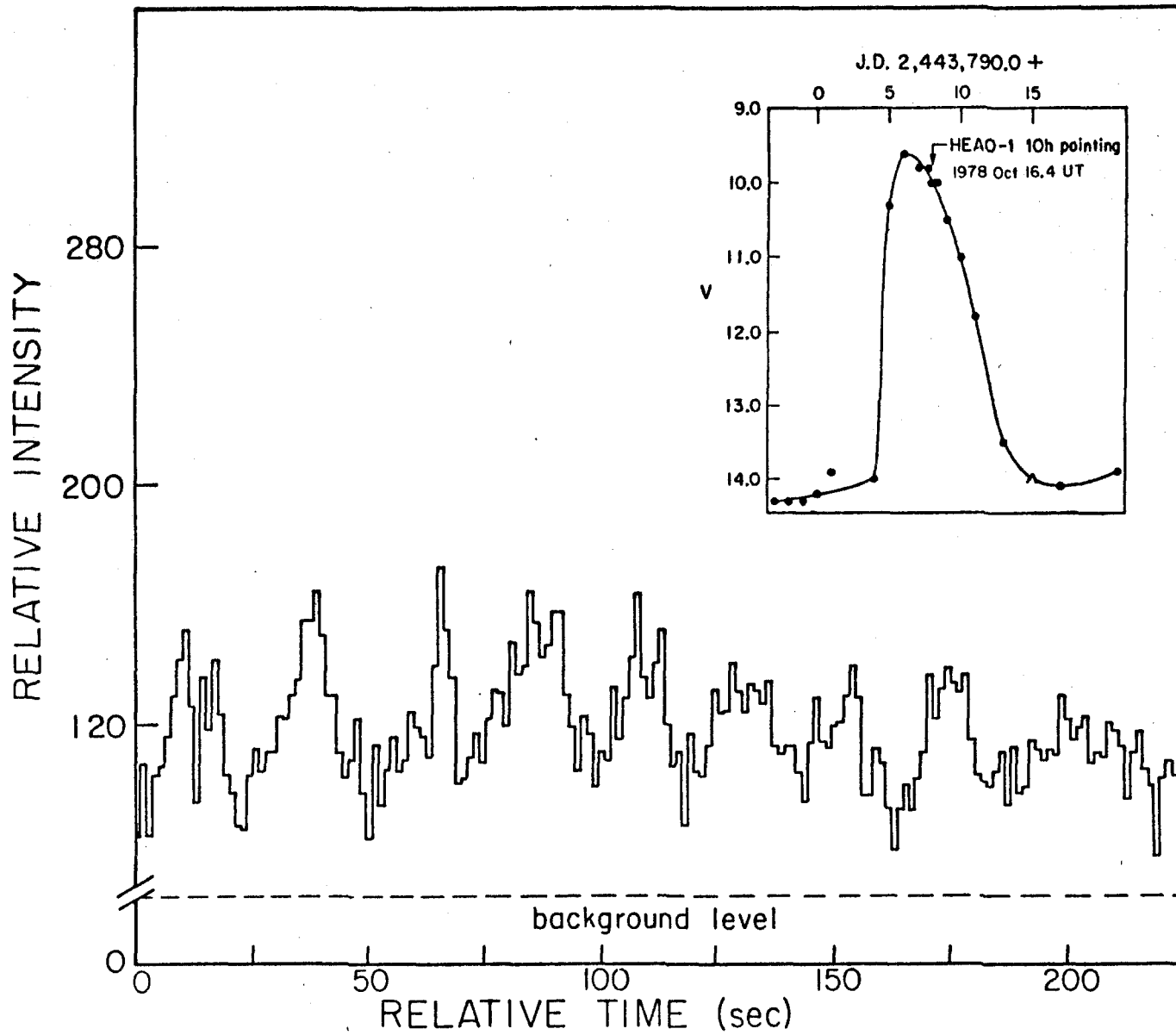
are shown. The periods that were used to plot the phases are given in the text.

Figure 6. The result of fitting a function of the form $F(t) = A e^{-S|t|/2} \cos \omega t$, where S is the strength of the random walk in phase, to the superposition of dwarf novae pulse trains. (a) The functional fit (solid line) to one orbit of SS Cyg data (bars), and (b) the residuals to the fit. (c) and (d) are similar to (a) and (b) but are for one orbit of U Gem data. The fits show that the strength of the random walk is much stronger in U Gem than in SS Cyg.

Figure 7. The X-ray intensity, pulsed fraction including white noise, period of the X-ray pulsation, and strength of the random walk in phase plotted versus time for (a) SS Cyg and (b) U Gem.

Figure 8. Power spectra generated from artificial data to show the effect on a sinusoid and an equal amplitude first harmonic of increasing the phase noise. In (a) the strength of the random walk is approximately the same as in SS Cyg, in (b) it is about four times greater, and in (c) it is more than eleven times greater than in (a). Figure 8c most nearly resembles the power spectra of U Gem (see Figure 4). Note how the first harmonic is washed out with an increase in phase noise. Also note the period shifts and multiple pseudo-periodicities that result from the random walk of the phase.

Figure 1



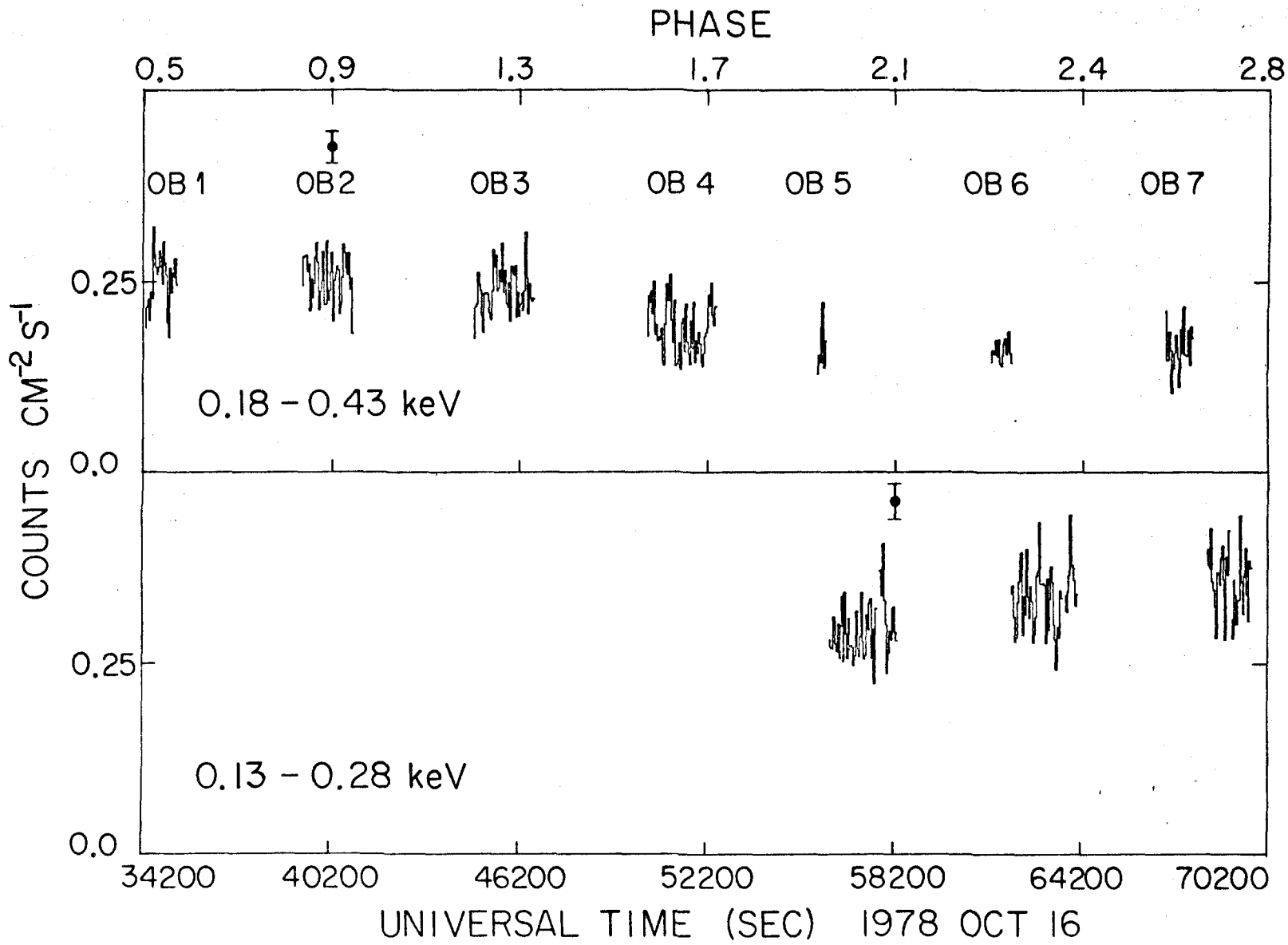


Figure 2

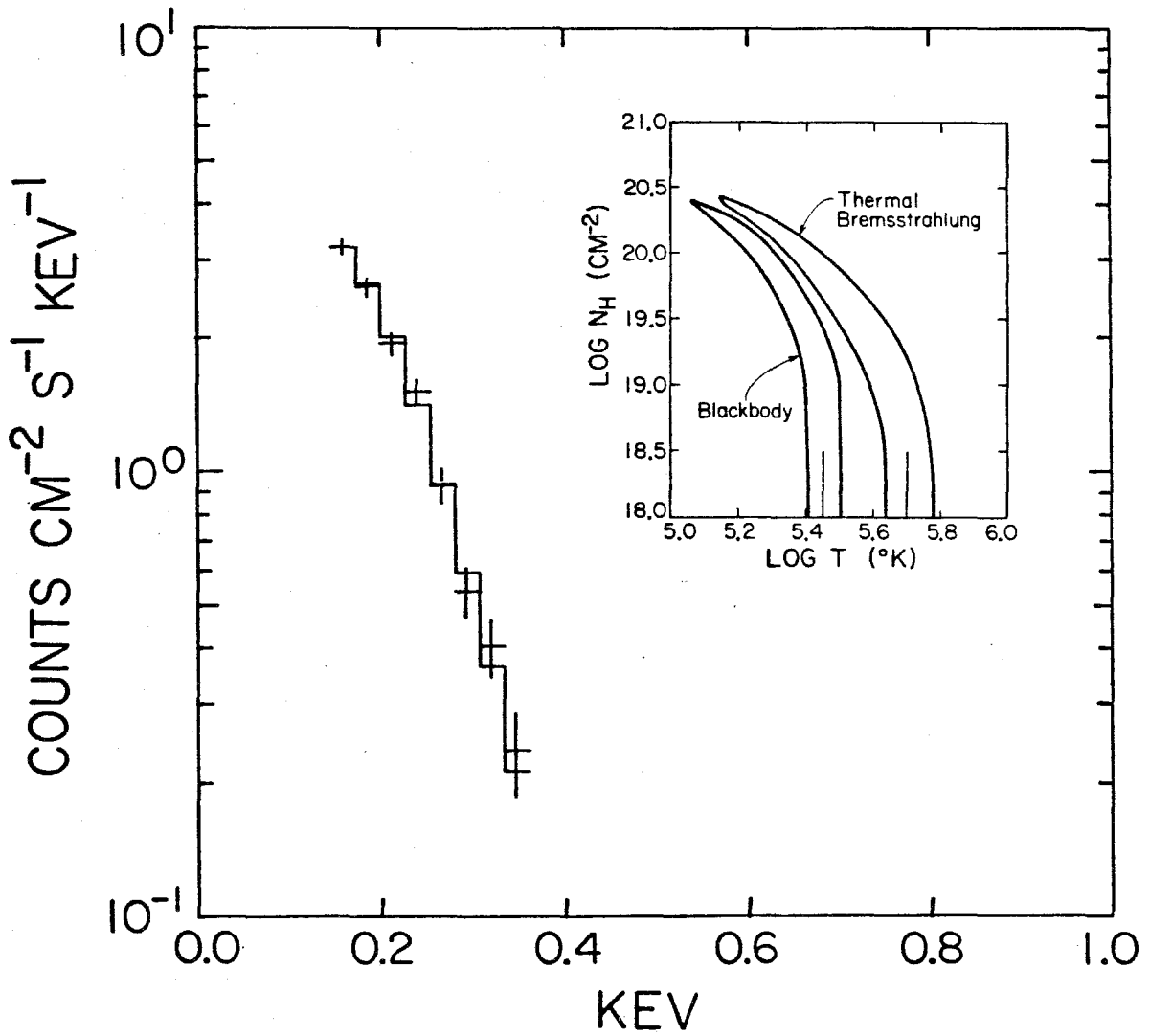


Figure 3

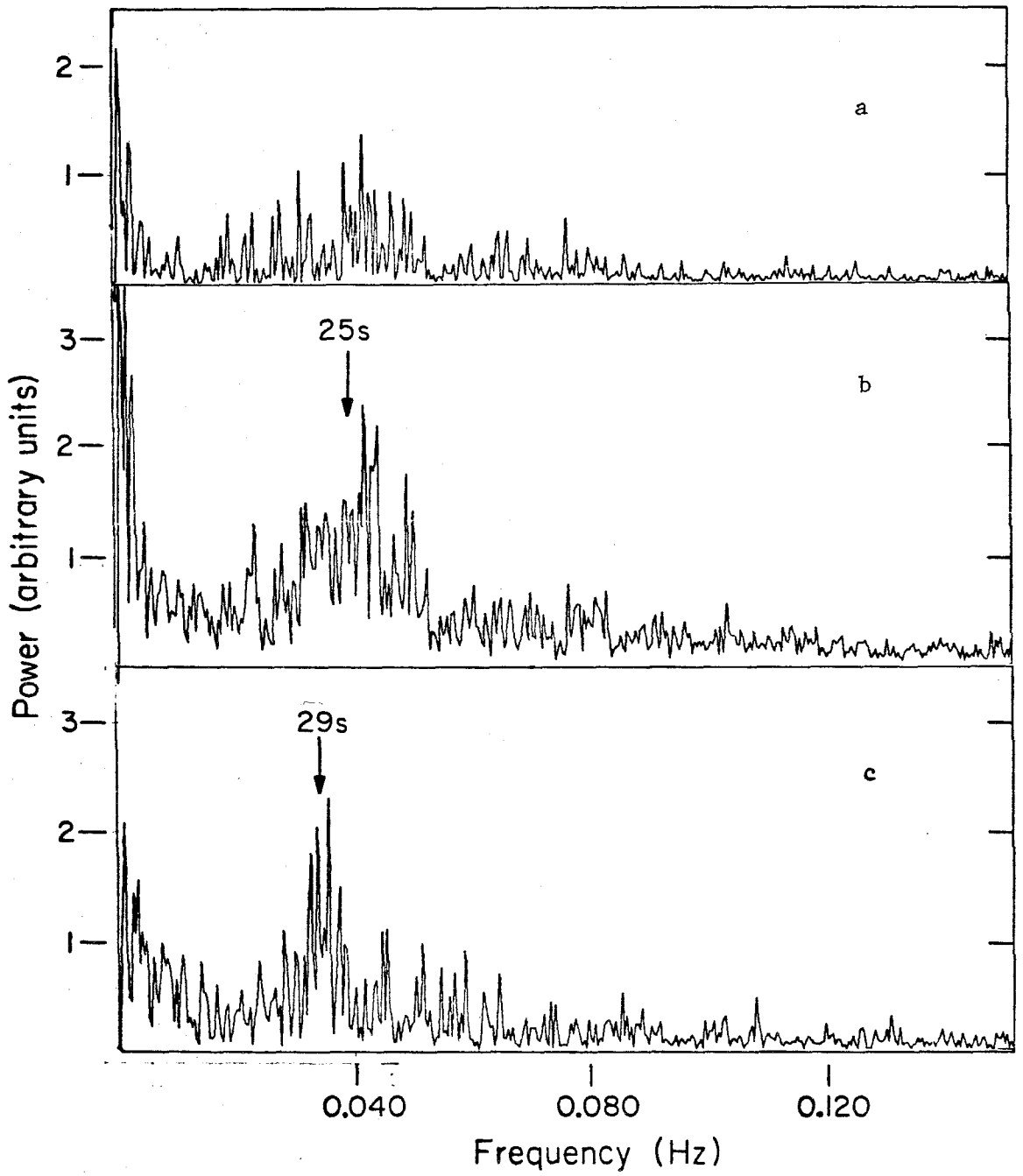
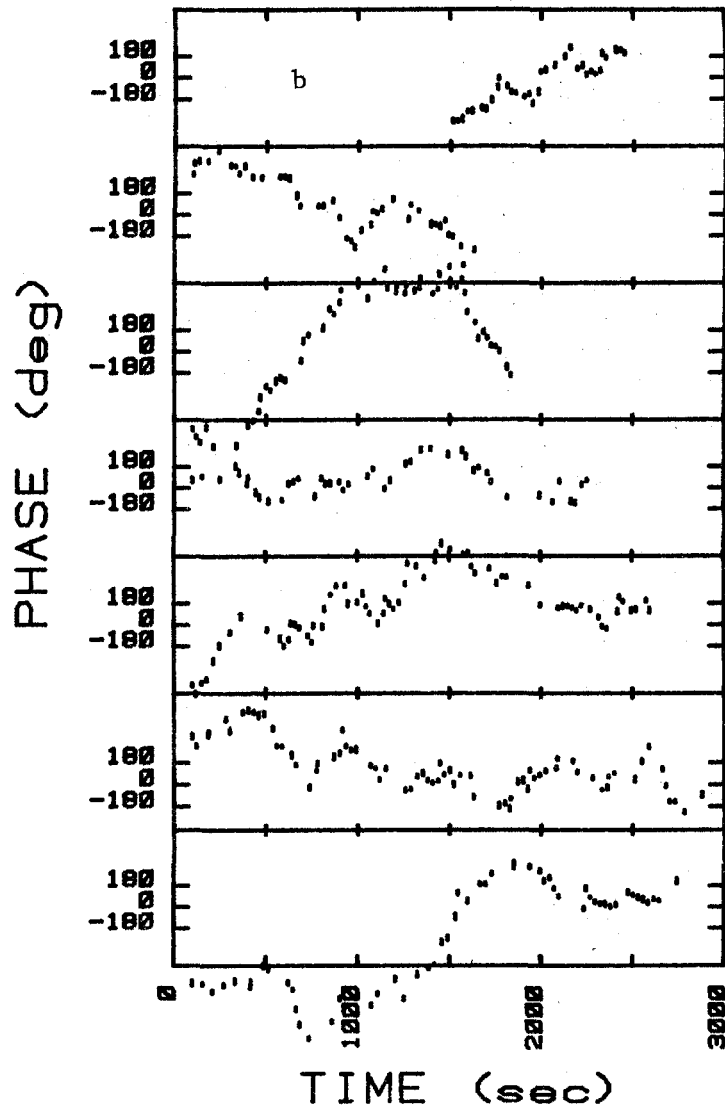
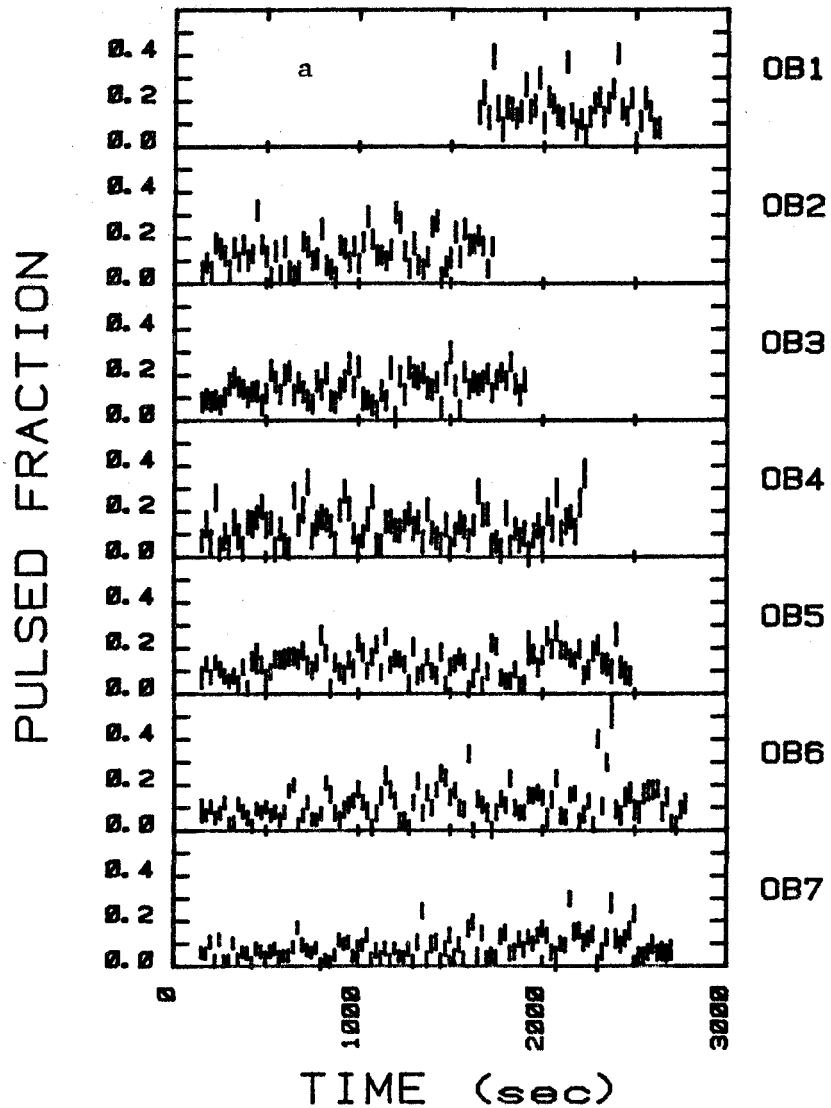


Figure 4

Figure 5



SS Cygni OB2

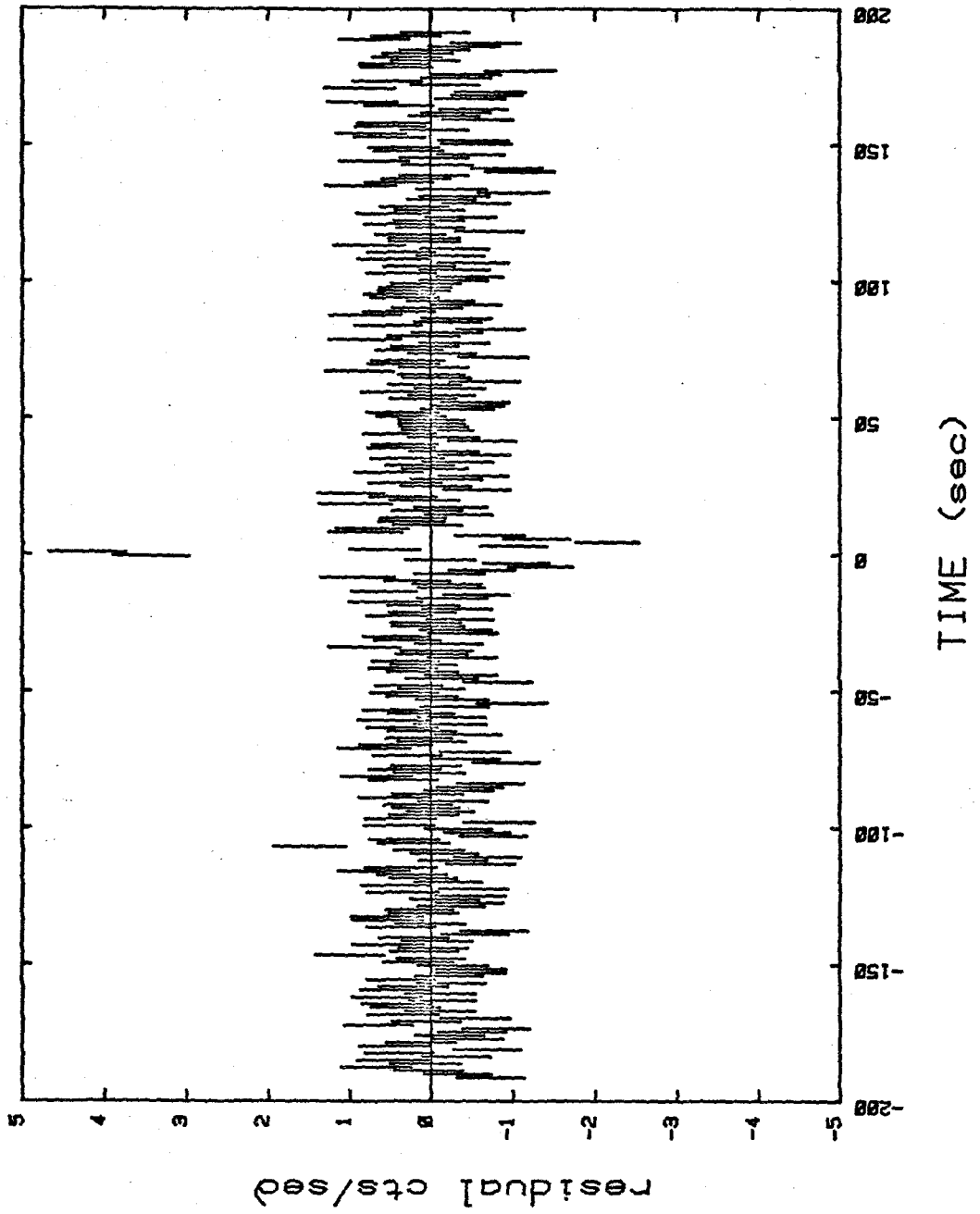


Figure 6a

SS Cygni OB2

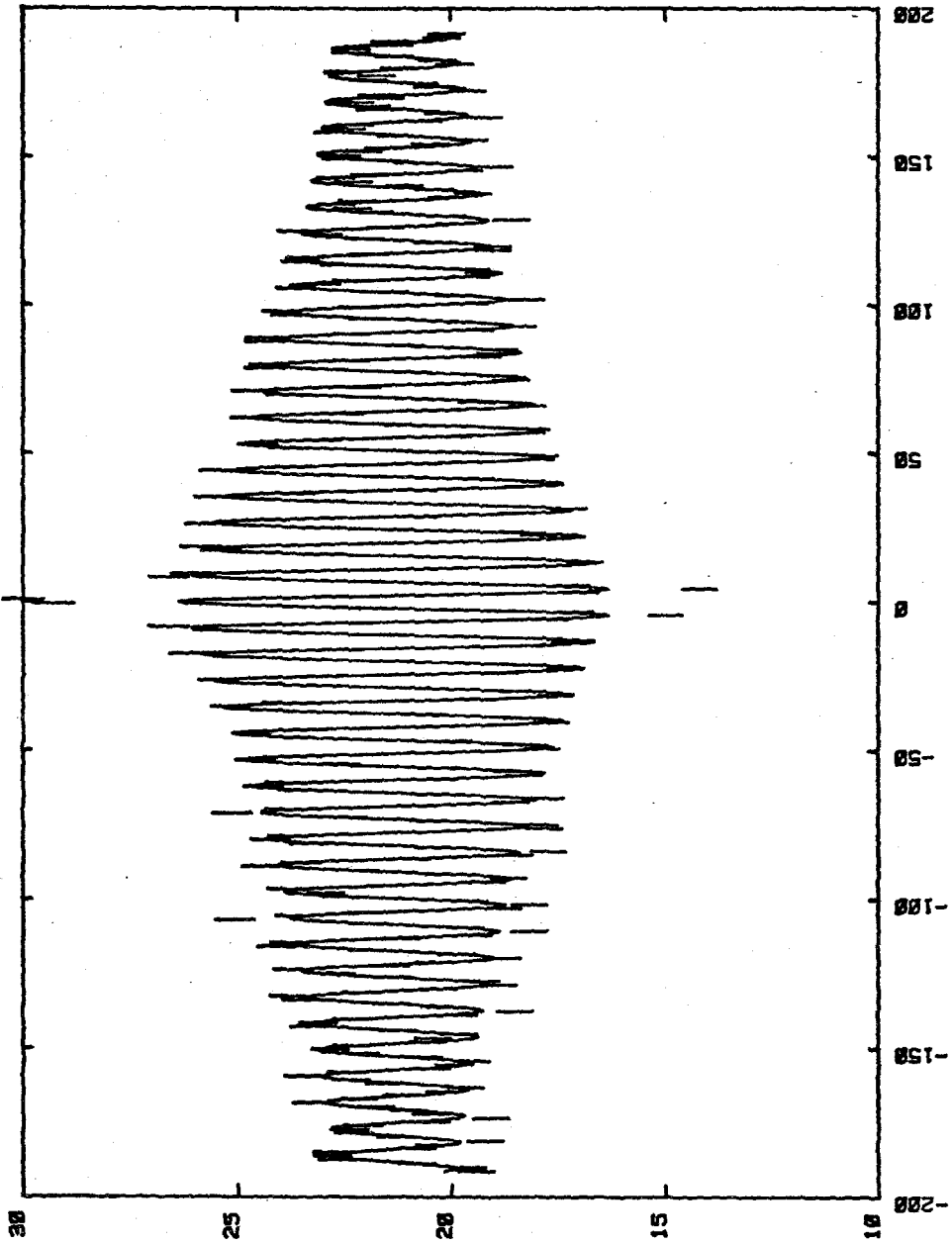


Figure 6b

U Gem OB7

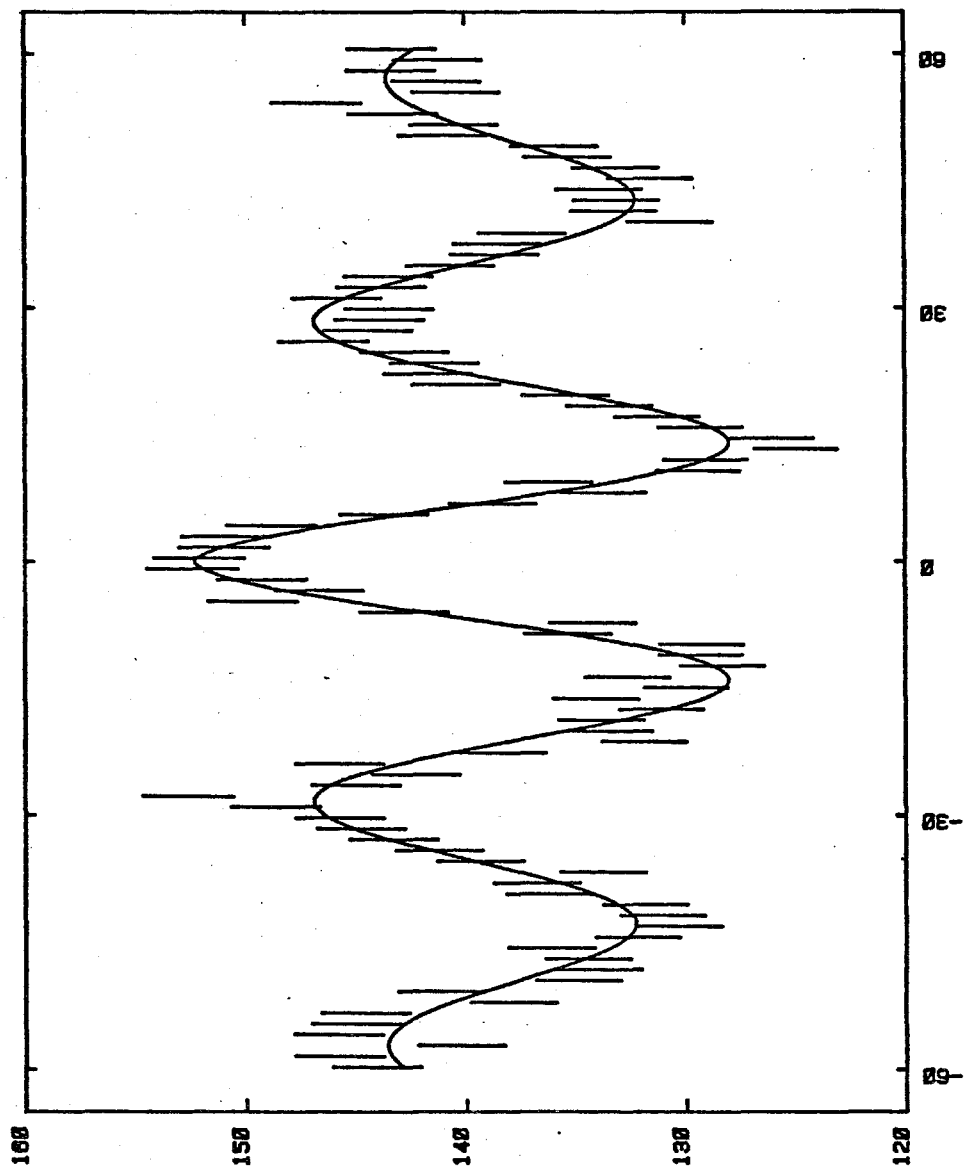


Figure 6c

U Gem OB7

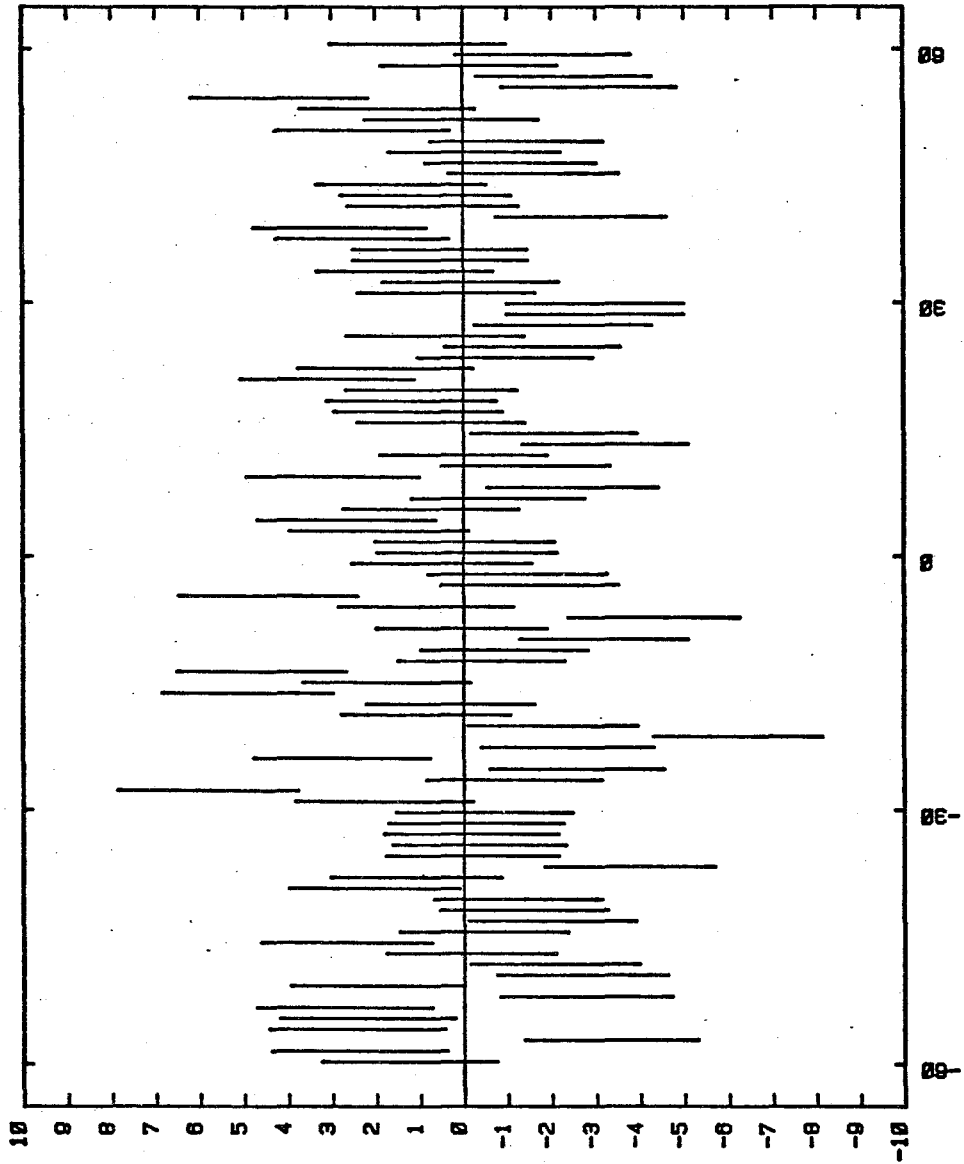


Figure 6d

SS Cygni

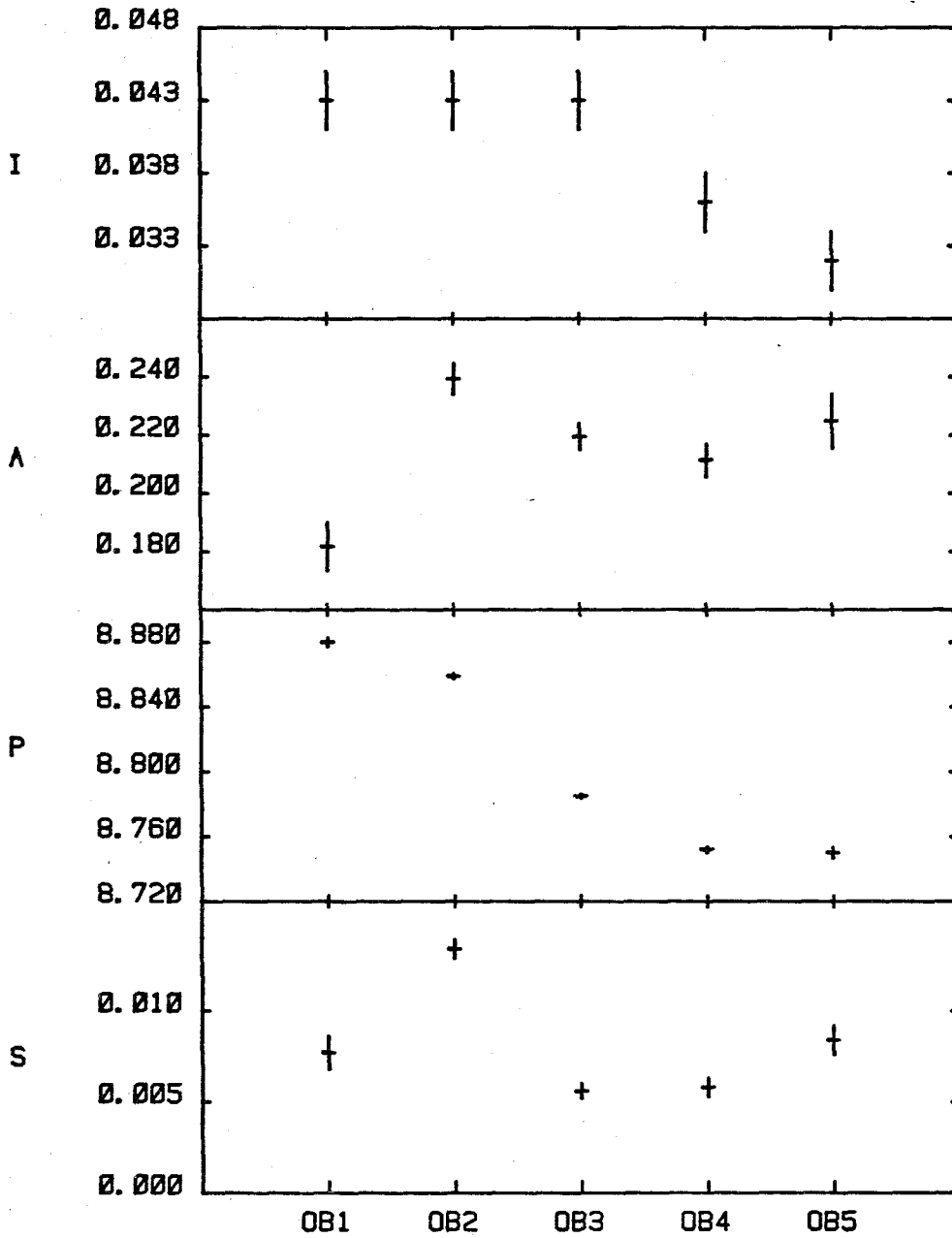


Figure 7a

U Geminorum

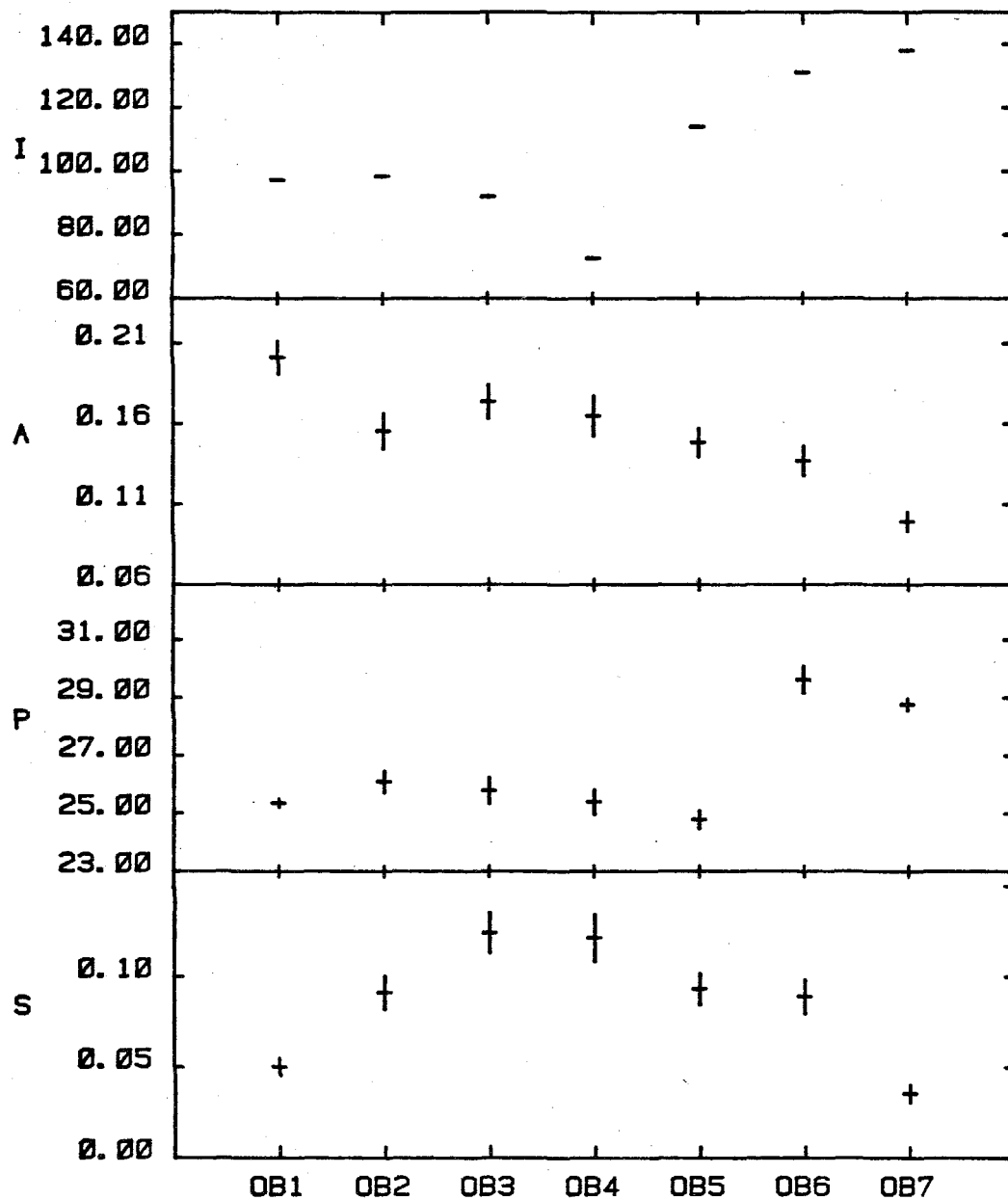


Figure 7b

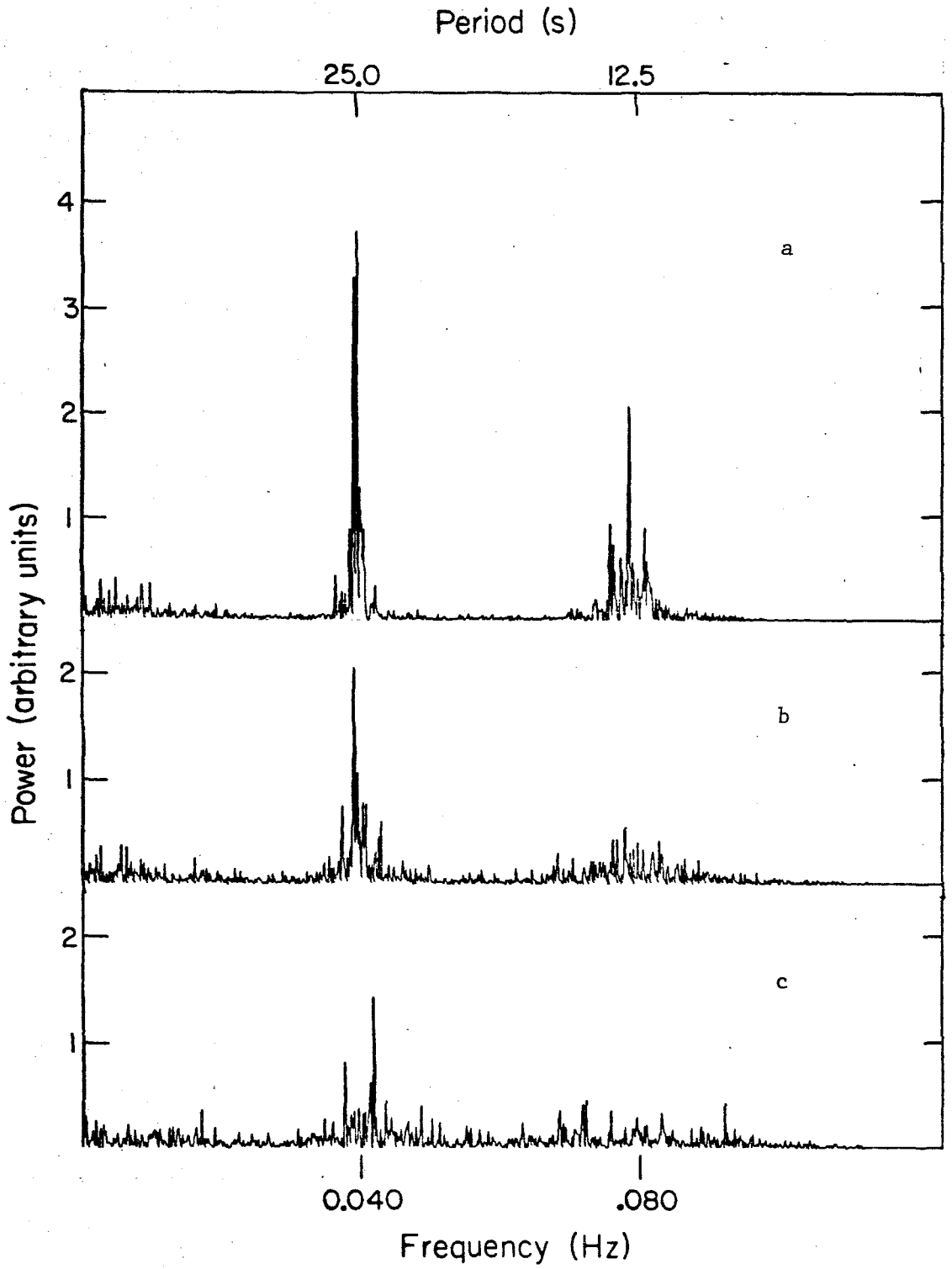


Figure 8

PAPER 3:

A SOFT X-RAY SURVEY OF
DWARF NOVAE IN OUTBURST

submitted for publication to the

Monthly Notices of the Royal Astronomical Society

in collaboration with

J.J.Nugent, S.R.Klein and G.P.Garmire

April 1979

1 INTRODUCTION

Our search for soft X-ray emission from dwarf novae in outburst was motivated by the detection of soft X-ray emission from SS Cyg during optical outbursts (Rappaport et al. 1974; Hearn, Richardson & Li 1976) and predictions of soft X-ray emission from cataclysmic variables (Warner 1974; Bath et al. 1974; Pringle 1977). Our program actually included ~ 130 cataclysmic variables, but in this paper we discuss only the survey of dwarf novae in outburst.

Cataclysmic variables are believed to be close binary systems in which a late-type star transfers matter onto a compact object via an accretion disc (see the reviews by Warner 1976 and Robinson 1976). The dwarf novae members of this class are distinguished by their small and frequent optical brightenings. These "outbursts" vary considerably from dwarf nova to dwarf nova in amplitude (2-5 mag.), duration (~ 2 days-2 weeks), and frequency (~ 10 days-30 years). The observation that among the dwarf novae there are several distinct types of outburst behavior has led to further subdivision with each category named for a prototype object. The U Gem (or SS Cyg) variety of dwarf novae have a fairly repeatable outburst profile: a rise to peak brightness in less than a day and a recovery which lasts for a few days. The Z Cam type occasionally, on the return from maximum light to their pre-outburst state, get stuck at an intermediate brightness level. Z Cam itself has been in such a "standstill" for more than two years. Finally, the SU UMa systems have short and frequent normal outbursts which are interspersed with much less frequent "superoutbursts," i.e., brighter and longer eruptions. All of these subclasses of dwarf novae are represented in the survey described in this paper.

In Section 2 of this paper we briefly describe the experiment and the procedure used in conducting the survey, and in Section 3 present the results of the survey. In Section 4 we discuss various explanations for the failure to detect X-rays from most of the erupting dwarf novae; in particular, we examine the roles of interstellar absorption, the spottiness of the X-ray coverage, the inclination of the source to the observer, source variability, self-absorption, and the source spectrum in the detectability of these objects. We are able to reject several of these alternatives because of the size of the sample involved. A comparison of these nondetections in the context of the positive detections of SS Cyg and U Gem illuminates our understanding of the critical parameters involved in detecting these low luminosity sources. Our results and conclusions are summarized in Section 5.

2 THE EXPERIMENT AND THE SURVEY

The data used for this survey were collected by a 380 cm^2 proportional counter sensitive to energies between 0.18 and 3 keV. The detector (LED1) was one in an array of similar detectors which spanned the energy range 0.18-60 keV and were collectively called the HEAO-A2 experiment (a complete description of which is given by Rothschild et al. 1979). The satellite performed mainly in a scanning mode, with the collimators tracing a 3° wide (FWHM) great circle across the celestial sphere in a plane perpendicular to the Earth-Sun line once every

30 minutes. Coaligned fields of view of 1.5° and 3° (FWHM) provided the spatial resolution in the scan direction. Regions of the sky were sampled over a period from days to weeks, depending on the ecliptic latitude of the region. For the low-energy detectors on HEAO-1 the scanning mission extended from mid-August 1977 to mid-May 1978. Subsequently, several pointing observations were conducted until attitude control of the satellite was lost in January 1979.

The survey was conducted as follows. At the beginning of the mission HEAO-1 Ephemerides of ~ 130 cataclysmic variables were sent to the American Association of Variable Star Observers and the Royal Astronomical Society of New Zealand Variable Star Section who generously agreed to simultaneously optically monitor these stars during the satellite observations. Included in the survey were ~ 65 dwarf novae. The variable star organizations sent us optical light curves of dwarf novae which were in eruption at the time of the satellite observations. We then searched the HEAO-A2 data for soft X-ray emission from these systems, superposing the scanning data over the duration of the outburst to get the best upper limits. Although the entire energy interval 0.18-3 keV was searched, the upper limits given here refer only to the energy band 0.18-0.43 keV because it is within this band that most of the observed high-energy flux appears in SS Cyg and U Gem during outburst.

3 RESULTS

Twenty-four outbursts from 19 dwarf novae were witnessed by HEAO-1. In Table 1 we summarize the salient facts from these observations. The

objects are listed according to the variable star convention (Kukarkin 1969). Given for each dwarf nova are its dwarf nova subclass, its characteristic magnitude range, with the peak magnitude during the outburst observed by HEAO-1 in parenthesis; the outburst date; the dates that were used in the superposition of X-ray data; the number of HEAO-1 scans in the superposition (the duration of a scan is ~ 15 s) the 3σ upper limits (or detections for SS Cyg and U Gem) in $\text{ct cm}^{-2} \text{s}^{-1}$; and comments where relevant. Note that superoutbursts were witnessed in Z Cha, VW Hyi and WX Hyi, and that Z Cam was observed during standstill. The range of upper limits is between 1 and 10% of U Gem's mean intensity of $0.2 \text{ ct cm}^{-2} \text{ s}^{-1}$. SS Cyg itself was detected at an intensity 20% of the average intensity observed for U Gem.

The wide range in upper limits for the different stars in Table 1 is due to (a) the spatial variability of the 1/4 keV sky background (by a factor of about three), which makes the noise level different from region to region of the sky, and (b) the variety in exposure times for the different sources. The collimator transmission correction for sources viewed off-axis is a substantial factor in reducing sensitivity to some of the objects.

The conversion from LED flux units ($\text{ct cm}^{-2} \text{s}^{-1}$) to $\text{erg cm}^{-2} \text{s}^{-1}$ depends on the assumed spectral parameters. This is illustrated in Fig. 1, where the flux for 1 LED flux unit (LFU) is plotted versus kT for various values of the hydrogen column density N_H , assuming a blackbody spectrum. The choice of a blackbody is only one possible characterization of the spectrum. The energy resolution of the LED1

detector at energies $< 1/4$ keV is so poor ($> 80\%$) that we simply cannot distinguish whether the true source spectrum is a blackbody, thermal bremsstrahlung, line emission, or a power law. A blackbody was chosen under the assumption that the X-ray emitting region is optically thick (see Pringle 1977).

The spectra for three cataclysmic variables (AM Her, U Gem and SS Cyg), whose characteristic blackbody spectral parameters have been measured by HEAO-1, have been noted in the figure, for the purpose of showing typical temperatures (25-30 eV) and N_H values ($\leq 10^{18}$ to $\sim 4 \times 10^{20} \text{ cm}^{-2}$). The dotted line shows the range of parameters permitted for SS Cyg at the 90% confidence level (see Section 4). For the temperature of 30 eV and N_H of 1×10^{20} which best fit the spectral data on SS Cyg (Section 4), 1 LFU implies a flux of $\sim 8 \times 10^{-10} \text{ erg cm}^{-2} \text{ s}^{-1}$. Therefore, the intensity of 0.04 LFU measured for SS Cyg (Table 1) implies a flux of $\sim 3 \times 10^{-11} \text{ erg cm}^{-2} \text{ s}^{-1}$. The average intensity observed for U Gem during the 1978 October outbursts was 0.2 LFU. The spectrum of ~ 25 eV and $N_H \leq 10^{18} \text{ cm}^{-2}$ measured during this observation implies a flux $\sim 1 \times 10^{-10} \text{ erg cm}^{-2} \text{ s}^{-1}$. All fluxes correspond to the energy band 0.18-0.43 keV only. The upper limits derived for the dwarf novae in the survey indicate, for a spectrum similar to that of SS Cyg, fluxes of order $2-20 \times 10^{-12} \text{ erg cm}^{-2} \text{ s}^{-1}$, and one-half this value for a spectrum like that of U Gem.

4 DISCUSSION

We have presented the upper limits to the soft X-ray emission from a large number of dwarf novae observed during their eruptive phases. We now explore the question of why only two of these objects were detected in soft X-rays.

4.1 COMPARISON OF THE OPTICAL AND X-RAY LIGHT CURVES AND PULSATIONS

SS Cyg and U Gem are visually among the brightest dwarf novae, and also among those suffering the largest change in magnitude during outburst. One might expect the X-ray brightness to be a monotonic function of the optical brightness and the change in optical brightness. Yet the correlation is not simple, as Fig. 2 shows. Here are illustrated the visual outburst profiles of 4 objects observed by HEAO-1: AY Lyrae, VW Hydri, SS Cyg and U Gem. AY Lyr, which is normally at $\sim 18^{\text{m}}.5$ (Patterson 1979) is the faintest star in the entire survey, yet it shows one of the largest changes in brightness ($\Delta m > 5$). VW Hyi also shows a larger brightness increase ($\Delta m \sim 5.5$) than SS Cyg and U Gem, and has a brightness at maximum ($8^{\text{m}}.7$) rivalling either of them. In comparison, the average peak brightness of the other dwarf novae in the survey was $\sim 12^{\text{m}}.6$, and Δm was $\lesssim 3$ mag. We also note in comparing the X-ray and optical intensities of U Gem and SS Cyg (see Table 1) that U Gem, which was several times brighter in X-rays than SS Cyg, was about 2 visual mag. fainter. Thus something other than a simple scaling relationship between the X-ray and optical light curves is at work.

Of possible relevance to the problem of dwarf novae detectability is the recent observation that ~ 20 -30% of the soft X-ray light from

both U Gem and SS Cyg during outburst is pulsed (Córdoba et al. 1979a, 1979b). The nature of the pulsation reveals that a soft X-ray/EUV source is the probable origin of the visual oscillations seen in ~ 20 cataclysmic variables, including many dwarf novae during outburst (Warner 1976; Robinson 1976). Thus we might expect that any cataclysmic variables showing visual pulsations should have a soft X-ray/EUV counterpart. In Table 1 we have noted those dwarf novae in which optical oscillations have been detected.

In SS Cyg, optical pulsations have been detected at all outburst phases (Patterson, Robinson & Kiplinger 1978; Horne and Gomer 1979; Patterson 1979). Only one X-ray observation of SS Cyg with fast-timing capability has been analyzed; in this observation, made at the peak of an optical light curve, a soft X-ray pulsation was detected (Córdoba et al. 1979a). No optical oscillations have been detected in U Gem, but a quasi-coherent X-ray modulation was found when the system was on the declining portion of a short outburst (Córdoba et al. 1979b). (It is not yet clear if pulsation phase noise is related to the outburst cycle or is a property of the individual dwarf nova; if the latter is true, then the lack of observed optical oscillations in U Gem may be due to the high degree of phase noise in the original X-ray oscillating component.)

If the turn-on of the optical pulsation signals the turn-on of the X-rays, then the visual observations of variability in the pulsed fraction (e.g., Stiening, Hildebrand & Spillar 1979) indicate that the X-ray emission may only occur during certain portions of the visual light curve. In VW Hyi visual oscillations are observed only when

$m_v \gtrsim 12.5$, far down on the declining portion of the light curve (see Fig.2). Extensive HEAO-1 coverage through both an entire superoutburst and normal outburst of VW Hyi, however, revealed no soft X-ray emission. This cannot be attributed to the fainter visual magnitude of the system at the time the visual oscillations are present because the energy in the optical pulsation is as great as the maximum energy in SS Cyg's visual pulsation (i.e. VW Hyi's visual pulsation amplitude is $\sim 2\%$, as compared with 0.02% for SS Cyg's pulsation which is observed when the star is at $m_v = 8.5$). Again, we do not find a simple correlation between X-ray and optical observations.

4.2 CONSIDERATIONS FROM THE X-RAY OBSERVATIONS OF U GEM AND SS CYG

A potentially illuminating investigation is to examine the characteristics of the two known dwarf novae X-ray emitters, SS Cyg and U Gem, and consider how variations in these characteristics affect the observable X-ray luminosity. Our approach will be to examine, in turn, each of several parameters measured for SS Cyg and U Gem and determine by how much the parameter must be varied to be consistent with the upper limits in Table 1. We will consider the source temperature, the combined effects of distance and interstellar absorption, self-absorption, and source variability. For the sake of discussion we will concentrate on measurable properties of the systems; other (inferred) quantities such as the mass accretion rate, mass of the white dwarf, and the size of the emitting region, will be ignored even though these properties are important.

(a) Temperature of the X-ray spectrum. Fig. 3 will serve as a guide for this discussion and the discussion of the hydrogen column density that follows. The figure combines results from the observations of SS Cyg and U Gem detailed in Córdova et al. (1979a, 1979b). Here are shown the 90% confidence χ^2 contours of hydrogen column density

(N_H) versus temperature (kT) for both assumed blackbody and thermal bremsstrahlung (i.e., exponential plus Gaunt factor) spectra. The best-fit spectral parameters for each source are indicated. These observations reveal that SS Cyg and U Gem have extremely soft components, with most of the emission occurring at EUV wavelengths. Referring to Fig. 3, the blackbody temperature is probably < 50 eV for SS Cyg and < 30 eV for U Gem. The spectral parameter error contours in the figure are large because the energy resolution is extremely poor for proportional counters operating at these low energies. The detector window thickness and lower level discriminator setting set the low energy threshold for detection, which is reached by a source with a temperature $\sim 1.5 \times 10^5$ K. Thus sources with temperatures $\sim 50\%$ lower than that of U Gem would be unobservable to LED1. As is clear from Fig. 3, even in the two detected dwarf novae a small change in temperature gives U Gem and SS Cyg nonoverlapping error contours, and pushes U Gem close to the LED1 threshold for detectability.

(b) Hydrogen column density. The column density N_H will depend on the distance to the source and the density of the material in the line-of-sight to the object.

The distances to cataclysmic variables are not accurately known. On the basis of their space density (Warner 1974a), it is believed that the observable dwarf novae are within a few hundred parsec. A recent spectrophotometric parallax for U Gem (Wade 1979) places it at $76 (\pm_{24}^{36})$ pc. On the basis of several kinds of observations, SS Cyg is thought to be somewhat farther away (~ 180 pc, Warner 1976). Recently measured absolute parallaxes for both U Gem and SS Cyg are 0.006 ± 0.005 ,

giving a lower limit to their distances which is consistent with the above measurements (Vasilevskis et al. 1975; Dahn 1979). Cruddace et al. (1974) discuss the opacity of the interstellar medium to soft X-rays and EUV, and find from a variety of measurements that the local medium is quite inhomogeneous in density and temperature. They conclude, however, that within 200 pc of the Sun the mean density is probably only 0.1 cm^{-3} , and more likely 0.2 cm^{-3} at greater distances in many directions. The error contours in Fig. 3 (for assumed blackbody and thermal bremsstrahlung spectra only) thus permit distances ≤ 400 pc for U Gem and ≤ 800 pc for SS Cyg; however, our lack of knowledge about the true nature of the emission spectrum creates an additional uncertainty in these upper limits to the distance.

We estimate the role that distance (including the corresponding greater absorption by the interstellar medium) may play in X-ray detectability by determining how much farther than U Gem the balance of dwarf novae must be in order to be consistent with the upper limits in Table 1. We have chosen U Gem instead of SS Cyg as the X-ray candle because U Gem's apparent visual magnitude at minimum and during its short outbursts is more typical of the majority of dwarf novae. We find that the nondetected dwarf novae discussed here would have to be more than three times farther than U Gem (scaling from U Gem's average X-ray intensity), or $\gtrsim 300$ pc. Excluding a fortuitious spatial distribution of the objects in this survey, this value is inconsistent with the dwarf novae space density (Warner 1974a). We conclude that differences in the X-ray fluxes because of distance and absorption by the

interstellar medium cannot explain the lack of detections for all of the dwarf novae represented here.

In the above we have attributed N_H to a uniform interstellar column, yet absorption in the vicinity of the source (presumably by the accretion disc) can equally affect our ability to detect a source of a given luminosity. If we assume that the scale height of the disc is similar for all systems, then the effect of self-absorption can be argued against by examining the U Gem and SS Cyg systems. The inclinations of these systems are not well known, but estimates of 67° for U Gem (Smak 1976) and 43° for SS Cyg (Warner 1976), coupled with their relatively low N_H values and the lack of orbital effects in their soft X-ray light curves (Córdoba et al. 1979a, 1979b), indicate that self-absorption is probably not a critical factor. The only exception to this may be systems with inclinations close to 90° , e.g., Z Cha (Warner 1974b).

By way of summarizing points (a) and (b), Fig. 4 shows the relative effects of distance, hydrogen column density, and a change in the temperature for an assumed spectral shape, on the observability of the object. Here the counts expected for a blackbody source are plotted versus kT for various values of N_H . The counts are normalized to the intensity and distance of SS Cyg (marked with a cross in Fig. 4; the SS Cyg values are those resulting from the best χ^2 fit to a blackbody spectrum). If the distance to a source with the same temperature as SS Cyg were twice that of SS Cyg, with twice as much N_H (assuming a uniform interstellar medium), then using Fig. 4, one estimates an intensity for the object of 0.5 SS Cyg counts $\times (D_{SS\ Cyg}/D_*)^2 = 0.125$ SS Cyg counts. Since SS Cyg

was observed at 0.04 LFU (Table 1), the intensity of the source which is twice as far is 0.005 LFU, or 4.3×10^{-12} erg cm⁻² s⁻¹ (see Fig. 2 for conversion from LFU to flux). This value is at the detection limit for many of the dwarf novae in this survey.

Conversely, the effects of a change in spectrum are demonstrated by reducing the temperature of a source that is at the distance of SS Cyg (i.e., moving along the $\log N_H = 20.0$ contour in Fig. 4 in the direction of decreasing kT). For a diminution in temperature by only 25% the source intensity is again at the threshold for detection.

As a last example, consider a source with the column density and temperature measured for U Gem and assume the source to be half the distance of SS Cyg. We locate in Fig. 4 the intersection of the $\log N_H \leq 19.0$ with $kT = 25$ eV and increase the value of the relative counts by 4 for the square of the distance. This source then ends up ~ 3 times brighter than SS Cyg even though its temperature is somewhat less.

Thus relatively small changes in the temperature and distance can produce the variety of behavior we see. If the column density of 10^{20} cm⁻² measured for SS Cyg is due to interstellar absorption and implies a distance of ~ 200 pc, as suggested by optical measurements, we think it unlikely that the rest of the dwarf novae are 2-3 times farther away, as would have to be the case to be consistent with the upper limits. If, on the other hand, most of the dwarf novae including SS Cyg are at about 200-300 pc, our results suggest that they may have temperatures $\sim 50\%$ lower than SS Cyg or U Gem. SS Cyg and U Gem may have greater temperatures due to higher white dwarf masses and/or higher mass accretion

rates. (The observation that the hard X-ray (2-25 keV) intensity of SS Cyg during quiescence is ~ 15 times greater than the 3σ upper limits to the hard X-ray flux from many other dwarf novae (Swank 1978) supports the distinctive nature of SS Cyg.) The sensitivity of the temperature and luminosity to these parameters is illustrated in Pringle (1977), where a study is made of the high-energy emission produced in the boundary layer where the accretion disc interacts with the white dwarf surface.

(c) X-ray variability. Large soft X-ray/EUV variability has been observed in scanning observations of SS Cyg and U Gem (Margon et al. 1978; Mason et al. 1978), but most of the time when these objects have been observed, they have been detected (Mason, Córdova and Swank 1978 and references therein). Recent long pointings at both objects by HEAO-1 have shown only a slow, monotonic change in soft X-ray brightness (Córdova et al. 1979a, 1979b). For the dwarf novae in the survey the mean number of LED1 scans per outburst was ~ 10 (with TW Vir at 1 scan and Z Cha at 107 scans representing the extremes in coverage). Thus it is unlikely that source variability can explain all of the nondetections.

5 CONCLUSIONS

U Gem and SS Cyg are thus far unique among dwarf novae in showing soft X-ray emission during outbursts. Our inability to detect soft X-rays from a large sample of other erupting dwarf novae may result from any or all of the following: extremely soft temperatures for the oscillating

high-energy component in these systems; a smaller area for the emission region; absorption by material in the vicinity of the source; and dilution of the flux due to distance and attenuation by the intervening hydrogen column. Some of the nondetections reported here are probably due to each of these factors. Nonetheless, we have demonstrated that fluctuations in the temperatures or column densities of sources with extremely soft spectra have the greatest effect on the apparent source flux; thus it is our feeling that most dwarf novae are not observed as soft X-ray sources by virtue of their low temperatures ($\lesssim 10^5$ K) or greater absorption. The relative importance of these contributing factors may be determined with EUV observations, refined orbital parameter estimations, and better distance determinations. More X-ray pointing observations of U Gem and SS Cyg during various outburst phases are also desirable so that the nature and origin of the X-ray emissions and their relation to optical phenomena may be better understood.

Table 1. HEAO-1 observations of erupting dwarf novae

Source	Type	λ Range (max during HEAO obs.)	Outburst Date*	Dates* of HEAO Superposition	No. of Scans	Visual Pulsations Detected**	Intensity [†] ct cm ⁻² s ⁻¹	Comments
RX And	ZC	10.3-13.6 (11.7)	530	529.7-532.4	2		< 0.0106	
TT Boo	UG	12 -->15 (13.3)	520	520.0-521.0	3		< 0.00885	
Z Cam	ZC	10.2-14.5 p (11.5)	Continuing	425.1-426.4	4	c	< 0.00664	Stardzill
"	"	(11.5)	"	600.9-609.4	14		< 0.00657	"
YZ Cnc	SU	11.0-14.6 p (12.7)	437	433.9-439.4	10	qc	< 0.00698	
SV CMI	ZC	13.0-16.3 p (13)	433	433.0-435.3	9		< 0.01212	
Z Cha	UG	11.8-14.3 (13)	367	372.7-379.5	107	c	< 0.00129	Superoutburst (~ 11 d)
SS Cyg	UG	8.1-12.1 (8.3)	669	674	6 h pointing	c, qc	0.04	X-ray pulsation detected
AB Dra	ZC	12.0-15.8 p (12.5)	375	374.6-377.5	51		< 0.00354	
"	"	(12.4)	387	386.5-388.5	33		< 0.00358	
AQ Eri	UG	12.5-16.5 (13.0)	573	572.7-573.4	3		< 0.00926	May be spurious outburst ^{††}
U Gem	UG	8.8-14.2 (9.0)	436	435.0-438.1	13		0.2	Peak intensity ~ 0.5 ct cm ⁻² s ⁻¹
"	"	(10.0)	795	798	10 h pointing	qc	0.2	X-ray pulsation detected
AH Her	ZC	10.2-14.7 p (11.5)	378	377.6-381.0	70	c	< 0.00425	
VW Byi	SU	8.5-14.0 (8.7)	442	445.6-464.6	80	c, qc	< 0.00280	Superoutburst (~ 11 d)
"	"	(9.7)	469	469.7-470.4	9		< 0.00843	
"	"	(8.4)	644	641.8-649.2	9		< 0.00897	Superoutburst (~ 15 d)
WX Byi	SU	10.7-14.2 p (11.5)	482	482.8-483.4	5		< 0.01602	Superoutburst (~ 17 d)
X Leo	UG	11.5-15.5 (12.1)	463	463.0-464.5	16		< 0.00405	
AY Lyr	SU	12.6-18.5 (13.1)	429	427.1-430.3	12		< 0.00971	
"	"	(13.1)	608	608.7-609.7	5		< 0.01290	
CT Lyr	UG	13.3-16.8 (12.3)	425	425.4-426.5	6		< 0.00478	
CN Ori	ZC	11.6-14.8 (12.3)	408	405.6-408.6	6	c	< 0.00164	
KT Per	ZC	10.7-15.0 (12.1)	537	536.6-545.5	6	c	< 0.00719	
TW Vir	UG	11.8-16 p (13.2)	493	493.7	1		< 0.4358	

* Julian day 2443000[†]

** c = coherent; qc = quasi-coherent

† Upper limits are 3 σ

†† Mattel (private communication)

References

- Bath, G. T., Evans, W. D., Paploizou, J. & Pringle, J. E., 1974.
Mon. Not. R. astr. Soc., 169, 447.
- Córdova, F. A., Chester, T. J., Tuohy, I. R. & Garmire, G. P.,
 1979a. Astrophys. J., submitted.
- Córdova, F. A. et al., 1979b, in preparation.
- Cruddace, R., Paresce, F., Bowyer, S. & Lampton, M., 1974. Astrophys.
J., 187, 497.
- Dahn, C. C., 1979. Private communication.
- Hearn, D. R., Richardson, J. A. & Li, F. K., 1976. Bull. Am. astr.
Soc., 8, 447.
- Horne, K. & Gomer, R., 1979. Private communication.
- Kukarkin, B. V., 1969. General catalogue of variable stars, Sternberg
 State Astronomical Institute of the Moscow State University, Moscow.
- Margon, B., Szkody, P., Bowyer, S., Lampton, M. & Paresce, F., 1978.
Astrophys. J., 224, 167.
- Mason, K. O., Córdova, F. A. & Swank, J. H., 1978. Proc. of the COSPAR
Symposium, Innsbruck, Austria, June 1978.
- Mason, K. O., Lampton, M., Charles, P. & Bowyer, S., 1978. Astrophys.
J. Letters, 226, L129.
- Patterson, J., Robinson, E. L. & Kiplinger, A. L., 1978. Astrophys. J.
Letters, 226, L137.
- Patterson, J., 1979. Private communication.
- Pringle, J. E., 1977. Mon. Not. R. astr. Soc., 178, 195.
- Rappaport, S., Cash, W., Doxey, R., McClintock, J. & Moore, G., 1974.
Astrophys. J. Letters, 187, L5.

- Robinson, E. L., 1976. Ann. Rev. Astron. & Astrophys., 14, 119.
- Rothschild, R., Boldt, E., Holt, S., Serlemitsos, P., Garmire, G.,
Agrawal, P., Riegler, G., Bowyer, S. & Lampton, M., 1979.
Space Sci. Instr., in press.
- Smak, J., 1976. Acta Astron., 26, 277.
- Stiening, R. F., Hildebrand, R. H. & Spillar, E. J., 1979. Submitted
to Pub. A.S.P.
- Swank, J. H., 1978. Private communication.
- Vasilevskis, S., Harlan, E. A., Lemola, A. R. & Wirtanen, C. A.,
1975. Lick. Obs. Publ., 22, part V.
- Wade, R. A., 1979. Astron J., in press.
- Warner, B., 1974a. M.N.A.S.S.A., 33, 21.
- Warner, B., 1974b. Mon. Not. R. astr. Soc., 168, 235.
- Warner, B., 1976. In IAU Symposium No. 73: Structure and Evolution
of Close Binary Systems, ed. P. Eggleton et al., p. 85, Dordrecht,
Reidel.
- Warner, B. & Brickhill, A. J., 1978. Mon. Not. R. astr. Soc., 183, 777.

Figure Captions

Fig. 1. Conversion from LED1 intensity (LFU) in $\text{ct cm}^{-2} \text{s}^{-1}$ to flux in $\text{erg cm}^{-2} \text{s}^{-1}$ for various values of N_{H} , assuming a blackbody spectrum. (a) $N_{\text{H}} \leq 1 \times 10^{19} \text{ cm}^{-2}$, (b) $N_{\text{H}} = 1 \times 10^{20}$, and (c) $N_{\text{H}} = 4 \times 10^{20}$. For comparison with the upper limits (expressed in (LFU) in this paper, the best-fitting spectral parameters for three cataclysmic variables observed by LED1 are indicated. The dotted line running through the SS Cyg value represents the spectral parameter extremes allowed by a χ^2 fit to the data (see Fig. 3).

Fig. 2. The visual light curve for four outbursting dwarf novae in the A2 survey. The data for AY Lyr, SS Cyg, and U Gem were supplied by the AAVSO; the data for VW Hyi were supplied by the Variable Star Section (R.A.S., New Zealand).

Fig. 3. The 90% confidence χ^2 contours for N_{H} as a function of kT for both SS Cyg and U Gem. A thermal bremsstrahlung (exponential plus Gaunt) and a blackbody model were fitted to the data. The crosses (SS Cyg) and vertical bars (U Gem) represent the best-fitting spectral values. The HEAO-1 low-energy detector used for this observation is insensitive to values of $\log N_{\text{H}}$ lower than 18.5.

Fig. 4. Predicted counts, assuming a blackbody spectrum, for a source as a function of N_{H} and kT , normalized to the best χ^2 fit values of the column density, temperature, and distance derived for SS Cyg (labeled with a cross).

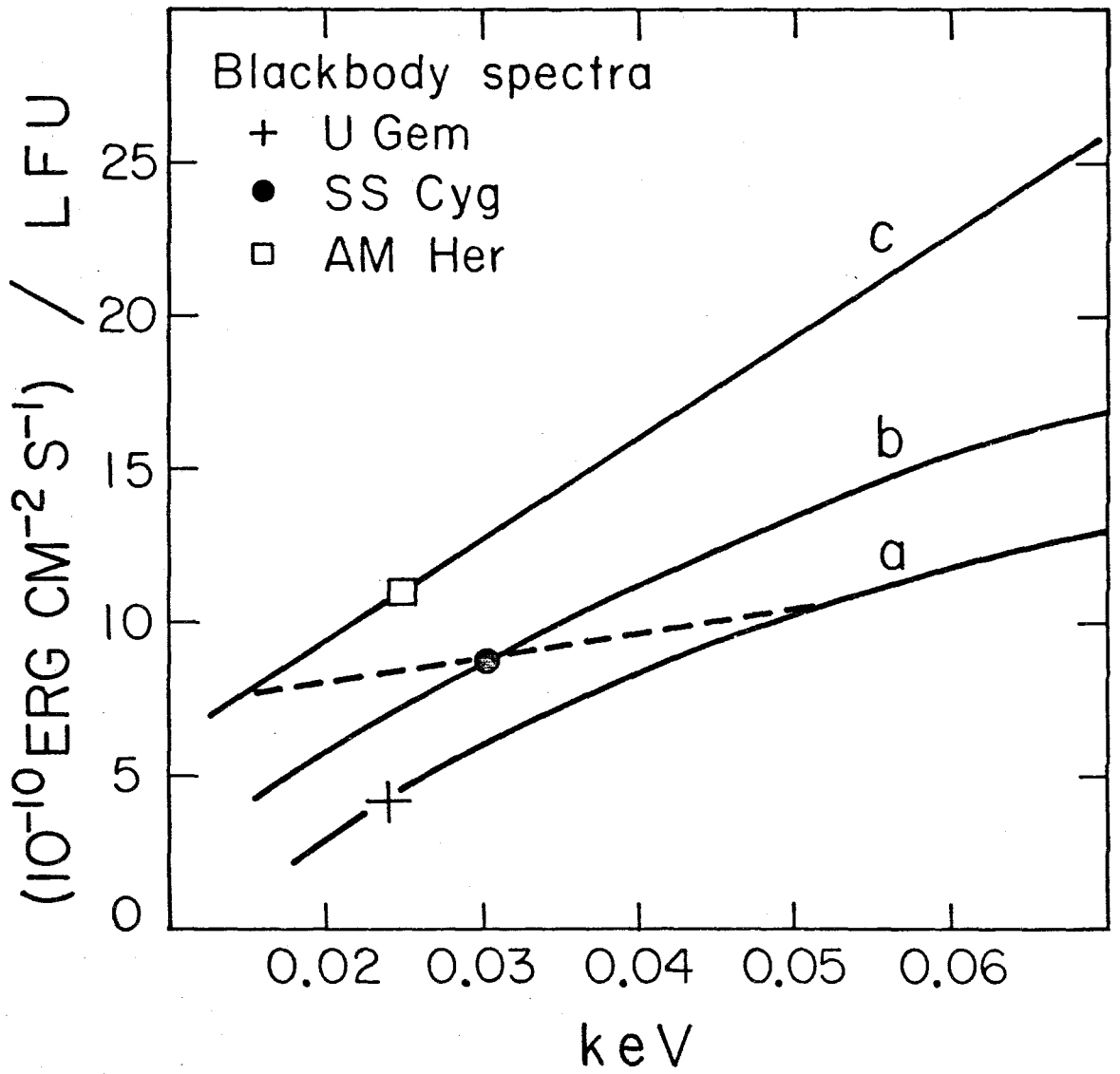


Fig. 1

JULIAN DAY 2,433,000+

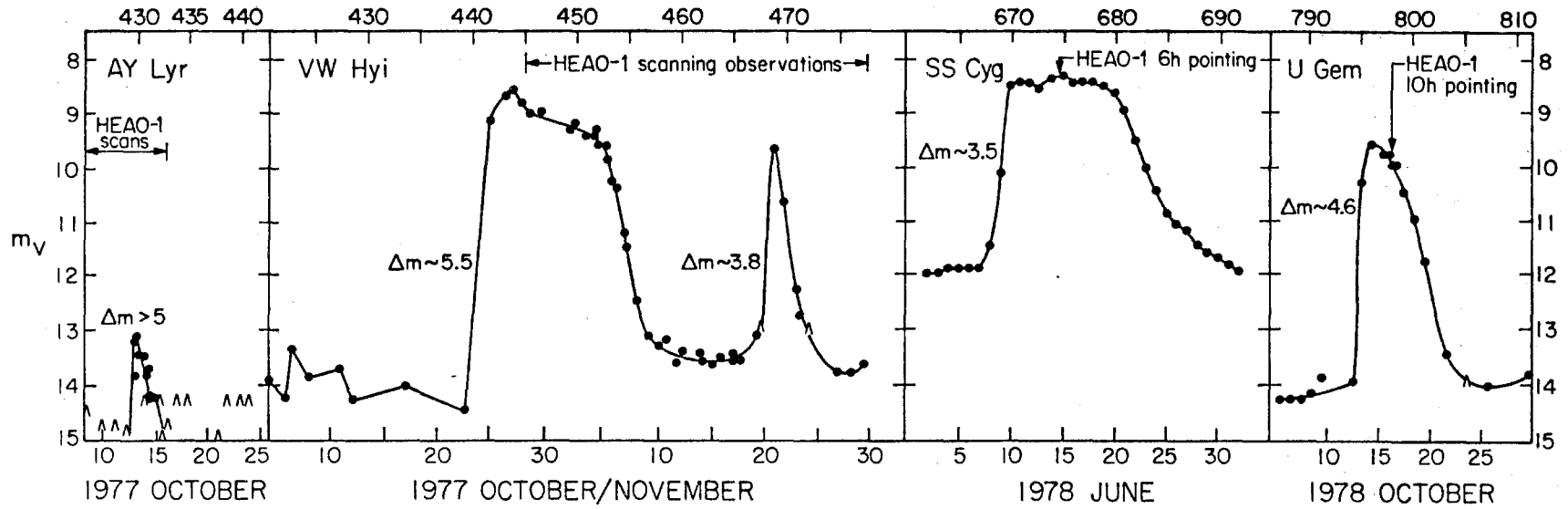


Fig. 2

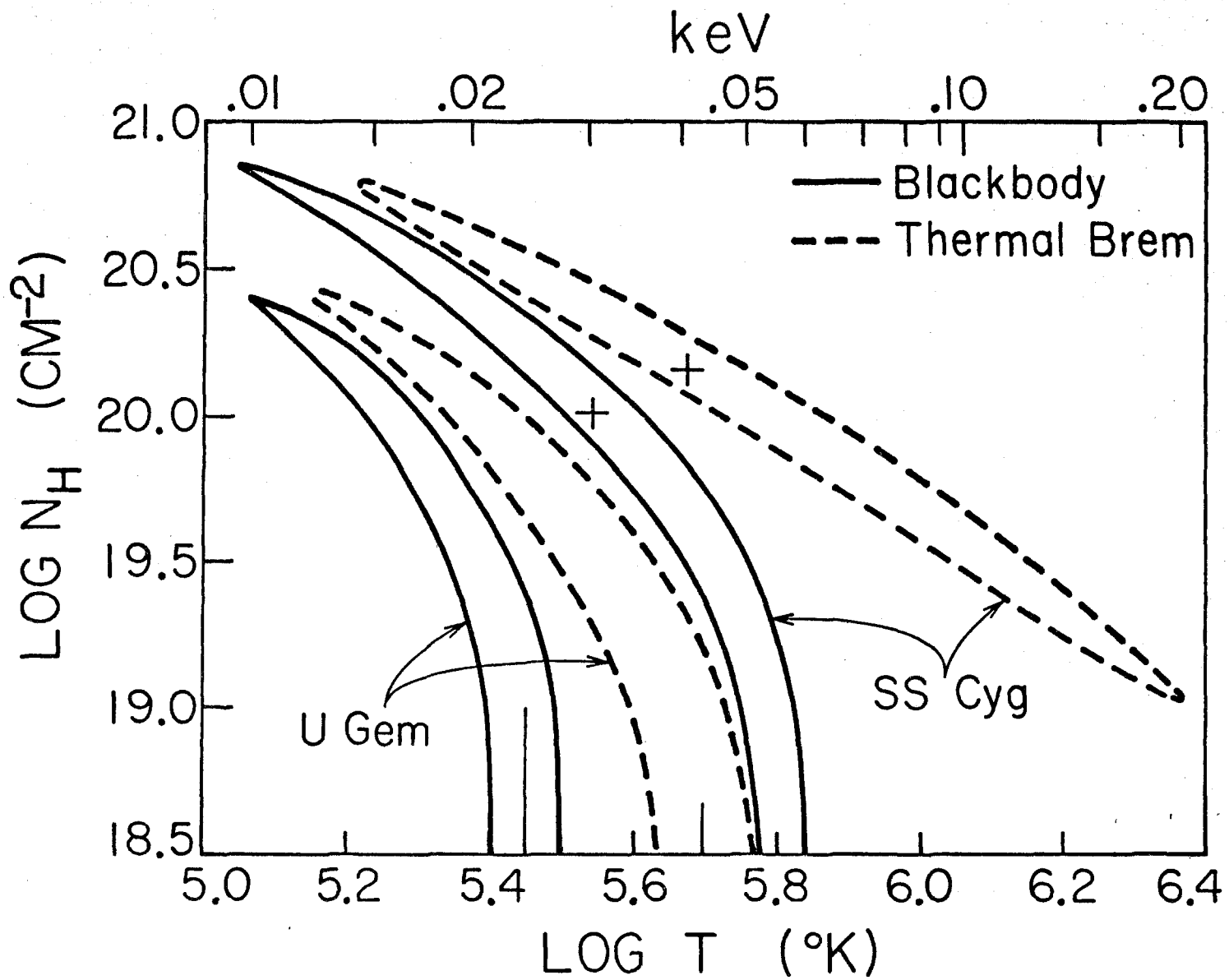


Fig. 3

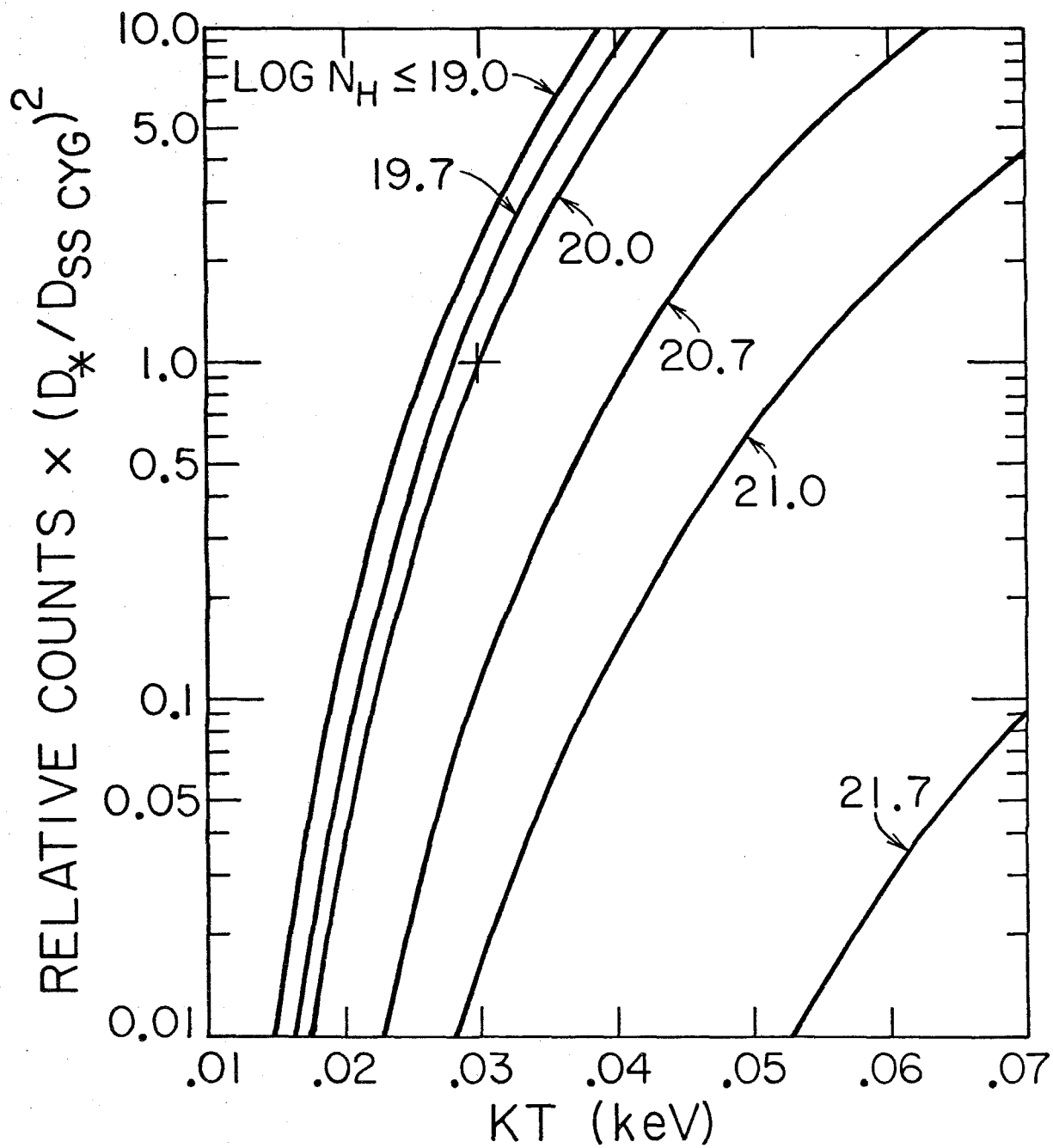


Fig. 4

PART II:
DWARF NOVAE IN QUIESCENCE

PREVIOUS X-RAY OBSERVATIONS OF DWARF NOVAE
DURING QUIESCENCE

X-rays from two dwarf novae have been detected during quiescence. Both SS Cygni and EX Hydrae have relatively hard X-ray spectra ($E > 2$ keV), and low luminosities ($L_x \sim 2 \times 10^{32}$ erg s⁻¹) comparable to their optical quiescent luminosities.

EX Hya was probably the first dwarf nova detected during any outburst phase. It was discovered in Uhuru data, but for a long time the X-ray flux was attributed to a nearby on the sky (0.4) richness class 3 cluster of galaxies, SC 1251-28 (Forman et al. 1978; Mushotzky et al. 1978). Actually it was Warner (1972) who, on the basis of positional coincidence alone, suggested that EX Hya was the optical candidate for the 5 Uhuru count source. Yet it was not until a good position was measured by Ariel V experimenters (Watson, Sherrington and Jameson 1978) and variability of the source was discovered (also Watson et al. 1978), that EX Hya became the leading candidate.

SS Cyg was first detected as a hard X-ray source during quiescence by ANS experimenters who observed both a hard X-ray component (1-7 keV) with a flux of 7×10^{-11} erg cm⁻² s⁻¹, and possibly (3.8 σ) a weak soft X-ray component (1/4 keV band) at a level of 4×10^{-12} erg cm⁻² s⁻¹. The hard X-ray flux during minimum visual light has been confirmed by Mason, Cordova and Swank (1978), Fabbiano et al. 1978, and Ricketts, King and Raine (1979); the average value is 1.6×10^{-10} erg cm⁻² s⁻¹. A thermal bremsstrahlung spectrum fits the data ($kT = 19$ keV) and iron line emission has been observed (Swank 1978, private communication).

Ricketts et al. (1979) discovered an inverse correlation between the hard X-ray and visual outburst light curves. The X-rays were observed to increase by two to three times their average quiescent state intensity both immediately before, and following, outbursts. During the outburst the hard X-ray flux is several times lower than the quiescent phase value (this result is confirmed by Swank 1979, private communication; see text of Paper 1). During quiescence the X-ray emission varies by a factor of five or more over periods of days (Ricketts et al. 1979), and by a factor of two over timescales of minutes (Mason, Cordova and Swank 1978).

The observations of Ricketts et al. is interpreted by them in terms of radial accretion onto a magnetized white dwarf; this interpretation is discussed in more detail in the Summary of this dissertation. Included in the Summary is a table with all of the dwarf novae X-ray observations during all phases of the light curve. The references for this brief review of past observations are also listed in the Summary.

PAPER 4:

THE DETECTION OF SOFT X-RAYS FROM EX HYDRAE

accepted for publication in the

Monthly Notices of the Royal Astronomical Society

in collaboration with

G.R.Riegler

January 1979

1 INTRODUCTION

This is one in a series of papers describing the results of a search for soft X-ray emission from cataclysmic variable stars using the A2 low energy detectors (0.15-3 keV) on the HEAO-1 satellite. Previously Córdova et al. (1977) summarized the soft X-ray observations of several dwarf novae which were undergoing optical outbursts at the time they were scanned by HEAO-1. Of these, only U Gem was detected in the 1/4 keV band (Mason et al. 1978). Since that investigation, SS Cygni has also been detected during a recent optical outburst (Córdova, Garmire & Tuohy 1978). In forthcoming papers we will also report on a search for soft X-rays from novae, recurrent novae, novalike objects, and dwarf novae in optical quiescence. Among the latter, only EX Hydrae, SS Cygni, and possibly AY Lyrae, have been detected as soft X-ray emitters. Here we report the results of HEAO-A2 scanning observations of EX Hya.

EX Hya is a southern ($\delta = -29^\circ$) dwarf nova with a binary period of 98 minutes (Mumford 1967) and a spectrum which shows evidence for an accretion disc (Kraft 1962). It is monitored by the Royal Astronomical Society of New Zealand Variable Star Section and the AAVSO. The former (Bateson 1978) communicates that EX Hya fluctuates almost continuously between visual magnitudes 12.8 and 13.2 with flare-like activity producing many minor peaks with magnitudes 12.2 to 12.6. There are

also several sharp minima fainter than magnitude 13.2. Major outbursts occur at long intervals, which average 465 days but vary within wide limits. In this respect, it is unlike the majority of dwarf novae which undergo outbursts on a timescale of tens of days. During the EX Hya outbursts, which last ≤ 4 days, its visual magnitude may increase to 10.0. During the X-ray observation reported here, Bateson reports that the system was not undergoing such an outburst, and was about magnitude 13.

Previous detections of a hard X-ray (2-10 keV) source consistent with the position and expected variability of EX Hya have been summarized by Watson, Sherrington & Jameson (1978). We report here the first detection of the source at energies less than 2 keV. Both the position and soft X-ray variability are consistent with the identification of EX Hya. This is the first observation of X-ray variability in the source on the timescale of an hour or less, and the first measurement of a column density to the source. We present a light curve from a 4-day HEAO-1 observation which shows no apparent orbital modulation. We also derive the best-fit (minimum χ^2) spectral parameters for the source. We compare this observation of EX Hya with the X-ray behavior of SS Cyg in optical quiescence, and discuss the observations in terms of models for the production of X-rays by accreting white dwarfs.

2 THE OBSERVATIONS

A new soft source was discovered in the HEAO-A2 low energy X-ray data of 1978 January 12-14. The detector used for the observation, described in detail by Rothschild et al. (1979), was a propane-filled

proportional counter sensitive in the 0.15 to 3 keV range. Two coaligned collimators with $1^{\circ}55 \times 2^{\circ}95$ and $2^{\circ}8 \times 2^{\circ}55$ fields of view (FWHM) were in front of the counter, which had a geometrical collecting area of 380 cm^2 .

The HEAO-A2 2σ error box for the soft X-ray source measures $0^{\circ}5$ in the scan direction and $3^{\circ}5$ perpendicular to the scan plane, and centers on EX Hya. It excludes the center of the southern cluster of galaxies SC1251-28, a source tentatively proposed as the candidate for the hard X-ray source observed near this position by several experimenters (see Watson, Sherrington & Jameson 1978, for a historical review). Other experimenters on HEAO-1, using a scanning modulation collimator, detected a 2-10 keV source at the same time as the 0.5-3 keV detection reported here. Their error box overlapping our error box is considerably smaller ($0.6[']^2$) and includes EX Hya (Schwartz et al. 1978). The positional coincidence between the hard and soft sources, plus the good agreement in spectrum (see below), argue that the hard and soft X-rays are emitted from the same source, and that the soft X-ray emission is an extension of the hard X-ray spectrum to lower energies. The large X-ray variability (reported here for the soft X-rays, and by Watson, Sherrington & Jameson 1978, for the hard X-rays) and lack of any other promising candidate in the error box argue that the optically active dwarf nova EX Hya is the X-ray source.

X-rays from EX Hya were detected only above 0.5 keV. In the 4 days during which the source was within 2° of the axis of the detector look-direction there were 17 scans of usable data, each

scan lasting for ~ 15 seconds. The most closely spaced scans occurred 1.2 hours apart. The source was detected at $2-7 \sigma$ above the X-ray background in 13 of the 17 scans. In Figure 1 the intensity of the source (0.5- 3 keV) versus time is plotted, utilizing data from both fields of view. Two of the scans (designated by dashed lines in Figs. 1 and 2) were made when the proportional counter high voltage setting differed from the nominal setting. To compare the intensities during these scans with the other scan intensities, the former values have been corrected assuming the best-fit source spectrum described below.

Clearly, the soft X-ray source is quite variable. In less than 1.2 hours, the intensity changed by a factor ~ 3 . Using the hypothesis of a constant source (and using only the 15 values measured with the same high-voltage setting), the observations yield a χ^2 of 46 for 14 degrees of freedom. The formal probability of obtaining this χ^2 from a steady source is $\ll 0.1\%$.

We have folded the data on the 1.6376 hour binary period (Mumford 1967). As is shown in Fig. 2, no correlation of soft X-ray intensity with orbital phase is apparent. We note, though, that there are only 17 points in the light curve. The optical eclipse is only 4 minutes long and we have only one, statistically poor, point during this phase (we have used the convention of assigning 0.0 phase to the center of the optical eclipse). The intensity at this phase is consistent with zero, but this may be fortuitous since there are a number of zero-intensity values throughout the orbital cycle. A pointed X-ray observation is needed to settle the question of X-ray orbital phase dependence, but we can see from the light curve that there is no evidence for an

X-ray modulation which lasts for $\gtrsim 15\%$ of the orbital cycle.

A large uncertainty in the spectral temperature derived by fitting such a weak source is inevitable. In Fig. 3 we present a χ^2 grid of column density of hydrogen (N_H) vs. thermal bremsstrahlung temperature (kT) using pulse-height data accumulated during the 5 source transits when the telemetry was in the proper mode for pulse-height readouts (scans used for the spectral fit are designated with diamonds in Fig. 1). The 1 and 2σ contours were derived using the prescription of Lampton *et al.* (1976). Clearly our measurements are consistent with any kT > 1 keV. For larger values of kT, a lower value of N_H is required to be consistent with the data. The best (minimum χ^2) thermal bremsstrahlung (plus Gaunt factor) fit to the soft X-ray data resulted for a temperature of ~ 5 keV, which was consistent with the bremsstrahlung temperature derived by fitting the HEAO-A2 medium energy X-ray (2-10 keV) data taken simultaneously. (The 2-10 keV data are being analyzed independently by Swank, who communicates a best fit temperature between 4 and 5 keV, and flux of 1.1×10^{-10} ergs $\text{cm}^{-2} \text{s}^{-1}$.) Assuming a temperature of 4.5 keV, we derive a hydrogen column density of $1.7 \left(\pm \begin{smallmatrix} 1.4 \\ 1.0 \end{smallmatrix} \right) \times 10^{21} \text{ cm}^{-2}$. This is in excess of the column density of $6 \times 10^{20} \text{ cm}^{-2}$ obtained using 21 cm measurements (Heiles 1975). Using these spectral parameters, we derive an average source flux of 8.6 ± 10^{-11} ergs $\text{cm}^{-2} \text{s}^{-1}$ in the bandpass of 0.7- 2 keV, and, utilizing the medium energy X-ray data, a total X-ray luminosity for the source of $\sim 2.4 \times 10^{32} \times (d/100 \text{ pc})^2 \text{ ergs s}^{-1}$ ($E = 0.15\text{-}10 \text{ keV}$).

3 DISCUSSION

3.1 COMPARISON WITH OTHER DWARF NOVAE

Among the dwarf novae, only EX Hya, SS Cyg and possibly AY Lyr have been found to emit X-rays during optical quiescence, and only U Gem and SS Cyg have been detected during optical outbursts. Other members of this class have been observed by HEAO-1, but no X-ray emission was detected from them (Córdoba et al. 1977). The HEAO-A2 upper limits on the hard X-ray (2-10 keV) emission from these other systems are ~ 15 times less than the flux detected from SS Cyg and EX Hya. Upper limits on the hard X-ray emission from 45 dwarf novae using Ariel V data have been measured by Watson, Sherrington & Jameson (1978).

It is interesting to compare the X-ray behavior of EX Hya with that of SS Cyg during optical quiescence. In Table 1 we summarize the spectral and temporal information which has been accumulated on these systems to date. Both SS Cyg and EX Hya have "hard" X-ray spectra, i.e., both were observed at $E > 0.5$ keV. Both have iron line features with equivalent widths expected for a gas of cosmic abundance at their respective temperatures. In addition, from measurements widely separated in time, it appears that the temperature of these systems can change by a factor of two, or greater. It is interesting to note from Table 1 that although the temperature of EX Hya changed by a factor of two between the OSO-8 satellite measurement (9.4 keV; Mushotzky et al. 1978) and the measurement of 4.5 keV reported here, the 2-10 keV flux did not change. This will be important in an interpretation of the mechanics of the X-ray production; see below.

As far as the temporal behavior is concerned, large intensity changes have been seen on the timescale of days or hours for both of these systems, and on the timescale of minutes for SS Cyg. The intensity variations of EX Hya reported here concern only the 0.5-3 keV band, and the finest time resolution is only 1.2 hours.

3.2 APPLICATION OF THEORETICAL MODELS

For the following discussion, we hypothesize that the X-rays are produced by accretion onto a degenerate dwarf. Recently, several models have been proposed.

I. Cold matter is shock heated as it falls radially onto a *strongly magnetic white dwarf*. Electrons, heated by collisions with the infalling heated ions, radiate through the cyclotron and bremsstrahlung processes. Some of this radiation is absorbed by the white dwarf, and reemitted as blackbody radiation. The resulting three-component spectrum (Masters 1978) has a hard X-ray bremsstrahlung component ($T_{\text{brem}} = 10^8 - 10^9$ K), a soft X-ray component ($T_{\text{bb}} = 10^5 - 10^6$ K), and a component due to the optically thick cyclotron radiation which peaks in the UV or optical region of the spectrum. The apportionment of the total flux among these components depends on the white dwarf mass, the magnetic field strength, and the accretion rate. To interpret the data in terms of Master's model, one needs to know the spectral flux in both the soft and hard X-ray components, and the respective temperatures, T_{bb} and T_{brem} . However, for EX Hya no soft X-ray flux was detected. This may be due to interstellar extinction, or the consequence of having a blackbody temperature $\lesssim 10$ eV, in which case the flux would be at wavelengths too soft for HEAO-1 to detect.

The low bremsstrahlung temperature of 5-10 keV implies, according to the Masters model, that we are in the regime where cyclotron cooling dominates over bremsstrahlung cooling, and that the mass of the white dwarf is $\sim 0.4 M$, and $B \geq 5 \times 10^7$ gauss. A large cyclotron plus black-body flux of 10^{-9} ergs cm^{-2} s^{-1} at temperatures less than 1×10^5 K is predicted. The optical colors of EX Hya ($B-V = -0.7$, $U-B = -1$; Mumford 1967) imply a temperature in excess of 20,000 K, and U band flux of $\sim 6 \times 10^{-11}$ ergs cm^{-2} s^{-1} . Since this contribution is also well below the predicted flux, most of the luminosity of the system would have to be emitted at ultraviolet wavelengths ($3 \times 10^4 \text{ K} \lesssim T \lesssim 1 \times 10^5 \text{ K}$). Although this model has been applied with some success to AM Her, which is believed to have a magnetic field $B \sim 10^8$ gauss, the model may not be particularly appropriate for EX Hya, for the following reasons.

(1) There is no evidence for a dependence of the X-ray intensity of EX Hya on orbital phase, as would be expected if a strong magnetic field forced the white dwarf to corotate with the binary period, and funnelled the accreting matter onto a fraction of the stellar surface. In AM Her there is a marked variation in both its hard and soft X-ray light curves (Swank et al. 1977; Tuohy et al. 1978). Of course, the observation described in this paper is insensitive to a coherent modulation which is much faster than the orbital period (e.g., DQ Her). There is no evidence from published optical data that such a fast oscillation exists in EX Hya.

(2) Optical observations also constrain the magnetic field strength to be much less than that of AM Her. The observation of line doubling

in EX Hya is interpreted as due to the presence of an accretion disc. In addition, many dwarf novae show emission lines with long wings which, if interpreted as due to Doppler broadening from rotation of the inner disc, imply velocities so large that the disc must extend nearly to the white dwarf surface (see Robinson 1976 for arguments).

A large magnetic field is expected to break up a disc at the radius where the energy density of the infalling material is equal to the magnetic energy density. Computing this radius requires knowledge of the density of the disc. The spectroscopic data on AM Her (see the review by Angel 1978) indicate that this radius must be $\gtrsim 10$ white dwarf radii. The absence of line doubling in AM Her and the fact that the emission lines have no steady broad component, are also consistent with a large magnetic field. More detailed optical spectroscopy, as well as circular polarization measurements of EX Hya are required, but from the evidence already in hand, the system does not appear similar to AM Her.

(3) The Masters model predicts a correlation between spectral temperature and L/f , where L is the total luminosity and f is the fraction of the white dwarf surface onto which the matter accretes. In Table 1 we list the temperature and flux detected from the source during two observations, widely separated in time. Note that although the temperature changed by a factor of two (from 9.8 keV to 4.5 keV), the flux remained the same. One plausible, if ad hoc, resolution is to postulate that f was greater when the accretion rate was higher (i.e., for the higher temperature observation).

II. The accretion disc is disrupted by a *weak magnetic field*. In this case the details of spherical accretion onto an essentially nonmagnetic white dwarf may apply. To disrupt the disc at a radius

fairly close to the white dwarf surface, say at twice the white dwarf radius, a magnetic field strength $B \sim 3 \times 10^4 \times \rho_{-10}^{1/2}$ gauss is required, where ρ_{-10} is the density of the accreting material. The calculations of Kylafis & Lamb (1978), which include the regime of high accretion rates, apply for $B \approx 6 \times 10^6 (L/10^{36})^{2/5}$ gauss. If their model is applicable to EX Hya, the measured temperature is not the shock temperature, but a bremsstrahlung temperature severely Comptonized because of the heavy inflow of matter. In our passband (0.5-3 keV) we do not have the sensitivity required to detect the kink in the 4.5 keV spectrum predicted for degraded bremsstrahlung emission. With respect to the lack of correlation between the temperature and luminosity, we must again insist, as we did in the previous model, that the fraction of the surface onto which the matter accretes changes when \dot{M} changes. For a weak magnetic field cyclotron cooling is unimportant, but a blackbody component, resulting from the energy lost by the absorbed and reflected photons, is still required.

III. It is clear from the hard X-ray temperature, and the presence of an iron line feature in both EX Hya and SS Cyg that the X-ray emission during optical quiescence is not coming from an optically thick boundary layer (Pringle 1977). However, X-rays may be produced in *strong shocks in an optically thin boundary layer* where the accretion disc grazes the white dwarf surface. Pringle & Savonije (1978) show that for low accretion rates ($\approx 10^{16} \text{ g s}^{-1}$) X-ray emission with temperatures up to $2 \times 10^8 \text{ K}$ is possible. The authors interpret the different X-ray behavior among the cataclysmic variables, and between quiescent and outburst

states for the same dwarf nova, as a consequence of varying rates of accretion. The hypothesis that the accretion is nonradial means that there is no requirement that the X-ray luminosity be dependent on temperature. However, the physics of the boundary layer in accreting white dwarf systems is poorly understood. No well-developed model for nonspherical accretion exists which can describe the physics involved in producing strong shocks, and hence predict the spectral and time-dependent behavior of these systems as a function of the mass accretion rate, plasma temperature, and physical parameters of the accreting white dwarf.

4 CONCLUSIONS

There are several observations which might elucidate the nature of the X-radiation from EX Hya. There is a need for fast-time resolution X-ray measurements over the course of an entire orbital cycle, a measurement of the UV luminosity, and detailed optical spectroscopy with an attempt to derive orbital parameters for the system. We also look forward to a deeper survey of dwarf novae by future spacecraft operating at X-ray and UV wavelengths. Such a study may settle the question as to whether the few dwarf novae detected as X-ray sources are unique among such systems, or brighter due to a fortuitous combination of factors such as distance, magnetic field strength, mass accretion rate, and/or white dwarf luminosity.

Table 1. X-radiation from dwarf novae during optical quiescence.

	EX Hydrae	SS Cygni
(i) Thermal bremsstrahlung temperature (keV)	4.5 ± 0.6 , ⁽¹⁾⁽³⁾	$10 \pm 0.5, 19 \pm 1.5, 30 \pm 10$ ⁽³⁾
(ii) N_H (10^{21} cm^{-2})	1.7 (± 1.4) ^{(1)*}	< 3.6 ⁽³⁾
(iii) Flux ($10^{-10} \text{ erg cm}^{-2} \text{ s}^{-1}$)		
(a) 0.15-0.4 keV	< 0.03 ^{(1)†}	< 0.05 ^{(4)†}
(b) 0.7-2 keV	0.86 ± 0.11 ⁽¹⁾	< 0.7 ^{(4)††}
(c) 2-10 keV	1.18 ⁽²⁾ ; 1.1 ± 0.25 ⁽³⁾	1.6 , range = 50% ⁽³⁾
(iv) Iron line feature		
(a) Line center (keV)	6.35 ± 0.2 ⁽²⁾	6.9 ± 0.1 ⁽³⁾
(b) Equivalent width (keV)	0.53 ± 0.04 ⁽²⁾	0.55 ± 0.02 ⁽³⁾
(v) Range of variability/timescale	3/hours ⁽¹⁾	5/days; ⁽⁵⁾ 2/minutes ⁽³⁾

(1) This paper.

(2) Incorrectly identified by Mushotzky et al. (1978); see Watson et al. (1978).

(3) Swank et al. (OSO-8 and HEAO-A2 hard X-ray results, in preparation).

(4) Córdova et al. (HEAO-A2 soft X-ray results, in preparation).

(5) Ricketts et al. (1978).

* Assumes $kT = 4.5 \text{ keV}$.

† 3σ upper limits for a $kT = 0.02 \text{ keV}$ blackbody.

†† 3σ upper limit for a flat spectrum.

References

- Angel, J. R. P., 1978. Ann. Rev. Astron. Astrophys., 16, 487.
- Bateson, F., 1978. Private communication.
- Córdova, F., Garmire, G. & Tuohy, I., 1978. IAU Circular No. 3235.
- Córdova, F., Tuohy, I. R., Nugent, J. & Garmire, G., 1977. B.A.A.S., 9, no. 4, 592.
- Heiles, C., 1975. Astron. & Astrophys. Suppl., 20, 37.
- Kraft, R. P., 1962. Astrophys. J., 135, 408.
- Kylafis, N. & Lamb, D., 1978. Submitted to Astrophys. J.
- Lampton, M., Margon, B. & Bowyer, S., 1976. Astrophys. J., 208, 177.
- Mason, K. O., Lampton, M., Charles, P. & Bowyer, S., 1978. Astrophys. J. Lett., 226, L129.
- Masters, A. R., 1978. Ph.D. Thesis, University of Illinois, Urbana, Illinois.
- Mumford, G. S., 1967. Astrophys. J. Suppl., 15, 1.
- Mushotzky, R. F., Serlemitsos, P. J., Smith, B. W., Boldt, E. A. & Holt, S. S., 1978. NASA 78097, GSFC.
- Pringle, J. E., 1977. Mon. Not. R. astr. Soc., 178, 195.
- Pringle, J. & Savonije, G., 1978. Preprint.
- Ricketts, M. J., King, A. R. & Raine, D. J., 1978. Submitted to Mon. Not. R. astr. Soc.
- Robinson, E. L., 1976. Ann. Rev. Astron. Astrophys., 14, 119.
- Rothschild, R., Boldt, E., Holt, S., Serlemitsos, P., Garmire, G., Agrawal, P., Riegler, G., Bowyer, S. & Lampton, M., 1979. Space Sci. Instr., in press.
- Schwartz, D., et al., 1978. In preparation.
- Swank, J., Lampton, M., Boldt, E., Holt, S., & Serlemitsos, P., 1977. Astrophys. J. Lett., 216, L71.

Tuohy, I. R., Lamb, F. K., Garmire, G. P., & Mason, K. O., 1978.

Astrophys. J. Lett., 226, L17.

Watson, M. G., Sherrington, M. R. & Jameson, R. F., 1978. Mon. Not. R.

astr. Soc., 184, 79.

Figure Captions

Fig. 1. The X-ray intensity (0.5-3 keV) of EX Hya for 4 days of HEAO-A2 observations beginning 1978 Jan 12.3. Each source transit was ~ 15 seconds long. The significance of the dashed lines and diamonds marking particular transits is explained in the text.

Fig. 2. The X-ray light curve of EX Hya. The data from Fig. 1 have been folded on the 1.6376 h binary period.

Fig. 3. A chi-square grid of hydrogen column density vs. temperature (energy) resulting from fitting the HEAO-A2 low energy X-ray data to a thermal bremsstrahlung spectrum with Gaunt factor. The source transits used in the spectral fitting are marked with diamonds in Fig. 1. The best (minimum χ^2) fit is shown by a cross. The best-fit temperature of 4-5 keV deduced from the HEAO-A2 medium energy X-ray data (2-10 keV) is shown by the double arrow near the top of the figure.

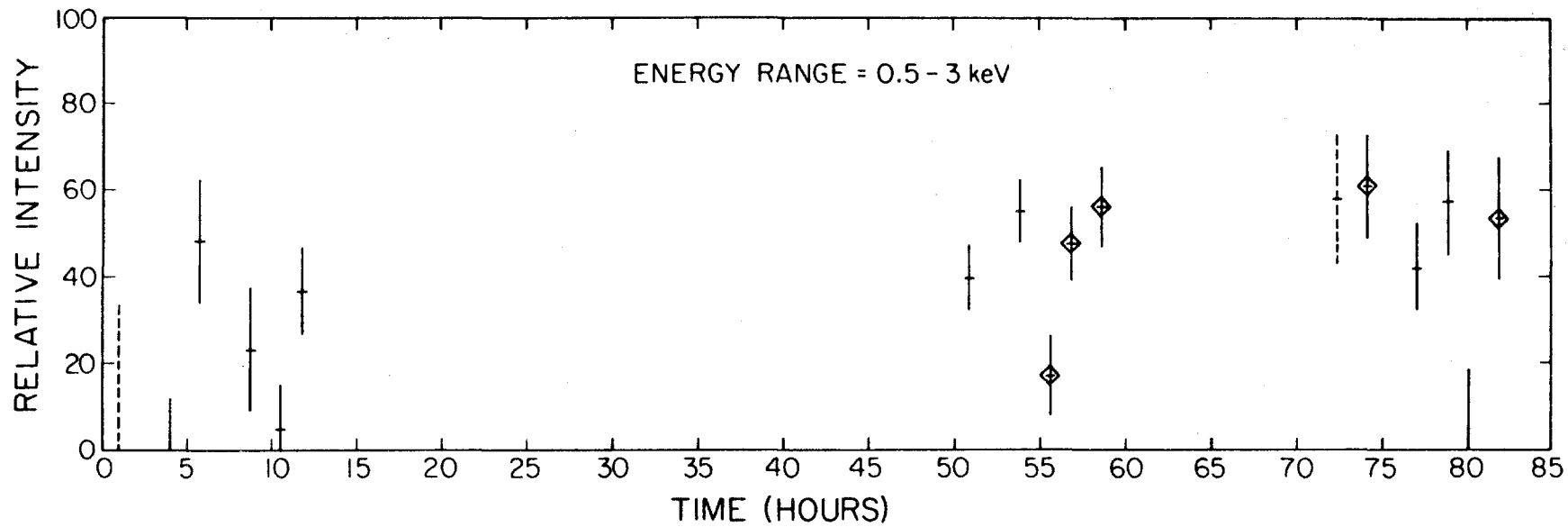


Figure 1

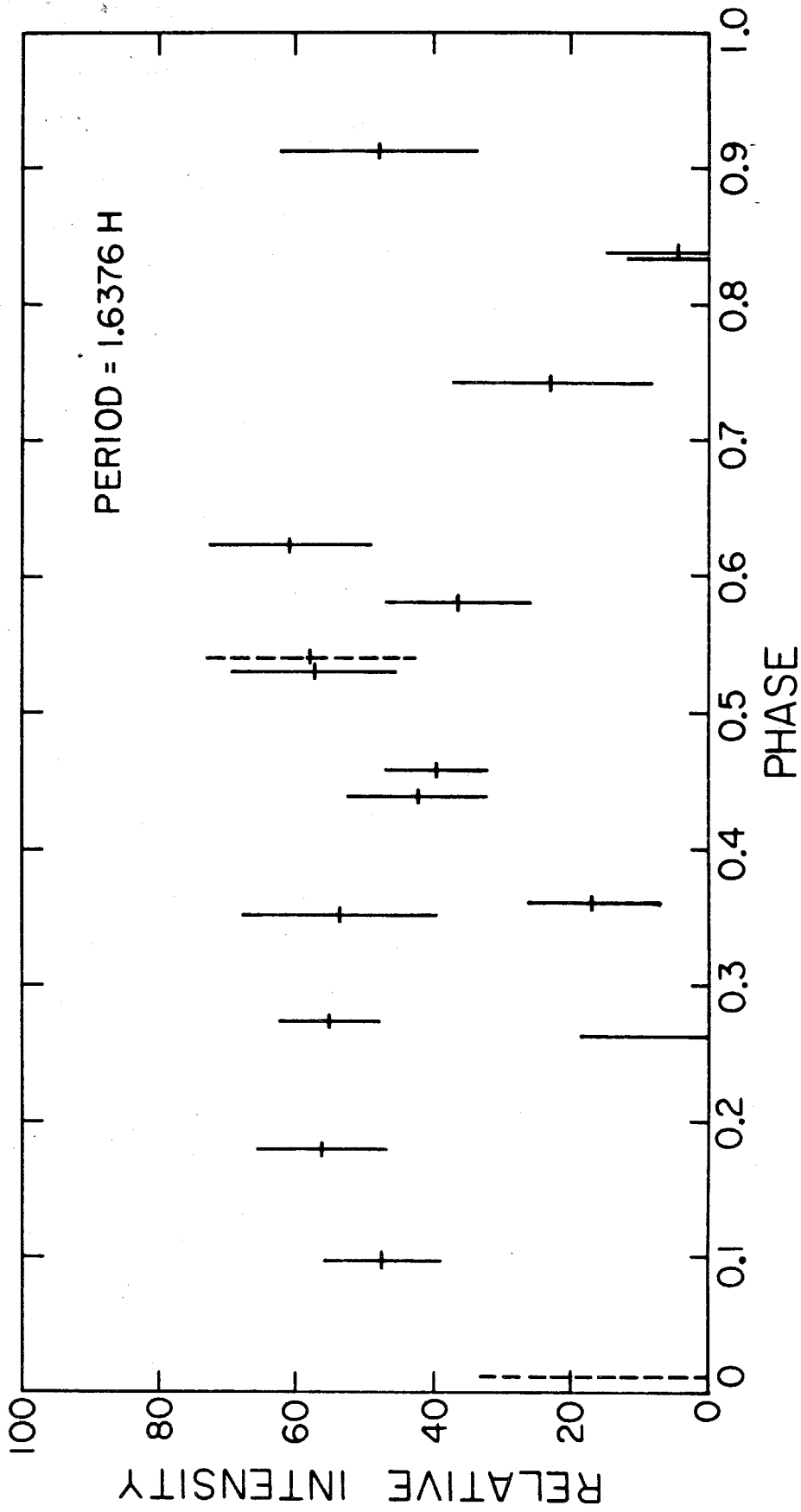


Figure 2

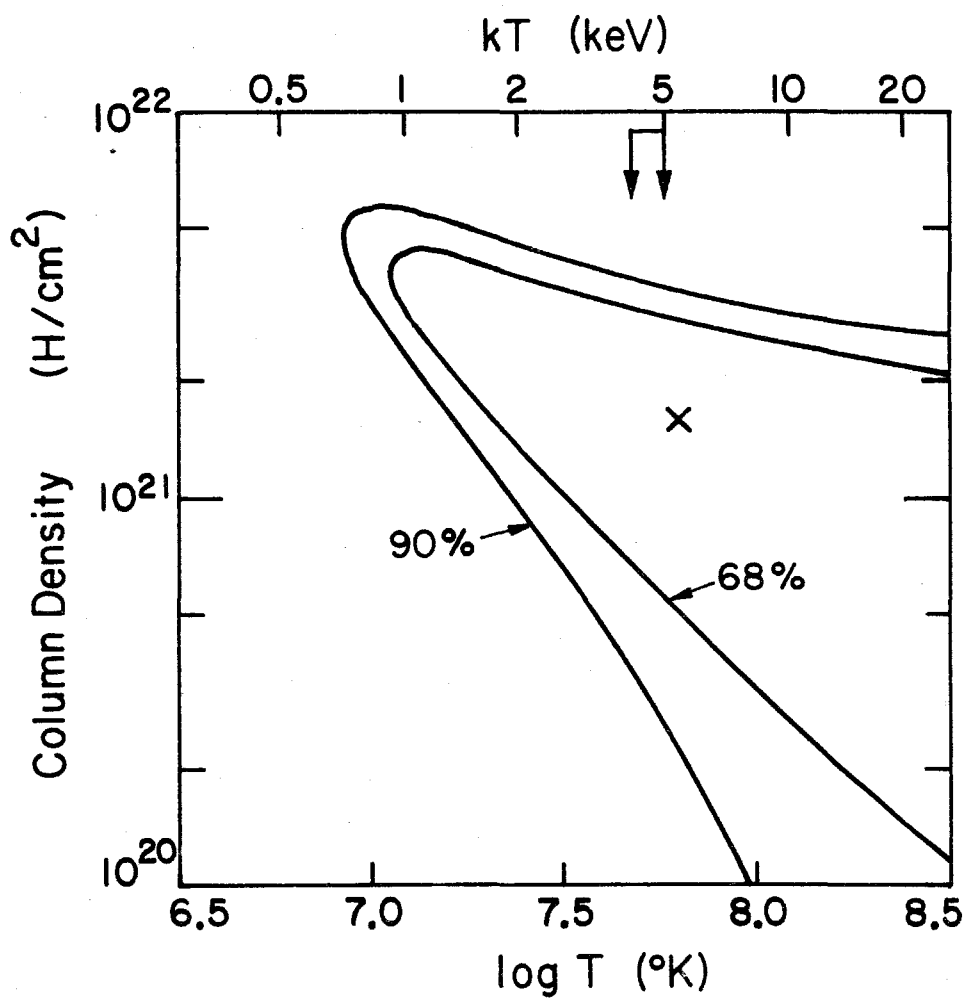


Figure 3

PAPER 5:

SOFT X-RAYS FROM THE VICINITY OF AY LYRAE

accepted for publication in Nature

April 1979

A low-intensity soft X-ray source has been discovered in a region of the sky containing the dwarf nova AY Lyrae. Figure 1 shows how the source, designated H1839+37, appeared in the superposition of HEAO-A2 scanning data that was taken 1977 October 9 with the low-energy detector LED1. The source was detected only in the energy interval 0.18-0.43 keV. The peak in Fig. 1 represents an intensity of 0.014 ± 0.0027 cts $\text{cm}^{-2} \text{s}^{-1}$ (5σ). An upper bound to the temperature of H1839+37 was derived by comparing the ratio of the source counts in different energy bands. If a thermal bremsstrahlung spectrum is assumed, $T_{\text{BR}} \leq 5 \times 10^6$ K, whereas a blackbody fit implies $T_{\text{BL}} \leq 1.4 \times 10^6$ K. A lower limit $T_{\text{BB}} \geq 1 \times 10^5$ K is set by the LED1 lower-level discriminator.

The region of the sky containing H1839+37 was scanned by HEAO-1 for several days. The light curve for the entire 1977 October observation is illustrated in Fig. 2a. Each point is the superposition of 1-5 individual scans made on a given day. For a single day, over

which the spin axis of the satellite is held fixed, an estimate of the variability of H1839+37 can be made independent of knowledge of the exact source position, i.e., without requiring corrections for the transmission of the LED1 collimator. Applying a χ^2 test to the 5 individual scans for October 9 (not shown here), the source is found to be constant at only the 10% confidence level ($\chi^2 = 7.68$ for 4 degrees of freedom). The source is definitely variable on longer timescales because when it was observed 6 months later it was not detected, even in a superposition of 5 1/2 days of scanning data. The upper limit to the intensity for that observation (1978 April 7-12) is $0.005 \text{ cts cm}^{-2} \text{ s}^{-1}$.

The centroid of the position error box for H1839+37 is at $\alpha = 18^{\text{h}} 38^{\text{m}} 58^{\text{s}}$, $\delta = +37^{\circ} 52' 4$ (1950 epoch). The error box, shown in Fig. 3, excludes the bright star Vega (α Lyrae). Also shown is the slightly overlapping error box for 4U1852+37, a hard X-ray source with an intensity of 0.57 ± 0.15 Uhuru flux units (UFU) (Ref 2; Jones 1979, private communication). The HEAO-A2 upper limit for hard X-ray emission from either H1839+37 or 4U1852+37 is 1/3 UFU (Swank, private communication).

H1839+37 was discovered in a survey of ~ 130 cataclysmic variable stars³; it corresponds to the position of one of the members of this class: the dwarf nova AY Lyrae. Three other dwarf novae have been identified with soft X-ray sources: SS Cygni, EX Hydrae, and U Geminorum. This, plus the fact that a search in the H1839+37 error

box has revealed no other promising candidates, make AY Lyr seem like a possible counterpart for H1839+37.

AY Lyr belongs to the subset of dwarf novae that have both normal outbursts and superoutbursts⁴. Patterson (ref. 4) reports that the quiescent visual brightness of the system is $V > 18$. At the time of the HEAO-1 sighting on 1977 October 9, AY Lyr was at $V > 14.8$ (Mattei, private communication). Assuming a flat response across the LED1 bandwidth, the 1/4 keV flux from a source at the position of AY Lyr is $\sim 1 \times 10^{-11} \text{ erg cm}^{-2} \text{ s}^{-1}$. The ratio of the X-ray to optical flux for the other dwarf novae in quiescence is less than or equal to unity (ref. 3). For AY Lyr, this ratio does not exceed unity only if the dwarf nova was as bright as $V \sim 15$ during the HEAO-1 observation. In Fig. 2b the 1977 October light curve of H1839+37 has been corrected for a source at the position of AY Lyrae, taking into account the transmission of the LED1 collimator. A comparison of the X-ray light curve with the AAVSO visual light curve for AY Lyr, which is shown in Fig. 2c, reveals that there was no increase in the X-ray activity during a short optical outburst of the dwarf nova⁵. There were only three LED1 scans during the October outburst; these occurred 0.4-0.6 days after the beginning of the outburst. A short visual outburst also occurred 1978 April 9 when AY Lyr was again being scanned by HEAO-1 (ref. 5), but no X-rays were detected from the object at that time either.

Part of the difficulty in interpreting this observation is in not having a good measurement of the X-ray spectrum of H1839+37. The

dwarf novae detected as X-ray sources appear to have two very different spectral components: a medium or hard X-ray ($E > 0.5$ keV) component which fits a thermal bremsstrahlung model with line emission⁶, and a soft X-ray ($E < 0.5$ keV) component whose spectrum may fit any of several models (ref. 3). The relative intensities of both components are correlated with the dwarf nova optical outburst. The soft component increases with increasing visual brightness, but the optically thin component is not uniquely correlated: in SS Cyg this component dramatically decreases during outburst⁷, while in U Gem the converse is observed⁸. In addition, the range of temperatures for the "hard" component spans an order of magnitude: from ~ 20 keV for SS Cyg to ~ 5 keV for EX Hya and U Gem (refs. 6 and 8). Therefore, with so few examples and such a wide range of behavior, it is not difficult to invoke a scenario for H1839+37 which is consistent with the X-ray behavior of dwarf novae.

For example, it is possible that in AY Lyr variable accretion onto a white dwarf primary could account for X-ray flaring during quiescence. If the spectrum were optically thin, then absorption by increased infalling material during outburst could produce a decrease in the bremsstrahlung X-rays (an effect similar to that observed in SS Cyg during outburst). The bright soft X-ray excess observed in SS Cyg during outburst may not appear in AY Lyr because the boundary layer between the white dwarf and the compact star in AY Lyr may not get hot enough to radiate soft X-rays. Differences in mass accretion rates during quiescence and outburst among all the dwarf novae may account for the range of observed behavior.

Our intention has been simply to point out a correspondence in the positions of the soft X-ray emitter H1839+37 and the dwarf nova AY Lyr, and to present all the pertinent data on both the X-ray and optical sources. It should be noted that a search of a set of 130 randomly distributed error boxes ($\sim 0.6^\circ \times 6^\circ$ in size), such as the cataclysmic variable survey, would have about a 40% chance of producing a positional coincidence with one or more of the ~ 50 soft X-ray sources in the HEAO-A2 Catalogue (in preparation). Thus there was a relatively high expectation of finding one fortuitous association of an X-ray source with a cataclysmic variable. If H1839+37 has a "steady" emission even a factor of ten below the HEAO-1 threshold, the X-ray telescope on the recently launched Einstein Observatory (HEAO-2) should be able to accurately locate it.

References

- 1 Rothschild, R. et al. Space Sci. Instr., 4, (in the press).
- 2 Forman, W. et al. Astrophys. J. Suppl. 38, 357 (1978).
- 3 Córdova, F. Ph.D. thesis (1979), California Institute of Technology.
- 4 Patterson, J. Astrophys. J. (submitted).
- 5 Bortle, J. AAVSO Circulars No. 85 (1977) and No. 91 (1978).

Additional information provided by AAVSO; Mattei, private communication.

- 6 Córdova, F. A. & Riegler, G. R. Mon. Not. R. astr. Soc. (in press).
- 7 Ricketts, M. J., King, A. R. & Raine, D. J. Mon. Not. R. astr. Soc. 186, 233 (1979).
- 8 Swank, J. H. et al. Astrophys. J. Lett. 226, L133 (1978).

Figure Captions

Fig. 1. A portion of the data from a superposition of soft X-ray (0.15-0.43 keV) scans on 1977 October 9. The intensity of the source at scan angle 61° was determined by making a least squares fit (the smooth line) to the data. The fitting procedure took into account the triangular response of the collimator, which had a 1.5° field of view (FWHM) in the scan direction. The area of the detector was 174 cm^2 .

Fig. 2a. The soft X-ray light curve of H1839+37 for 1977 October.
b. The light curve of H1839+37 corrected for a source at the position of AY Lyr. c. The AAVSO visual light curve for AY Lyr covering the HEAO-1 observation.

Fig. 3. H1839+37 error box (90% confidence), also showing the positions of Vega, the dwarf nova AY Lyrae, and the error box for a 4U source.

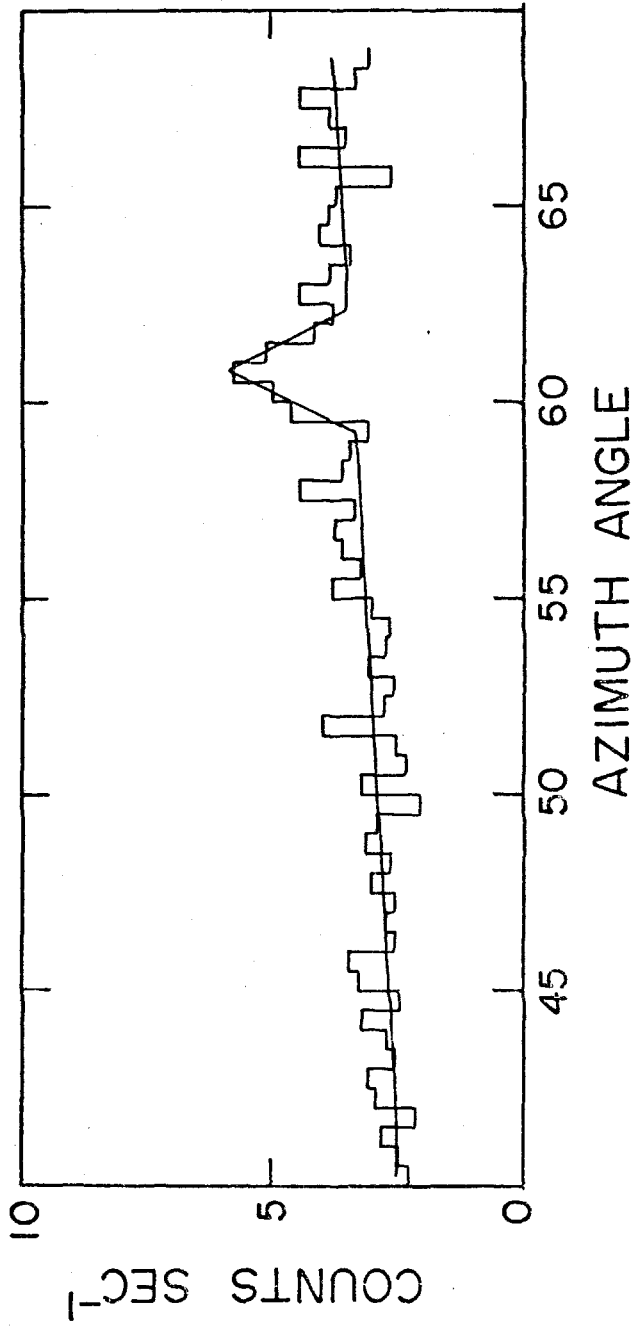


Fig. 1

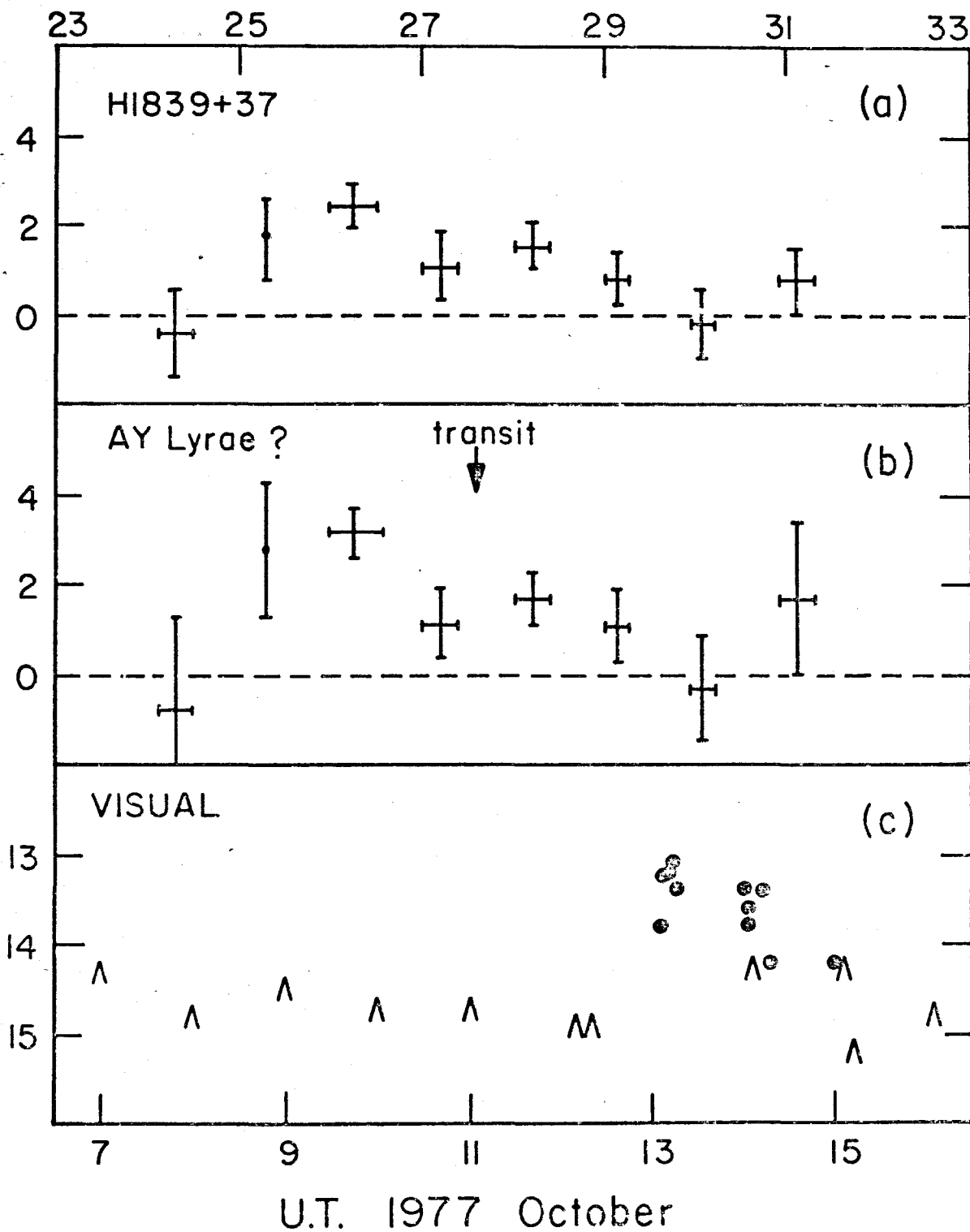
JD2443400⁺

Fig. 2

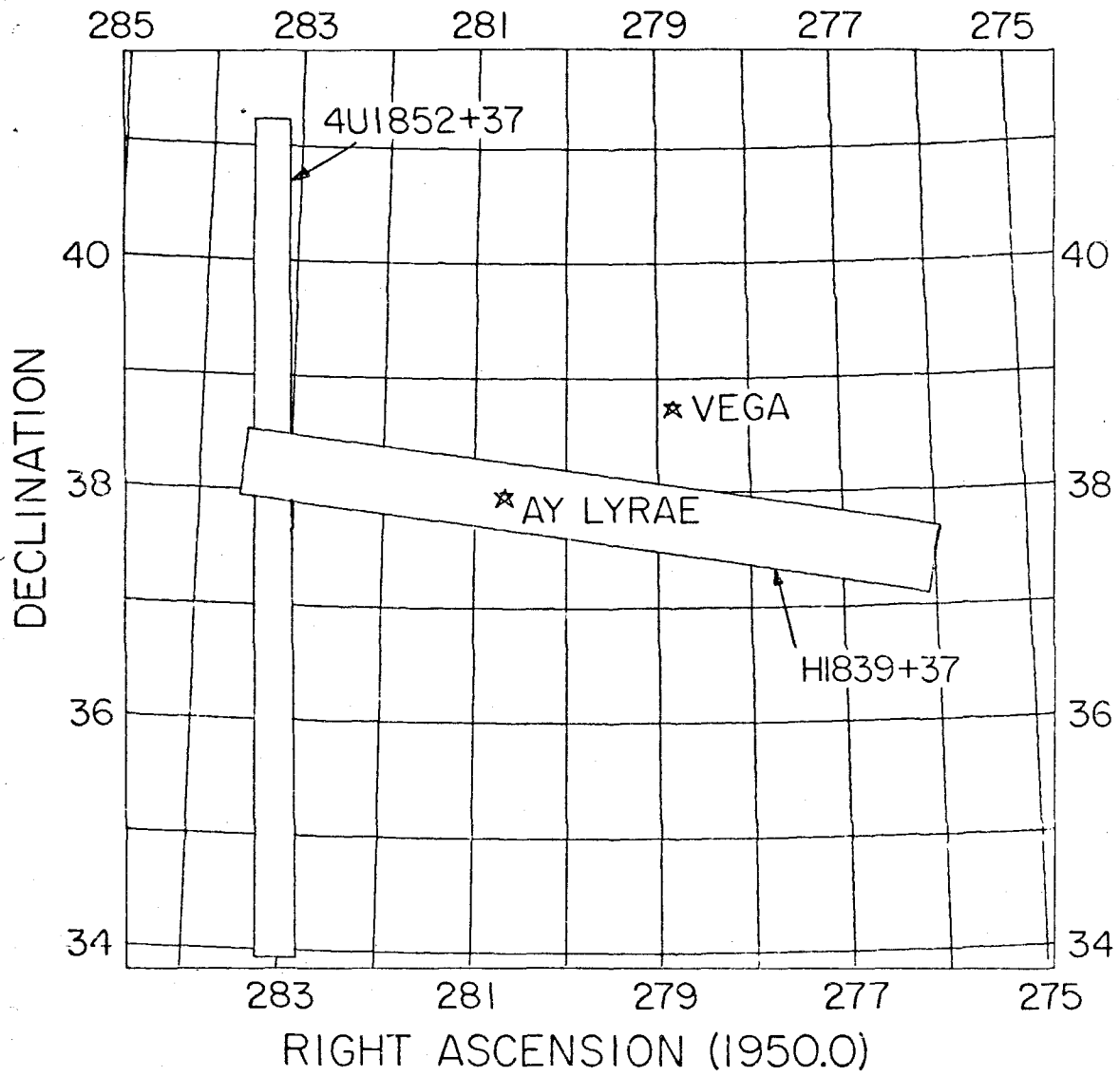


Fig. 3

PAPER 6:
A SOFT X-RAY SURVEY OF
DWARF NOVAE IN QUIESCENCE
in preparation

1 INTRODUCTION

To date, X-ray emission has been reported from the following dwarf novae during quiescence: SS Cygni (Ricketts, King & Raine 1978; Mason, Córdova & Swank 1978; Fabbiano et al. 1978), EX Hydrae (Watson, Sherrington & Jameson 1978 and references therein; Córdova & Riegler 1979), and possibly AY Lyrae (Córdova & Garmire 1979). The discoveries of soft X-ray emission from EX Hya and AY Lyr were made during a systematic search for soft X-rays (0.2-3 keV) from ~ 130 cataclysmic variables using HEAO-1 data. The results of the survey have been reported for dwarf novae in outburst (Córdova et al. 1979). Here we report the upper limit to the soft X-ray flux from dwarf novae during their optically quiescent state. Our derived flux limit is an average over the entire sample of well-known dwarf novae; we do not present upper limits for individual objects. Our intention is to provide a useful number for application in theories attempting to explain the mass accretion process in dwarf novae and the origin of the dwarf novae visual luminosity. The individual flux limits for selected prominent dwarf novae will be presented later in connection with our HEAO-A2 (Einstein Observatory) guest investigatorships of ~ 20 cataclysmic variables.

2 THE EXPERIMENT AND THE SURVEY

All of the data for this survey were taken with one of the low energy detectors of the A2 experiment on HEAO-1. LED1 is a collimated gas proportional counter with an area of 174 cm^2 and sensitivity in the energy range 0.18-3 keV. In the nominal scanning mode of HEAO-1, the detector sweeps out a band 3° (FWHM) wide in a great circle perpendicular to the Earth-Sun line. For the survey described here only the narrowest field of view of 1.5° (FWHM) in the scanning direction was used in order to limit the contribution of the diffuse X-ray background. The X-ray observatory rotated once every ~ 33 min, thus exposing a source in this field of view for ~ 8 s per rotation. On average, only 4 LED1 scans per day provided useful data. Each source remained in the LED1 field of view for at least a few days, depending on its ecliptic latitude. The entire sky was scanned by HEAO-1 in a 6 month period.

The survey described here was accomplished by determining the times of HEAO-A2 transit of each of the ~ 65 dwarf novae that are monitored by the American Association of Variable Star Observers and the Royal Astronomical Society of New Zealand Variable Star Section

(see Table 1 for a listing of these objects). Knowing the satellite aspect from an on-board star camera, the positions of each of these objects along the satellite scan path could be determined. We then determined the background level at the source location on the date of transit. The data base spans the first 6 months of HEAO-1 observations (Aug. 18, 1977-Feb. 18, 1978).

A technique used to increase our sensitivity to weak sources was to superpose for each day all the scans made that day. For this preliminary survey our search was limited to looking at each of the individual days of superpositions, rather than one superposition over all the days of possible viewing. This method is favored for variable emitters, whose intensity is only a fraction of the bright and (spatially) variable X-ray sky. (See, for example, the observation of AY Lyrae in Córdova & Garmire 1979; the enhanced X-ray background in the region of AY Lyr made the source, which was observed at 5σ level on one day only, disappear in the background noise when several adjacent days were added together.) Work is in progress to superpose several adjacent days of data to search for constant sources below the limits quoted here.

Another technique for detecting weak sources, whose emission was limited to only a certain portion of the total LED1 energy interval, made use of the detector electronics which sorted the event rates into broadband scalers. All scalers were visually inspected for the signatures of point sources. Since the evidence from known dwarf novae X-ray emitters reveals a well-resolved two-component spectrum (with $E \sim 0.5$ keV as the apparent dividing line), we made separate evaluations of the flux limits for scalers spanning the intervals 0.18-0.43 keV and 0.74-2 keV.

3 RESULTS

The results are summarized in Table 2. For each energy interval the average background rate is given. This is followed by the upper limit for a nominal value of four scans (the upper limit was calculated using the prescription of Gursky & Schwartz 1974). The conversion to flux units is given for an assumed flat spectrum across the band, and including the average detector efficiencies (Rothschild *et al.* 1979). For comparison, the rates (with a 20% correction for the collimator transmission) for EX Hya (ten scans over two days) and AY Lyr (four scans on one day) are also given.

4 DISCUSSION

4.1 A REVIEW OF X-RAY BEHAVIOR OF DWARF NOVAE

Dwarf novae appear to have a two-component high-energy spectrum: a soft, perhaps optically thick component with $kT < 50$ eV and a "hard," optically thin component with $kT > 2$ keV. There is evidence that both components may be present at some level all the time, although the correlation of the temperature and luminosity with outburst phase does not appear to be simple.

We have previously investigated numerous hypotheses for the failure to detect soft X-rays from ~ 25 erupting dwarf novae (Córdova *et al.* 1979). We concluded, from an analysis of the spectrum of SS Cygni and U Geminorum, the only dwarf novae detected during outburst, that the temperatures of most of the nondetected objects were probably so low that most of their emission was in the EUV, below the HEAO-1 low-energy

threshold; although for any individual source other factors, such as distance and variable absorption, could also be important. The same arguments may also apply for the soft X-ray component of dwarf novae during quiescence. The evidence suggests that the rate of accretion onto the white dwarf during minimum may be 10-100 times lower than the outburst accretion rate (Warner 1976); the luminosity is probably a sensitive function of this rate (Pringle 1977).

The flux from AY Lyrae during quiescence ($\sim 1 \times 10^{-11}$ erg cm⁻² s⁻¹ in the 1/4 keV band) is rather surprising if interpreted as due to an optically thick component with $T \sim 3 \times 10^5$ K (i.e., the spectrum of U Gem and SS Cyg during outburst), in view of the fact that AY Lyr was at $V > 15$ mag during the observation, and no X-ray emission was detected from many optically brighter objects. A second thorn in this model is that during an outburst of AY Lyr three days after its detection there was no apparent X-ray emission from the source. We might, however, interpret the AY Lyr X-ray flux during quiescence as due to a variable, optically thin component whose origin is the same as that of the hard X-ray components of EX Hya and SS Cyg during quiescence (Córdova & Riegler 1979). Then we might understand AY Lyrae's outburst behavior as due to a softening of the source spectrum resulting from absorption of the X-ray flux by the accreting material. Such a scenario may also be evoked to explain the behavior of SS Cyg: the outburst flux at optical minimum is seen to rise sharply at the beginning of the outburst and quickly diminish (within a day) below the preoutburst level (Ricketts, King & Raine 1979). Swank (1979) reports that when

SS Cyg was at the peak of an optical outburst there was a residual hard X-ray flux with $kT < 10$ keV (in contrast to Swank's measurement of 20 keV for an optically quiescent period six months earlier) and an intensity four times lower than the quiescent state intensity.

During quiescence, the hard X-ray fluxes measured for SS Cyg and EX Hya ($\sim 2 \times 10^{-10}$ erg cm⁻² s⁻¹) are of the same order as the optical fluxes (3400-6000 Å) measured for these systems. Thus a large part of the optical emission may be reprocessed X-ray emission. It might be supposed that all dwarf novae should have an X-ray component to account for the bulk of the optical luminosity, and that the X-ray flux during quiescence should scale approximately as the apparent optical magnitude (of course, the outer parts of the disk itself must make an unspecified contribution to the visual light).

The brightness of the dwarf novae in our survey is mostly concentrated within four magnitudes ($\sim 12^m-16^m$); SS Cyg and EX Hya are among the brightest at minimum light, with apparent visual magnitudes of ~ 12 and ~ 13 respectively. For many dwarf novae in the survey $V \sim 14$; U Gem is an example. Thus, in visual light these latter systems are a few times fainter than EX Hya. Our soft X-ray upper limits are only four times lower than the observed flux from EX Hya; thus our observations are consistent with the quiescent visual magnitude relationships between dwarf novae. The differences in apparent magnitudes among the objects may be due to the effects of inclination to the observer and distance, among other things.

EX Hya and SS Cyg are probably unique in some aspect; they may have more intense magnetic fields or higher white dwarf masses -- either of which could stimulate a higher mass accretion rate during quiescence.

4.2 THEORETICAL CONSIDERATIONS

The X-ray observations of dwarf novae during quiescence are inconclusive; it is difficult to interpret such a wide variety of behavior from such a small number of systems. One interesting start in this direction is the scenario envisioned by Pringle & Savonije (1978) which interprets the hard X-ray emission as due to strong (radial) shocks in the boundary layer. These shocks will only occur within a restricted range close to $\dot{M} \sim 1 \times 10^{16} \text{ gm s}^{-1}$; for higher accretion rates the hard X-ray emission is absorbed and reemitted at lower temperatures ($\sim \text{few} \times 10^5 \text{ K}$). The recent observation of hard X-rays ($kT = 5 \pm 3 \text{ keV}$) from U Gem during outburst (Swank *et al.* 1978) can also be explained in this model as due to an increase in mass accretion from a rate somewhat less than $10^{16} \text{ gm s}^{-1}$ up to this critical value for the production of hard X-rays. In this model, SS Cyg may have an accretion rate at maximum $\dot{M} \gtrsim 10^{17} \text{ gm s}^{-1}$. If the optical light at minimum is largely due to reprocessing of the hard X-rays, the differences between the dwarf novae visual magnitudes at minimum may be due more to a variety of mass accretion rates than a variety of distances.

4.3 THE EMISSIVITY OF CATACLYSMIC VARIABLES AND THEIR CONTRIBUTION TO THE X-RAY BACKGROUND

For pedagogical reasons we felt it would be of interest to calculate the volume emissivity of cataclysmic variables in general, and also their contribution to the diffuse X-ray background. These calculations have been carried for dwarf novae in outburst only by Rappaport et al. (1974) who overestimated the luminosity of the majority of dwarf novae, and allowed them a greater space density than is probably correct. Rappaport et al. derived a luminosity about two orders of magnitude smaller than the calculated value required to produce the soft ($E < 0.5$ keV) X-ray background; our survey of dwarf novae in outburst (Córdova et al. 1979) and Warner's (1974) estimation of the space density of dwarf novae increase this discrepancy by two additional orders of magnitude!

Most of the X-ray flux from dwarf novae during visual minimum appears to be emitted at a higher temperature than the flux at outburst. The integrated volume emissivity of the X-ray background between 2 and 10 keV is $\sim 2 \times 10^{30}$ erg pc⁻³ s⁻¹ (Schwartz & Gursky 1974). The upper limit to the hard X-ray (2-25 keV) flux at minimum from at least the few variables examined (e.g., U Gem, AY Lyr, VW Hyi, SS Aur, and the ex-novae DQ Her and RR Pic) is about 15 times lower than the flux from SS Cyg (Swank 1979); therefore, $L_x \lesssim 1 \times 10^{31}$ erg s⁻¹ for these systems, assuming a distance of 100 pc. Warner (1974) estimates that the space density of cataclysmic variables is $n \sim 1 \times 10^{-6}$ pc⁻³, with dwarf novae and ex-novae contributing about equal numbers. Thus we estimate that the emissivity nL_x for all cataclysmic variables is

$\sim 1 \times 10^{25} \text{ pc}^{-3} \text{ s}^{-1}$; this falls short of the emissivity required to produce the X-ray background by $\sim 2 \times 10^5$.

5 CONCLUSION

We have searched for soft X-ray flux from a sample of ~ 65 dwarf novae during optical quiescence and found X-ray emission from the vicinity of only two of these objects. Our upper limits to the soft X-ray emission from the remainder of the dwarf novae are only two or three times less than the observed intensities of AY Lyr and EX Hya. Thus a deeper survey may produce more detections. Alternatively, the range in observed temperatures is so large (from $\sim 3 \times 10^5$ K for SS Cyg and U Gem during outburst to $\sim 2 \times 10^8$ K for SS Cyg during quiescence) that both the soft and hard X-ray components in many of these systems may be outside our detector bandpass. Thus it is also of interest to do surveys for EUV and hard ($E > 2$ keV) X-ray emission from these stars.

A fruitful investigation would be hard X-ray observations throughout the outburst cycle to search for spectral softening and intensity variability; particularly illuminating would be simultaneous soft and hard X-ray observations throughout the duration of an outburst to look at the relationship between the spectral components. In addition, pointing observations of SS Cyg and EX Hya in hard X-rays might reveal the nature of the hard X-ray component. A particularly vexing problem is the relationship of the hard X-ray emission to the soft, pulsing component which appears during outburst in U Gem and SS Cyg (Córdoba 1979 and references therein).

Note added in proof:

Soft X-rays (0.7-2 keV) from the dwarf nova SS Aurigae have been recently detected using HEAO-1 data superposed over several adjacent days (Agrawal 1979, private communication). The weak detection ($3-4\sigma$) at 0.84 ct s^{-1} is consistent with the upper limit of 0.9 ct s^{-1} reported here.

Table 1

Dwarf Novae in the Survey

RX And	TU Leo
AR And	AY Lyr
DX And	CY Lyr
UU Aql	LL Lyr
VZ Aqr	EQ Mon
EY Aql	V2051 Oph
SS Aur	CN Ori
TT Boo	CZ Ori
UZ Boo	RU Peg
Z Cam	TZ Per
AF Cam	UV Per
SY Cnc	UW Per
YZ Cnc	FO Per
AA Cnc	KT Per
SV CMi	TY Psc
HT Cas	BV Pup
KU Cas	RZ Sge
Z Cha	WZ Sge
WW Cet	UZ Ser
BV Cen	HW Tau
V436 Cen	SU UMa
AL Com	SW UMa
SS Cyg	BC UMa
EM Cyg	TW Vir
EY Cyg	
V630 Cyg	
V632 Cyg	
V811 Cyg	
AB Dra	
AH Eri	
AQ Eri	
U Gem	
AW Gem	
IR Gem	
AH Her	
CH Her	
AG Hya	
EX Hya	
VW Hyi	
WX Hyi	
X Leo	
T Leo	
TT Leo	

Table 2. Dwarf novae in quiescence: Upper limits and comparison stars

Source Designation	Energy Interval (keV)	Source Rate (ct s ⁻¹)	3 σ Upper Limit (ct s ⁻¹)	Flux (10 ⁻¹¹ erg cm ⁻² s ⁻¹)
Survey star	0.18-0.43		1.5	0.7
AY Lyrae	"	3.0 \pm 0.6		1.4
Survey star	0.74-2		0.9	2.8
EX Hydrae	"	2.9 \pm 0.4		8.5

References

- Córdova, F. A., 1979. Ph.D. thesis.
- Córdova, F. A., Nugent, J. J., Klein, S. R. & Garmire, G. P., 1979.
Submitted to Mon. Not. R. astr. Soc.
- Córdova, F. A. & Garmire, G. P., 1979. Submitted to Nature.
- Córdova, F. A. & Riegler, G. P., 1979. Mon. Not. R. astr. Soc., in press.
- Fabbiano, G., Gursky, H., Schwartz, D. A., Schwarz, J., Bradt, H. V.
& Doxsey, R. E., 1978. Nature, 275, 721.
- Gursky, H. & Schwartz, D., 1974. In X-ray Astronomy, eds R. Giacconi
& H. Gursky, Dordrecht, Reidel.
- Mason, K. O., Córdova, F. A. & Swank, J. H., 1978. Proc. of the
COSPAR Symposium, Innsbruck, Austria, June 1978.
- Pringle, J. E., 1977. Mon. Not. R. astr. Soc., 178, 195.
- Pringle, J.E. and Savonije, G.J., 1978, preprint.
- Rappaport, S., Cash, W., Doxsey, R., McClintock, J. & Moore, G., 1974.
Astrophys. J. Lett., 187, L5.
- Ricketts, M. J., King, A. R. & Raine, D. J., 1979. Mon. Not. R. astr.
Soc., 186, 233.
- Rothschild, R., Boldt, E., Holt, S., Serlemitsos, P., Garmire, G.,
Agrawal, P., Riegler, G., Bowyer, S. & Lampton, M., 1979. Space
Sci. Instr., 4, in press.
- Schwartz, D. & Gursky, H., 1974. In X-ray Astronomy, eds R. Giacconi
& H. Gursky, Dordrecht, Reidel.
- Swank, J. H., 1979. Private communication.
- Swank, J. H., Boldt, E. A., Holt, S. S., Rothschild, R. E. & Serlemitsos,
P. J., 1978. Astrophys. J. Lett., 226, L133.

- Warner, B., 1976. In Structure and Evolution of Close Binary Systems,
ed P. Eggleton et al., Dordrecht, Reidel.
- Watson, M. G., Sherrington, M. R. & Jameson, R. F., 1978. Mon. Not.
R. astr. Soc., 184, 79.

SUMMARY

In the discussion sections of the papers included here we have examined the merits of previous models for the nature of the X-ray emission, and shown how our observations constrain future theoretical work. We now enumerate the highlights of our investigation, including the work of other experimenters as well. For convenience, we have listed all X-ray observations of dwarf novae in the accompanying Table.

1. *The X-rays provide only a small fraction of the outburst luminosity.* Dwarf novae appear to be low-luminosity sources at all wavelengths and at all phases of the light curve. Even during eruptions their absolute visual magnitude, M_V , is ≥ 3 ; thus their maximum luminosity is only slightly greater than that of the Sun. The ratio of the X-ray to optical luminosity is ≈ 1 during quiescence, but during outburst it is $\leq 10^{-2}$. Optical observations of Z Cha, a dwarf nova which shows a prominent eclipse of the entire disk and the compact star, reveal that during quiescent light the dominant emission appears to come from areas near the white dwarf and from the bright spot at the outer edge of the disk, but during outburst the visual light comes from a brightening of the entire disk (Warner 1974).

2. Unlike most of the visual light, *the X-ray emission appears to come from a region near the white dwarf at all phases of the light curve.* The visual light curves of both U Gem and EX Hya show eclipses of the bright spot. Yet in long HEAO-1 pointing observations, neither the hard X-rays from EX Hya (Swank 1979), nor the soft X-rays from U Gem (reported here), showed evidence for eclipses. Thus

TABLE

X-RAY OBSERVATIONS OF DWARF NOVAE

OB = outburst
Q = quiescence

	<u>Detecting Instrument</u>	<u>Energy band (keV)</u>	<u>Flux ($\text{erg cm}^{-2} \text{s}^{-1}$)</u>	<u>Reference</u>	
A.	<u>SS Cyg</u>				
	OB	MIT rocket	0.15 - 0.28	5×10^{-10}	15
	OB	SAS-3	0.15 - 0.28	$(3-5) \times 10^{-11}$	7
	same OB	ASTP "	0.08 - 0.25 "	9×10^{-11} $< 1.5 \times 10^{-11}$	10 "
	same OB	HEAO-1 "	0.13 - 0.5 2 - 25	4.5×10^{-11} 4×10^{-11}	1 17,4
	same Q	ANS "	0.15 - 0.28 1 - 7	4×10^{-12} 7×10^{-11}	8 "
	same Q	HEAO - 1 " "	0.15 - 0.5 0.7 - 2 2 - 25	$< 5 \times 10^{-12}$ $< 7 \times 10^{-11}$ 1.6×10^{-10}	4 4 11,5
	Q	Ariel V	2 - 18	$(2-5) \times 10^{-10}$	16
B.	<u>U Gem</u>				
	same OB	HEAO - 1 "	0.15 - 0.5 2 - 10	2×10^{-10} 2.4×10^{-11}	12 18
	OB	HEAO - 1	0.13 - 0.5	9×10^{-11}	3
	same Q	HEAO - 1 "	0.15 - 0.5 2 - 15	$< 1 \times 10^{-12}$ $< 5 \times 10^{-12}$	12 18
	Q	Ariel V	2 - 18	$< 1.9 \times 10^{-11}$	21
C.	<u>EX Hya</u>				
	Q	Uhuru	2 - 7	7.7×10^{-11}	6
	Q	Ariel V	2 - 18	7.6×10^{-11}	21
	Q	OSO - 8	2 - 10	1.1×10^{-10}	13
	same Q	HEAO - 1 " "	0.15 - 0.5 0.7 - 2 2 - 10	$< 3 \times 10^{-12}$ 8.6×10^{-11} 1.2×10^{-10}	4 4 17,4
D.	<u>AY Lyr</u>				
	Q	HEAO - 1	0.15 - 0.5	1×10^{-11}	2

the X-ray emission, at least during the pointing observations accomplished to date, did not come from the bright spot. The temperature of the hard component plus the short timescale of the pulsations in the soft component are evidence that both the hard and soft X-ray sources are associated with the white dwarf or inner regions of the disc.

3. *The outburst is probably due to enhanced mass accretion throughout the disk, and not to thermonuclear burning.* The white dwarf participates in the outburst (evidence the hard X-ray flare at the beginning of the outburst in both SS Cyg and U Gem, and the soft X-ray pulsations during outburst in both these systems). It is still not clear, however, exactly how the outburst is triggered, or just what part (i.e. active/passive) the white dwarf plays in the outburst.

The clearest evidence for a mass accretion event rather than nuclear burning as the outburst energy source comes from changes in the X-ray spectrum at the start of an eruption. The observed spectrum has at least two components: a hard ($E > 2$ keV) component that fits a thermal bremsstrahlung spectrum (note Iron emission lines) and a soft ($E < 0.5$ keV) component whose spectral nature is uncertain due to poor energy resolution at these wavelengths. Neither component shows much evidence for absorption: for the hard X-ray spectrum $N_H \leq 10^{22} \text{ cm}^{-2}$, (the HEAO-1 medium energy detector is insensitive to a smaller N_H), while for the soft X-ray spectrum $N_H \leq 10^{21}$.

The soft X-rays appear at a significant level only during outburst; at that time the soft X-ray intensity increases by ~ 100 times. The observations are, at present, simply not extensive enough to show how the soft X-ray intensity depends on the outburst phase; therefore, it cannot be determined exactly how the soft and hard X-ray components are related.

No hard X-rays are observed from U Gem during quiescence, but during outburst they appeared (in the only such observation reported to date) along with the optical rise to peak light. The hard X-ray emission was strongest on the first day of the outburst and thereafter either decreased or disappeared; the observations were not sensitive enough to distinguish between these possibilities.

In contrast, for SS Cyg the hard X-ray emission was observed during quiescence at a level at least 15 times greater than for any other dwarf nova except EX Hya. On the rise to visual outburst this hard component increased sharply by two to three times, and just as sharply decreased in less than a day to a factor of four below its quiescent state intensity. The temperature also dropped: from 20 keV to less than 10 keV, but with no measurable increase in N_H (Swank 1979).

This is exactly the behavior predicted by Kylafis et al. (1978) for degenerate dwarfs undergoing variable mass accretion. The authors have shown that the X-ray and UV spectrum depends sensitively on the mass accretion rate and on the white dwarf mass.

The spectrum produced by accretion onto non-magnetic degenerate dwarfs has three components: i) a hard X-ray bremsstrahlung component produced by the hot, post-shock region where the matter cools and comes to rest on the stellar surface, ii) a soft X-ray blackbody component produced by bremsstrahlung photons that are absorbed by the white dwarf surface and re-emitted, and iii) secondary radiation produced by Compton heating of infalling matter above the shock.

The regimes where the various components dominate are illustrated in Kylafis *et al.* (1978). Basically, for low accretion rates the standoff shock is many white dwarf radii from the central star, and a hard X-ray spectrum with temperatures up to 45 keV may be observed. For a one solar mass white dwarf, a transition occurs at about $\dot{M} \sim 10^{17} \text{ gm s}^{-1}$; this is when the freefall time scale is approximately equal to the cooling timescale (for either bremsstrahlung or Compton cooling). As the accretion rate is increased to $\sim 10^{18} \text{ gm s}^{-1}$ the electron scattering optical depth from the emission region to infinity reaches unity. At still higher accretion rates Compton scattering will severely degrade the bremsstrahlung spectrum and the observed temperature will appear much lower than the shock temperature. Much of the luminosity will come out at EUV and soft X-ray wavelengths. When \dot{M} has increased to $\geq 10^{19} \text{ gm s}^{-1}$ (i.e. similar to the accretion rate calculated for SS Cyg in outburst from a variety of measurements) then the bremsstrahlung fit to the observed spectrum gives a temperature that is less than 2 keV; all of the flux comes out as soft X-rays or EUV.

This model is, then, qualitatively compatible with the observations of SS Cyg and U Gem, particularly if SS Cyg is allowed a mass accretion rate about ten times higher than that of U Gem at all phases of the light curve. The model even predicts that no turnover will be observed in the degraded bremsstrahlung spectrum because of the contribution by secondary radiation which produces a shoulder between the blackbody and hard components.

The difficulty with this model is that the luminosities it predicts are $\sim 10^3 - 10^5$ times higher than the observed dwarf novae X-ray luminosities. (There is also a difficulty for the observation of EX Hya -- see Paper 4 -- which does not appear to satisfy the requirement of the model that posits a correlation between the temperature and the luminosity; more observations are required to check this.)

The difficulty with the luminosity can be circumvented if the area of the emitting region is much smaller than the white dwarf surface. At least two possibilities emerge. The first is that the white dwarf has a "small" magnetic field ($B \ll 10^6$ gauss; circular polarization measurements exclude fields higher than this) which disrupts the disk and channels some of the material onto a fraction of the white dwarf surface. Ricketts *et al.* (1979) interpreted their hard X-ray observations of SS Cyg as due to variable accretion by a white dwarf with $B = 10^6$ gauss. The observation that there are only two dwarf novae (SS Cyg and EX Hya) with hard X-ray emission during quiescence is not incompatible with the observation that only 3% of white dwarfs have magnetic fields of such strength (Stockman 1979, private communication).

Yet the detection of pulsations at 9s for SS Cyg confines the emitting region to an area very close to the white dwarf, if the clock that drives the pulsations is the Keplerian period of the inner disk/boundary layer. The broadened optical emission lines (extending out to $\sim 4000 \text{ km s}^{-1}$ for SS Cyg) also indicate that the disk must extend very close to the white dwarf surface. In addition, there has been no report of any stable modulation of the light from any of the dwarf novae discussed here -- at any wavelength. Such a modulation would be expected if the flow onto the compact star were anisotropic. All of these observations severely constrain the size of the magnetic field.

An alternative way of accreting the matter onto only a fraction of the degenerate star's surface has been proposed by Pringle and Savonije (1978) who suggest that hard X-ray emission may occur even for disk accretion. For low enough accretion rates ($\dot{M} \sim 10^{16} \text{ gm s}^{-1}$) temperatures up to 20 keV may be reached if strong shocks occur in the boundary layer. The requirements for this to happen are i) that the emitting region is sufficiently optically thin so that the X-rays can escape, and ii) that the cooling time of the shocked gas for free-free emission is much greater than the adiabatic expansion timescale of the shocked gas. An equal amount of radiation at soft X-ray/EUV wavelengths should result from absorption and re-emission of the hard X-ray flux by the white dwarf and inner disk. For accretion rates $\dot{M} \gtrsim 10^{16} \text{ gm s}^{-1}$ hard X-ray emission is suppressed and most of the energy is emitted as soft X-rays ($T \sim 2 - 5 \times 10^5 \text{ K}$). The details of this hypothesis have not yet been reported.

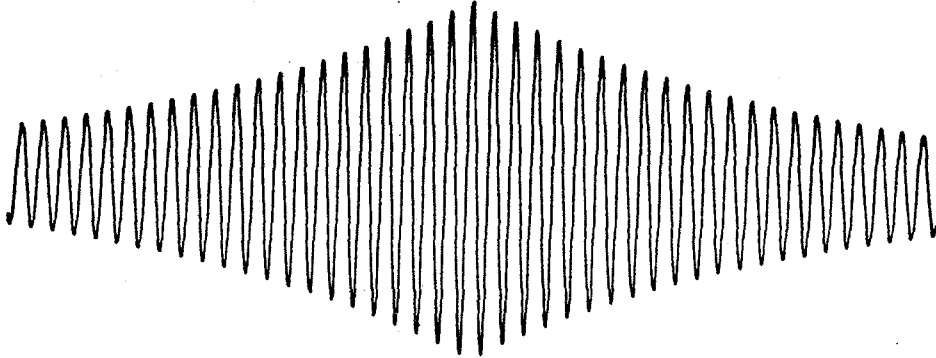
4. The X-ray variability implies that *the mass transfer onto the white dwarf is a highly unstable process*. The hard X-rays from SS Cyg and EX Hya are observed to flicker by a factor of two or three; for SS Cyg, where good time resolution was available, this modulation was observed on a timescale of minutes. The evidence of unstable soft X-ray pulsations shows that the region near the white dwarf may be quite turbulent. In addition, the evidence for visual quasi-periodic oscillations with the same behavior as the quasi-periodic pulsation observed for U Gem, but with longer timescales, shows that most of the visual and soft X-ray light may come from different portions of an unstable disk that has temperature enhancements or blobs which can feign stability, in spite of vicious stresses, for several hours, or even days.

5. *Not all dwarf novae are detected as X-ray emitters*. The ones which are have both a hard and a soft component; this is further evidence that these components are related. Since the emission from the known dwarf novae X-ray emitters is weak, the lack of X-rays in most of these objects may be one of degree; the known emitters may have higher white dwarf masses or small magnetic fields (in contrast to no magnetic field); this would, in turn, induce a higher rate of accretion onto the compact star, and hence higher temperatures and luminosities.

REFERENCES

- * 1. Cordova et al. 1979a, submitted to Ap. J.
- * 2. Cordova, F.A. and Garmire, G.P. 1979, Nature, in press.
- * 3. Cordova et al. 1979b, in preparation.
- * 4. Cordova, F.A. and Riegler, G.R. 1979, M.N.R.A.S., in press.
- 5. Fabbiano et al. 1978, Nature, 275, 721.
- 6. Forman et al. 1978, Ap. J. Suppl., 38, 357.
- 7. Hearn, D., Richardson, J. and Li, F. 1976, Bull. A.A.S., 8, 447.
- 8. Heise et al. 1978, Astr. and Ap., 63, L1.
- 9. Kylafis et al. 1978, Proc. of COSPAR Symp., Innsbruck, Austria,
June 1978.
- 10. Margon et al. 1978, Ap. J., 224, 167.
- 11. Mason, K.O., Cordova, F.A. and Swank, J.H. 1978, Proc. of COSPAR
Symp., Innsbruck, Austria, June 1978.
- 12. Mason et al. 1978, Ap. J. (Letters), 226, L129.
- 13. Mushotzky et al. 1978, NASA 78097, GSFC.
- 14. Pringle, J.E. and Savonije, G.J. 1978, preprint.
- 15. Rappaport et al. 1974, Ap. J. (Letters), 187, L5.
- 16. Ricketts, M.J., King, A.R. and Raine, D.J. 1979, M.N.R.A.S., 186, 233.
- 17. Swank, J.H. 1979, private communication.
- 18. Swank et al. 1978, Ap. J. (Letters), 226, L133.
- 19. Warner, B. 1972, M.N.R.A.S., 158, 425.
- 20. _____ 1974, M.N.R.A.S., 168, 235.
- 21. Watson, M.G., Sherrington, M.R. and Jameson, R.F. 1978, M.N.R.A.S.,
184, 79p.

* papers included in this dissertation



"Progress in solving the majority of problems in astrophysics results neither from a steady advance along predictable paths, nor from a series of Kuhnian revolutions, in which old paradigms, like old oil lamps, are exchanged for new. Rather it is more often the result of an anarchical melee in which progress is more analogous to a random walk..."

G.T.Bath 1978
Q. Jl. R. astr. Soc.,
19, 442.

"I like cataclysmic variables because they go boom,boom, BOOM."

R.A.Wade

private communication

APPENDIX A

EXPERIMENT DESCRIPTION

1. Introduction

The A2 experiment on the High Energy Astronomical Observatory HEAO-1 is a collaboration between scientists at the Goddard Space Flight Center, the California Institute of Technology, the Jet Propulsion Laboratory, and the University of California at Berkeley. The experiment objectives are the mapping of the diffuse X-ray sky between energies of 0.2 and 60 keV, and the study of the temporal and broadband spectral characteristics of discrete sources. The experiment consists of 6 multi-anode, multi-layered, collimated gas proportional counters of 3 types which are designated according to the energy ranges they span: HED (high energy detector, 2.5-60 keV), MED (medium energy detector, 1.2-20 keV), and LED (low energy detector, 0.2-3 keV).

A complete description of the entire A2 experiment is given in Rothschild et al. (1979). Since only the detector designated LED1 was used to collect the data comprising the subject material of this thesis, the discussion of the physical characteristics of the experiment in Section 2 concerns only this detector. The progress of an X-ray photon intercepted by LED1 is traced in Section 3. Included in this section is a description of a novel telemetry program that was specifically designed for the SS Cygni pointing and was subsequently used for the U Geminorum pointing. This program was conceived in order to handle both fast timing (80 ms) measurements and rapid (20 ms) direct pulse

height readouts for time-resolved spectral analysis. In Section 4 techniques used in the reduction of the data for this dissertation are described. Special attention is given to an analysis technique used for producing aspect-corrected, background-subtracted light curves from pointing data.

HEAO-1 was launched 1977 August 12 into a circular orbit with an apogee of 445 km and an inclination of $22^{\circ}75'$. The mission continued until 1979 January when the gas supply used for attitude control ran out.

2. LED1 Characteristics

a) General

The configuration of the A2 detectors on the satellite is shown in Figure 1. The detectors are oriented 90° to the spin (z) axis. In the normal scanning mode the satellite rotates clockwise about the sun-pointed +z-axis with a nominal 33 min period. The spin axis is stepped $0^{\circ}5'$ every 12 h in order to remain pointed at the sun. Each spacecraft rotation sweeps a 3° (FWHM) wide great circle on the sky through the ecliptic poles. In the scan direction two coaligned fields of view provide apertures of $1^{\circ}5'$ and 3° (FWHM). Figure 2 is a schematic illustration of the field of view of an A2 collimator.

A cross-sectional view of LED1 is shown in Figure 3. The detector is comprised, in order progressing from back to front, of a multi-wired gas proportional counter, a thin window and window support, a commandable calibration device that may be rotated in and out of the

Figure 1

Configuration of the six detectors within the Cosmic X-ray (A-2) Experiment and its position in the HEAO-1 observatory. The three axes of the spacecraft are labeled and the sense of the rotation is shown.

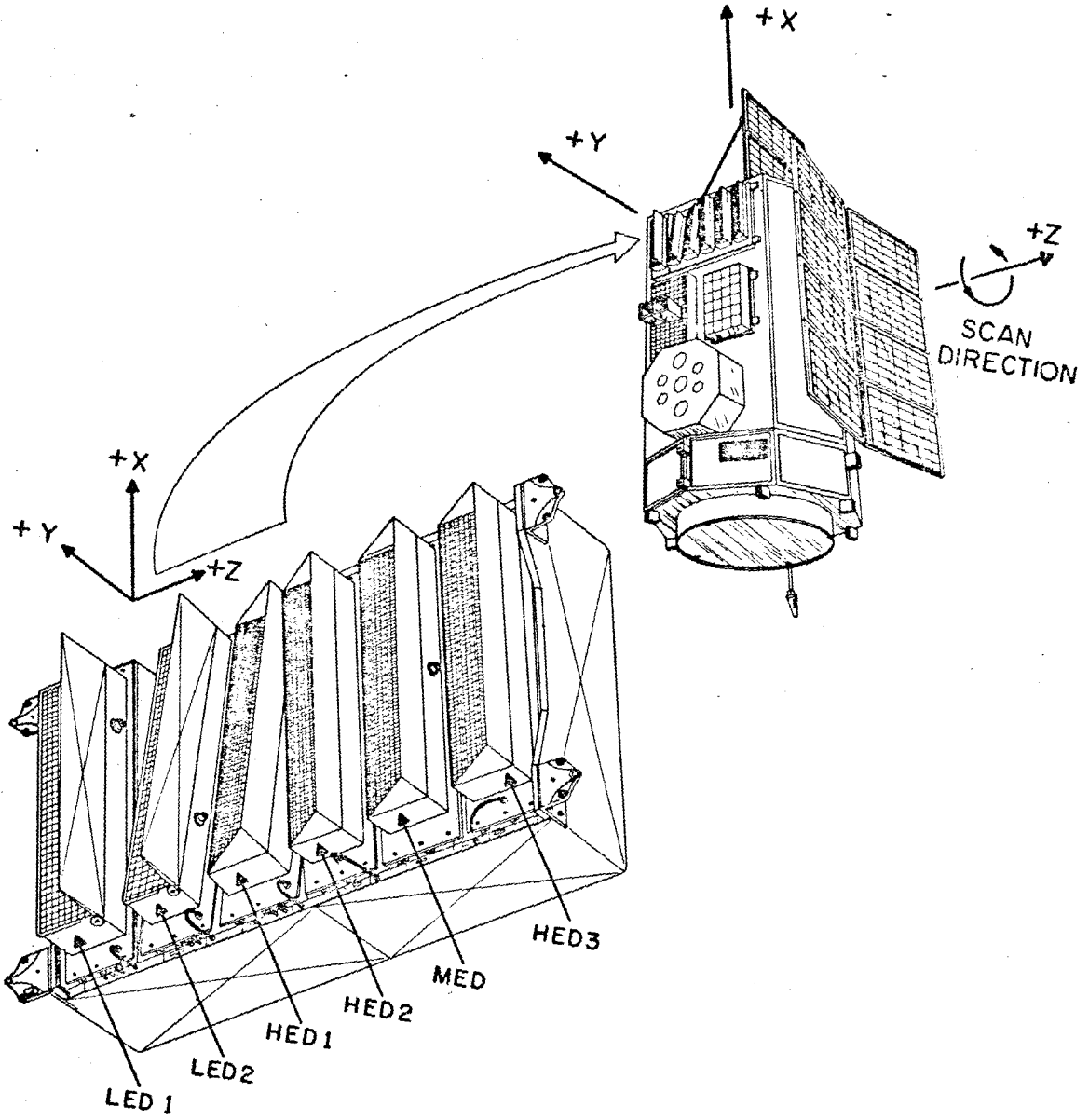


Figure 1

Figure 2

Schematic illustration of the LED1 collimator fields of view (FOVs).
In the direction normal to the scan path both FOVs are 3° FWHM;
in the parallel direction they are 1.5° and 3° FWHM.

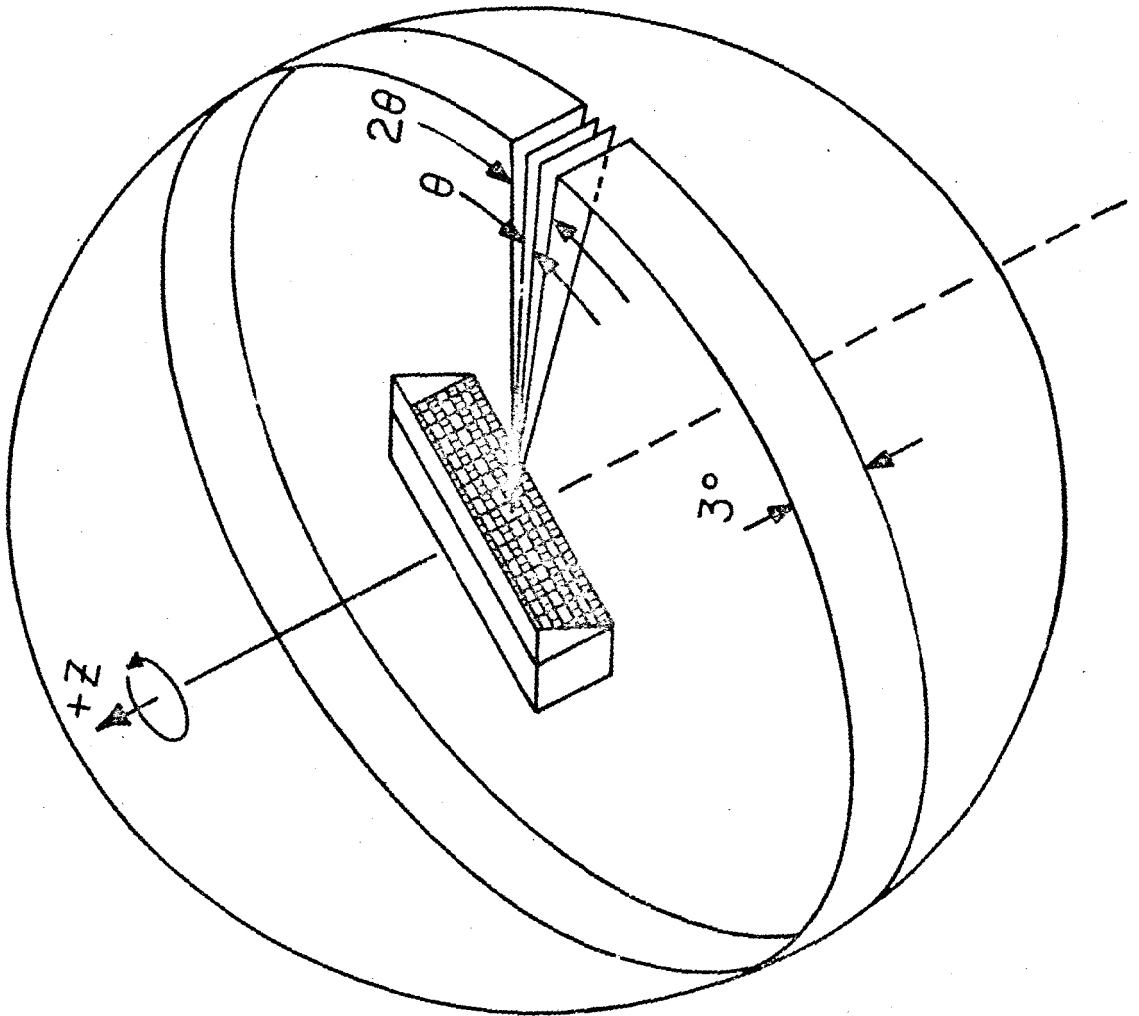
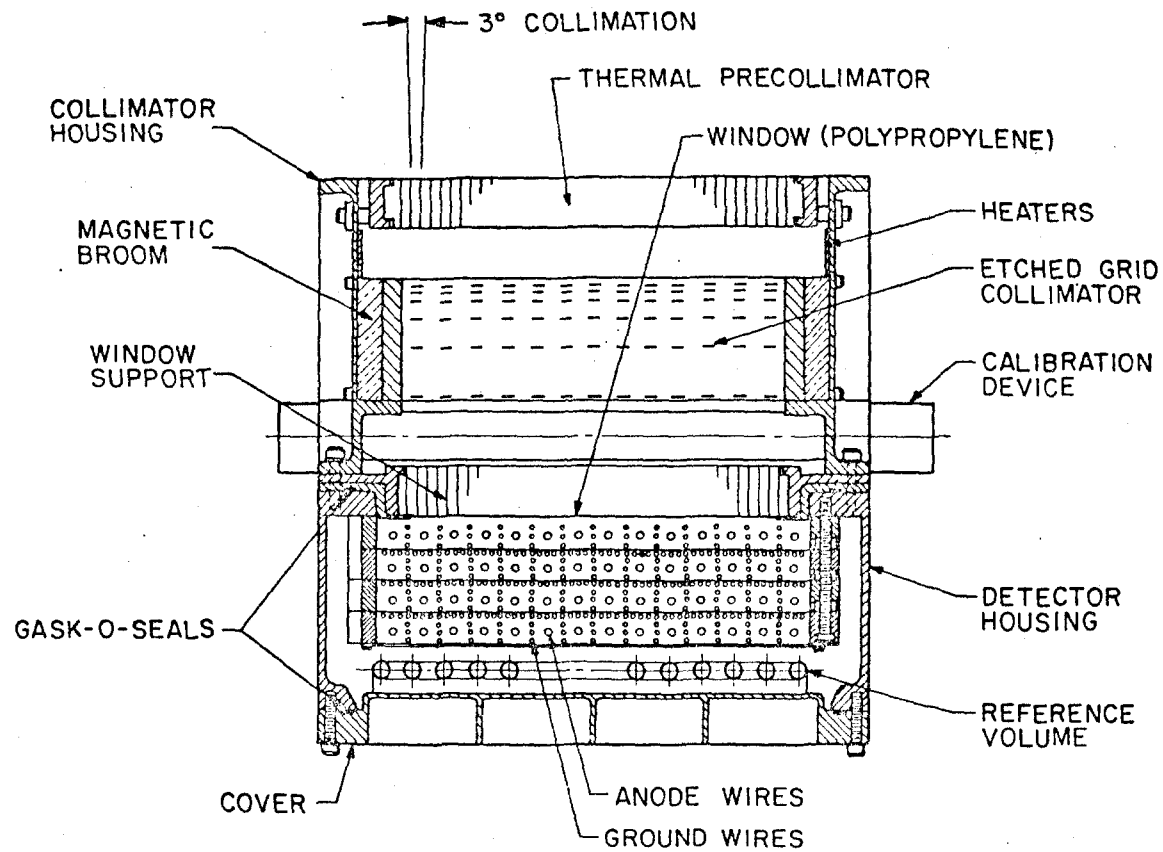


Figure 2

Figure 3

Cross-sectional view of LED1.



LED CROSSSECTION

Figure 3

field of view, an etched-grid collimator to provide the fields of view, a magnetic "broom" to reject electrons with energies < 40 keV, a heater to minimize temperature gradients, and a precollimator that acts as a thermal baffle to minimize heat loss into space and to minimize temperature gradients.

The physical characteristics of LED1 are summarized in Table 2-1. In the next few subsections the following particulars of the detectors are detailed: the design of the counter itself, the collimator transmission, the window and gas efficiencies, and the uncertainties in the calibration of the detector area.

b) Configuration of the gas cells

As illustrated in Figure 4, LED1 contains 4 physical layers. These are grouped electronically into 3 data layers. The first (front) layer is designated M1 and has separate electronic readouts for the left and right alternating cells (L1, R1). The second data layer, M2, electronically combines the second and third physical layers and also has separate left and right anode groupings (L2, R2). The third data layer, which is the fourth physical layer, is a "veto" layer, designated V1. It is used to discriminate against charged particles which may mask as X-ray events in the counter. Charged particles, unlike X-ray photons, have long ionization paths and hence are likely to trigger more than one anode layer. The technique of rejecting events that trigger more than one layer is called anti-coincidence. A side layer, V2, is also used for vetoing contaminating particles. Since V2 does not look through the collimator, it only receives penetrating radiation through the side walls.

Table 2-1

Nominal and Measured LEDL Characteristics

Position on satellite	"Deck" (90° to spin axis)
Type	Multi-wired, multi-layered, collimated gas proportional counter
(1) Gas/pressure	propane/200 torr
(2) Anode high voltage	1813 volts
Energy range	0.18-3 keV
(3) Energy resolution (FWHM relative)	$15.146 E_e^{-0.525}$
Entrance window material/thickness	polypropylene plus carbon coating/ 1.4×10^{-4} cm
Layer depths	M1 (front): 1.372 cm M2 (mid) : 2.437 cm V1 (back) : 1.372 cm
Collimation: FOV/solid angle	L (left) : 1°55 x 2°95/1.43 msr R (right) : 2°80 x 2°55/2.47 msr
(4) Open area	L : 174 cm ² R : 205 cm ²

$$(1) \text{ Pressure}(0^\circ \text{ C}) = p(T) \times \frac{273.16}{273.16+T(^{\circ}\text{C})}$$

In March 1978, T was raised for the rest of the mission to 15-20° C (see Garmire, NASA Final Technical Report, March 1979).

- (2) Commandable high voltage setting could be raised or lowered in discrete units of 33 V to alter the detector gain ($\sim 1.6 \times 10^4$ at 1800 V). For several satellite orbits during the SS Cyg and U Gem pointings, the high voltage was raised 2 levels to ~ 1880 V; this reduced the low-energy threshold from 0.18 keV to 0.11 keV.

- (3) Roughly, FWHM relative = $2.35 \sqrt{W/E}$ where W is the mean ionization energy of the gas (~ 28 eV/ion pair for propane). The true pulse-height response was measured using on-board radioactive calibration sources.
- (4) Detector areas were derived by normalizing the expected intensity of known (constant) cosmic X-ray sources. The values given here may be 13% too high; see text.

Figure 4

Detector grid connections. Cell-to-cell anode interconnections are labeled.

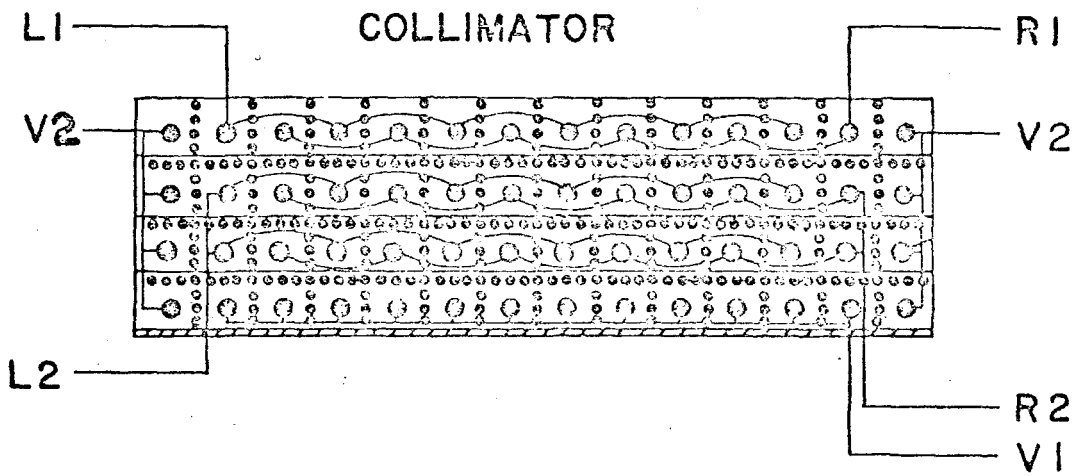


Figure 4

c) Collimation

The mechanical collimator in front of the detector is designed so that the left cells (L1, L2) of the proportional counter have one field of view, while the right cells (R1, R2) have a coaligned field of view approximately twice as large. Since the left and right cells are identical and their signals pass through a common amplifier, logic circuitry, and pulse height analyzer, the difference between the left and right cells is a measure of the true X-ray source intensity; systematic contributions from the detector background are practically eliminated (see Section 4 for applications). The fields of view and the solid angles of the left and right cell groupings are given in Table 2-1. The collimator response was calibrated before launch, and re-calibrated after launch using the September 1977 and March 1978 transits of the Crab Nebula, a constant X-ray source (Riegler 1976, 1978). Figures 5 a and 5 b show the collimator transmissions in the x-y and y-z planes.

d) Detector performance: window transmission, gas absorption efficiency, and energy resolution

The basic aim is to get as many X-ray photons as possible through the detector window, and then to stop them in the gas volume. The intrinsic efficiency of the counter may be written

$$\epsilon(E) = \exp(-t_w/\lambda_w)(1 - \exp(-t_g/\lambda_g))$$

where $\epsilon(E)$ is the counter efficiency for an X-ray photon of energy E, $t_w(t_g)$ is the window (gas) thickness, and $\lambda_w(\lambda_g)$ is the absorption mean

Figure 5

The transmission curves for the LED1 collimator fields of view.

(a) x-y plane, (b) y-z plane.

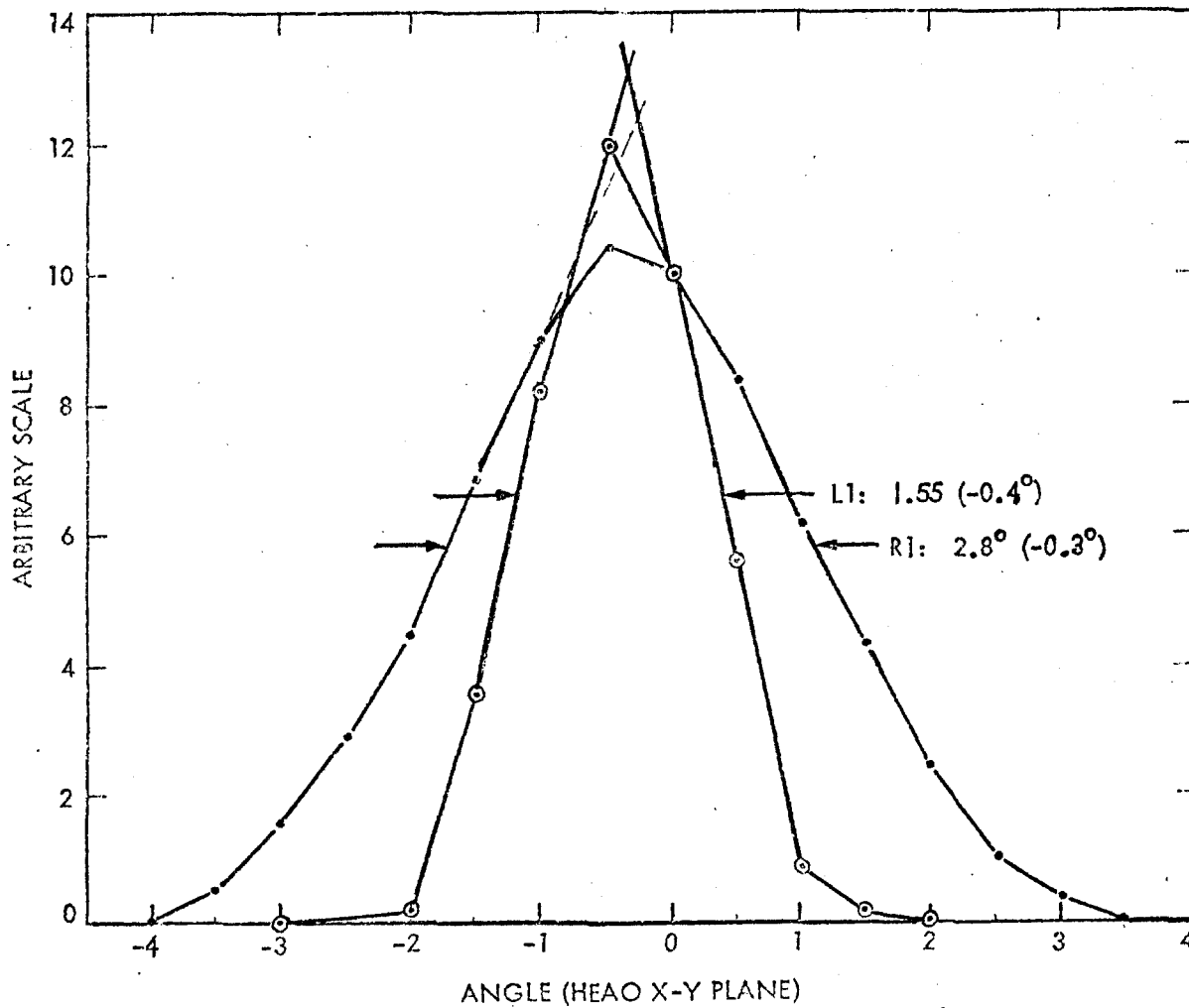


Figure 5a

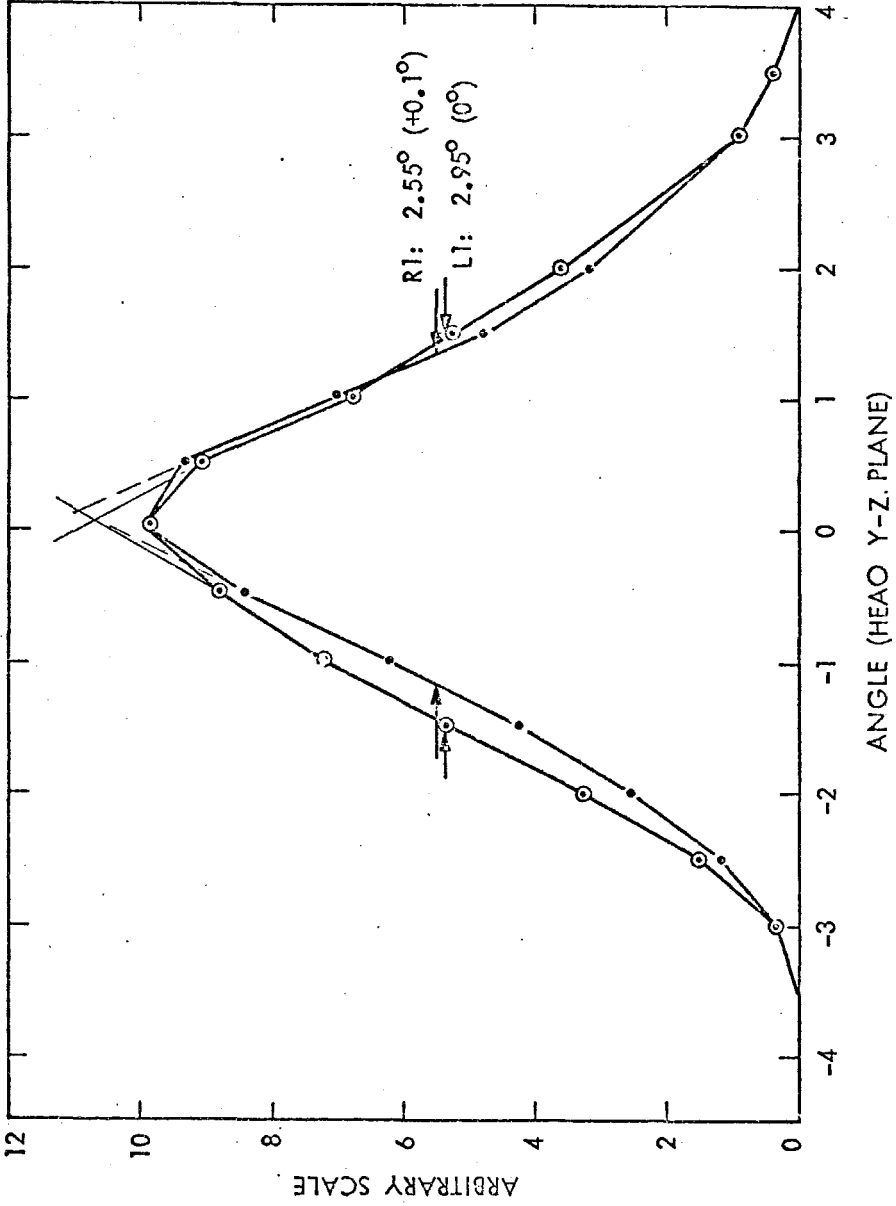


Figure 5b

free path in the window (gas) at the energy E. The thickness of the window and gas cell layers are given in Table 2-1. At the carbon K-edge (284 eV) the window is almost totally absorbing; hence, the transmission band below this energy is often referred to as the "carbon band" or the "1/4 keV band."

The combined window-plus-gas efficiency curves for each counter layer (M1, M2, V1) and M1 + M2 are shown in Figure 6. These are the efficiencies that are folded through the incident spectrum of a cosmic X-ray source observed by LED1, resulting in a determination of the true source flux.

The spectral resolution of LED1 at various calibration lines is listed in Table 2-2. The resolution values (given as relative FWHM at the energies listed) from both the laboratory measurements and the theoretical determination are given. The former have been fit to a Gaussian curve.

e) Calibration device

A commandable rotating calibration source in the collimator emits the characteristic X-radiation of carbon, fluorine and aluminum, using a ${}_{96}\text{Cm}^{244}$ (α -emitter) source with a 17.6 yr half-life. This source illuminates M1, M2, and V1. A fixed calibration source in the detector gas volume emits characteristic X-radiation of silicon (1.74 keV $\text{K}_{\alpha\beta}$ line) after fluorescence from a ${}_{26}\text{Fe}^{55}$ source with a 2.6 yr half-life; this source illuminates only V2. Frequent in-flight calibrations insure that the gain of the detector is always known (see Section 3-c for the gain equation).

Figure 6

The LED1 quantum efficiency for various cell configurations.

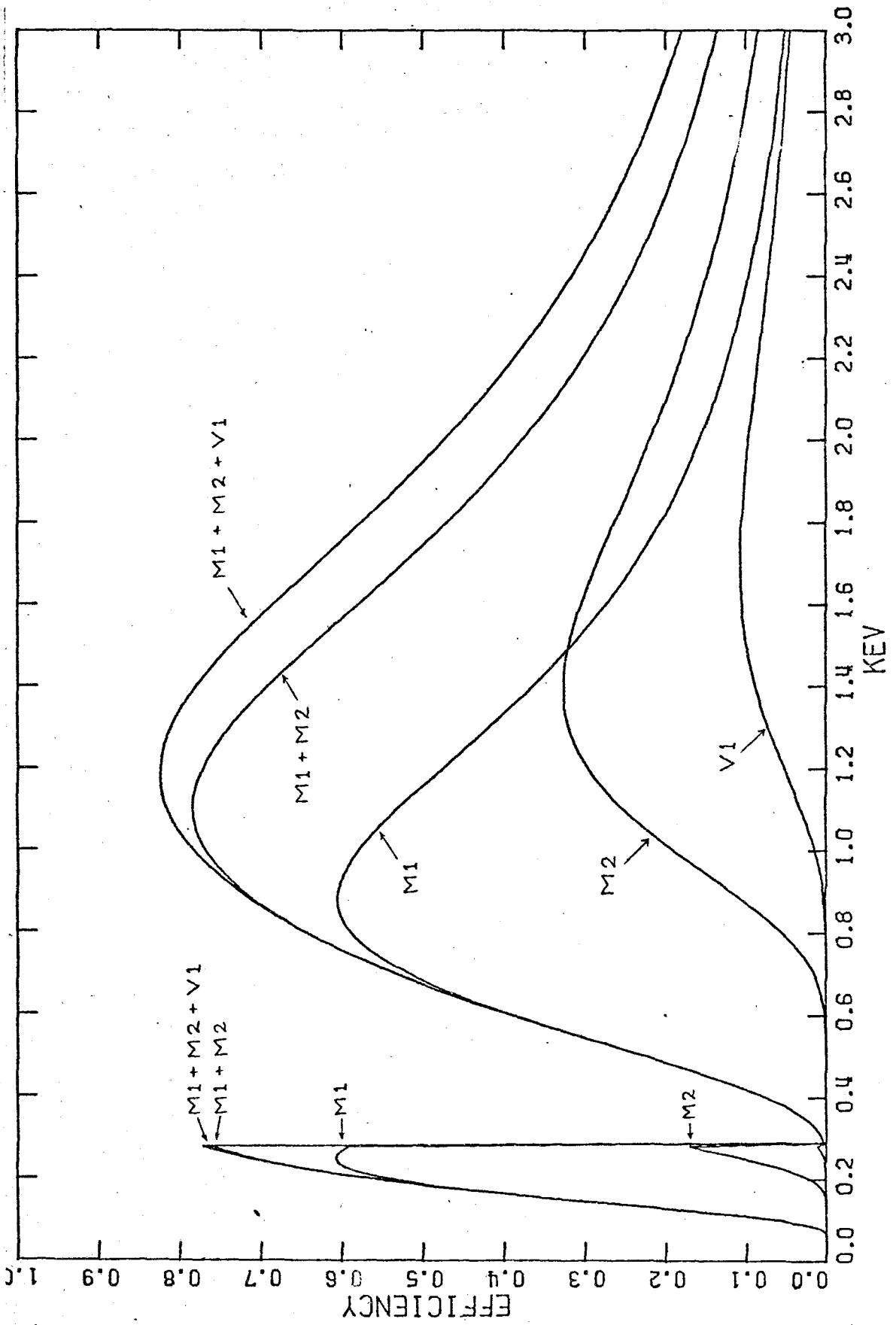


Figure 6

Table 2-2

LED1 Spectral Resolution Summary

Line	Energy (eV)	Calc. ⁽¹⁾ FWHM	Theor. ⁽²⁾ FWHM
C	282	0.804	0.768
F	677	0.493	0.496
Na	1041	0.387	0.400
Mg	1257	0.348	0.364
Al	1490	0.317	0.334
Si	1742	0.290	0.309
P ⁽³⁾	2020	0.267	0.287
Cl ⁽³⁾	2636	0.230	0.251

(1) From least-squares power-law fit: $\text{FWHM}_{\text{rel}} = 18.912 E^{-0.560}$ (E in eV)

(2) For $W = 30$ eV/ion pair, $F = 1$: $\text{FWHM}_{\text{rel}} = 12.898 E^{-0.5}$ (E in eV).

(3) Resolution broadening due to the presence of Si from diffusion pump oil; not included in least-squares fit.

f) Detector area

The effective geometrical detector area (not including window absorption) is somewhat reduced from the theoretical value owing to the presence of the various collimators in front of the detector, the rotating calibration source, and stiffening bars. The determination of the true detector area is accomplished by calibrations using known, constant cosmic X-ray sources. Most X-ray sources are variable; an exception is the Crab Nebula. From ~ 30 measurements spanning 8 years, the Crab has been found to be a steady X-ray source producing a constant spectrum between 2 and 60 keV. Averaging over all these measurements, Toor and Seward (1974) derived the best-fitting spectral parameters for the Crab, using a power law spectrum of the form $I = A E_{\text{keV}}^{-\alpha}$ where I is the differential energy flux and E is the photon energy. The best-fitting values were $A = 9.7 \pm 1.0$ and $\alpha = 1.10 \pm 0.03$. A hydrogen column density for the Crab of $\sim 3 \times 10^{21} \text{ cm}^{-2}$ was measured by Charles et al. (1973). In principle these spectral parameters could be applied to any satellite observations of the Crab, without foreknowledge of the detector area; the resulting computed intensity could then be compared to the predicted intensity using the Toor and Seward normalization, and the detector area would thus be calibrated.

Early in the HEAO-1 mission, the LED1 area determination was made by fitting Crab data using approximate values for A and α of 9 and 1, respectively, on the assumption that the spectral intensity did not sensitively depend on the exact choice of these parameters (Charles (1978)). The resulting area determinations are given in Table 2-1.

These are the values used throughout this dissertation, and for all LED1 observations written up before April 1979 by LED collaborating institutions.

Only recently has a re-examination of this calibration been made (Mason 1979). This was motivated by inconsistencies which emerged in attempts to match HEAO-1 spectra of discrete sources across the LED-MED energy ranges (overlap extends from $\sim 1-3$ keV). The ratio of the LED1 and MED intensities for several sources was 0.87. It was realized that the origin of this discrepancy could result from an overestimation of the LED1 area. Further tests showed that for energies > 2 keV, the Crab normalization is relatively insensitive to the exact choice for α and A , but since the Crab spectrum turns over (due to absorption) in the LED1 bandpass, for $E < 2$ keV the normalization turns out to be very sensitive to the fitted spectral parameters. When the more precise Toor and Seward spectral values were used, instead of the approximate values quoted earlier, the area of LED1 was computed to be 0.87 lower than the previous determination. Further checks on this new area determination included doing a χ^2 fit to the LED1 spectrum letting α and N_H be free parameters. The resulting best-fitting value for α was just that of Toor and Seward's, while N_H was $3 \times 10^{21} \text{ cm}^{-2}$, the value which was used all along.

More checks are currently underway by collaborating institutions; if the new result bears out, all LED1 intensities previously quoted will have to be divided by the 0.87 correction factor.

3. How an Event Gets Processed and Telemetered

a) General

The path of adventure^{*} of the X-ray photon that we eventually record is the following. A photon in the field of view of the collimator enters the gas volume after passing through the thin counter window. The photon is absorbed in the gas, ejecting a photon-electron which begins an avalanche process in the high electric field of the anode wire. The charge amplification process has been reviewed by Giacconi et al. (1968). The event processing subsequent to the deposition of charge on the anode is described by Birsa, Glasser, and Ziegler (1972). In short, the voltage pulse is amplified and "cross-examined" by the digital electronics to see if it is acceptable, i.e., it must pass preset low and high level discriminator thresholds and satisfy the anti-coincidence logic that checks for charge particle events (Section 2-b). Good (X-ray) events are pulse-height analyzed, that is, the amplitude of the input signal is converted into a digital number. At the same time the rates from various sets of anodes are output by scalars. Thus both the energy and arrival time of each X-ray event are tagged. The problem is how to "economically" get this information back to an experimenter on the ground; each A2 experiment is allocated only 200 bps. The sorting and packaging of the data is handled in the data selector system, to be discussed below. Three types of information are sent to the experimenter: scalar rates, PHA data, and housekeeping

* Eddington, 1916.

data. The latter concerns the status of the instrument itself (pressure, temperature, voltages, anti-rates, etc.). The scaler and PHA are presently discussed in more detail.

b) Scalers

There are 8 scalers; each counts the rate from a designated anode grouping. In this way layer and field of view information is associated with each scaler rate. If the scaler is electronically linked to voltage discriminators, additional broadband energy information may also be had. The nominal scaler energy thresholds, fields of view, and layers are given in Table 3-1. Note that scaler 5(6) is the "1/4 keV band" (Section 2-d).

c) PHA

The pulse height analysis (PHA) electronics sorts the signal according to its amplitude and the information is compressed into 64 energy channels using a pseudo-logarithmic scheme. In general, the readout mode is commanded to drop the most significant bit so that only 31 PHA channels are output. The energy thresholds for each channel (the "gain" of the detector) are determined by frequent calibrations in orbit (Section 2-d). For the nominal high voltage mode the following relationship between the PHA channel number (CHN) and the energy (E in keV) was derived:

$$E = 0.02160 \times \text{CHN} + 0.04000 \quad (\text{layer 1})$$

The lower threshold was 0.18 keV.

Table 3-1

Nominal Scaler Designations

Scaler	Broadband (keV)	FOV	Layer
1(2)	0.18-3	left (right)	1
3(4)	0.18-3	left (right)	2
5(6)	0.18-0.43	left (right)	1
7(8)	0.74-2	left (right)	1

d) Data Selector

The processed information eventually ends up in the data selector system. An on-board computer, which can be communicated with from the ground by use of special commands, is directed as to how the information is to be formatted and subsequently telemetered to the ground tracking stations. The format information is stored in two kinds of memory banks: a fixed-format Read Only Memory (ROM) and a variable-format sequential access memory (RAM). The former comes in two varieties: ROM II requests scaler data and high speed (80 ms) data, while ROM I asks for scaler data and PHA data sampled every 10.24 s (fastest possible ROM sampling for PHA). To acquire both high-resolution temporal and spectral data, these telemetry formats are automatically switched every ~ 30 min (which corresponds to a satellite rotation). The scalers have 1.28 s resolution in both formats, and prove to be the most useful data for looking at source fluctuations and broadband spectral characteristics of weak sources.

The other type of memory bank in the data system, the RAM, allows a user to program the data selector himself to ask for data in a format suited for a particular observation. Often a user can also "borrow" telemetry allocated to another detector; the RAM instructs the satellite computer as to how the shuffling of bits is to be made.

e) SS CYG RAM

For the SS Cyg pointing a special RAM was written by J. Swank (GSFC) in collaboration with G. Garmire (CIT). A copy of the program is in the Caltech RAM library. By borrowing TM from the medium

energy detector (MED) of the A2 experiment the following data were simultaneously acquired and telemetered: 80 ms broadband data (0.2-3 keV), 1.28 s scaler data, and "direct" pulse height analysis data wherein each PHA count was timed to within 20 ms. (This contrasts with the usual method of PHA sampling which integrates the data over 10.24 s (ROM I) or 40.96 s (ROM II), thus sacrificing timing information.) Each PHA channel in the special RAM was only one energy channel wide (normal mode had 1:2 ratio).

The advantages of this special RAM were multifold. A 9 s soft X-ray pulsation was discovered in the SS Cyg data. The existence of continuous 80 ms data made it possible to make a sensitive search for harmonics of the 9 s pulsation by superposing pulse trains. In addition, the 20 ms PHA data permitted a search for pulse phase-dependent spectral changes. This special RAM was used again for the U Gem pointing.

The readout and reset delays in the 20 ms data-taking mode caused a deadtime in the counting. This was corrected for by calculating the ratio of 1.28 s scaler data to the direct PHA data. This ratio (summed over L1, L2, R1, and R2) was 1.289 for the SS Cyg background data, and 1.653 for the source-plus-background data (Tuohy 1979).

For several orbits of the SS Cyg and U Gem observations an increased high voltage mode was used (see Footnote (2) Table 2-1). In-flight calibrations produced the following gain equation:

$$E \text{ (keV)} = 0.01338 \times \text{CHN} + 0.04006.$$

Thus each PHA channel was ~ 13 eV wide, in contrast to the channel width of ~ 22 eV in the nominal high voltage mode. The low-energy threshold

in the increased high voltage mode was reduced from 180 eV to 110 eV.

4. Data Reduction

a) General

The data were transmitted from the satellite to the ground tracking station, then to NASA/GSFC, and finally to collaborating institutions where they were analyzed. The data were organized on magnetic tape in sequential 40.96 s "major frames" that were, in turn, subdivided into thirty-two 1.28 s readouts (scaler data). Each major frame (MF) had a universal time associated with it, as well as aspect information and housekeeping data. In addition, depending on the telemetry format in which the data were taken (Section 3), each MF contained either PHA data with 10.24 s readouts, or 80 ms timing data (no spectral resolution) plus 40.96 s PHA readouts.

The analysis of the spectral and temporal behavior of discrete sources required the extraction of a "clean" set of data: background-subtracted, aspect-corrected, and free of charged particle contamination. Flags associated with each MF indicated data that were suspect due to a low earth-horizon angle, high-voltage instability, high anti-coincidence rates and/or parity bit errors. In the end, though, the best check on the data quality was always visual inspection of the raw data.

b) Upper Limits

In the dwarf novae survey paper included in this dissertation the upper limits to the intensity of a large number of stars are presented. It was decided to use the standard method of calculating the sensitivity

of a source (Gursky and Schwartz 1974) for uniformity, although this method may underestimate the standard error by a factor of two for the non-uniform background considered here.

The LED1 sensitivity (3σ) in the 1/4 keV band (layer 1, left FOV) is:

$$j_{\min} = 3 f(\phi - \phi_0)^{-1} A^{-1} \sqrt{B/(Nt)}, \text{ where}$$

$f(\phi - \phi_0)$ is the collimator transmission to the source;

A is the effective geometrical detector area (174 cm^2);

B is the total background rate ($\sim 5-10 \text{ ct}/1.28\text{s}$);

N is the number of scans over the source; and

t is the exposure time of a source for a single scan ($\sim 8\text{s}$).

The conversion from HEAO-1 $\text{ct cm}^{-2} \text{s}^{-1}$ to flux is spectrum dependent; in the dwarf novae survey paper (Chapter III) we give conversions assuming various spectral parameters. A rough estimation of the conversion can be made by assuming a flat spectrum over a bandwidth which is assigned an average efficiency. In the 1/4 keV band the detector efficiency is $\sim 50\%$ (see Figure 7) and the bandwidth is $\sim 0.25 \text{ keV}$. Using the conversion from keV to ergs ($1.6 \times 10^{-9} \text{ erg keV}^{-1}$), the 3σ upper limit for a source viewed on axis becomes

$$j_{\min} \sim 1.4 \times 10^{-11} \text{ erg cm}^{-2} \text{ s}^{-1}.$$

Typically, N equals 10, so that the upper limits are around $4 \times 10^{-12} \text{ erg cm}^{-2} \text{ s}^{-1}$.

c) Spectral analysis

Pulse height data were used for the spectral fitting. The net source spectrum was obtained by subtracting background data from a source-free region of the sky adjacent to the source. An analytical model of the incident spectrum is multiplied by a detector response matrix. The result is then compared to the net PHA data using a χ^2 test (the errors on the individual data points are the statistical errors). An inferred incident spectrum is obtained by dividing the best-fit PHA data by the spectrum-dependent channel-by-channel efficiencies. The parameter bounds are determined using the criteria of Lampton, Margon and Bowyer (1976).

The two models of the incident spectra that were used for the analysis in this thesis were a thermal bremsstrahlung spectrum (exponential plus Gaunt) and a blackbody spectrum. The functional forms for the photon number spectrum (dN/dE in photons $\text{cm}^{-2} \text{s}^{-1} \text{keV}^{-1}$) are:

i) Exponential plus Gaunt

$$\frac{dN}{dE} = \frac{C}{E} e^{-E/KT} g(E,KT) e^{-\sigma(E)N_H}$$

where $g(E,KT)$ is the energy-dependent Gaunt factor (Kellogg, Baldwin and Koch 1975) and $\sigma(E)$ are the photoelectric absorption coefficients calculated by Brown and Gould (1970); and

ii) Blackbody

$$\frac{dN}{dE} = A \frac{E^2}{e^{E/KT} - 1} e^{-\sigma(E)N_H}$$

d) Charged particle contamination

In spite of the anti-coincidence logic and the magnetic broom

described in Section 2a, there was still some particle contamination, particularly when the collimator viewed perpendicular to the magnetic field vector. Especially in the earth-viewing data where the X-ray countrate is generally low is this undesirable contribution noticeable. Unfortunately, this effect does not scale as the field of view, so that the FOV subtraction technique (described in Section 4-3) is not applicable. Instead, a charged particle "flag" was contrived to roughly estimate the charged particle intensity. This flag was calculated by subtracting the rate in V2 (the guard layer) from the (normalized) upper-level discriminator rate. Figure 7 shows a plot of the flux from the earth as a function of the charged particle count rate (N_e) in the 1/4 keV band for both FOV's. Pointing data for which N_e was less than 3000 were acceptable for fast timing analysis. For spectral analysis and for producing light curves from scans, data for which N_e was less than 1000 were used.

e) Light curves

A light curve is a plot of the intensity of a source as a function of time (or phase, if the source has a binary period). Light curves were made for all the sources discussed in this thesis, but different techniques had to be applied for scanning and pointing data. For EX Hydrae and AY Lyrae, only scanning data were available. In both cases the X-ray sky background was a significant fraction of the total count-rate. The net source intensity was derived by doing a nonlinear least squares fitting (Marquardt gradient expansion algorithm; see Bevington 1969)

Figure 7

Countrate for the $3^{\circ} \times 3^{\circ}$ and $1.5^{\circ} \times 3^{\circ}$ fields of view as a function of the charged particle countrate (Ne). Data are for the 1/4 keV band only and were taken while LED1 viewed the dark Earth.

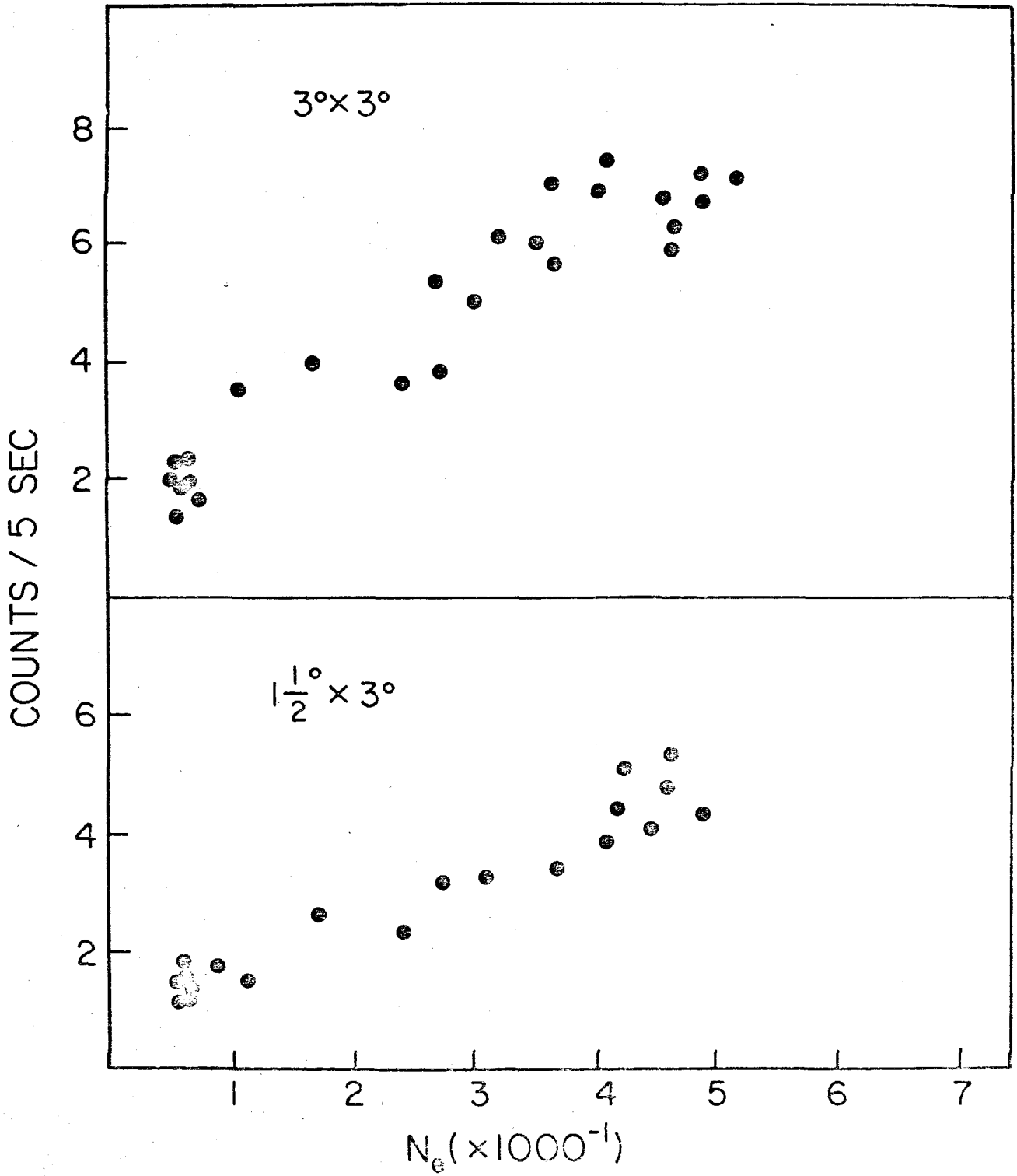


Figure 7

to a continuous interval of data which included the source and adjacent source-free sky. A low-order polynomial was the model for the background, while the triangular response function of the collimator served to model the source profile. Iterations were made until an acceptable χ^2 fit was achieved.

The extraction of an uncontaminated signal from pointing data presented a challenge. Figures 8a-h show the raw count rates for each scaler during the SS Cyg pointing. On first inspection, these unprocessed light curves show large variability on a timescale of minutes; it will be shown that this is due to spacecraft dithering off and on the source, and to background variability. To aid in the interpretation of these plots, and the remainder of the plots and tables in this discussion, a time log of the SS Cyg observation is given in Table 4-1. Individual sections of scanning, pointing, and Earth viewing data are labeled for reference later in the text.

The unique collimation design of the A2 detectors, which had two coaligned fields of view, permitted elimination of background that scaled as the ratio of the solid angles subtended by the FOV's. (The effect of instrumental background, which does not scale as this ratio, will be treated later.) The rates in the left (L) and right (R) FOV's are:

$$R = \Omega_R A_R B + T_R A_R S + \text{internal detector background}$$

$$L = \Omega_L A_L B + T_L A_L S \quad " \quad " \quad "$$

where Ω_i (solid angle), T_i (collimator transmission), and A_i (detector area) are properties of the individual detector FOV, and B (background rate) and S (source rate) are observed quantities. We shall ignore the small contribution from the internal background until later.

Figure 8

The raw countrate data for the entire SS Cygni pointing observation. Figures (a) through (h) represent the broadband scalers 1 through 8, respectively. (See Table 3-1 for band-passes and fields of view of each scaler.) Each data point is an average over one telemetry "major frame" (40.960s).

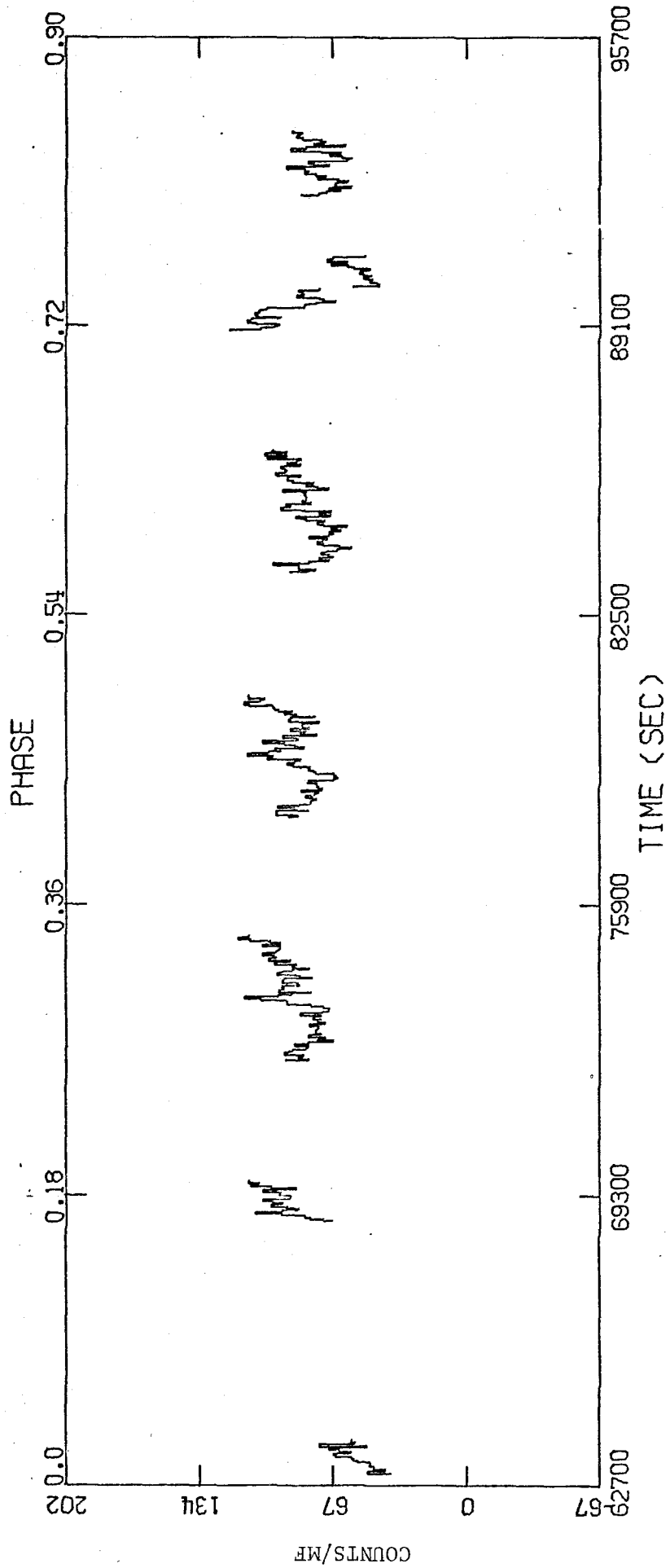


Figure 8a

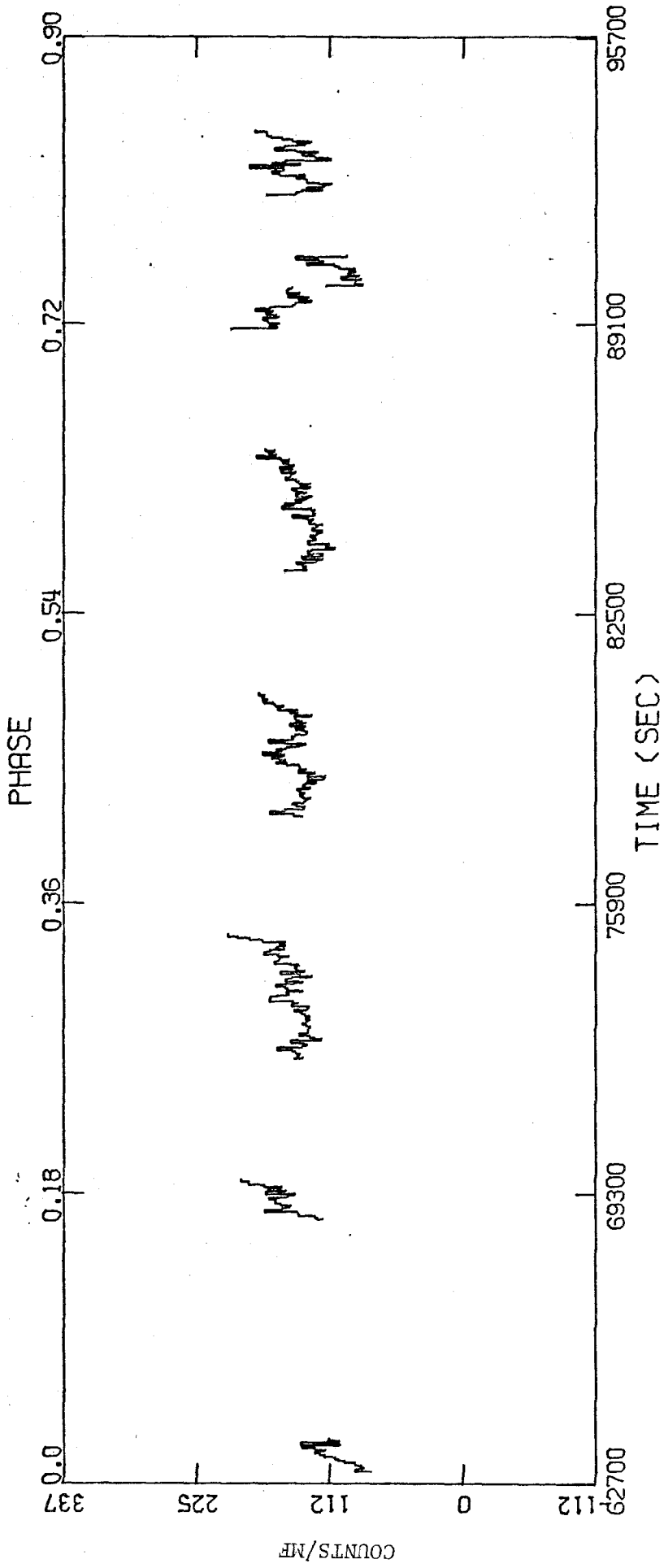


Figure 8b

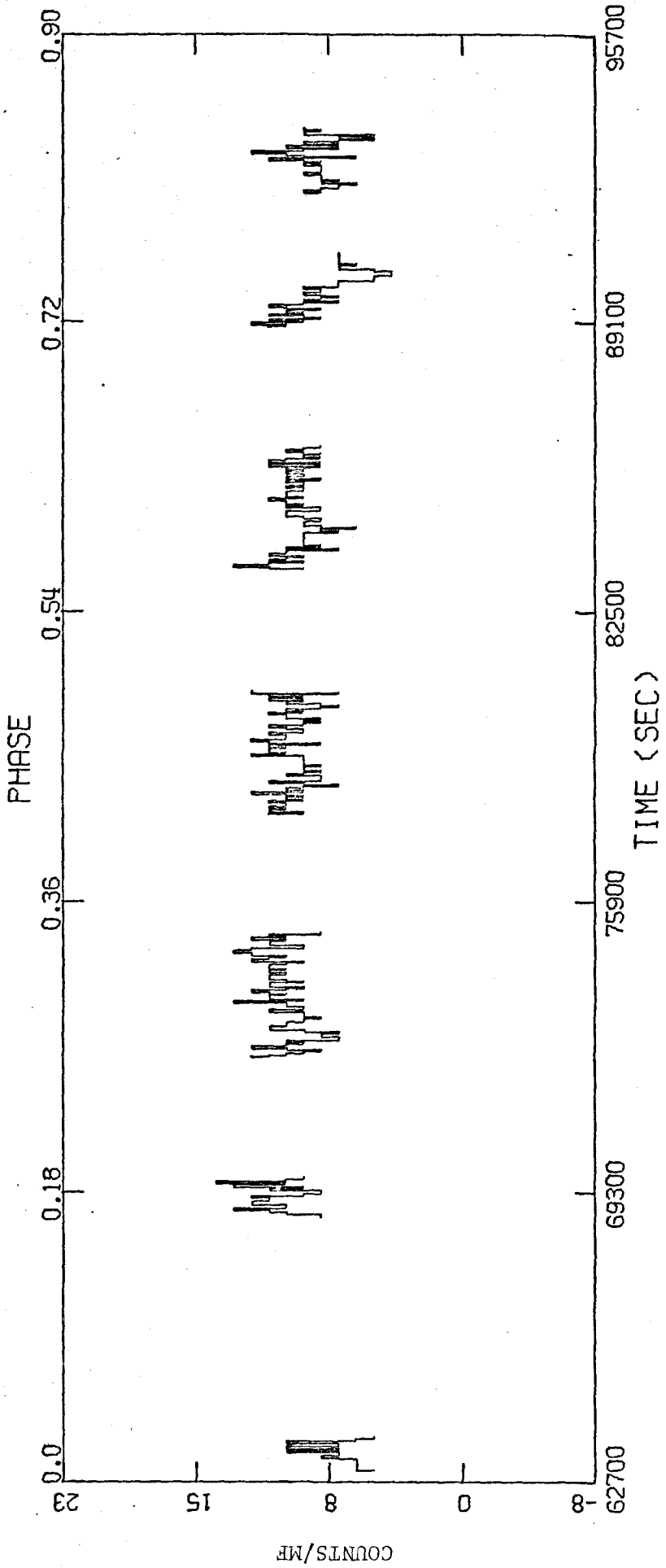


Figure 8c

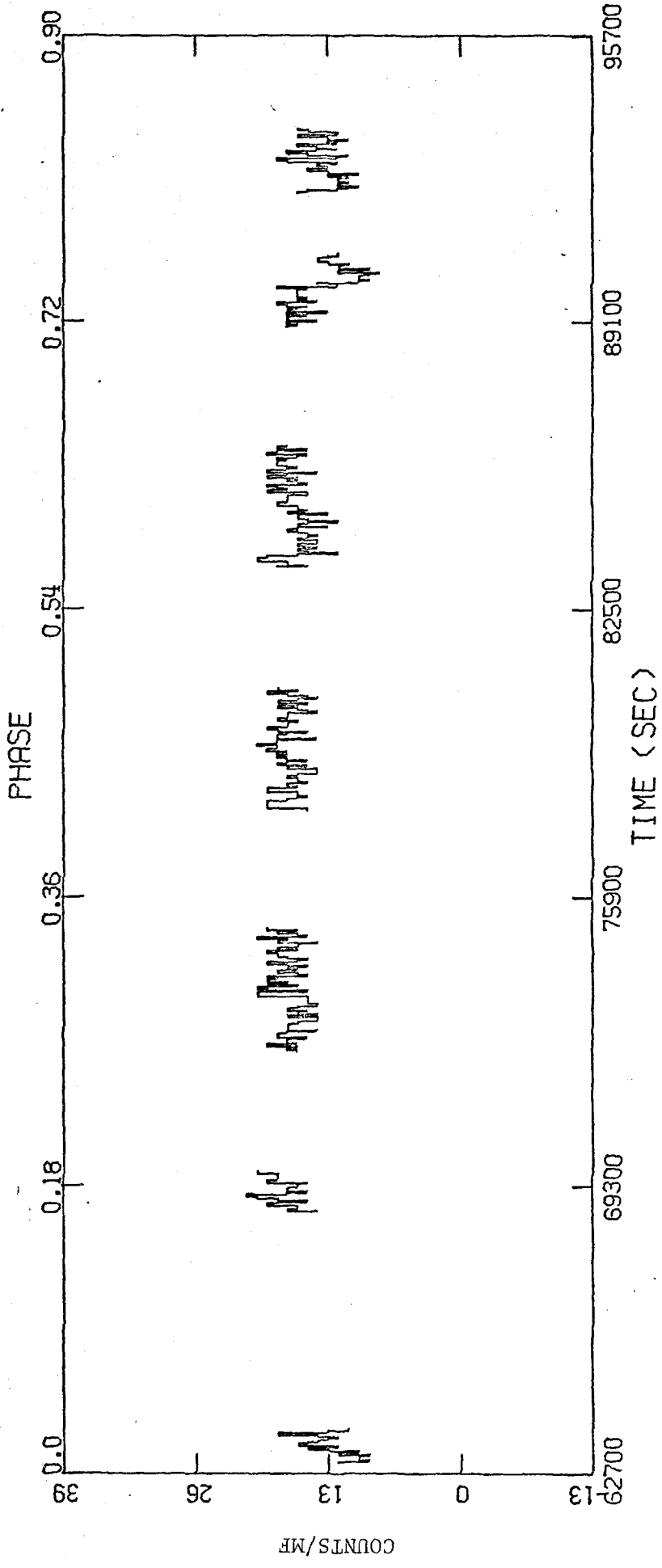


Figure 8d

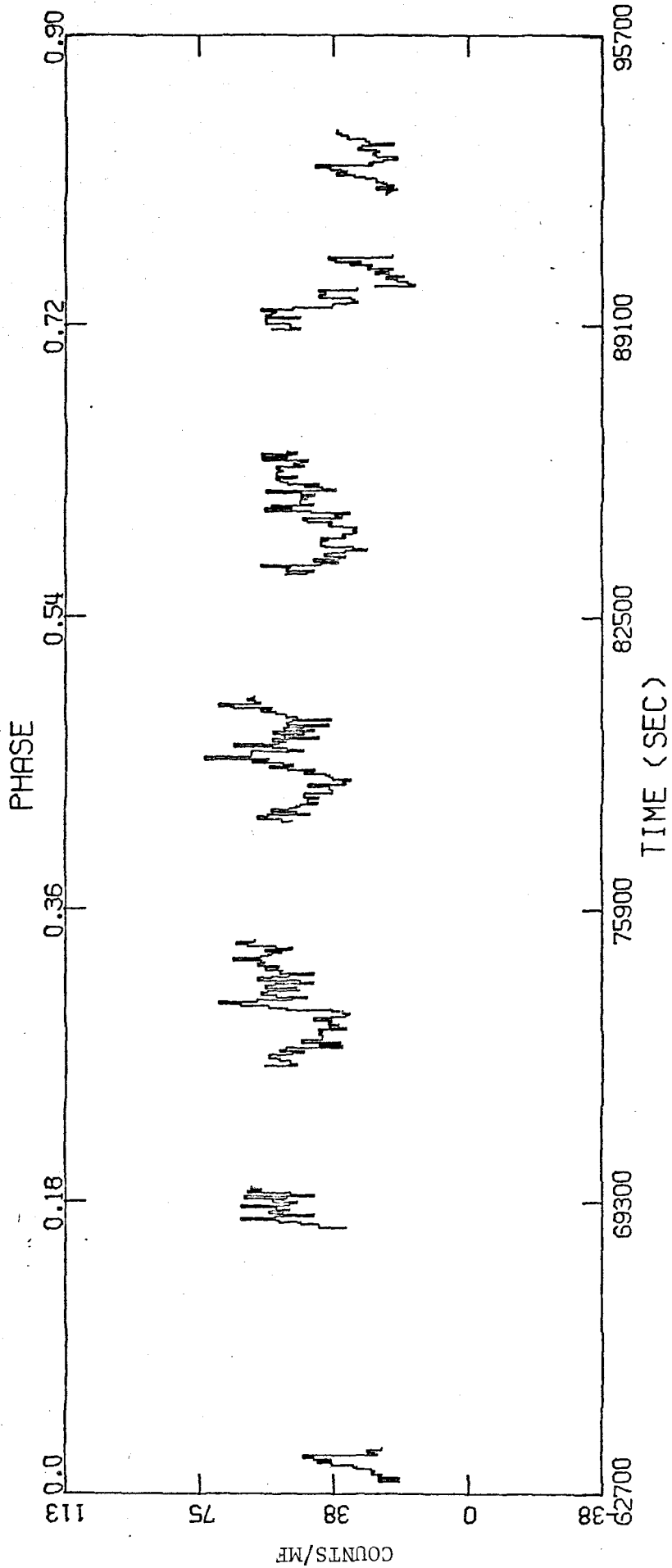


Figure 8e

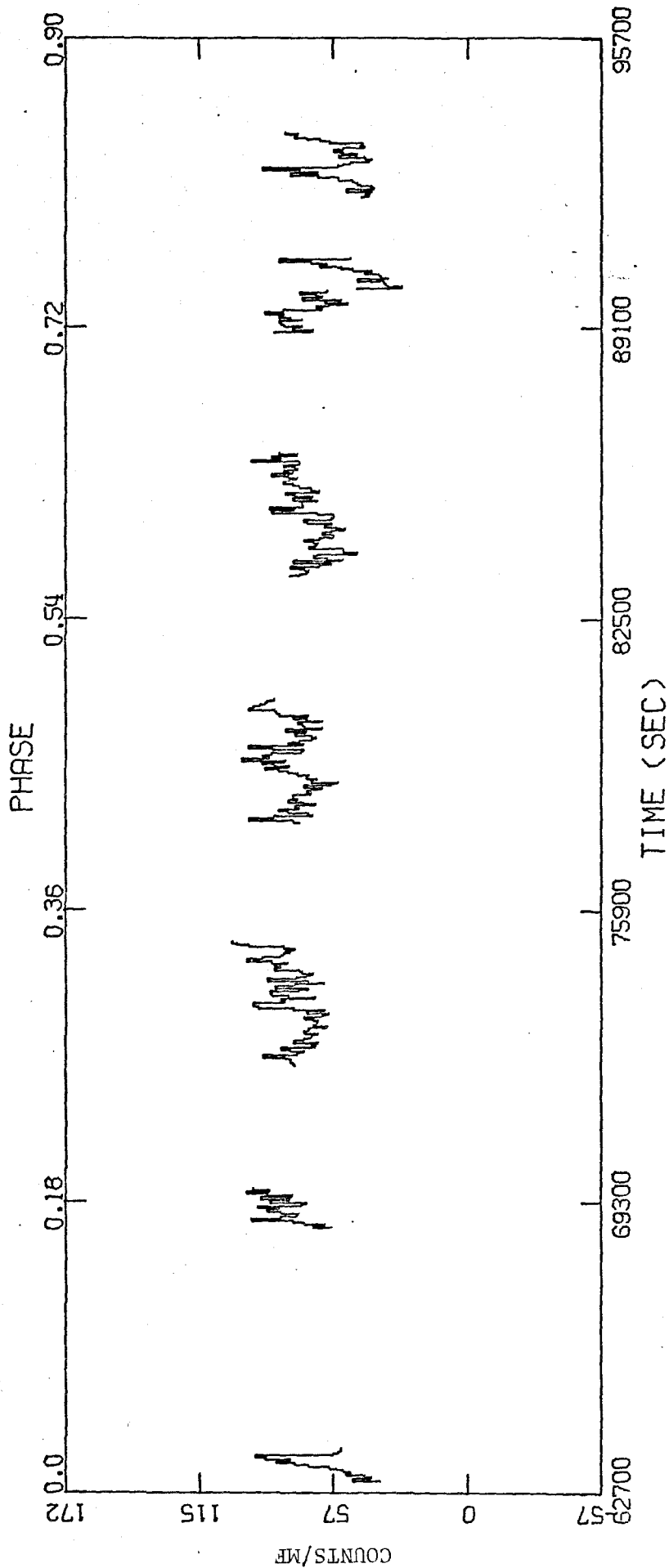


Figure 8f

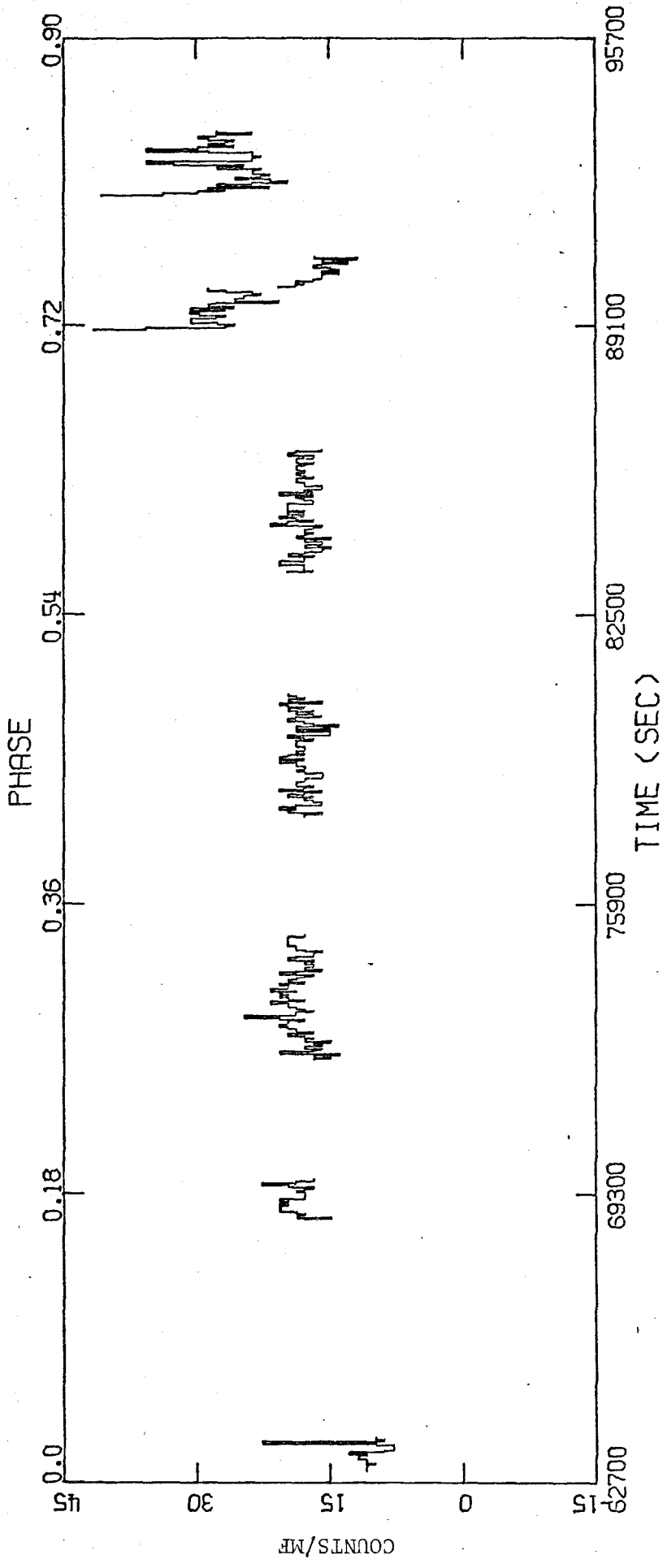


Figure 8g

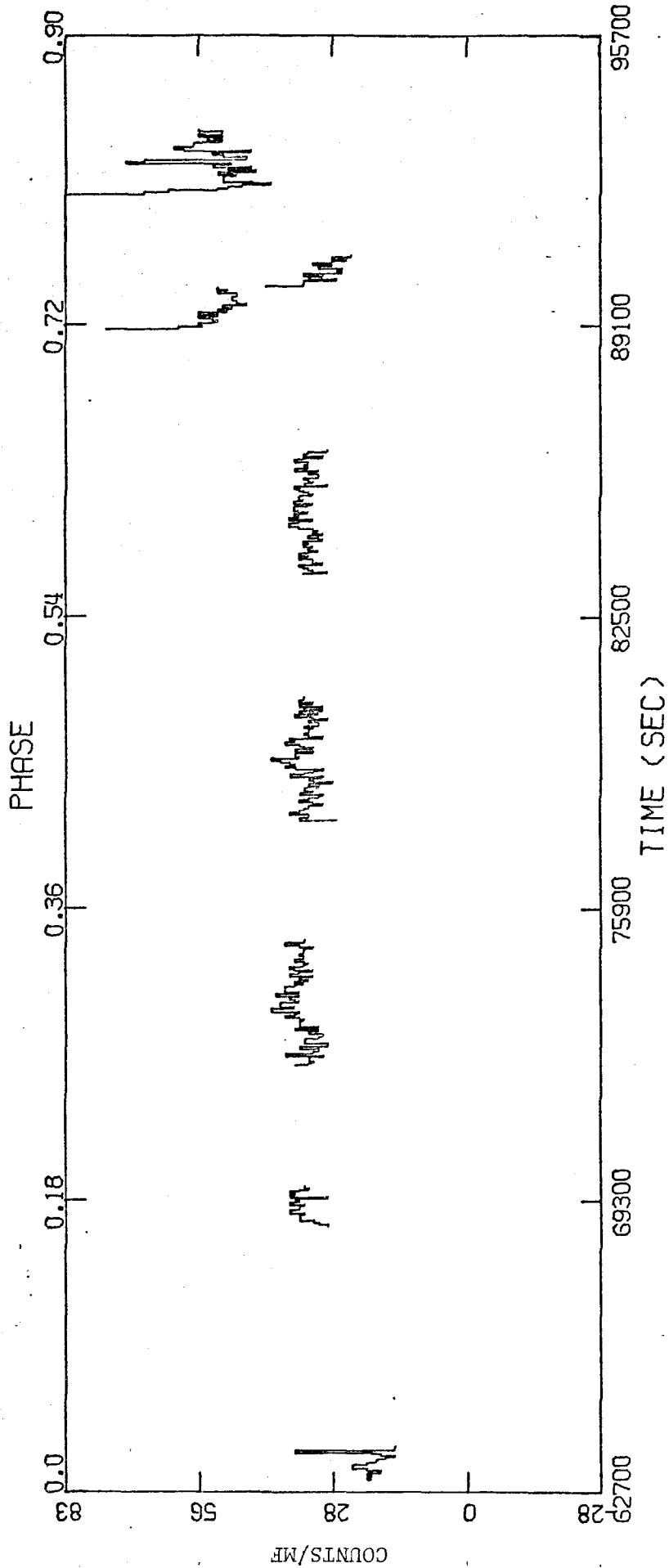


Figure 8h

Table 4-1

SS Cygni Log

Designation ⁽¹⁾	U.T. (s)	Sun	HV ⁽²⁾	TM Format ⁽³⁾
1978 June 14 U.T.				
S1	62998-63203	Day	0	ROM 1
	63203-63817	Night	"	"
OB1	68732-69674	Day	"	"
OB2	72378-74385	Night	"	"
	74385-75245	Day	"	"
OB3	77907-79914	Night	"	"
	79914-80733	Day	"	"
OB4	83478-85485	Night	"	SS Cyg RAM
	85485-68304	Day	"	"
1978 June 15 U.T.				
OB5	2607-3490	Night	+2	"
S1	3490-4328	Night	"	"
DE	4410-4696	Night	"	"
S3	5679-7154	Day	"	"

(1) OB is pointing data; S is scanning data; DE is dark earth viewing data.

(2) HV = 0 is normal HV mode; HV+2 is increased 2 levels (see footnote (2) in Table 2-1).

(3) See Section 3-d.

The equations for the source and background rates follow:

$$S = \frac{\gamma L - R}{\gamma A_L^T L - A_R^T R} \quad (1)$$

$$B_i = \frac{1}{A_i \Omega_i} \left(\frac{A_L^T R - A_R^T L}{\gamma A_L^T L - A_R^T R} \right) \quad (2)$$

where $\gamma = \frac{\Omega_R A_R}{\Omega_L A_L}$ (3)

If $S = 0$, $\gamma = R/L$, so that γ may be evaluated by comparing the ratios of the FOV's in a source-free region.

The ratio γ is a good check on whether a weak source is present in the data. One may calculate a γ' for any stretch of data by finding the FOV ratio, and then compare γ' with the value γ determined from source-free regions. The former figure will be lower if a source is present because the observed source intensity is independent of the FOV.

Figures 9a-d are plots of the ratios of the FOV's during the SS Cyg pointing for the 4 sets of scalers shown in Figures 8a-h; the values for γ and γ' are listed in Table 4-2. The γ values were derived using scanning data for each of the two high-voltage settings used during the pointing. The γ' values were derived using data taken when LED1 was pointed within 0.75 of SS Cyg. It is apparent from a comparison of these figures that the source is only present in scalers 1(2) and 5(6); this is consistent with a very soft source spectrum. (See Table 3-1 for a list of the energy ranges covered by each scaler.)

Figure 9

The ratio of the counts in the two collimator fields of view, $\sim(3^\circ \times 3^\circ) / (1.5^\circ \times 3^\circ)$, utilizing the scaler data shown in Figures 8. (a) the ratio of scaler 2 to scaler 1, (b) the ratio of scaler 4 to scaler 3, etc.

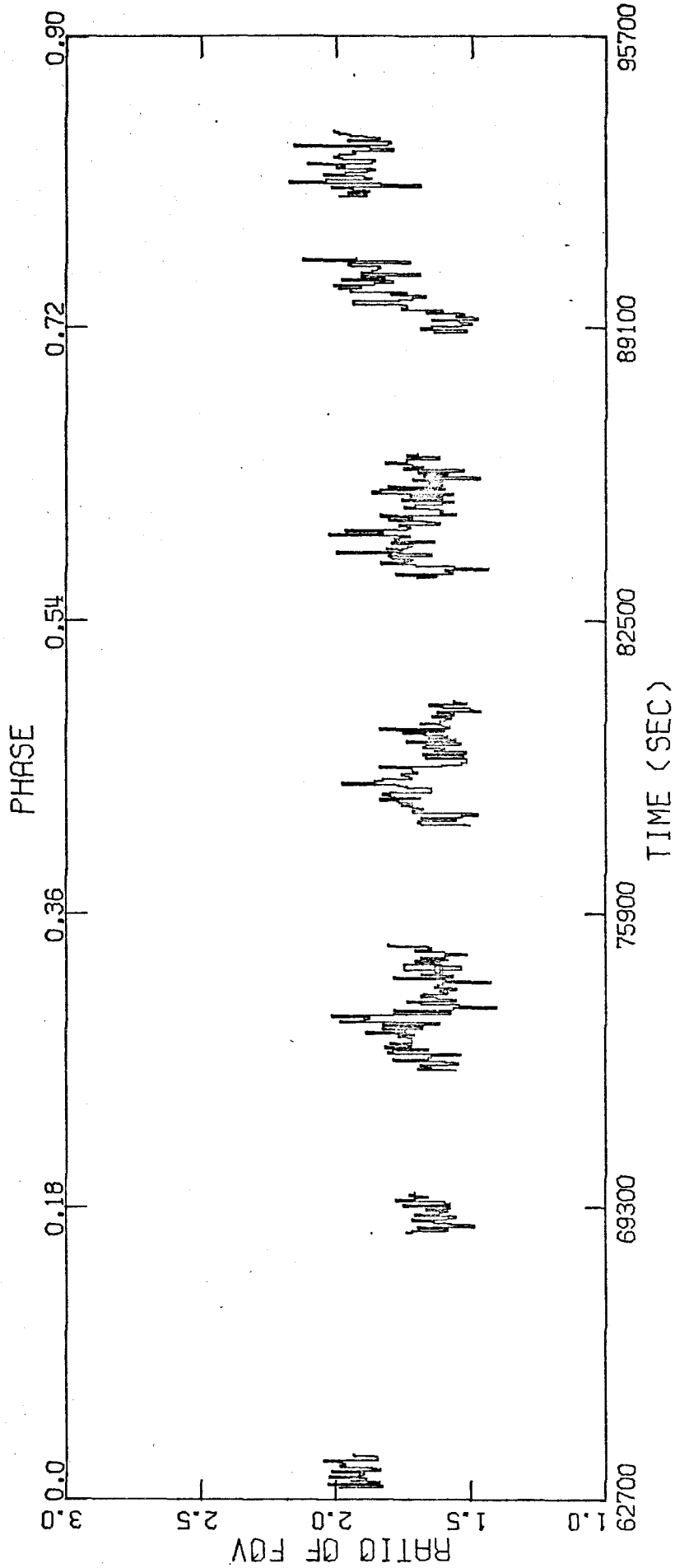


Figure 9a

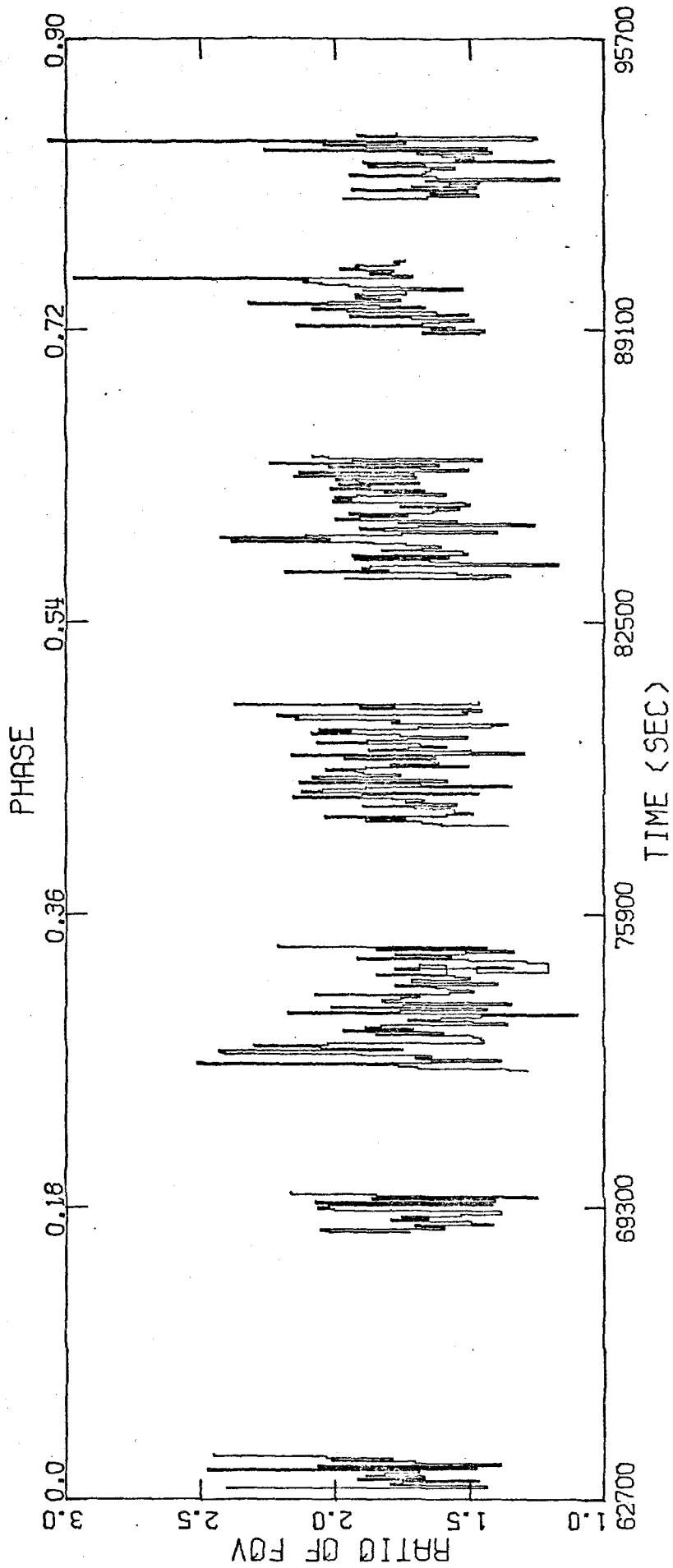


Figure 9b

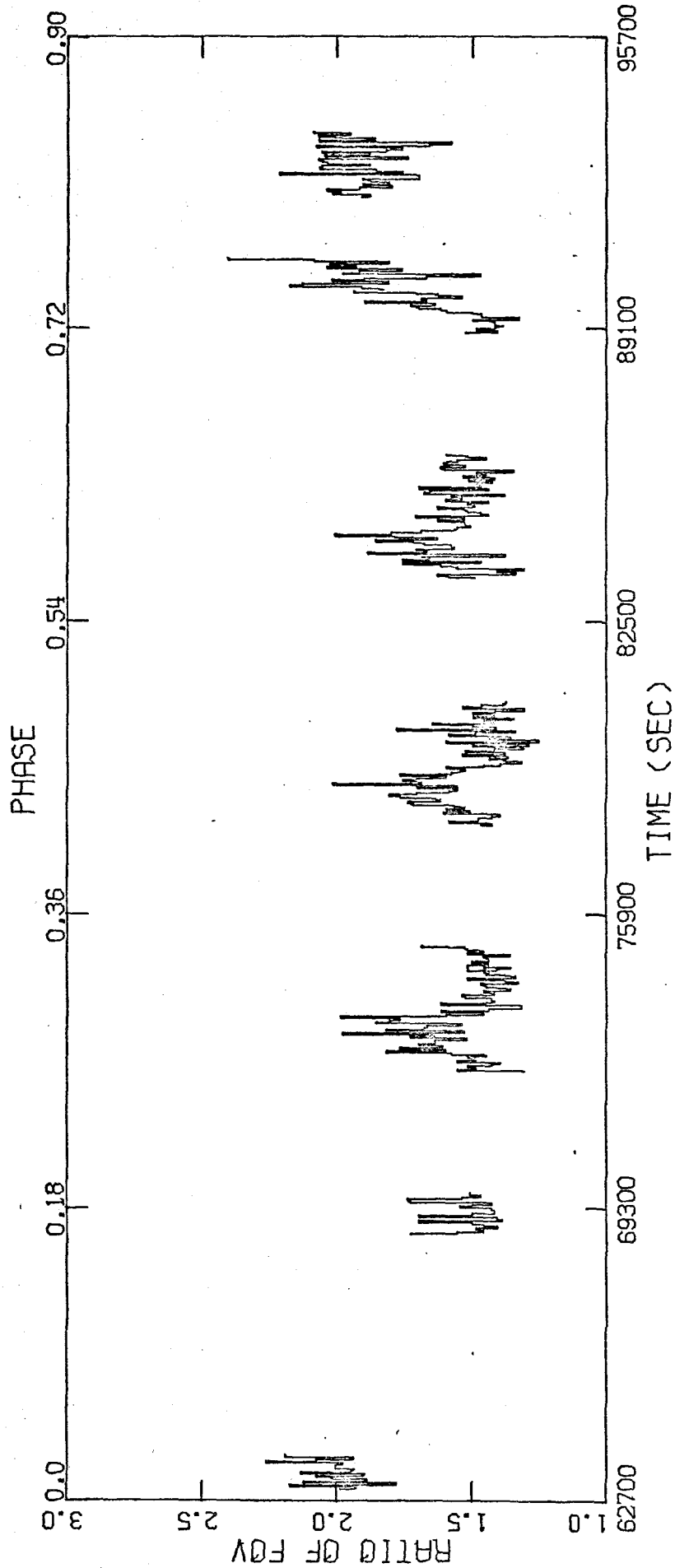


Figure 9c

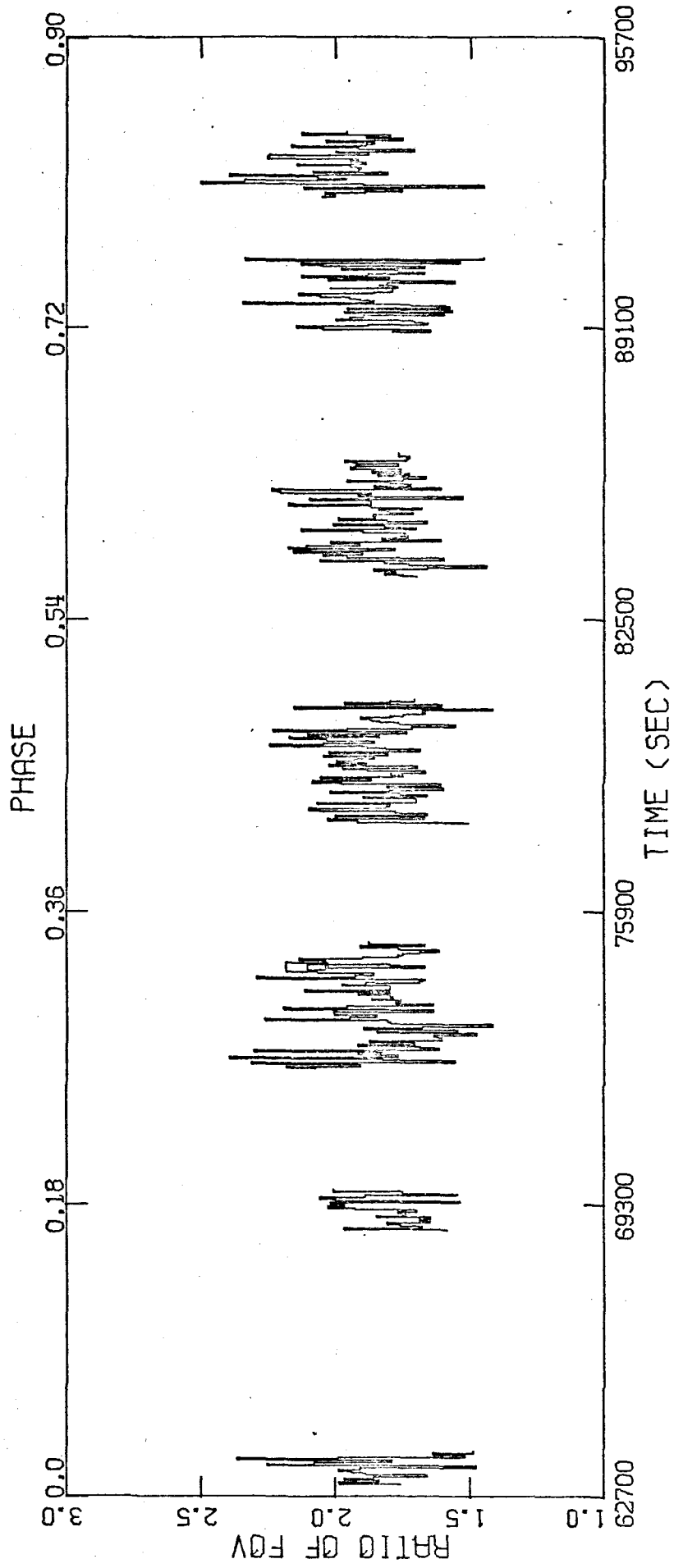


Figure 9d

Table 4-2

SS Cygni FOV Ratios

Designation	Scalers				
	2/1	4/3	6/5	8/7	
S1	$\left\{ \begin{array}{l} 1.93 \pm 0.07^{(2)} \\ 1.62 \pm 0.09 \end{array} \right.$	1.86 ± 0.33	2.02 ± 0.12	1.86 ± 0.24	normal HV setting
OB2 ⁽¹⁾					
S3	$\left\{ \begin{array}{l} 1.94 \pm 0.10 \\ 1.58 \pm 0.07 \end{array} \right.$	1.69 ± 0.34	1.92 ± 0.15	1.99 ± 0.20	increased HV setting
OB5 ⁽¹⁾					

(1) Only those sections of the OB's for which the transmission to SS Cyg was $\geq 75\%$ were used for this calculation.

(2) Errors are the standard deviations.

Other values that must be known to derive the true source intensity S in Eqn. 1 are the areas associated with the two fields of view, and the collimator transmission. A discussion of the uncertainty in the area is given in Section 2-e. This uncertainty affects only the final normalization since it is a scaling factor; it does not affect the ratios of the areas. In this discussion the area values given in Table 2-1 are used.

To date, the values for the transmission T have only been determined for discrete offsets in units of 0.5° (Figure 5). This is not useful for pointing observations where the detector axis never wanders off the source by more than 0.7° . A triangular beam profile was assumed for continuous transmission function.

In constructing the light curve, the source aspect is critical. The aspect is provided by GSFC using data from an on-board star sensor. Each 1.28 s frame of data has aspect information associated with it. In principle, then, the transmission to the source can be determined as a function of time and the spacecraft motion corrected for. Figure 10 illustrates the satellite motion during the SS Cyg pointing (Conroy 1979). The wandering of the satellite off and on the source may appear surprisingly periodic (see the effect on raw count rates in Figures 8a, b, e, and f). As the satellite completes a revolution about the Earth (~ 94 min.), it experiences torques due to air drag, the gravity gradient along the satellite, and the interaction of the Earth's magnetic field with any magnetic moments of the satellite (Gursky and Schwartz 1974). The satellite begins to drift until it reaches a critical offset from the target ($\sim 0.7^\circ$), whereupon it is stopped by

Figure 10

Illustration of the satellite aspect wandering during the SS Cygni observation. The Figure was kindly supplied by M. Conroy of the HEAO-A3 experiment at SAO.

the attitude control system (control moment gyros). To conserve gas, it is allowed to drift back and forth across the source within a preselected offset limit. Unfortunately, due to relatively infrequent gyro-rate updates and occasionally inadequate star sensor data, the GSFC aspect solution may be in error by $\sim 0.1^\circ$. Another uncertainty is introduced by our lack of knowledge of the exact offset of LED1 with respect to the spin axis. Numerous iterative tests were performed on the SS Cyg data in order to determine the correction to the GSFC aspect; mainly these amounted to stepping the predicted source azimuthal angle by 0.05° , applying the transmission corrections, and testing for the best fit to a "constant" source. The timescale of SS Cyg's variability is short compared to the bin length (40.96s) used in this calculation.

It was found, after many iterations, that the GSFC aspect was suitable for the SS Cyg light curve. For U Gem, a correction of -0.1° had to be applied to the source azimuthal angle. To show how sensitively the light curves depend on the aspect correction, we have generated transmission curves and the corresponding light curves using the raw SS Cyg data and aspect corrections which differed by only 0.1° in the azimuthal angle. Figure 11a shows the light curve using the GSFC aspect, and Figure 12a shows a light curve with the 0.1° change in scan angle. The respective collimator transmission curves for each FOV are illustrated in Figures 11b,c and 12b,c.

Figure 11

The final corrected SS Cygni light curve, generated using the data from scalers 5 and 6 (1/4 keV band) which are illustrated in Figures 8 (e) and (f). The X-ray sky background has been subtracted using the differencing technique between the fields of view, as described in the text. The aspect was corrected for by using the GSFC fit to star sensor data. The collimator transmission function for this aspect is shown for the small field of view in Figure 11 (b) and for the large field of view in Figure 11 (c).

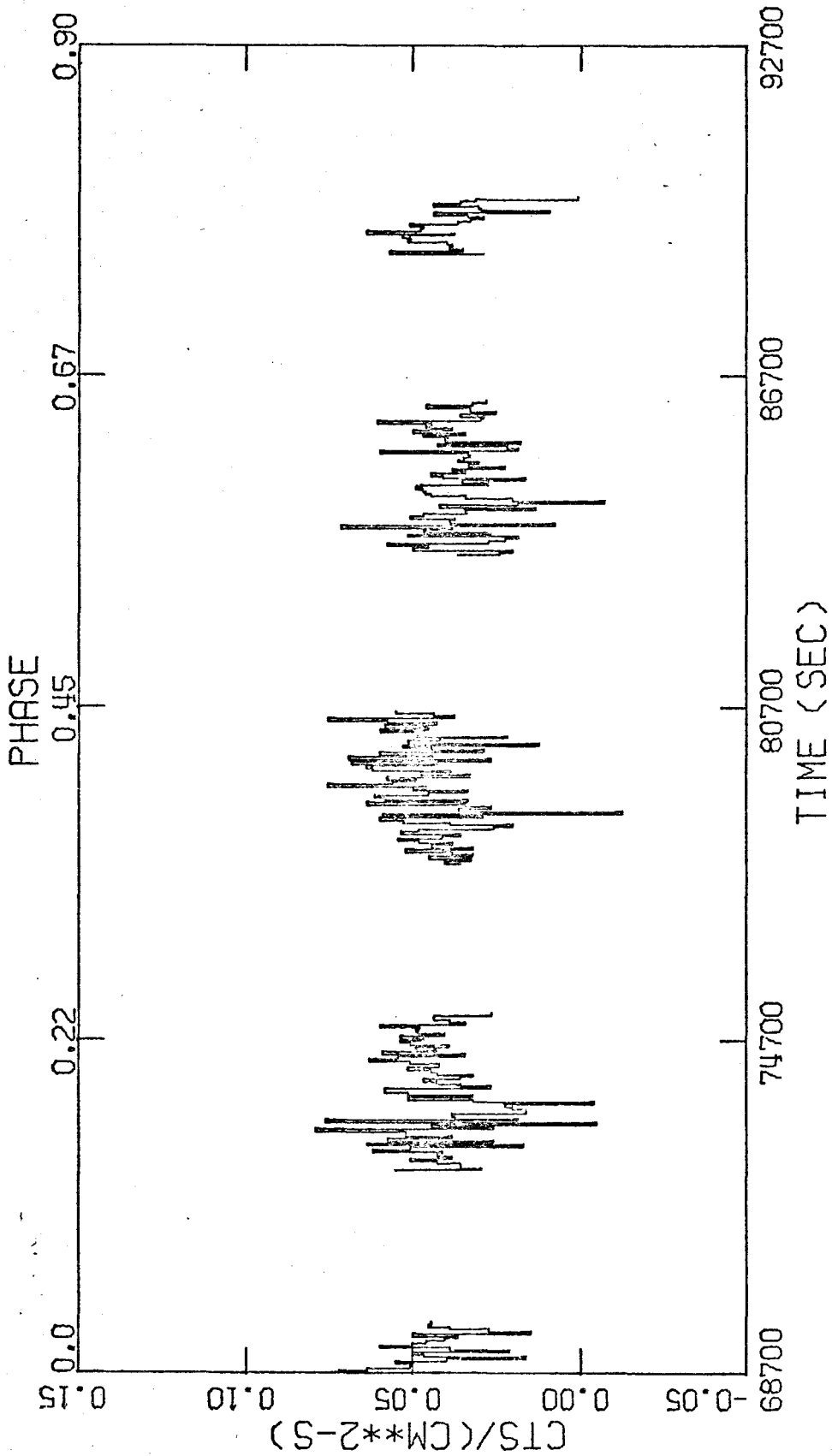


Figure 11a

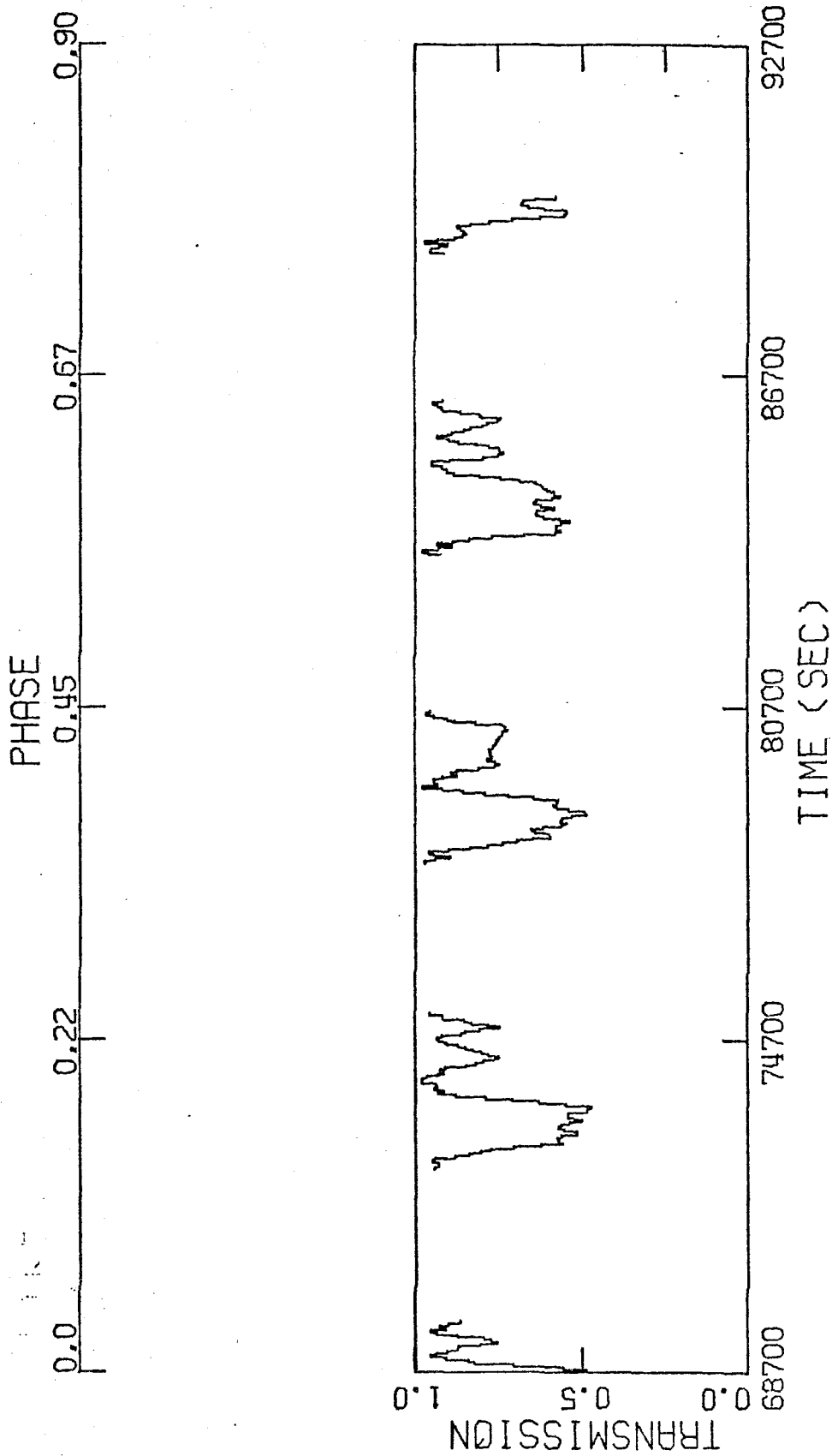


Figure 11b

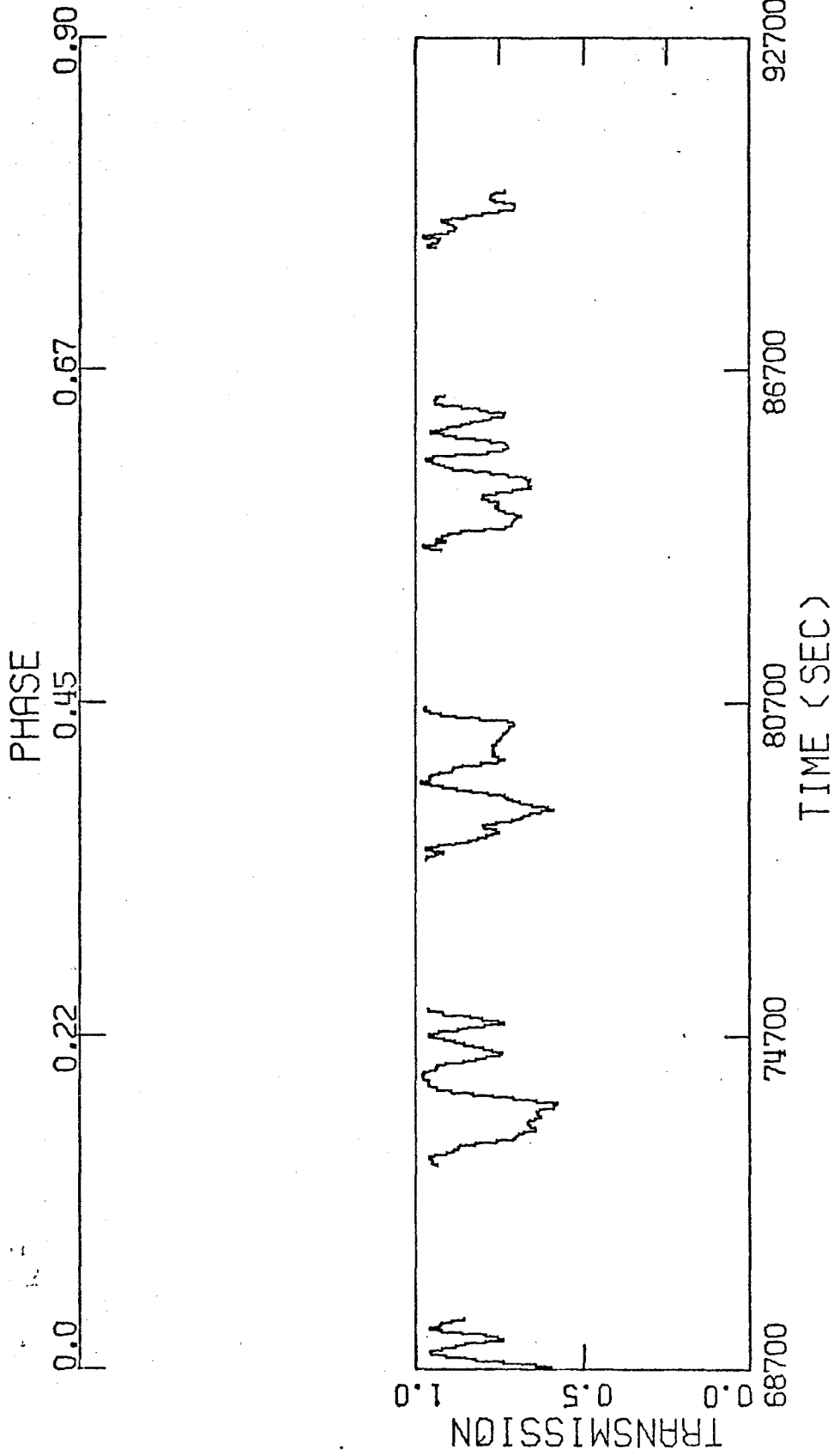


Figure 11c

Figure 12

Same as Figures 11 (a), (b), and (c), but with a "correction" to the GSFC aspect solution amounting to a shift in the source azimuthal angle by only 0.1° . These Figures, when compared with Figure 11, show how sensitive the light curve is to relatively small changes in the value used for the aspect correction.

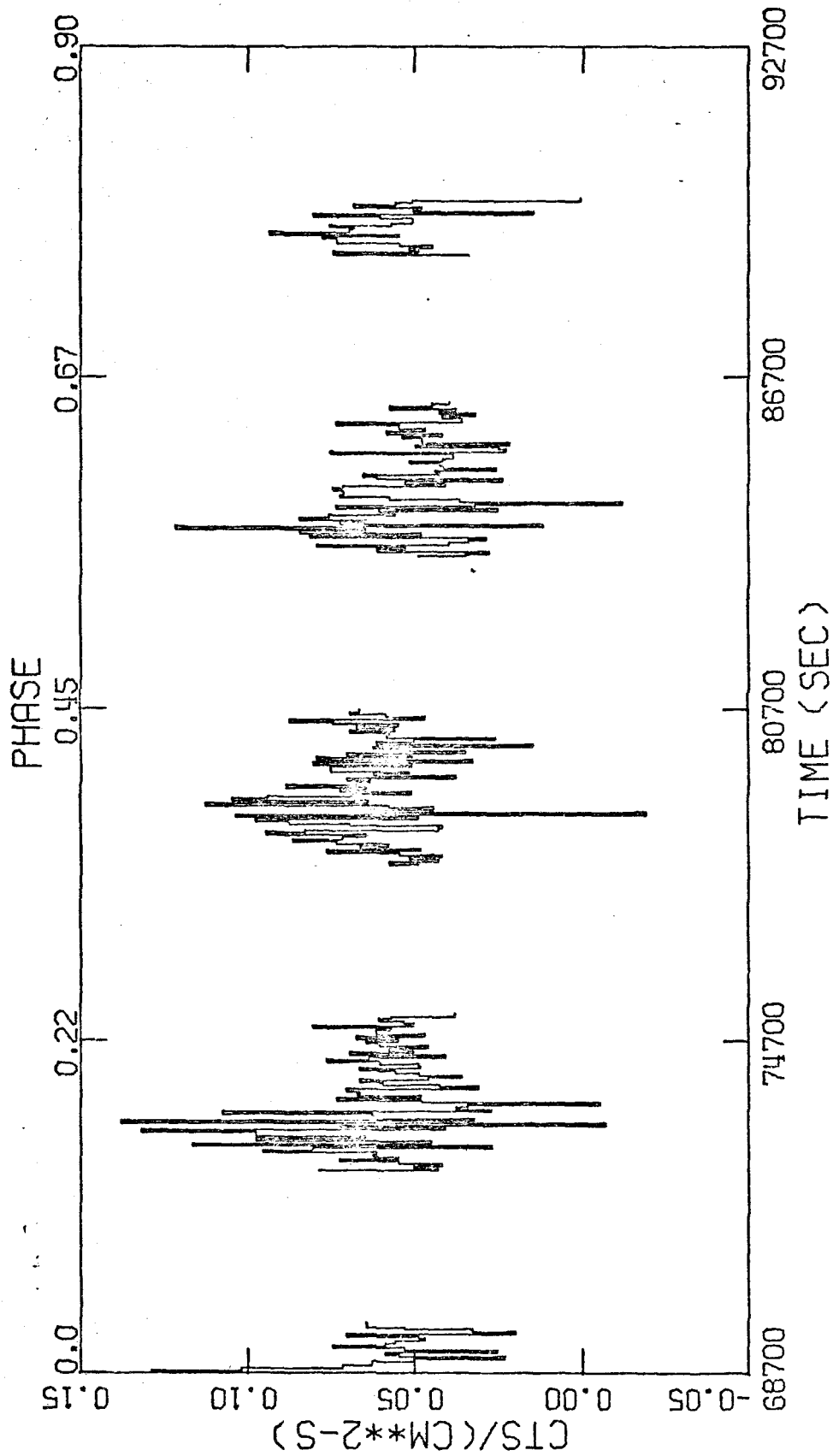


Figure 12a

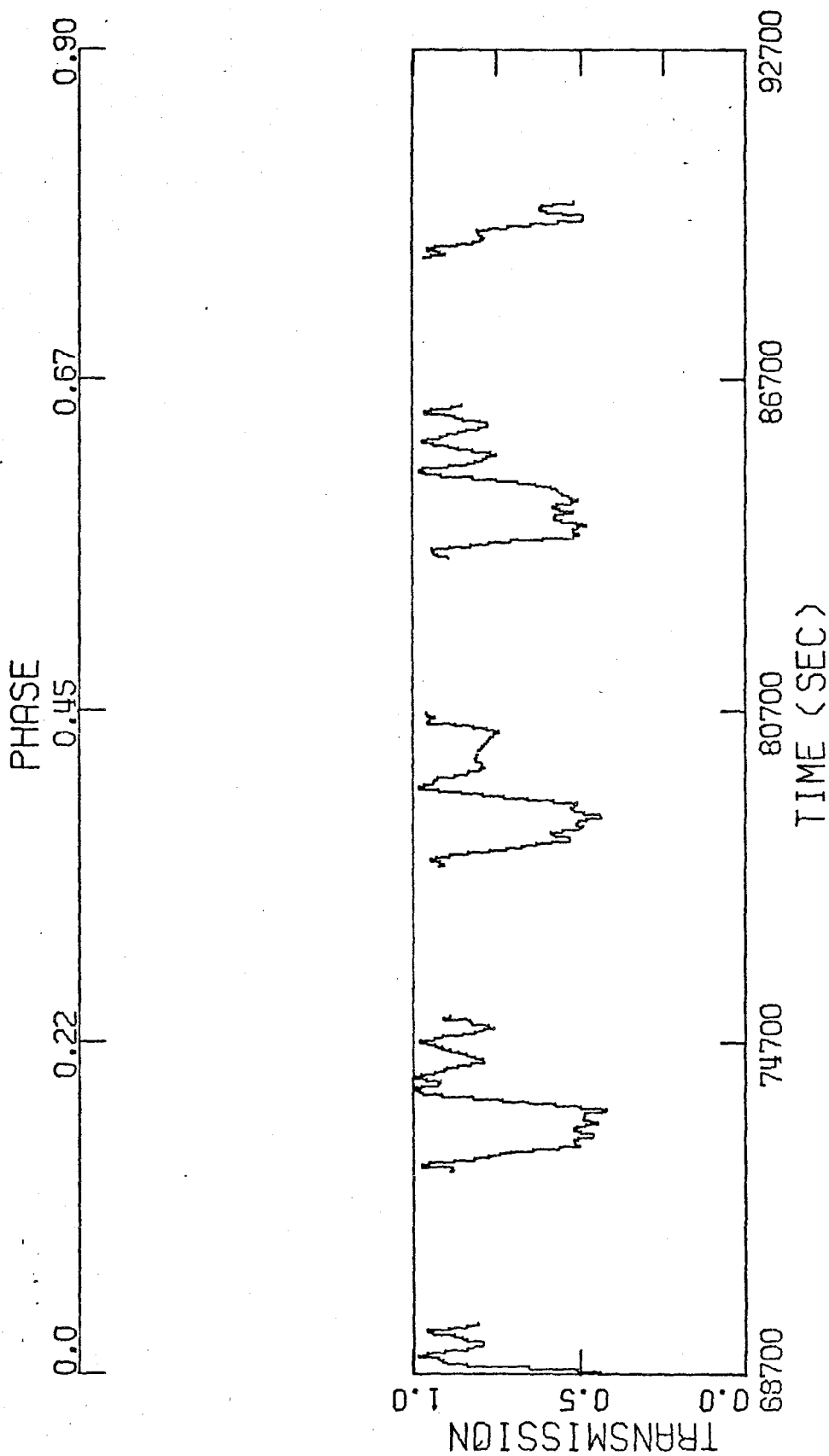


Figure 12b

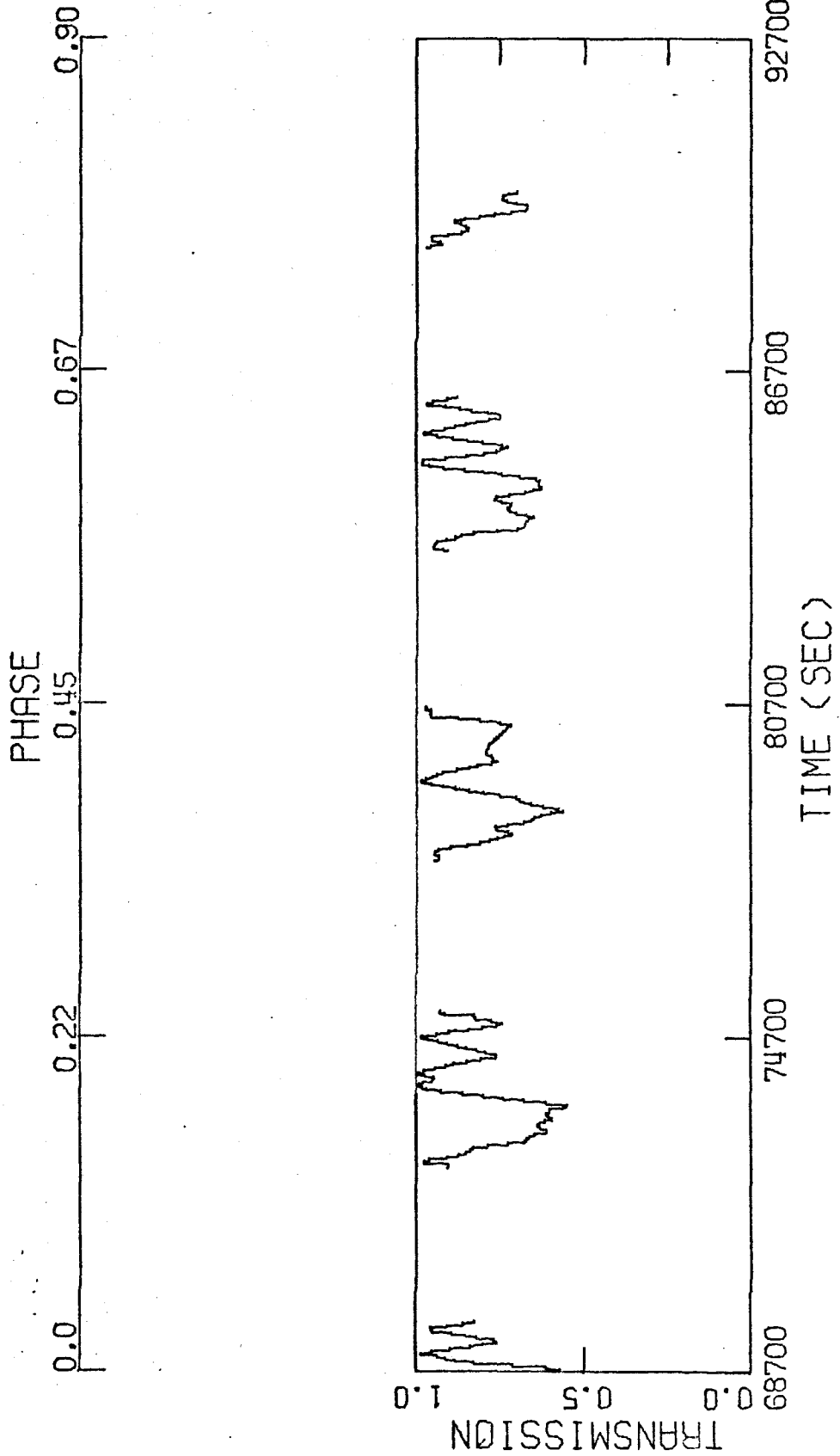


Figure 12c

For the above discussion, the instrumental background has been ignored. We now estimate its effect on the calculated source intensity. Figure 13 shows the countrate per PHA channel versus energy for LED observations of the detector door (cover closed), the dark Earth, a typical sky region, and a very bright sky region. The contribution to the countrate from the dark Earth may be taken as the instrumental background. The dark Earth flux is due to scattering of cosmic background X-rays and to precipitation of trapped electrons into the atmosphere with subsequent bremsstrahlung. The sunlit Earth (not represented in Figure 15) is very bright below 1 keV due to fluorescence of atmospheric oxygen and nitrogen produced in the illumination of the Earth by solar X-rays.

For the SS Cyg pointing there was only one stretch of dark Earth data; it occurred in the increased high voltage mode (see Table 4-2). To estimate the instrumental background for the normal high voltage mode, we used dark Earth data from an earlier pointing. The rates for the instrumental background during both high voltage modes were ~ 0.2 ct/1.28s for both FOVs; this amounted to only a few percent of the total background rate. This value for the instrumental background was then subtracted from the scanning data, which were taken just before and just after the pointing, and a revised value for γ was derived. Then all the pointing data were corrected for instrumental background and the new γ was used to derive the source intensity S (Eqn. 1).

In producing the light curves only electron-free data were used since electrons, like the instrumental background,

Figure 13

Pulse-height distribution for X-rays entering LED1 from a bright region of the diffuse X-ray sky (\square), a typical sky region (o), the dark Earth (Δ), and with the protective cover closed (\times). Error bars are 1σ statistical uncertainties only.

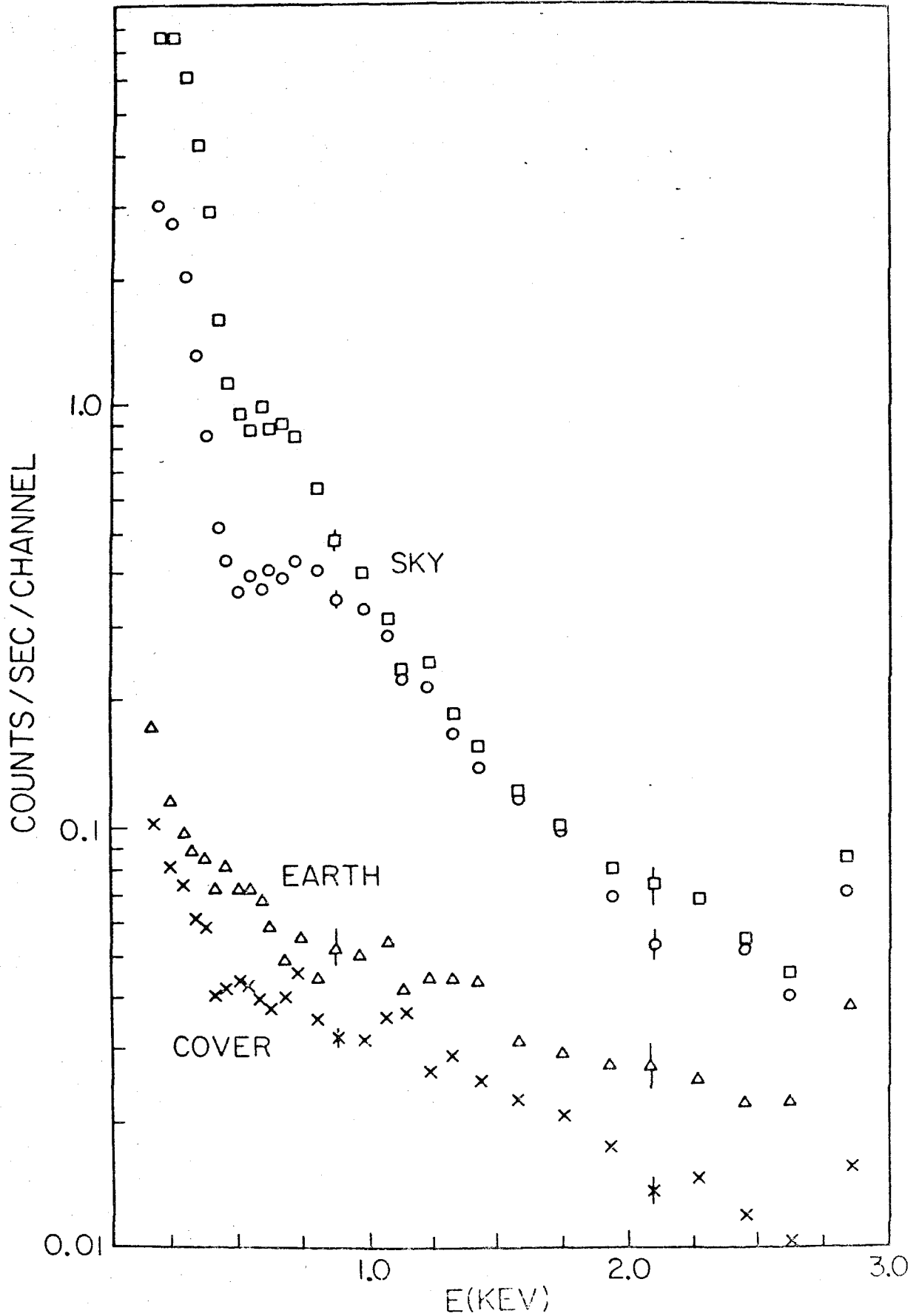


Figure 13

also do not scale as the FOV. The figure for γ should be calculated from dark Earth data and source-free scanning data near the time of the observation. As an illustration of the effects of choosing a γ -value that is too small, and of not accounting for instrumental background, Figure 14 shows 3 light curves of SS Cyg. Figure 14a is assuming $\gamma = 1.81$, a value communicated to us by a collaborating institution on the basis of several background measurements using data from early in the HEAO-1 mission; Figure 14b is for $\gamma = 1.95$, a value derived by averaging over the SS Cyg and U Gem scanning data; Figure 14c is for $\gamma = 2.05$, a value calculated from the SS Cyg observation alone when instrumental background was taken into account. Only for Figure 14c has the instrumental background been subtracted. The resulting satellite orbit (OB) average intensities for each assumed value of γ are listed in Table 4-3. Comparing the plots, or comparing the actual numbers in Table 4-3, it is apparent that while the choice of γ affects the absolute intensity, it does not affect the relative point-to-point intensities; this is because the source is never very far off axis. It is also clear that a correction for instrumental background is not necessary if the contribution of this background is as low as it was during this observation.

Figure 14

The light curves for SS Cygni using various values for the ratio of the fields of view (see text for derivation of this value). (a) for a ratio equal to 1.81, (b) for 1.95, and (c) for 2.05. The last Figure is the only one that includes a correction for instrumental background. The average values of each disjoint section of data for each value of the ratio plotted here are listed in Table 4-3.

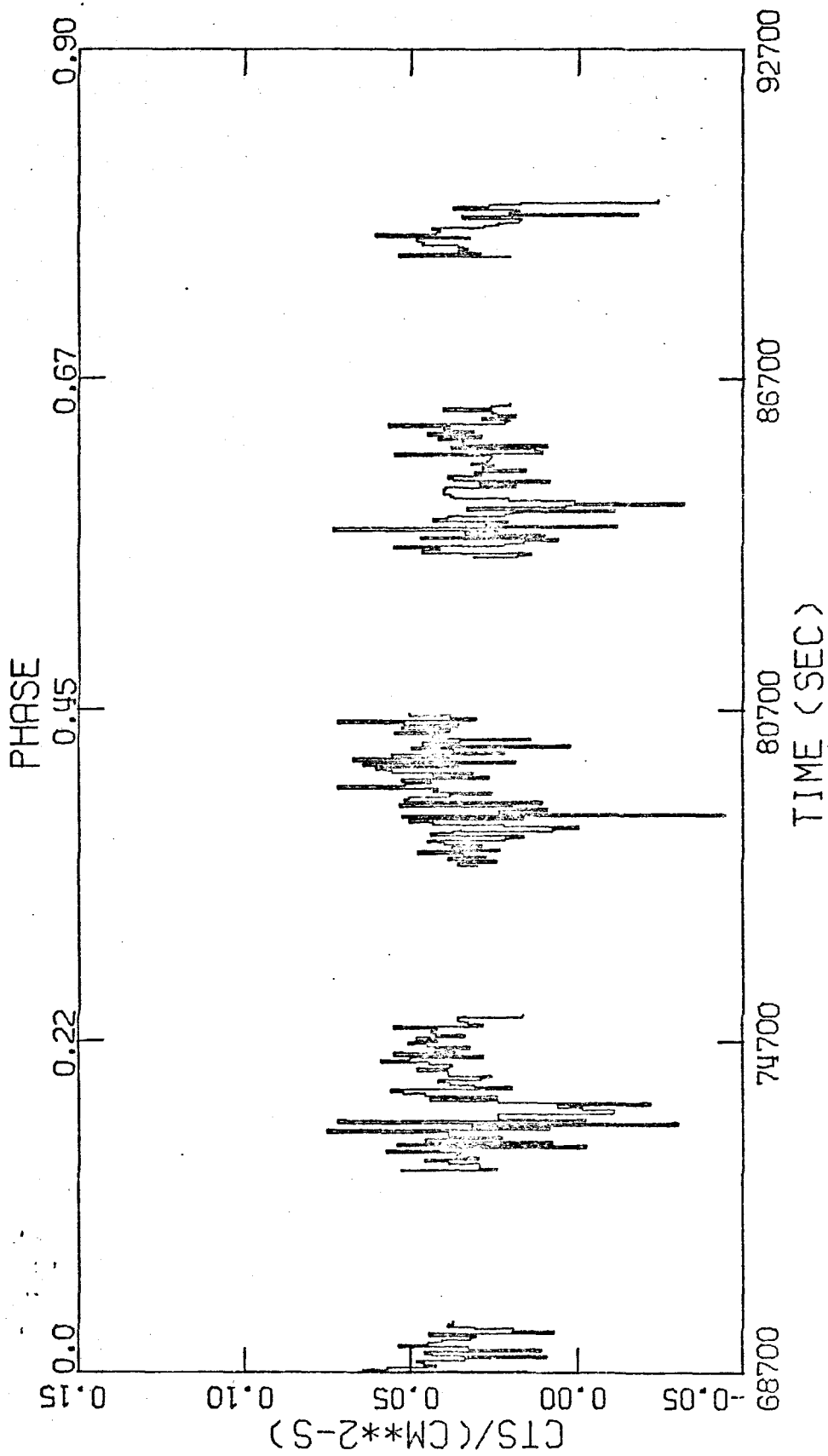


Figure 14a

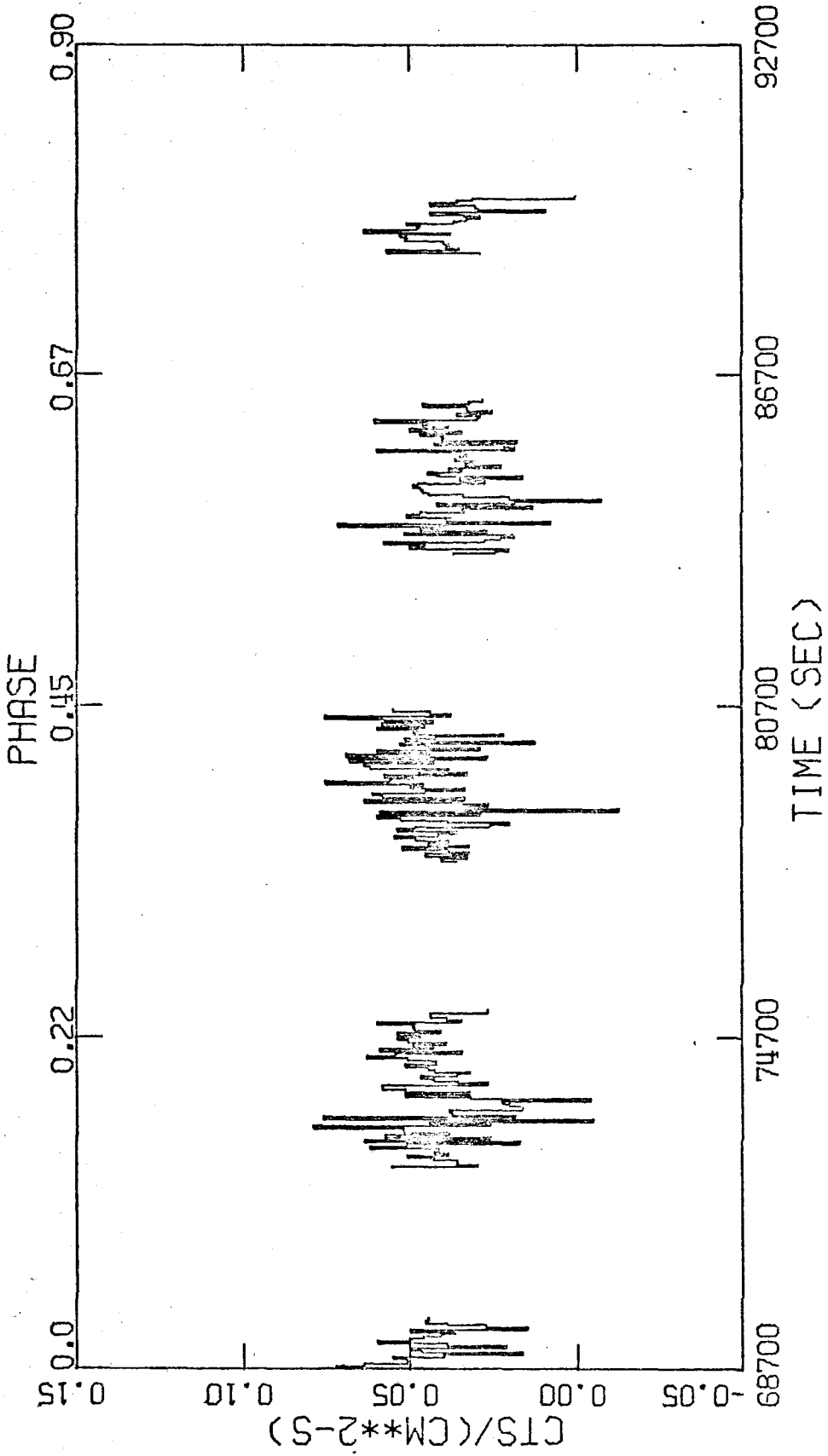


Figure 14b

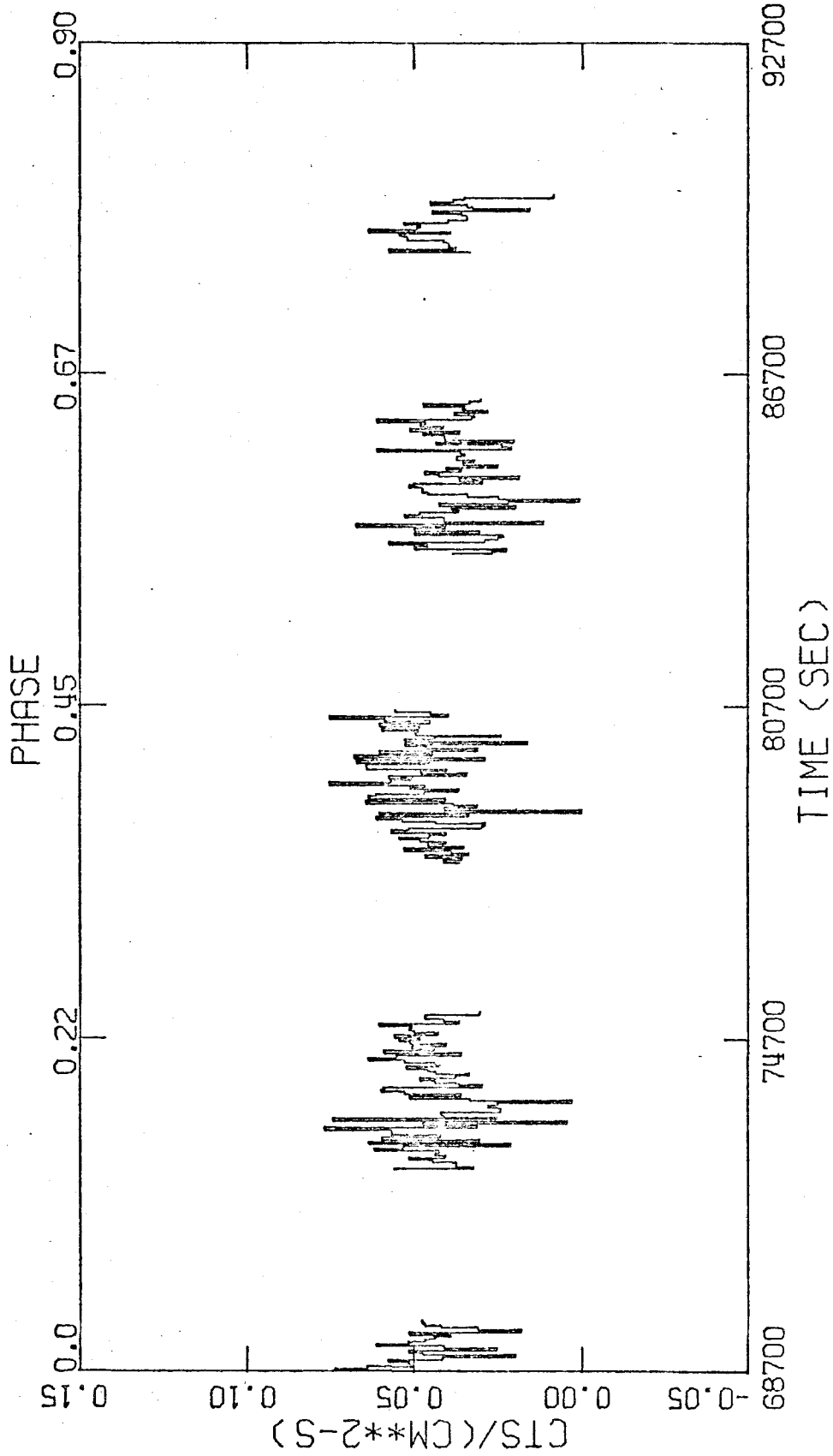


Figure 14c

Table 4-3

SS Cygni

Background-Subtracted, Aspect Corrected Source Intensity⁽¹⁾

Designation/	γ	$\text{Ct cm}^{-2} (1.28 \text{ s})^{-1}$		
		1.81	1.95	2.05 ⁽²⁾
OB1		.046±.004	.056±.003	.058±.003
OB2		.043±.003	.054±.002	.057±.002
OB3		.047±.003	.058±.002	.061±.002
OB4		.035±.003	.046±.002	.048±.002
OB5		.038±.004	.049±.003	.052±.003

(1) Errors are the statistical errors plus the correction for the transmission.

(2) For $\gamma = 2.05$, the instrumental background was subtracted from the raw data before applying the FOV ratio technique.

References for Appendix A

- Bevington, P. R., Data Reduction and Error Analysis for the Physical Sciences (McGraw-Hill, New York), 1969.
- Birsa, F. B., Glasser, C. A., and Ziegler, M. M. 1972, 1.5 to 38 keV X-ray Experiment System for High Altitude Sounding Rockets, NASA Report X-661-72-80.
- Brown, R. L. and Gould, R. J. 1970, Phys. Rev. D., 1, 2252.
- Charles, P. A. 1978, private communication.
- Charles, P. A., Culhane, J. L., and Tuohy, I. R. 1973, Mon. Not. R. Astr. Soc., 165, 355.
- Conroy, M. 1979, private communication.
- Eddington, A. 1916, reprinted in Nature, 1979, 278, 213.
- Giacconi, R., Gursky, H., and Van Speybroeck, L. P. 1968, Annual Reviews of Astronomy and Astrophysics, 6, 373.
- Gursky, H. and Schwartz, D. in X-ray Astronomy, ed. by R. Giacconi and H. Gursky (D. Reidel: Dordrecht-Holland), 1974.
- Kellogg, E., Baldwin, J. R., and Koch, D. 1975, Astrophys. J., 199, 299.
- Lampton, M., Margon, B. and Bowyer, S. 1976, Astrophys. J., 208, 177.
- Mason, K. O. 1979, private communication.
- Riegler, G. R. 1976, 1978, In-house technical reports.
- Rothschild, R., Boldt, E., Holt, S., Serlemitsos, P., Garmire, G., Agrawal, P., Riegler, G., Bowyer, S., and Lampton, M. 1979, Space Science Instrumentation, in press.
- Toor, A. and Seward, F.D. 1974, Astronomical J., 79, 995.
- Tuohy, I.R. 1979, private communication.

APPENDIX B

THE PROGRAM PTIMING

This computer program fits a sinusoid to individual pulses or groups of pulses; it outputs the arrival time of the pulses, their amplitude and mean, and the chi-squared values of the fits.

The data set which is analyzed in the example included here is on a disc labeled FXC.ALLCYG.AGAIN (unit 80). All of the data are on one file which is read as

$$ITO, M, (H(j), j=1, M), (V(j), j=1, M).$$

ITO is the reference start time of the observation in milliseconds; M is the total number of bins of data (each bin is 1.280 seconds long); H are the data in counts per bin; and V are the respective variances of the counts (these are greater than the statistical uncertainties because corrections for background subtraction and aspect have been included).

Following the listing of the Fortran program are the sets of arrival times, amplitudes and means generated for a fit to independent sets of four consecutive pulse periods of SS Cygni.

```

// EXEC FORTG
//FORT DD *
COMMON H,V,A,B,C,F,I,P,S,W,T,J,L,ICT
REAL*4 H(34000),V(34000)
COMMON AMPL,PHASE,BMEAN
REAL*4 I
AAVE = 0.
BAVE = 0.
READ(80) ITO,M,(H(J),J=1,M),(V(J),J=1,M)
READ(5,5) L,IDSC
WRITE(6,7) L,IDSC,ITO
WRITE(90) L,IDSC,ITO
WRITE(6,8)
C J IS A 'DO LOOP' PARAMETER WHICH STEPS THROUGH THE DATA WITH STEPS OF L
J=-L
C W IS ANGULAR FREQUENCY
PERIOD = 8.8
W = 2.*3.14159/PERIOD
ITOTAL = 0
ICT = 0
IEACH = 0
ICYCLE=0
C FIT A SINUSOID TO L BINS OF DATA
1 CONTINUE
J=J+L
ICYCLE=ICYCLE+1
A = 0.
B=0.
C=0.
D=0.
E=0.
F=0.
G=0.
HH=0.
I=0.
N1 = 0
DO 2 K=1,L
N=J+K
IF(N.GT.M) GO TO 3
RH=H(N)
C THROW OUT BAD DATA
IF (RH.LE.-10.) GO TO 2
T=1.280*N
X=COS(W*T)
Y=SIN(W*T)
Z = 1./V(N)
X1 = Z * RH
A=A+X*X*Z
B=B+X*Y*Z
C=C+X*Z
D = D + X*X1
E = E + Y*X1
F=F+Y*Z

```

```

G=G+Y*Y*Z
HH=HH+Z
N1 = N1 + 1
I = I + X1
2 CONTINUE
C EXCLUDE THOSE INTERVALS WHICH HAVE TOO LITTLE DATA
IF (N1.LT.4) GO TO 1
Z=1./HH
A=A*Z
B=B*Z
C=C*Z
D=D*Z
E=E*Z
F=F*Z
G=G*Z
I=I*Z
X=((E-F*I)*(A-C*C)-(D-I*C)*(B-F*C))/((A-C*C)*(G-F*F)-(B-F*C)**2)
Y=(D-I*C-X*(B-F*C))/(A-C*C)
C AMPL, PHASE, BMEAN ARE THE FITTED VALUES
AMPL=SQRT(X*X+Y*Y)
PHASE=ATAN2(X,Y)
BMEAN = I - AMPL*C*COS(PHASE) - AMPL*F*SIN(PHASE)
A = AMPL
P = PHASE
C CHI COMPUTES THE CHI-SQUARED VALUE OF THE FIT
CALL CHI
CHIMIN = S
BMEAN = B
AAVE = AAVE + AMPL
BAVE = BAVE + BMEAN
ITOTAL = ITOTAL + 1
C THIS PART COMPUTES THE UNCERTAINTIES IN THE FITTED VALUES
C IT WAS DEEMED THAT ONLY 10 PERCENT ACCURACY WAS NEEDED IN FINDING CHIMIN + 1
CHI1 = CHIMIN + 1.
CHI11 = CHIMIN + 1.1
CHI09 = CHIMIN + .9
CALL TIME
TMAX = T
C FIND UNCERTAINTY IN AMPLITUDE
C TRY ZERO AMPLITUDE
SIGT = 0.
A = 0.
CALL CHI
C S0 SAVES THE VALUE OF CHISQUARED FOR A ZERO AMPLITUDE PULSE
S0 = S
XLEFT = 0.
XRIGHT = AMPL
IF (S.LE.CHI11) GO TO 10
GO TO 11
C ENTERS HERE IF NOT CONSISTENT WITH ZERO AMPLITUDE
10 SIGT = 10.
C FIND MAX POSSIBLE AMPL IF CONSISTENT WITH ZERO AMPLITUDE
12 A = AMPL
13 A = A + .3
CALL CHI
IF (S.LT.CHI09) GO TO 13
C THIS IS CORRECT. WORK IT OUT . .
XRIGHT = A - 3.

```

```

XLEFT = A
IF (S.LE.CH11.AND.S.GE.CH109) GO TO 20
C ENTERS HERE IF CONSISTENT WITH ZERO AMPLITUDE
11 CONTINUE
A = (XLEFT + XRIGHT) * .5
CALL CHI
IF (S.LE.CH11.AND.S.GE.CH109) GO TO 20
IF (S.GT.CH11) XLEFT = A
IF (S.LT.CH11) XRIGHT = A
GO TO 11
20 SIGAMP = ABS(AMPL - A)
A = AMPL
IF (SIGT.GT.9.) GO TO 30
C FIND UNCERTAINTY IN ARRIVAL TIME OR PHASE
21 P = P + .3
CALL CHI
IF (S.LT.CH109) GO TO 21
XRIGHT = P
XLEFT = P - .3
IF (S.LE.CH11.AND.S.GE.CH109) GO TO 40
22 P = (XLEFT + XRIGHT) * .5
CALL CHI
IF (S.LE.CH11.AND.S.GE.CH109) GO TO 40
IF (S.LT.CH11) XLEFT = P
IF (S.GT.CH11) XRIGHT = P
GO TO 22
40 CALL TIME
SIGT = ABS(T-TMAX)
C SUBROUTINE TIME FINDS THE TIME OF THE MAXIMUM CLOSEST TO THE CENTER OF
C THE INTERVAL. IF THE MAXIMUM OF THE PULSE WITH AN ARRIVAL TIME 1
C SIGMA AWAY FROM THE BEST FIT ARRIVAL TIME HAS SKIPPED A PERIOD,
C THE FOLLOWING STATEMENT CORRECTS FOR THAT SKIP
IF (SIGT.GT.(PERIOD/2.)) SIGT = PERIOD - SIGT
GO TO 30
41 SIGT = 10.
30 CONTINUE
IEACH = ICT - IEACH
IFLG = 0
IF ((S0-CHIMIN).GT.6.635) IFLG = 1
WRITE(6,6) ICYCLE,TMAX,AMPL,BMEAN,CHIMIN,N1,SIGT,SIGAMP,S0,IFLG
WRITE(90) ICYCLE,TMAX,AMPL,BMEAN,CHIMIN,N1,SIGT,SIGAMP,S0,IFLG
IEACH = ICT
GO TO 1
3 WRITE(6,6) ITOTAL
GPF = AAVE / BAVE
AAVE = AAVE / ITOTAL
BAVE = BAVE / ITOTAL
WRITE(6,336) AAVE,BAVE,GPF
336 FORMAT(/1X,'THE MEAN AMPL IS ',F10.3,'THE MEAN AVE IS ',F10.3,
1 'THE PULSED FRACTION IS ',F10.3/)
STOP
5 FORMAT(2I5)
6 FORMAT(I10,4F10.1,I10,3F10.1,I10,F10.1)
7 FORMAT(1X'THE DATA ARE SUMMED OVER',I4,3X'BINS (1.28 SEC PFR BIN)'
1 ,5X'FOR SCALAR ',I3,5X'THE START TIME IS',I10,' MSLC'//)
8 FORMAT(3X,'ICYCLE',6X'TIME',6X'AMPL',6X'MEAN',5X'CHISQ',5X'NBINS',
1 3X'SIGMA T',3X'SIGMA AMPL'//)
9 FORMAT(1X//)

```

```

END
SUBROUTINE CHI
COMMON H,V,A,B,C,F,I,P,S,W,T,J,L,ICT
REAL*4 H(34000),V(34000)
REAL*4 I
B = I - A*C*COS(P) - A*F*SIN(P)
ICT = ICT + 1
S = 0.
DO 4 K=1,L
N=J+K
T=1.280*N
RH=H(N)
IF (RH.LE.-10.) GO TO 4
Z = A*COS(W*T-P) + B
S = S + (Z-RH)**2/V(N)
4 CONTINUE
RETURN
END
SUBROUTINE TIME
COMMON H,V,A,B,C,F,I,P,S,W,T,J,L,ICT
REAL*4 H(34000),V(34000)
REAL*4 I
T = T - 1.28*L * .5
K = (W*T-P) / (2.*3.14159) + .5
T = (2*3.14159*K + P) / W
RETURN
END
//DATA DD *
      7 56
//FT80F001 DD UNIT=SYSDA,DISP=OLD,VOL=SER=CITSL2,DSN=FXC.ALLCYG.AGAIN
//FT90F001 DD UNIT=SYSDA,
// DISP=(NEW,KEEP),SPACE=(TRK,(1,1),RLSE),VOL=SER=CITSL2,
// DSN=FXC.PTIME07.DSC56
//

```

THE DATA ARE SUMMED OVER 20 BINS (1.28 SEC PER BIN) FOR SCALAR 56 THE START TIME IS 68732184 MSEC

ICYCLE	TIME	AMPL	MEAN	CHISO	NBINS	SIGMA T	SIGMA	AMPL
1	21.5	5.1	12.3	13.6	28	0.6	2.2	19.2
2	56.0	7.5	18.5	22.8	28	0.4	2.4	32.3
3	92.3	6.6	19.4	15.8	27	0.5	2.5	23.2
4	127.0	6.2	14.7	40.7	28	0.4	1.9	50.2
5	163.7	13.7	19.5	40.3	28	0.2	1.9	91.7
6	198.9	7.4	21.2	76.9	28	0.3	1.9	92.6
7	234.1	8.6	24.6	33.3	28	0.3	1.9	55.0
8	269.9	3.7	17.5	52.9	28	0.6	1.6	57.8
9	305.2	3.6	13.4	20.6	28	0.6	1.5	26.7
10	341.5	1.9	14.4	40.2	28	1.2	1.5	41.7
11	376.4	6.9	18.9	34.3	28	0.3	1.6	52.2
12	413.7	1.8	19.4	25.2	28	1.4	1.7	26.3
13	447.9	10.1	20.7	28.1	28	0.2	1.7	61.4
14	484.6	10.1	23.3	24.2	28	0.3	1.9	53.1
15	518.8	7.0	26.8	38.7	28	0.4	2.0	50.2
16	553.9	3.4	17.0	36.0	28	0.8	1.9	39.2
17	590.0	3.5	16.2	41.8	28	0.7	2.0	45.2
18	624.7	9.6	22.5	28.1	28	0.3	2.0	52.6
19	660.5	5.4	19.1	32.5	28	0.5	1.7	41.9
20	695.3	7.9	22.8	29.7	28	0.3	1.7	49.7
21	739.1	5.0	18.3	55.7	28	0.5	1.5	65.0
22	769.1	5.4	14.3	17.4	27	0.4	1.5	29.4
23	804.4	5.5	20.1	46.6	28	0.4	1.7	57.3
24	841.4	3.9	23.7	68.9	28	0.6	1.7	73.7
25	876.8	3.6	21.3	38.1	28	0.7	1.8	42.3
26	911.5	3.0	25.4	31.0	28	0.9	1.9	33.5
103	3671.9	9.6	22.0	31.5	28	0.2	1.6	64.8
104	3711.9	1.8	14.0	42.3	28	1.3	1.5	43.6
105	3745.7	6.6	14.6	48.3	28	0.3	1.4	67.1
106	3782.9	6.5	19.5	24.2	28	0.3	1.6	41.0
107	3815.7	3.5	17.1	15.3	28	0.6	1.5	20.3
108	3852.8	7.1	19.6	18.0	28	0.3	1.6	37.8
109	3887.3	6.9	22.6	25.3	28	0.3	1.9	39.1
110	3922.0	8.3	21.9	36.2	28	0.3	1.7	59.5
111	3960.6	1.7	17.5	30.4	28	10.0	1.6	31.4
112	3999.9	3.9	17.0	31.1	28	0.6	1.7	36.4
113	4027.8	11.8	20.1	39.5	28	0.2	1.8	84.2
114	4070.0	13.9	25.1	41.9	28	0.2	2.2	86.5
115	4107.4	0.6	13.8	24.4	28	10.0	1.8	24.5
116	4142.0	7.9	19.0	32.7	28	0.4	2.2	46.6
117	4178.9	2.3	16.3	35.4	28	1.3	2.0	36.7
118	4211.5	6.5	15.4	35.7	28	0.4	2.0	46.1
119	4247.3	17.0	25.6	26.7	28	0.2	2.4	80.8
120	4282.4	7.0	20.4	27.0	28	0.5	2.6	34.4
122	4353.9	9.6	19.2	45.1	28	0.4	2.4	60.1
123	4389.0	4.8	19.1	45.3	28	0.7	2.3	49.7
124	4424.5	9.0	20.2	33.9	24	0.3	2.5	45.7
125	4459.7	8.2	21.1	36.6	28	0.4	2.3	49.4
126	4495.8	5.5	19.2	21.8	28	0.6	2.2	28.1
127	4531.7	9.4	15.3	45.8	28	0.3	2.2	64.0
128	4567.9	5.3	16.2	42.7	28	0.6	2.3	48.3
129	4604.0	7.9	18.1	39.0	28	0.4	2.2	50.7
130	4640.6	8.8	18.4	28.6	28	0.4	2.2	43.9
131	4676.1	7.2	17.3	42.0	28	0.4	2.2	52.5
132	4710.2	5.2	15.6	32.9	26	0.6	2.3	38.3
133	4745.0	10.0	26.2	12.6	28	0.4	2.5	28.6
134	4788.6	8.3	17.8	34.2	28	0.4	2.3	45.9

135	4822.3	5.8	15.4	29.1	28	0.6	2.2	35.7
136	4858.5	6.4	14.0	29.5	28	0.5	2.0	39.1
137	4893.9	5.7	14.1	31.7	28	0.5	2.0	40.7
138	4930.0	4.3	14.2	33.3	28	-0.6	1.9	38.9
139	4967.4	3.1	18.3	36.2	28	-0.8	1.7	39.2
140	4996.4	4.1	20.6	40.9	28	-0.6	1.8	46.5
141	5032.8	8.7	26.7	34.8	26	0.3	1.9	55.8
142	5068.1	12.7	25.7	23.1	25	0.2	1.8	70.4
143	5111.5	10.5	27.3	51.3	26	0.1	1.7	155.9
144	5146.5	7.4	19.3	46.5	28	0.3	1.6	68.0
145	5182.5	9.0	18.6	38.0	28	0.2	1.5	69.8
146	5218.0	4.8	12.8	25.8	28	0.4	1.5	36.9
147	5253.4	10.2	16.5	22.2	28	0.2	1.4	69.5
148	5287.4	5.1	19.1	41.8	28	0.4	1.5	53.1
149	5323.5	9.3	21.5	40.3	26	0.3	1.6	71.9
150	5361.0	9.3	19.6	27.9	28	0.2	1.6	60.3
151	5398.3	0.6	14.7	38.5	28	10.0	1.5	38.6
152	5431.8	5.5	14.2	54.8	28	0.4	1.5	68.5
153	5466.2	12.9	21.1	34.1	28	0.2	1.6	94.7
154	5500.5	6.6	20.5	24.9	28	0.3	1.7	40.3
155	5536.1	6.2	15.2	31.1	28	0.4	1.6	45.8
156	5570.7	2.9	12.6	40.5	28	0.7	1.6	43.9
157	5605.7	0.8	20.3	54.2	28	0.3	1.8	77.4
158	5640.8	6.3	22.3	66.3	28	0.4	2.0	76.6
159	5676.8	8.6	22.3	67.9	28	0.3	1.9	87.7
160	5712.5	4.6	19.1	38.3	28	0.6	1.9	44.3
161	5748.4	5.8	14.7	59.6	28	0.4	1.6	72.1
162	5784.5	5.0	19.6	25.0	28	0.5	1.9	32.8
163	5820.4	7.6	19.6	24.6	26	0.3	1.9	42.0
164	5856.8	9.3	21.1	24.0	28	0.3	1.7	51.5
165	5898.8	8.1	20.4	52.7	28	0.3	1.8	73.5
166	5927.6	8.5	22.6	30.6	28	0.3	1.7	55.9
167	5963.4	12.2	21.7	17.6	26	0.2	1.7	70.1
168	6001.0	1.3	18.7	60.1	28	10.0	1.6	60.8
169	6035.2	6.9	20.2	40.4	28	0.3	1.6	59.1
170	6079.4	14.7	28.1	49.3	28	0.2	1.8	113.8
171	6113.8	6.6	22.5	25.9	26	0.4	1.9	39.7
172	6148.6	10.2	23.3	36.1	28	0.2	1.9	67.3
173	6183.5	7.2	21.8	43.3	28	0.4	1.8	58.8
174	6218.7	7.5	22.4	43.1	28	0.4	1.9	58.2
175	6253.4	3.2	22.4	39.0	28	0.8	2.0	41.7
176	6290.5	10.7	23.7	59.9	28	0.3	2.0	90.4
177	6327.1	5.4	19.2	20.9	28	0.5	1.7	30.4
178	6361.9	4.3	22.6	30.8	28	0.6	1.9	36.2
179	6397.6	9.3	23.2	10.5	24	0.3	2.0	32.3
180	6434.7	5.1	28.1	36.2	28	0.5	1.9	43.3
181	6469.9	10.0	30.7	30.8	28	0.3	1.9	60.0
257	9189.9	8.2	16.3	28.6	28	0.3	1.4	60.1
258	9232.9	5.6	17.8	37.7	28	0.4	1.6	50.9
259	9268.8	13.2	23.8	44.7	28	0.2	1.6	108.9
260	9297.9	7.2	21.3	43.3	28	0.3	1.7	62.0
261	9335.7	0.8	18.6	56.1	28	10.0	1.6	56.4
262	9368.6	2.1	13.0	32.5	28	0.9	1.4	34.6
263	9411.4	4.9	16.9	22.7	28	0.4	1.5	33.2
264	9439.6	5.0	21.4	29.6	28	0.5	1.6	38.9
265	9483.2	5.1	18.5	49.9	28	0.5	1.7	58.8
266	9518.2	9.2	21.8	23.3	28	0.3	1.7	49.3
267	9552.2	8.9	22.8	35.6	28	0.3	1.8	58.8
268	9586.2	3.2	13.6	22.9	28	0.7	1.8	26.3
269	9625.6	10.7	17.7	44.0	28	0.2	1.8	76.9
270	9662.4	6.4	23.4	17.4	28	0.4	2.2	26.6
271	9697.2	7.7	21.6	38.4	28	0.4	2.2	51.0
272	9732.4	12.1	20.9	33.2	28	0.2	2.1	69.5

273	9766.8	10.5	21.7	34.7	28	0.3	2.0	62.2
274	9803.1	12.0	21.4	40.7	28	0.2	1.9	78.3
275	9837.4	8.5	16.5	34.3	28	0.3	1.9	55.7
276	9873.2	11.8	21.9	28.5	28	0.2	2.0	60.4
277	9914.0	4.8	13.6	47.0	28	0.6	1.9	53.0
278	9941.8	14.9	19.9	36.2	28	0.2	2.1	87.4
279	9978.2	8.7	20.9	26.6	27	0.4	2.2	42.8
280	10021.0	6.7	22.2	25.1	28	0.5	2.3	33.8
281	10055.4	2.5	14.1	29.3	28	1.3	2.2	30.6
282	10090.5	4.3	16.6	37.7	28	0.7	2.3	41.3
283	10127.2	7.2	13.2	50.3	28	0.4	2.2	60.2
284	10162.1	3.8	17.5	48.1	28	0.8	2.1	51.0
285	10196.5	5.6	20.8	16.6	28	0.6	2.1	23.3
286	10232.9	7.7	19.7	25.6	28	0.4	2.2	39.2
287	10267.5	9.3	19.9	33.4	28	0.3	2.0	52.9
288	10304.1	9.8	21.4	35.0	28	0.3	2.1	57.4
289	10337.2	8.7	22.5	33.6	28	0.3	2.2	50.1
290	10372.9	12.2	26.2	32.0	28	0.2	2.1	64.6
291	10408.6	9.0	28.5	37.7	28	0.3	2.1	56.4
292	10451.5	6.0	20.7	43.4	28	0.4	1.7	55.1
293	10487.2	5.5	19.9	42.1	28	0.4	1.7	52.5
294	10522.5	10.0	21.2	36.6	28	0.2	1.7	72.1
295	10557.7	8.9	24.7	53.9	28	0.3	1.7	80.9
296	10592.3	8.5	19.4	17.9	28	0.3	1.6	48.7
297	10627.6	17.9	30.4	42.5	28	0.1	1.8	143.3
298	10663.0	8.4	23.9	26.9	28	0.3	1.7	51.8
299	10698.4	10.3	22.2	33.3	28	0.2	1.6	73.4
300	10733.7	9.7	25.6	65.0	28	0.2	1.7	96.5
301	10765.8	0.2	17.3	53.4	28	0.8	1.5	53.4
302	10804.6	5.6	17.6	31.3	28	0.4	1.6	43.4
303	10839.1	7.0	18.7	23.2	28	0.3	1.6	41.6
304	10873.1	12.0	24.5	19.7	28	0.2	1.9	63.7
305	10917.3	19.6	32.7	30.5	28	0.1	2.1	119.9
306	10951.5	5.8	23.4	41.2	28	0.5	2.0	49.4
307	10988.5	4.5	21.1	37.8	28	0.6	2.0	43.2
308	11024.2	7.4	22.8	35.8	28	0.4	2.1	49.2
309	11057.9	12.7	22.2	37.0	28	0.2	1.9	82.2
310	11094.9	4.7	14.3	37.1	28	0.5	1.8	44.3
311	11129.6	5.3	20.4	40.8	28	0.5	2.0	48.5
312	11165.5	2.0	17.0	32.2	28	1.3	1.8	33.5
313	11197.6	12.7	23.4	24.6	28	0.2	2.0	66.5
314	11239.9	5.4	19.5	47.7	28	0.5	1.9	56.2
315	11276.0	9.7	17.9	57.2	28	0.2	1.8	85.0
316	11310.7	6.7	19.1	50.9	28	0.4	1.9	63.7
317	11346.1	5.7	18.3	21.8	28	0.4	1.8	31.2
318	11381.6	6.1	15.9	22.6	28	0.4	1.9	33.8
319	11416.9	8.3	23.2	34.1	28	0.3	2.1	51.3
320	11450.4	8.2	20.7	51.7	28	0.3	2.0	69.2
321	11487.1	1.5	14.0	35.2	28	0.0	1.8	36.0
322	11522.0	4.3	17.7	39.0	28	0.6	1.9	44.4
323	11557.2	8.2	24.2	23.3	28	0.3	2.0	39.0
324	11592.3	10.2	25.2	37.1	28	0.3	2.1	62.0
325	11626.4	6.8	22.5	48.0	28	0.4	2.1	59.2
326	11662.7	8.9	21.8	37.7	28	0.3	1.9	57.7
327	11697.8	14.5	32.3	32.2	28	0.2	2.3	75.2
328	11741.8	4.5	22.4	53.0	28	0.6	1.8	59.1
329	11776.6	10.4	28.4	30.2	28	0.2	1.9	59.7
330	11809.6	13.0	29.6	79.8	28	0.2	1.8	130.4
331	11844.3	4.7	24.2	39.9	28	0.5	1.8	47.6
332	11881.4	3.0	20.8	59.7	28	0.7	1.5	63.5
333	11915.4	4.0	22.7	21.7	28	0.6	1.6	27.6
334	11951.1	8.4	23.7	28.1	28	0.3	1.7	51.6
335	11988.0	3.5	22.0	15.9	24	0.7	1.7	10.8

413	14786.7	8.6	18.4	37.9	28	0.3	1.6	66.2
414	14823.4	3.8	14.1	20.4	28	0.5	1.4	27.6
415	14857.4	7.4	13.8	19.1	28	0.3	1.4	45.6
416	14892.9	8.0	15.5	49.3	28	0.3	1.5	77.0
417	14927.7	5.4	14.3	67.7	28	0.4	1.5	80.7
418	14962.5	6.1	18.8	70.8	28	0.4	1.6	85.2
419	14996.1	8.3	17.4	32.7	28	0.3	1.6	59.6
420	15033.7	2.5	5.4	51.6	28	0.7	1.2	55.3
421	15068.0	10.1	16.2	40.1	28	0.2	1.6	78.6
422	15108.1	1.4	11.7	51.0	28	10.0	1.6	51.7
423	15146.7	4.0	11.8	31.2	28	0.6	1.7	36.5
424	15181.6	4.1	12.3	29.2	28	0.6	2.0	33.6
425	15216.3	9.7	16.6	51.9	28	0.3	2.0	75.3
426	15251.4	6.0	15.0	43.1	28	0.5	1.9	52.3
427	15286.9	1.0	11.7	35.9	28	10.0	1.9	36.2
428	15320.5	2.6	6.9	22.3	28	0.9	1.8	24.4
429	15357.6	5.5	11.0	19.0	28	0.5	1.9	27.3
430	15393.2	10.0	10.4	50.1	28	0.3	1.9	78.1
431	15427.9	6.1	16.5	49.0	28	0.5	2.1	57.8
432	15466.2	0.6	17.9	21.7	28	10.0	1.9	21.8
433	15498.4	9.0	17.1	29.2	28	0.3	2.0	51.0
434	15532.7	9.2	14.5	28.3	28	0.3	1.7	54.6
435	15576.6	11.9	18.0	55.5	28	0.2	1.9	95.2
436	15611.8	4.9	15.5	19.5	28	0.5	2.0	25.7
437	15645.6	7.8	13.4	25.0	28	0.3	1.8	43.4
438	15682.3	1.7	9.0	35.4	28	10.0	1.7	36.4
439	15715.6	3.6	11.6	25.7	28	0.6	1.7	30.1
440	15752.5	4.1	10.6	25.7	28	0.6	1.7	31.7
441	15785.8	4.0	11.4	29.1	28	0.6	1.9	33.8
442	15826.6	5.0	9.0	48.1	28	0.5	1.9	55.9
443	15855.2	5.9	9.9	47.2	28	0.4	1.9	57.2
444	15891.5	6.9	14.1	30.1	28	0.4	1.9	41.9
445	15934.8	7.8	14.3	25.3	28	0.4	1.9	40.3
446	15970.6	5.1	15.8	40.4	28	0.6	2.1	46.7
447	16004.5	10.5	22.2	25.8	28	0.3	2.1	48.9
448	16038.6	12.6	20.9	35.7	28	0.2	2.2	71.0
449	16074.3	6.8	11.3	38.4	28	0.4	1.9	52.1
450	16109.2	4.3	12.7	30.8	28	0.6	1.9	36.2
451	16143.8	1.4	8.8	27.4	28	10.0	1.6	28.1
452	16182.1	4.5	13.2	27.1	28	0.5	1.7	34.0
453	16216.1	14.7	19.1	44.9	28	0.2	1.7	117.0
454	16251.8	6.3	19.9	30.6	28	0.4	1.7	44.8
455	16285.6	7.2	18.7	25.0	28	0.3	1.6	44.6
456	16329.1	14.6	22.4	28.3	28	0.2	1.6	106.0
457	16363.9	6.0	13.1	27.4	28	0.3	1.5	43.2
458	16398.9	4.7	15.8	30.3	28	0.4	1.5	39.6
459	16432.6	7.0	15.4	54.3	28	0.3	1.5	75.7
460	16470.0	7.7	11.8	62.2	28	0.2	1.4	88.4
461	16506.3	4.3	14.5	36.0	27	0.5	1.6	43.3
462	16539.6	9.5	19.9	45.5	28	0.3	1.9	70.3
463	16575.6	3.4	15.8	37.9	28	0.7	1.9	41.2
464	16608.9	10.4	21.2	29.7	28	0.3	2.0	57.0
465	16643.8	17.1	25.6	46.0	28	0.2	2.1	113.1
466	16680.8	2.0	15.6	34.7	28	1.4	1.7	35.9
467	16722.6	3.5	12.8	48.5	28	0.7	1.7	52.5
468	16756.9	6.5	16.9	36.0	28	0.4	1.7	50.3
469	16791.0	2.6	14.4	16.6	28	0.9	1.6	19.2
470	16827.4	8.9	16.9	19.2	28	0.3	1.5	51.9
471	16862.4	3.8	17.2	44.3	28	0.6	1.7	50.1
472	16897.6	5.4	19.3	42.3	28	0.4	1.6	53.7
473	16932.2	5.1	19.0	35.6	28	0.5	1.6	45.4
474	16967.3	3.5	18.6	41.2	28	0.6	1.6	45.7
475	17003.4	3.4	17.4	30.6	28	0.7	1.7	34.8

476	17038.8	6.4	22.1	37.0	28	0.4	1.8	50.1	
477	17082.1	11.9	24.7	35.4	28	0.2	1.9	75.4	
478	17117.3	6.5	18.4	32.7	28	0.4	1.8	46.0	
479	17152.7	12.1	22.5	48.2	28	0.2	1.9	85.8	
480	17186.8	4.0	21.9	52.1	28	0.7	2.0	56.1	
481	17223.1	8.9	19.0	33.7	28	0.3	2.0	55.8	
482	17258.3	7.8	22.5	31.0	28	0.3	1.9	47.9	
483	17294.2	4.1	18.8	31.8	28	0.6	1.8	37.3	
484	17328.0	0.7	13.0	58.7	28	10.0	1.6	58.9	
485	17361.9	9.6	20.8	22.1	28	0.2	1.8	53.1	
486	17396.0	8.3	25.3	31.9	28	0.3	1.8	54.2	
487	17432.2	7.1	19.2	26.5	28	0.3	1.5	45.7	
488	17474.9	6.0	22.0	41.0	28	0.4	1.7	54.1	
489	17506.0	0.9	15.8	53.2	28	10.0	1.5	53.6	
490	17547.3	1.4	19.1	25.8	28	10.0	1.6	26.5	
141 262	565	20234.8	6.8	27.1	50.2	28	0.4	1.8	64.3
	566	20270.0	7.2	19.4	70.9	28	0.3	1.6	92.2
	567	20305.9	10.2	17.7	39.5	28	0.2	1.6	82.2
	568	20338.9	2.4	12.7	100.3	28	0.8	1.5	102.9
	569	20376.8	3.2	18.2	44.1	28	0.7	1.6	48.3
	570	20412.9	6.4	15.5	29.8	28	0.3	1.5	48.5
	571	20448.2	9.8	18.1	63.6	28	0.2	1.5	105.4
	572	20482.7	11.3	23.2	50.7	28	0.2	1.6	97.1
	573	20517.4	6.1	18.9	58.2	28	0.3	1.8	81.0
	574	20552.5	8.6	22.3	34.1	28	0.3	1.8	57.7
	575	20588.3	1.1	16.1	24.1	28	10.0	1.6	24.5
	576	20623.1	9.5	22.1	45.5	28	0.3	1.6	78.9
	577	20659.1	9.1	23.0	44.5	28	0.3	1.7	72.5
	578	20696.5	1.5	17.0	51.2	28	10.0	1.6	52.1
	579	20736.9	7.8	23.1	52.2	28	0.3	1.7	71.1
	580	20771.7	11.4	24.3	33.4	28	0.2	1.8	70.2
	581	20806.3	4.8	18.9	30.5	28	0.5	1.8	37.5
	582	20840.0	5.9	14.3	31.1	28	0.4	1.8	42.2
	583	20876.0	6.9	16.2	45.6	28	0.4	1.9	58.8
	584	20909.4	3.5	10.6	47.9	28	0.7	1.8	51.7
	585	20945.8	3.2	7.4	58.6	28	0.8	1.8	61.8
	586	20988.3	5.8	12.6	32.8	28	0.5	2.0	42.0
	587	21023.0	10.4	10.7	31.0	28	0.2	1.8	66.2
	588	21057.8	4.6	17.1	26.4	28	0.6	2.0	31.9
	589	21094.2	14.2	18.6	33.8	28	0.2	1.9	90.4
	590	21123.4	1.0	12.8	36.3	28	10.0	1.8	36.6
	591	21162.3	10.7	17.4	34.8	28	0.2	1.8	68.1
	592	21198.0	9.3	18.8	31.3	28	0.3	2.0	53.5
	593	21233.9	2.8	11.9	35.8	28	0.9	1.9	37.9
290									

THE MEAN AMPL IS 6.973 THE MEAN AVE IS 18.836 THE PULSED FRACTION IS 0.370